AD-A058 115 LOS ALAMOS SCIENTIFIC LAB N MEX F/G 11/2
DEVELOPMENT OF PYROLYTIC GRAPHITE/SILICON CARBIDE COMPOSITE MAT--ETC(U)
JUN 78 T C WALLACE, G E CORT, J J DAMRAN W-7405-ENG-36
UNCLASSIFIED AFRPL-TR-78-46-VOL-1 NL

1 OF 3
AD A058 115

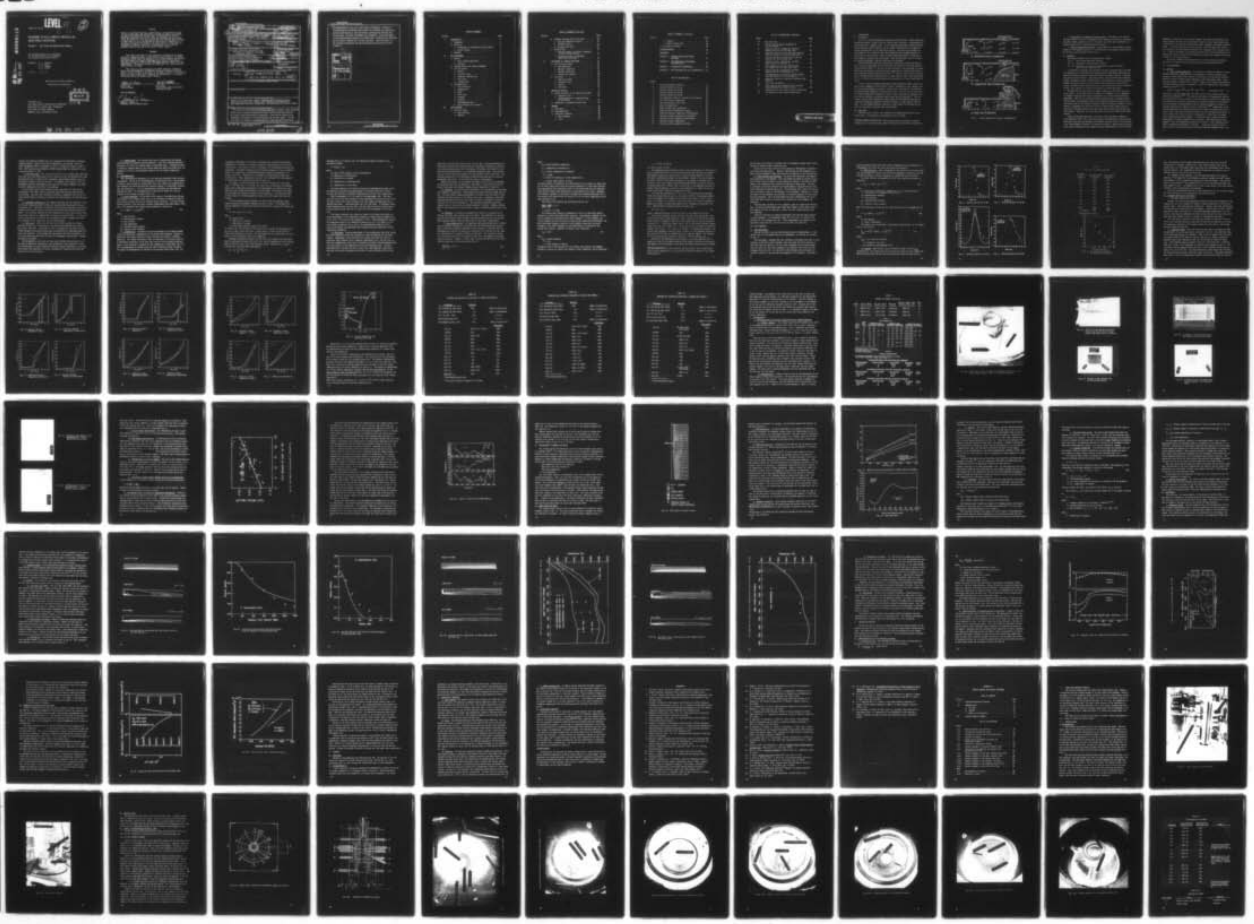

ADA058115

AD No.
DDC FILE COPY

LEVEL III

(2)

AFRPL-TR 78-46

A057982
981

DEVELOPMENT OF PG/SiC COMPOSITE MATERIALS FOR ROCKET-NOZZLE APPLICATIONS

VOLUME I - THE INJECTOR DEPOSITION FURNACE

LOS ALAMOS SCIENTIFIC LABORATORY
OF THE UNIVERSITY OF CALIFORNIA
LOS ALAMOS, NEW NEXICO 87545

AUTHORS: T. C. WALLACE
G. E. CORT
J. J. DAMRAN
M. C. CLINE

JUNE 1978

Approved for Public Release;

Distribution Unlimited.

DDC
RECEIVED
AUG 28 1978
E

Prepared for:
AIR FORCE ROCKET PROPULSION LABORATORY
DIRECTOR OF SCIENCE AND TECHNOLOGY
AIR FORCE SYSTEMS COMMAND
EDWARDS AFB, CALIFORNIA 93523

78 08 23 006

NOTICES

"When U.S. Government drawings, specifications, or other data are used for any purpose other than a definitely related government procurement operation, the Government thereby incurs no responsibility nor any obligation whatsoever, and the fact that the Government may have formulated, furnished, or in any way supplied the said drawings specifications or other data, is not to be regarded by implication or otherwise, or in any manner liscensing the holder or any other person or corporation, or conveying any rights or permission to manufacture, use or sell any patented invention that may in any way be related thereto."

FOREWORD

This report published in three volumes was submitted by Los Alamos Scientific Laboratory (LASL) of the University of California, Los Alamos, New Mexico, 87545, under the auspices of U.S. Energy Research and Development Administration Contract W-7405-ENG. 36, to the Air Force Rocket Propulsion Laboratory (AFRPL) under AFRPL MIPR agreement F04611-76-X-003, JON-305909JQ. The work was directed for LASL by Mr. T.C. Wallace and for AFRPL by Major J.G. Dean.

This report has been reviewed by the AFRPL Technical Information Office and is releasable to the National Technical Information Service (NTIS). At NTIS it will be available to the general public. This technical report has been reviewed and is approved for publication; it is unclassified and suitable for general public release.

Lester E. Tepe

LESTER TEPE
Project Manager

W.W. Wells

W.W. WELLS
Acting Chief, Space & Ballistic Propulsion Branch

FOR THE COMMANDER

Charles R. Cooke

CHARLES R. COOKE
Director, Solid Rocket Division

62302F

UNCLASSIFIED
SECURITY CLASSIFICATION OF THIS PAGE (When Data Entered)

(18) (19) REPORT DOCUMENTATION PAGE

READ INSTRUCTIONS BEFORE COMPLETING FORM

1. REPORT NUMBER: AFRPL-TR-78-46-Vol-I
2. GOVT ACCESSION NO.
3. RECIPIENT'S CATALOG NUMBER: (9) Rept.

(6) 4. TITLE (and Subtitle): DEVELOPMENT OF PYROLYTIC GRAPHITE/SILICON CARBIDE COMPOSITE MATERIALS FOR ROCKET-NOZZLE APPLICATIONS, Volume I. The Injector Deposition Furnace,

5. TYPE OF REPORT & PERIOD COVERED: Final 1 July 1975 to 31 December 1976 (21)
6. PERFORMING ORG. REPORT NUMBER

7. AUTHOR(s): (10) T. C. Wallace, G. E. Cort, J. J. Damran and M. C. Cline

8. CONTRACT OR GRANT NUMBER(s): F04611-76-X-003; F04611-76-X-003 Amendment Number 1

9. PERFORMING ORGANIZATION NAME AND ADDRESS: Los Alamos Scientific Laboratory of the University of California, Los Alamos, New Mexico, 87545

10. PROGRAM ELEMENT, PROJECT, TASK AREA & WORK UNIT NUMBERS: Project No. 62302F; BPSN: 305908 (16) (17) 09

11. CONTROLLING OFFICE NAME AND ADDRESS: Air Force Rocket Propulsion Laboratory, Director of Science and Technology, Air Force Systems Command, Edwards AFB, CA 93523 (11)

12. REPORT DATE: June 1978
13. NUMBER OF PAGES: 205

14. MONITORING AGENCY NAME & ADDRESS(if different from Controlling Office): (12) 213 p.

15. SECURITY CLASS. (of this report): UNCLASSIFIED

15a. DECLASSIFICATION/DOWNGRADING SCHEDULE: N/A

16. DISTRIBUTION STATEMENT (of this Report)
Unlimited
(15) W-7405-ENG-36
MIPR-F04611-76-X-003

17. DISTRIBUTION STATEMENT (of the abstract entered in Block 20, if different from Report)

18. SUPPLEMENTARY NOTES

19. KEY WORDS (Continue on reverse side if necessary and identify by block number)
chemical vapor deposition, computer modeling, data acquisition system, deposition kinetics, heat transfer, high temperature instrumentation, high temperature materials, pyrographite, recirculating flow, silicon carbide

20. ABSTRACT (Continue on reverse side if necessary and identify by block number)
A series of instrumented engineering tests with a chemical vapor deposition furnace used to prepare pyrographite/silicon carbide codeposited material for rocket nozzle applications is described. Flow into the furnace is an axisymmetric confined jet with high Reynolds and low Mach number. The gas flow within the furnace is characterized by a large separated flow region

DD FORM 1 JAN 73 1473 EDITION OF 1 NOV 65 IS OBSOLETE
S/N 0102-014-6601

UNCLASSIFIED
SECURITY CLASSIFICATION OF THIS PAGE (When Data Entered)

21135Ø

with associated hot spot and a high level of turbulence. Methods of instrumenting and collecting data, methods for defining the furnace and process characteristics, test procedures, recording and reducing data, data analysis, and model development are documented. Analytical models of the furnace during transient and steady state operation were developed and the results compared with the data obtained. Characterization of the coatings obtained and the associated deposition kinetics are also presented.

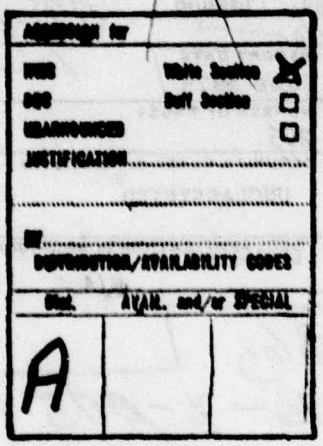

TABLE OF CONTENTS

TABLE OF CONTENTS (continued)

TABLE OF CONTENTS (continued)

LIST OF ILLUSTRATIONS

▼

LIST OF ILLUSTRATIONS (continued)

PRECEDING PAGE BLANK

I. INTRODUCTION

A. Background

In 1971, at Atlantic Research Corporation*, the Air Force Rocket Propulsion Laboratory started a study of silicon carbide (SiC) additions to continuously nucleated pyrolytic graphite (PG). In the codeposited material, pyrolytic graphite and silicon carbide (PG/SiC), the SiC phase is deposited in a PG matrix as needles perpendicular to the deposition surface. This structure provides reinforcement in the c-direction and vastly improved shear strength between the a-b layers of the PG matrix. Also, the bond between the PG/SiC coating and an ATJ** graphite substrate was outstanding. Even in mechancial tests to failure, no coating separations from the substrate were observed.[1]

Early development involved small-throat rocket-nozzle inserts and exploratory firings to establish target compositions and structure and gather preliminary performance data.[2-7] As this work was successful, work was begun to design, fabricate, and evaluate the PG/SiC-coated, large-throat, rocket-nozzle inserts under advanced ICBM test firing conditions.[8-11] Most of the work was on scaling up the coating process from 25-mm-(1-in.-)-diam inserts to 89-, 178-, and 318-mm (3.5-, 7-, and 12.5-in.-)-diam inserts with coatings 3.3-7.6 mm (0.150-0.300 in) thick.

As the coating development progressed toward making the larger diameter inserts, major changes in the deposition furnace configuration were required (Fig. 1), and the percentage of acceptable coated inserts decreased.[11] A requirement for demonstrating capability to reproducibly coat a nose cap for the rocket-nozzle throat package led to even more drastic furnace configuration changes, and a yet lower percentage of acceptable coated nose caps were produced.[12] The conclusion was that more fundamental understanding of the deposition process was required in designing apparatus for making deposits on large inserts and nose caps. The Los Alamos Scientific Laboratory (LASL) began a study with the Air Force in July 1975, to provide that understanding.

B. Objective

This work was to improve the capability for making PG/SiC-coated rocket-nozzle parts. The expected accomplishments were as follows.

---

*Atlantic Research Corporation, 5390 Cherokee Avenue, Alexandria, Virginia.

**Trade name of a premium grade graphite supplied by Union Carbide Corporation.

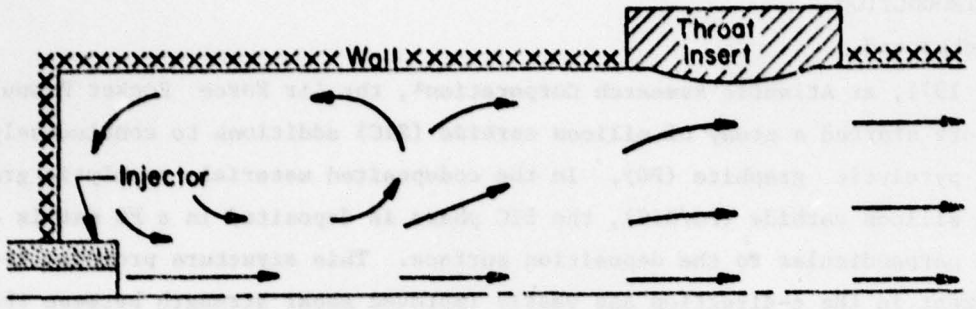

A - Small Throat Insert Configuration

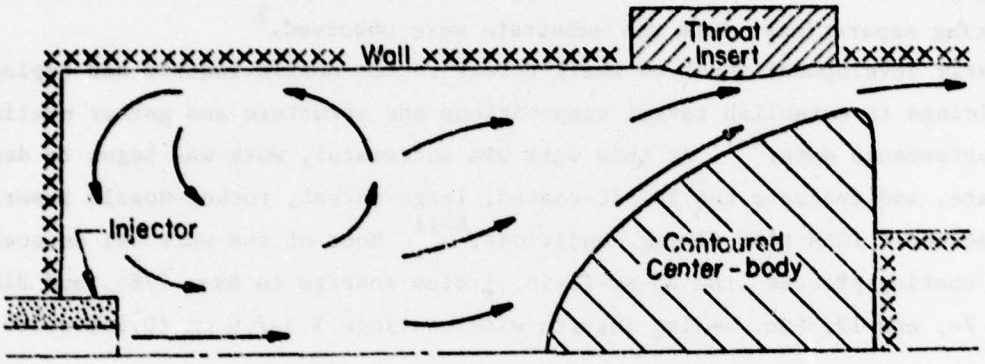

B - Large Throat Insert Configuration

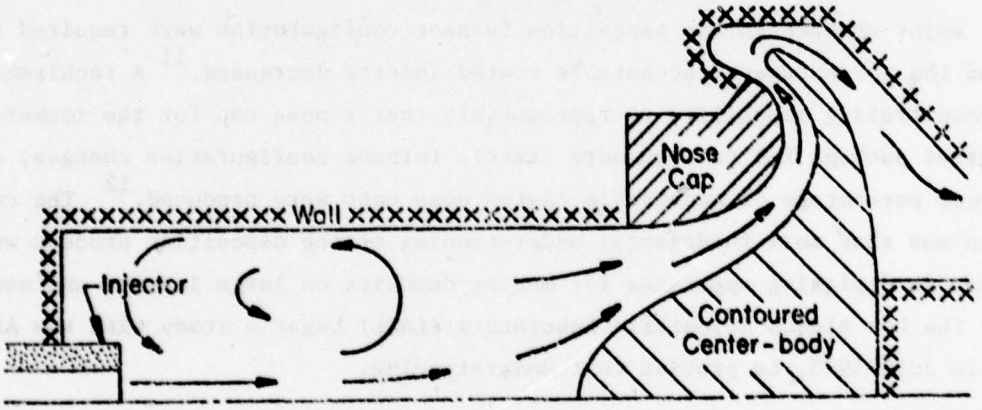

C - Nose Cap Configuration

Fig. 1. Various deposition canister configurations.

1. Development of a deposition process model. Development of an analytical model complete enough for designing furnace geometry and fixtures and specifying power inputs, mass flow rates of reactants, and other input conditions for coating nozzle parts of differing shapes and sizes.

2. Control system specification. Specification of fully automatic control system for the deposition process. System definition and complete specification. No detailed circuit design or fabrication.

C. Approach

This report consists of the following three volumes.

Vol. I. The Injector Deposition Furnace.

Vol. II. The Channel Flow Depositing Furnace.

Vol. III. Comparison of Deposition Furnaces and a Generic Process Control System Specification.

To establish a data base for validation the model developed and to document the operation of an existing PG/SiC coating furnace, LASL asked (LASL Order No. L66-17503-1)Atlantic Research Corporation (ARC) to perform a series of engineering tests at their facility. LASL specified the test procedures and instrumentation. Deposition furnace modifications for instrumentation, furnace operation during the tests, and part of the coating characterization were done by ARC. Volume I documents these engineering tests, characterizes the injector deposition process, and compares the results obtained with the model developed.

The model had to be an efficient, simple design tool for PG/SiC coating of nozzle parts. If the model were too complex, too expensive, or too demanding of computer facilities for routine application, its utility would be greatly diminished. Early in the injector deposition furnace work, it became apparent that the model fluid dynamics would be very complex (primarily because of a recirculation zone in the furnace) and would require an extensive computer facility. Further, it appeared that the flow field for coating throat inserts would be drastically different from that for nose caps, and the model would become even more complex. Therefore, the study objectives could not be achieved using ARC's furnace.

Using information developed to that point and an available computation fluid mechanics code[13] that could treat steady, two-dimensional, turbulent boundary layer flow with heat addition and chemical reactions (but not recirculation flow), LASL designed a channel flow deposition furnace. Design criteria included an inlet configuration that permited accurate specification of the fluid flow

parameters at the start of the coating chamber, equivalent flow conditions for throat inserts and nose caps, better heat transfer to parts being coated, more economical use of power and coating gases, easier assembly, and higher production rates. The furnace was built and run at LASL. The test matrix for the runs was designed to provide maximum information for comparison with the model kinetics. Volume II documents the fabrication details and the data obtained from the engineering tests, characerizes the deposition process, and compares the results obtained to the model developed.

Volume III compares the characteristics of the two deposition furnaces, describes the models developed, and gives control system specifications.

II. THE EXPERIMENTS

A. General.

1. Prior process experience. The composite coatings are applied to heated graphite substrates (1800-2500 K) by an atmospheric-pressure chemical vapor deposition (CVD) process that involves the pyrolysis of a diluted (N_2 diluent) mixture of methyl trichlorosilane (CH_3SiCl_3 or MTS) and methane (CH_4). Other hydrocarbons may be used in place of CH_4.[14] When a fluid element containing CH_4 is heated rapidly to 1500 K (or higher), a series of consecutively irreversible reactions occur;[15,16] i.e.,

$$CH_4 \xrightarrow{k_1} 1/2C_2H_6 \xrightarrow{k_2} C_2H_4 \xrightarrow{k_3} C_2H_2 \xrightarrow{k_4} \cdots \{\text{precursor}\} \longrightarrow PG, \qquad (1)$$

where the k's are the appropriate 1st-order reaction rate constants that are temperature dependent.[16,17] The chemistry and physics of pyrographite deposition (the nature of the PG precursor in the gas phase, the effect of energy gradient effects near the wall, the kinetics of precursor formation, soot formation in the gas phase, and pyrographite structure deposited relative to types of precursor species) are complex and poorly understood.[18-20] Examination of the relative magnitudes of the known reaction rate constants indicates that pyrolysis of CH_4 is the rate-controlling kinetic step (all succeding steps in Eq. (1) occur at much faster rate) and that a temperature of 1500 K must be reached before significant pyrolysis begins. A literature search failed to find any kinetic data on thermal decomposition of CH_3SiCl_3. Mass spectrometric data suggest[21] that the decomposition proceeds in two ways. First, CH_3SiCl_3 decomposes by sequential detachment of chlorine atoms and, second, the Si-C bond is broken and various silicon- and carbon-containing fragments form. The

rate of the first process is approximately twice that of the second.

Once the precursor species have formed in the gas stream, the deposition rate is very dependent on flow conditions. Figure 1 shows typical configurations of deposition canisters that contain the part to be coated. The process gas ($\sim$ 97 vol % N_2 + CH_4 and CH_3SiCl_3) is introduced into the canister through a water-cooled injector at Reynolds numbers of 7000 near the inlet based on the canister i.d. For the larger throat inserts and nose caps, the practice has been to place a contoured centerbody in the canister to try to maintain flow conditions equivalent to those of the small-throat insert configuration. The deposition canisters may be heated by either resistance or induction heating. Optical pyrometer readings are made on the surface of the part being coated, and the power to the furnace is varied to maintain a constant substrate temperature.

When an injector is used, there will always be a recirculation region near the canister inlet. The physical characteristics of the recirculation flow will depend on the internal geometery of the canister, wall and centerbody temperatures, process gas flow rates, physical properties of the diluent, and the injector i.d. Therefore, the time-thermal history of the precursors in the recirculating flow region will differ from that of those in the nonrecirculating region.

When all these complex factors are properly controlled, the SiC phase deposits as needles perpendicular to the deposition surface, providing reinforcement in the c-direction and vastly improved shear strength between the a-b layers of the codeposited PG matrix. Reasonably uniform coatings have been obtained over axial distances of 75- to 125 mm along the substrate at rates up to 0.5 mm/h. Uniform distribution of accicular SiC in the PG matrix can be maintained given 0.1-0.4 weight fractions of SiC. The experimental data available indicate that the PG and SiC deposition rates are essentially independent of each other. The deposition rates of both increase monotonically with increasing concentrations of CH_4 and CH_3SiCl_3, respectively. The deposition rate of SiC apparently decreases drastically with a temperature increase from 1900 to 2200 K. This factor emphasizes the requirement for accurate control of the temperature along the substrate surface.

2. Approach. A model complete enough for use in designing furnace geometry and fixtures and specifying power inputs, mass flow rates of reactants, and other input conditions for coating nozzle parts of differing shapes has a number

of interactive computation elements that must be validated against a reliable data base. The data base must contain information on the nature and efficiency of power input to the deposition furnace, transient and steady state thermal characteristics of the deposition furnace, heat transfer to the process gas, hydrodynamic flow during the deposition, and dependence of coating characteristics (deposition rate, microstructure, etc.) on process conditions. A review of available data showed that the data base was inadequate to cover all the requisite areas.

It was determined that the most effective way to establish the data base was to enter into a contract (LASL order No. LL6-17503-1) with ARC to provide engineering services for conducting instrumented PG/SiC codeposition runs. The work was divided into three tasks. The first was modification of an existing deposition furnace to accommodate additional instrumentation. Included also were installation and operation of a data acquisition system. LASL furnished the additional instrumentation and data acquisition system.

The second task was to run deposition tests using a straight-tube geometry similiar to that shown in Fig. 1A. This effort involved two subtasks. The first was to get data on the flow field within the deposition canister and on furnace temperatures during transient and steady state heating tests with flowing nitrogen. The second was to get similiar data during actual coating runs.

The third task was to have been the performance of deposition tests using a curved annular passage similar to that shown in Fig. 1C, but the contract funds were depleted by the second task.

B. Coating furnace and process equipment.

Initially ARC was the only company that had extensive experience with PG/SiC codeposition. Therefore, as they had complementary work in progress, the least expensive way to assemble the initial data base was to perform these engineering tests at their facility. Appendix A details the modification of the ARC process gas equipment and deposition furnace. The instrumentation requirements and calibration methods are described in Appendices B and C, respectively.

C. Test Procedure

1. General. The tests were planned to provide enough data to explain the factors involved in coating nonreproducibility and to verify that the analytical model could predict conditions in the furnace. The latter objective was particularly important because of the complex flow anticipated owing to the jet injector and the complicated furnace configuration. All of the tests described involved the same basic furnace configuration, and they were conducted in the sequence

listed. The tests are divided into four categories for discussion: cold-flow, transient heatup, steady flow holds at temperature, and coating. The first three designated 15601 (see Appendix D) were all conducted on March 16 and 17, 1976. The coating tests, designated 15800 through 15809 (see Appendix D), were conducted on May 6-7, 1976.

2. Cold-flow tests. The cold-flow tests were run to answer basic questions about the flow field downstream from the injector by use of a movable Pitot tube. The objective was to locate the jet boundaries and determine whether they were affected by changes in the N_2 flow rate. For example, the location of the reattachment point and determination that the flow is axially symmetric are basic pieces of information that affect the modeling.

The cold-flow tests also provided an early opportunity to exercise the hydrodynamic code, VNAP, without requiring iterations with the heat-transfer calculations. They were also intended to provide a comparison with the jet velocity profile when the furnace was heated, but unfortunately, no such data were taken.

3. Transient heating test. The transient heating test was intended to verify the heat conduction model, without the complications introduced by the recirculating flow. Comparison of measured and calculated temperatures during the transient was possible without iterations between the flow and heat conduction models. The transient heating test was integrated with the normal furnace start up procedure and did not significantly increase the overall effort. It also provided an opportunity to exercise the instrumentation and to measure the transient response of the furnace for control system design.

4. Flow tests. These were the basic tests used to verify the furnace modeling through use of hydrodynamic calculations from VNAP and heat transfer calculations from AYER. Conducting the tests at several N_2 flow rates and power levels allowed the relative scaling laws and sensitivity to modeling assumptions also to be verified. If any unexpected temperatures had been encountered, the flow tests would have been used to guide the subsequent coating tests. However, this was not necessary.

Not attempting to coat parts in these tests allowed the objectives to be met without additional constraints, thus permitting a wider latitude in power and flow settings. It also allowed the substrate surface temperature to be measured without the possibility of errors introduced by radiation scattering and absorption in the coating gas.

5. Coating tests. The coating tests were to characterize the coating achieved using the relevant process parameters. They also provided additional opportunity to verify the thermal models as described above. Although we hoped to develop a chemical kinetics and coating deposition model from these data, the complexity of the jet flow prevented doing so for the injector deposition furnace.

D. Instrumentation.

The instrumentation necessary for this study was determined from the above requirements. Review of the instrumentation at ARC showed that it was necessary to design a data acquisition system (DAS) that could support the program fully. LASL designed the system and gave ARC technical support in installing, calibrating, and operating it. All the instrumentation equipment was specified and furnished by LASL. The instrumentation is described in Table B-I, and its location in the furnace is shown in Fig. A-6.

1. Flow velocities. To get data on the injector characteristics and gas flow pattern in the furnace inlet tube, it was necessary to measure the gas velocity profile across the tube at different axial locations. To obtain the gas velocity profile, total and static pressure measurements were made using a Pitot tube. The expression that relates these pressures to velocity is

$$V = \left(2gRT \left(1 - P_s/P_t\right)\right)^{1/2} , \qquad (2)$$

where

V = gas velocity

g = gravitational constant

R = gas constant

T = gas temperature

P_s = absolute static pressure

P_t = absolute total pressure.

2. Temperatures. To support the data requirements of the AYER and VNAP codes, the inside wall temperatures of the furnace were measured. Figure A-6 shows that the furnace consisted of many different parts made of different materials. The thermal resistance across the interface of two parts could not be determined accurately; so the heat flow could not be calculated accurately. Hence, it was necessary to measure the wall temperature of each major part, as well as temperatures at several axial and radial positions within the parts. The number of measurements was limited by the available space (Fig. A-6), the

instruments obtainable, and the wish to minimize heat transport pertubations. Parameters T-1 through T-14 represent temperature measurements of the various furnace parts. All except T-4 and T-10 through T-12 were measured using optical pyrometers. The W/W-Re thermocouple that measured parameter T-4 was included to explore the feasibility of using thermocouples, instead of pyrometers, in a furnace controller. Parameters T-10 through T-12 were measured using Type T thermocouples. Other temperature parameters (T-15 through T-20) were measured by thermocouples as described below and in Table B-I.

3. Power. The power generated in the furnace susceptor is a necessary input to the AYER code. To provide this input, two cooling water flow measurements, seven temperature measurements, and measurements to calculate the power supplied by the 10-kHz motor-generator set were made. The furnace input power that the AYER code requires is power from the susceptor. The susceptor power is what remains of the motor-generator output after the losses have been subtracted.

The total furnace power parameter, W-1 (EI cos ϕ), was measured using signal conditioning equipment designed and built at LASL. The parameter W-2 (EI) was measured to verify the electrical power factor to which the furnace was tuned.

$$PF = EI \cos \phi \; / \; EI = \cos \phi \quad , \tag{3}$$

where

PF = power factor
E = RMS value of voltage
I = RMS value of current
ϕ = phase angle between voltage and current.

The furnace coil was paralleled with capacitance to present the motor-generator set with a power factor near unity. A power factor of unity occurs when the current and voltage are in phase. The motor-generator set can deliver its rated power at rated efficiency under these conditions.

Assuming an adiabatic process, the I^2R loss in the furnace coil was determined by measuring the water flow rate (F-5), and the temperature of the cooling water at the coil inlet (T-17) and discharge (T-20). Equation (4) is used to calculate I^2R loss from these measurements.

$$Q_1 - Q_2 = \int_{T_1}^{T_2} m \, C_p \, dt \tag{4}$$

Assuming that C_p is constant over the temperature range of interest, this expression becomes

$$Q = mC_p(T_2 - T_1), \tag{5}$$

where

Q = power (I^2R) picked up by the cooling water

m = mass flow of cooling water

C_p = specific heat constant

T_2 = temperature of discharge water

T_1 = temperature of inlet water.

The power removed by the furnace fixtures and instrumentation sight ports was similarly calculated from measurements of the water flow rate in these circuits and the inlet and exhaust temperatures (T-17 and T-19, respectively).

Only one parameter, F-5, is listed in the measurement list. The water flow rate in the coil was obtained by first measuring the total flow rate in all the water loops (F-5), then turning off the coil supply and measuring the remaining flow rates. Subtration gives the coil flow rates. If inconstant water supply pressure varied the flow rate, the flow rate of the two circuits would be calculated from the same ratio to main flow (F-5) determined in the above test.

The furnace radiation and conduction losses to the room's environment required measurement of the temperature parameters, furnace exterior temperature (T-10, T-11, T-12) and the room temperature (T-18). These measurements supplied the temperature data for the simplified equation $Q_T = h_r + h_c$, where Q_T = the total energy transferred and h_r and h_c are characteristic functions of the furnace and furnace room materials that interface with each other and of their temperature difference.

4. Flow rates. Accurate measurement of the reactant gas flow rates (along with some temperature data) was necessary to study the kinetics of the PG/SiC process. Measurement of MTS flow rate (F-4) and N_2 flow rate (F-1 and F-2) along with inlet pressure (P-3), substrate temperature (T-7), and the other inside wall temperatures, would help to determine and verify the MTS disassociation rate with respect to the temperature and the SiC deposition rate. Accurate determination of the mass flow rate of CH_4 (F-3), was required to help determine and, verify which parameters controlled (or were a function of) the total

deposition rate of PG/SiC and the ratio of PG to SiC. Accurate measurement of these flow rates(and wall temperatures) was necessary to establish a data base for furnace scaling as well as to determine, if possible, the reason for the previous nonreproduceability of the deposition process at ARC. Flow controllers were used to adjust and regulate the CH_4 and MTS reactant flow rates. The inherent properties of the deposition process dictated the need for accurate measurement and control of the mass flow rates of these gasses.

Small fluctuations in the nitrogen flow were not critical, but knowledge of the actual flow rate was necessary. Therefore, a flow controller was not used for this gas, but accurate flowmeters were installed (F-1 and F-2).

5. Pressure. The inlet pressure parameter, P-3, was measured to determine inlet pressure fluctuations. This parameter was also required as VNAP code input. The wall static pressure measurements P-1 and P-2 were specified to help determine the flow pattern in the furnace inlet tube. Originally, these wall pressure measurements were the only source of data for defining the velocity flow field in the recirculating jet. Wall pressure measurements ware most commonly used to obtain data for sudden expansion of gasses. However, development of the moveable Pitot tube provided a means of obtaining significantly more data.

6. Position. To relate the parameters P-4 and P-5 to position in the furnace, the Pitot tube location had to be known. The parameters D-1 and Ø-1 were the Pitot tube's linear distance from the injector face and its plus and minus angular position from the center line of the nozzle, respectively.

7. Data-sampling rate. The sampling rates were specified after estimating the transient response of the furnace and the PG/SiC deposition process. After reviewing the physical properties of the furnace, it was felt that the characteristic equation to express its temperature as a function of time would be a second-order (or higher) differential equation. The transient response to a step power input would be similar to that of an over-damped second-order electrical system. However, a "worst case" solution was obtained by the modeling the furnace as a first-order system (Eq. 6).

$$\frac{T_f - T_t}{T_f - T_i} = e^{-t/\tau}, \qquad (6)$$

where

T_f = final substrate temperature

T_t = temperatue of substrate at t

T_i = initial temperature of substrate

e = 2.71828

t = hours for substrate to reach temperature T_t

τ = furnace time constant in hours.

The time constant is defined as the time required for the output to reach 63.2% of its final steady state value after being subjected to a step input function. From experimental data (supplied by ARC) it was ascertained that the substrate would achieve steady state temperature in approximately four hours. Assuming the transient response of the furnace followed this simplified equation, Eq. 6, the furnace would reach 99.75% (or within 5° K) of its final temperature in six time constants (4 h).

The furnace time constant was calculated from Eq. (6).

$$\frac{2033 - 2028}{2033 - 294} = e^{-4/\tau}$$

τ = 0.684 h = 41 min.

The furnace time constant is analogous to that of an electrical system defined by a first-order differential equation. The frequency response of this type of system can be obtained from a Bode diagram.[22] On this diagram, the corner frequence is that at which the system output amplitude has decreased 3 db. The 3-db system frequency response is then bounded by zero and the corner frequence. The corner frequency is also identified as a function of the system time constant. Equation (7) depicts this correlation.

$$f_{cf} = 1/2\pi\tau \quad , \qquad (7)$$

where

f_{cf} = corner frequency

π = 3.14

τ = time constant of system.

Through the use of this equation and the furnace time constant, the highest frequency to which the furnace will respond (corner frequency) can be calculated.

$$f_{cf} = 0.0039 \text{ cycles/min}$$

or, one cycle per 257 min.

The sampling theorem stipulates that if the rms spectrum of a time function g(t) is identically zero at all frequencies above W Hz, then g(t) is uniquely determined by giving its ordinates at a series of points spaced 1/2 W apart, the series extending throughout the time domain. However, for this theorem to be valid, a perfect filter must be applied to the signal of interest with a cutoff at W Hz, or the signal spectrum being sampled must be perfect and have no energy above W Hz. Neither case is practical, so the sampling rate must be greater than 2W samples/s to prevent the aliasing* error, present in all sampling data systems, from being exceptionally large.

To reduce the aliasing error[23] to < 1% in a time division multiplexing (TDM) data system with two poles of filtering, the ratio of sampling frequency (f_s) to the signal 3-db frequency (f_{cf}) must be less than 30. Here the two poles of filtering are provided by the furnace since its transient response is defined by at least a second-order equation with a damping ratio greater than one. Substituting the 0.0039-cycle/min frequence into

$$30 = f_s / f_{cf} , \tag{8}$$

gives a sampling frequency of 0.117 per min, or one sample per 8.6 min.

The process variables (power, reactant flow rate, and cooling water flow rate) had much faster time constants ($\sim$ 20s). However, the CVD furnace temperatures could not respond to this 20-s time constant and the process resolution exceeded 20s. Experience showed that if one of the process variable changed drastically (MTS flow turned off), $\sim$ 15 min was required to obtain an obserable change in the process. If 15 min is two-thirds of a process time constant, the process time constant is then 22.5 min. From Eq. (7) the frequency response is one cycle per 141.3 min or a sample rate of 4.7 min per sample. The frequency of the room temperature fluctuation required a similar sampling rate.

Therefore, the sampling rate used during steady state operation was one sample per 5 min, which seemed adequate on the basis of the above calculations. The sample rate was increased to one sample per minute during transient heating

*The misrepresentation of the frequency and amplitude of the recorded signal when the data sampling rate is too much lower than the frequency of the signal being measured.

and cooling of the furnace to prevent loss of information during these periods because of unknown furnace characteristics.

We are not sure that the error from aliasing in TDM systems is germane to this particular application. However, ensuring that the data sampling rate meets these requirements lends that much more credibility to the recorded data.

8. Data accuracy and recording. The end-to-end inaccuracy requirements were specified as ± 2% maximum. This requirement was based on several factors, one of which was the accuracy of data required as inputs to the AYER and VNAP codes or for comparison with conditions predicted by these codes. The need to ascertain the process kinetics and reproduceability characteristics dictated an inaccuracy no greater than ± 2%. The parameters that control the process were not entirely known at the beginning of the program. Therefore, to relate the effect of one parameter upon another, an accurate signature of each parameter was necessary. The ± 2% requirement was also a prerequisite for an accurate data base on which a process control system was to be designed and specified.

The data were recorded on 1/2-in. magnetic tape in a seven-track IBM format. The data-recording medium and format were chosen to allow easy access to the computer facility at LASL and to reduce the cost of data reduction and data handling.

Table B-I outlines the complete measurement list and the range required for each parameter. All parameters except F-3, F-4, F-6, T-7, and W-2 were required for the nitrogen flow test. Those measurements not required by the deposition tests were P-1, P-2, P-4, P-5, D-1, Ø-1, T-4, and T-16.

III DATA OBTAINED

A. Cold Flow Tests.

Because the Pitot tube was moved during each set of measurements, a time history plot of the pressure data is not meaningful, so they are not included in App. D.

The instrument readings that were recorded on continuous DAS scans at each position on the Pitot tube's traverse were the static and total pressure at the Pitot tube (P-4 and P-5), the two static pressures in the coating camber wall (P-1 and P-2), the static pressure in the injector tube (P-3), and the nitrogen flow rate (F-5). At each Pitot tube location, the continuous scan lasted at least 45 s and the data were sampled at 3-s intervals. This gave a

total of about 15 data points that could be averaged for each instrument (a few points at the start and end of each scan were skipped).

1. Data reduction. After averaging the data points for each Pitot position, subtracting zero offsets for the initial instrument calibration, and converting from gauge to absolute pressure, we reduced the data as follows.

The fluid velocity as measured by a Pitot tube pressure difference is found from

$$V = C_p \{ 2 g (P_0 - P_1)/\rho \}^{1/2} , \tag{9}$$

where

C_p = Pitot tube coefficient, assumed equal to 1.0 (usually found by calibration to be between 0.98 and 1.02)

g = gravitational constant

ρ = fluid density

P_o = absolute total perssure

P_1 = absolute static pressure.

Use of the ideal gas law and the fact that velocities are low changes Eq. (9) to

$$V = C_p \{2gRT(P_o - P_1)/P_1\}^{1/2} , \tag{10}$$

where

R = gas constant

T = static temperature.

This equation was normalized to the maximum fluid velocity, at the centerline of the injector.

$$\frac{V}{V_{max}} = 0.83 \frac{A_1}{Q} \{2gRT(P_o - P_1)/P_1\}^{1/2} , \tag{11}$$

where

V_{max} = jet centerline velocity

Q = volumetric flow rate

A_1 = injector cross-sectional area.

2. Results. The relative velocity plotted in Figs. 2-6 is V/V_{max}, defined above. The figures show that the velocity profile is very symmetrical about the centerline, and that the three flow rates have the same profile.

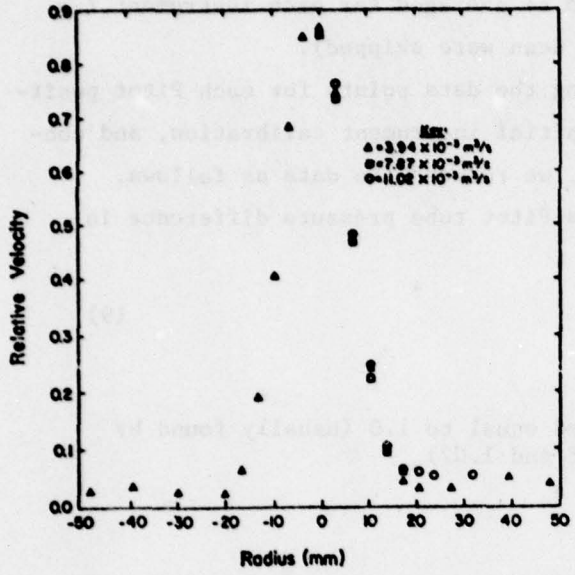

Fig. 2. Velocity profile at 51 mm.

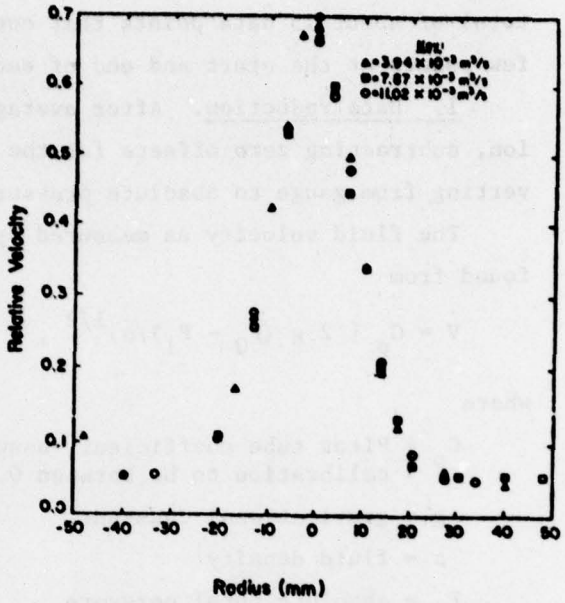

Fig. 3. Velocity profile at 102 mm.

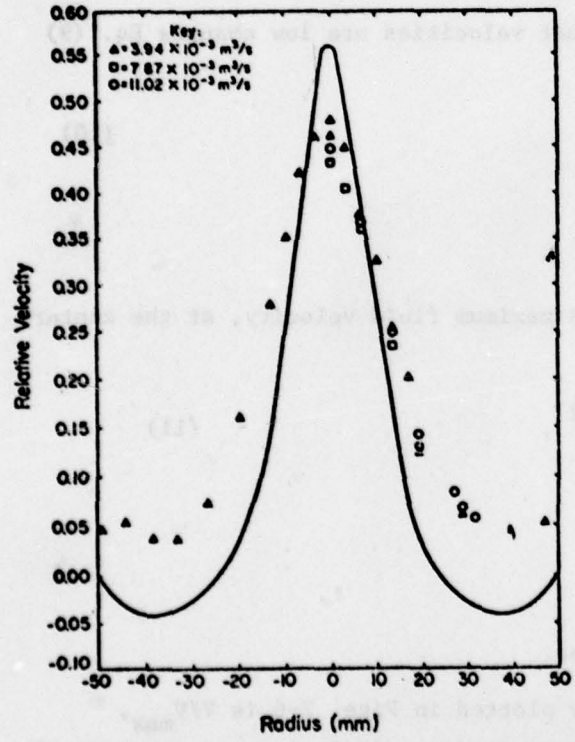

Fig. 4. Velocity profile at 152 mm.

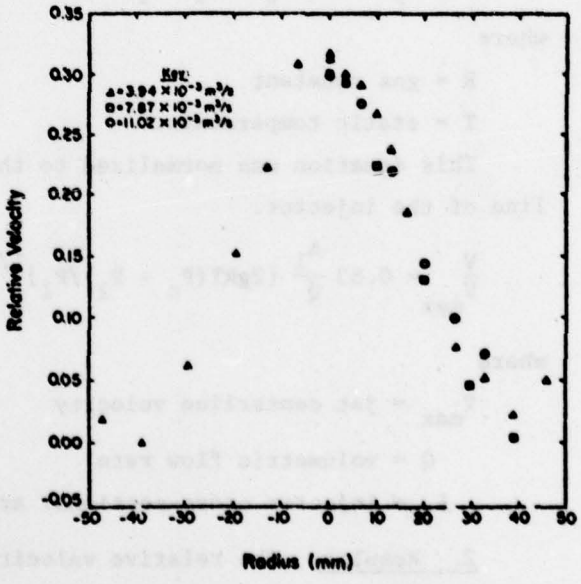

Fig. 5. Velocity profile at 203 mm.

TABLE I

EXIT GAS TEMPERATURE TRAVERSE

Distance from Wall (mm)	N_2 Flow Test[a] (T, K)	Coating Test[a] (T, K)
13	1315	1269
25	1326	1281
38	1322	1298
51	1326	1289
64	1312	1286
76	1308	1278
89	1305	1273
102	1311	1266
114	1304	1267
Average	1314	1279

[a] Average of 10 scans.

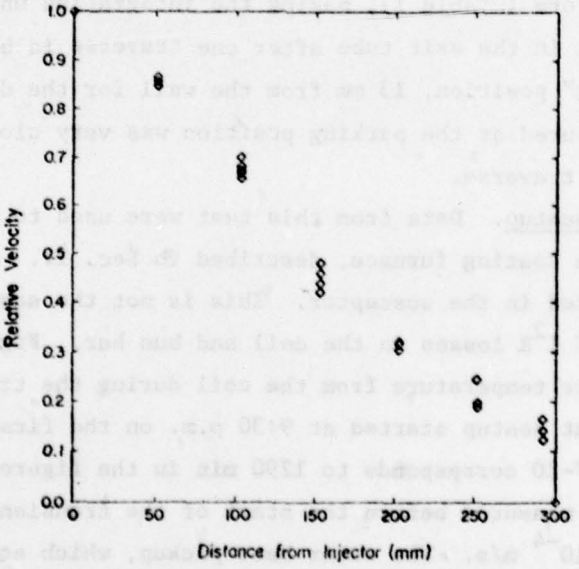

Fig. 6. Jet centerline velocity vs distance from injector.

Also, the velocity profiles agree reasonable well with those that Gortler[24] predicted for a circular, turbulent jet. This theory predicts that the jet spreads with a 12° half-angle, which would place the reattachment point 213 mm from the injector. The experimental profile 203 mm from the injector (Fig. 5) indicates this is true in the cold flow test.

In a symmetric plane expansion, the recirculating regions are often not symmetric,[25] although, for the axisymmetric geometry, Macagno and Hung[26] showed that symmetric flow is maintained regardless of Reynolds number. Nevertheless, there is some evidence[27] that asymmetries can occur at high Reynolds number and high diameter ratios. An asymmetric jet in the coating furnace could cause severe problems in data interpretation and modeling.

The velocities measured near the coating furnace wall are not accurate because the Pitot tube could not be oriented with the flow direction.

B. Transient Heat and N_2 Flow Tests.

1. Exit gas temperature profile.

Because flow velocity and temperature profiles are not fully developed at the furnace exit, it is not possible to measure a single temperature in the exit gas stream to get a true mixed-mean gas temperature. Instead, the W/W-Re thermocouple T-15 was able to traverse the exit tube diameter. With the flow velocity profile predicted by VNAP, this permits an integrated mixed-mean temperature to be calculated. The measured temperature profiles in both the N_2 flow tests and coating tests were very uniform (Table I), making the integration unnecessary.

The probe stuck in the exit tube after one traverse in both tests and was left in its "parking" position, 13 mm from the wall for the duration of the test. The temperature measured at the parking position was very close to the average measured during the traverse.

2. Transient heatup. Data from this test were used to calibrate the AYER thermal model of the coating furnace, described in Sec. IV. One important input is the power generated in the susceptor. This is not the same as the total furnace power because of I^2R losses in the coil and bus bar. Figure 7 shows the measured outlet water temperature from the coil during the transient heatup test. (The transient heatup started at 9:30 p.m. on the first day. Therefore, time zero in Figs. 7-20 corresponds to 1290 min in the figures in App. D.) The coil water flow was measured before the start of the transient heatup test and found to be 1.93×10^{-4} m/s. The water heat pickup, which equals the I^2R losses, was then subtracted from the total power input to the coil. (The small additional heat input to the coil cooling water caused by convection and radiation from the

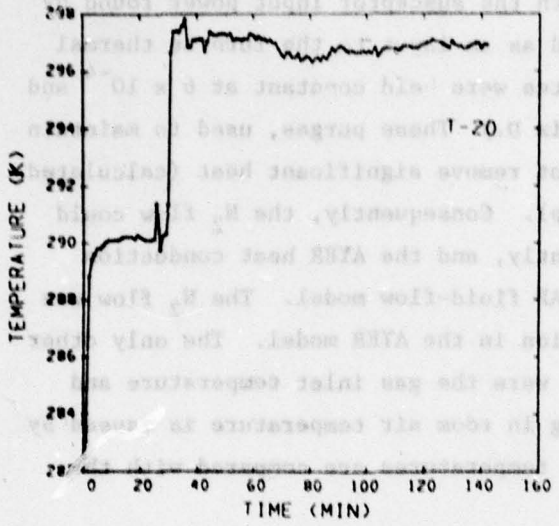

Fig. 7. Coil outlet water temperature.

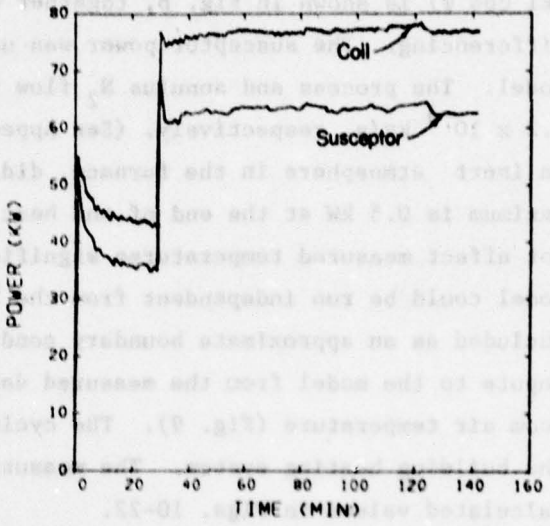

Fig. 8. Coil and susceptor input power.

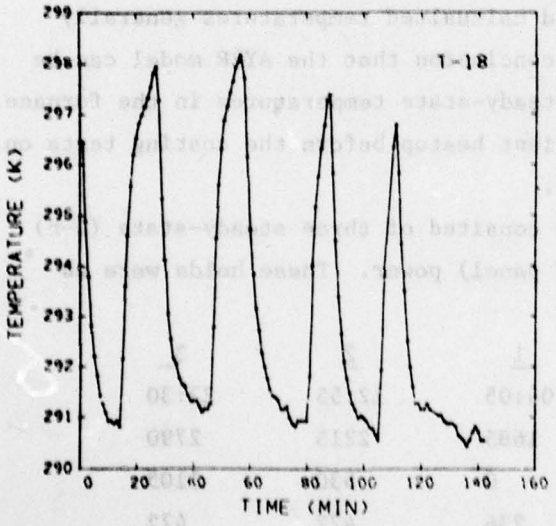

Fig. 9. Room air temperature.

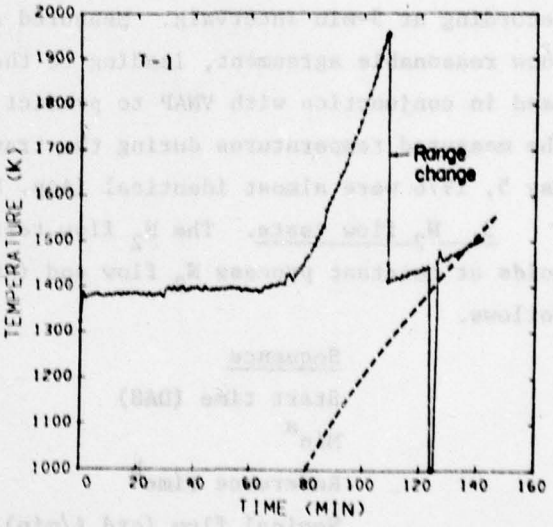

Fig. 10. Upper canister wall temperature. T-1 was not calibrated for interval before range change.

furnace o.d. was calculated and found to be negiligible). The coil input power (EI cos ∅) is shown in Fig. 8, together with the susceptor input power found by differencing. The susceptor power was used as an input to the furnace thermal model. The process and annulus N_2 flow rates were held constant at 6×10^{-4} and 1.2×10^{-4} kg/s, respectively. (See Appendix D.) These purges, used to maintain an inert atmosphere in the furnace, did not remove significant heat (calculated maximum is 0.5 kW at the end of the heat up). Consequently, the N_2 flow could not affect measured temperatures significantly, and the AYER heat conduction model could be run independent from the VNAP fluid-flow model. The N_2 flow was included as an approximate boundary condition in the AYER model. The only other inputs to the model from the measured data were the gas inlet temperature and room air temperature (Fig. 9). The cycling in room air temperature is caused by the building heating system. The measured temperatures are compared with the calculated values in Figs. 10-22.

The temperature slope discontinuity measured by Milletron instruments at T-5 and T-7 (Figs. 13 and 15) is an artifact of the instrument as it comes on range. The other two Milletron instruments at T-2 and T-9 were not connected to the DAS during these tests, but in the transient heatup at the start of the coating tests, T-2 showed the same behavior at T-5 and T-7. The instrument at T-9 did not come on range until after the N_2 flow was increased and the DAS was recording at 5-min intervals. Measured and calcualted temperatures generally show reasonable agreement, leading to the conclusion that the AYER model can be used in conjunction with VNAP to predict steady-state temperatures in the furnace. The measured temperatures during the transient heatup before the coating tests on May 5, 1976 were almost identical (App. D).

3. N_2 flow tests. The N_2 flow tests consited of three steady-state (1-h) holds at constant process N_2 flow and (ARC panel) power. These holds were as follows.

Sequence	1	2	3
Start time (DAS)	04:05	12:55	22:30
Min[a]	1685	2215	2790
Reference time[b]	0	530	1105
Nominal flow (std ℓ/min)	236	472	472
Nominal power (kW)	45	45	60

[a] Used in figures in App. D.

[b] Used for figures in this section.

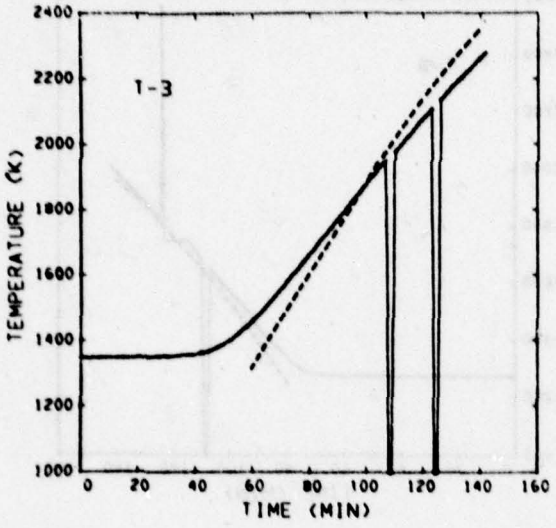

Fig. 11. Canister surface temperature (upper).

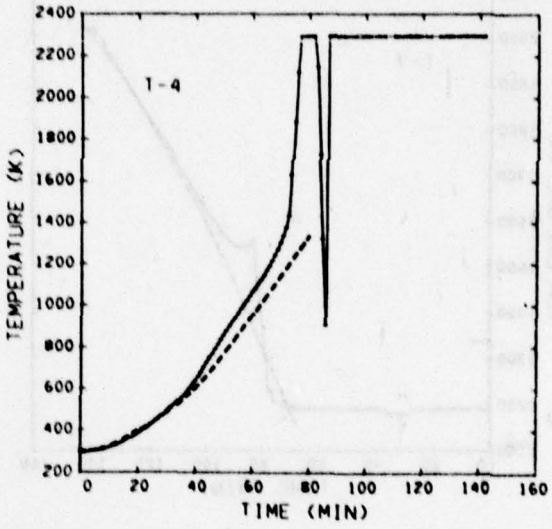

Fig. 12. Substrate backside temperature (thermocouple).

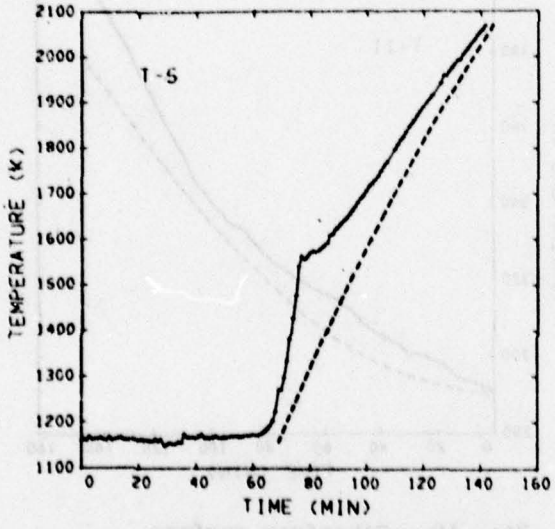

Fig. 13. Substrate backside temperature (pyrometer).

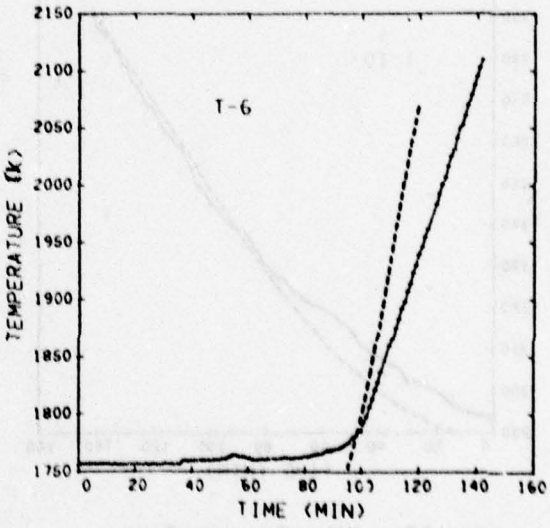

Fig. 14. Canister surface temperature (mid-height).

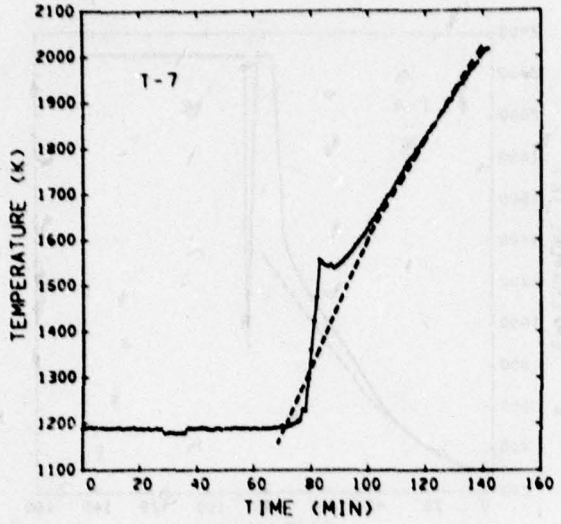

Fig. 15. Substrate surface temperature.

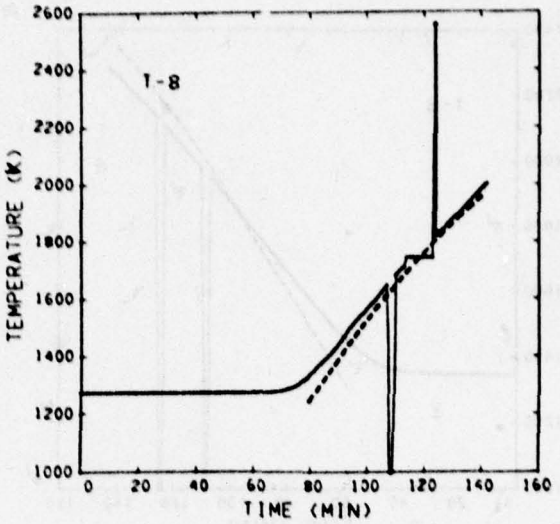

Fig. 16. Canister surface temperature (lower).

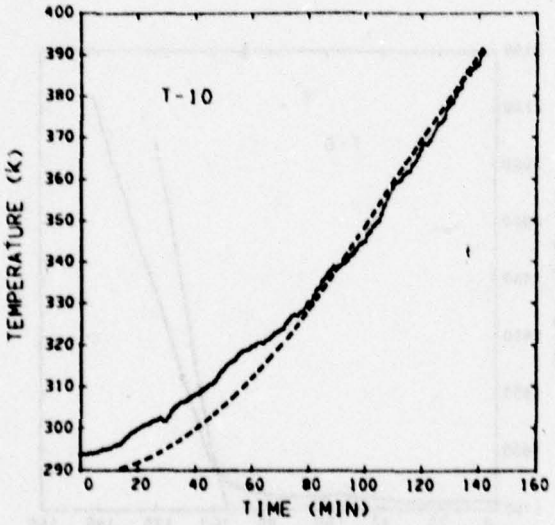

Fig. 17. Fiberfrax surface temperature (upper).

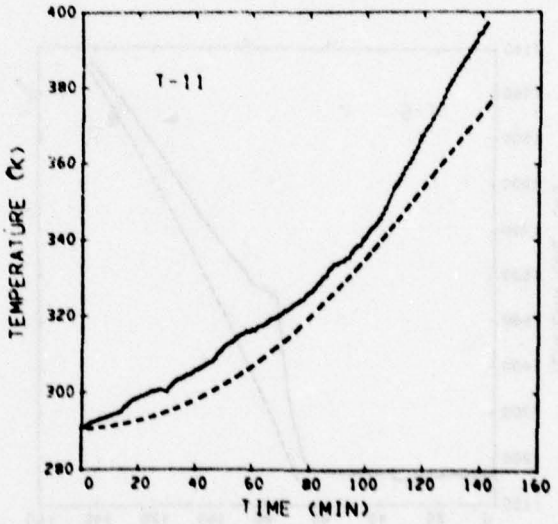

Fig. 18. Fiberfrax surface temperature (mid-height).

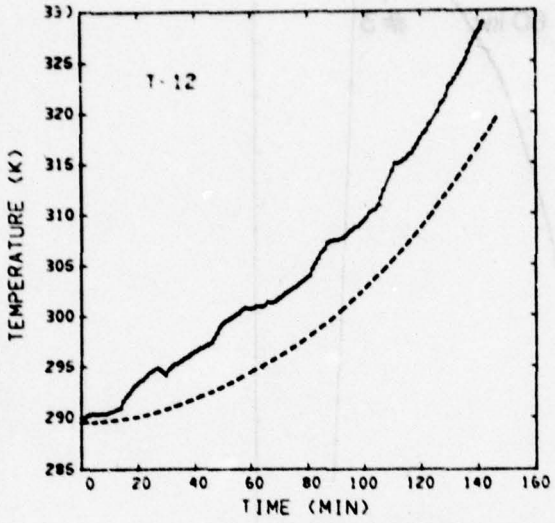

Fig. 19. Fiberfrax surface temperature (lower).

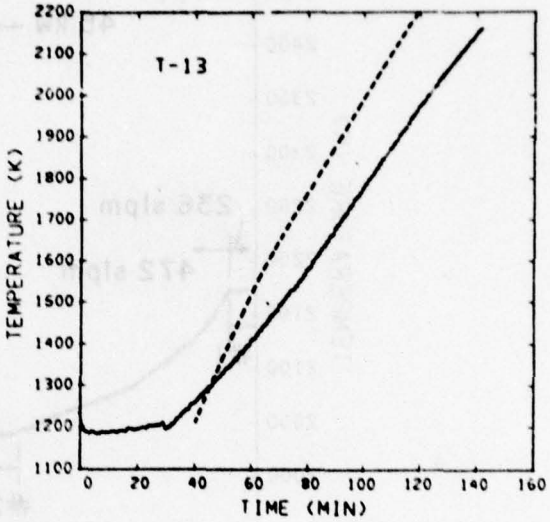

Fig. 20. Susceptor surface temperature (upper).

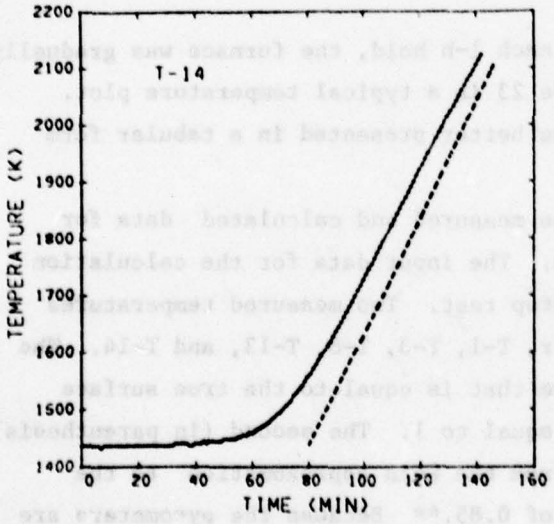

Fig. 21. Susceptor surface temperature (lower).

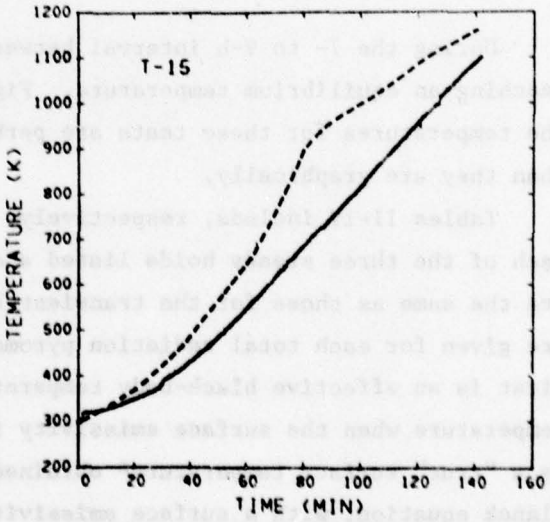

Fig. 22. Exhaust gas temperature.

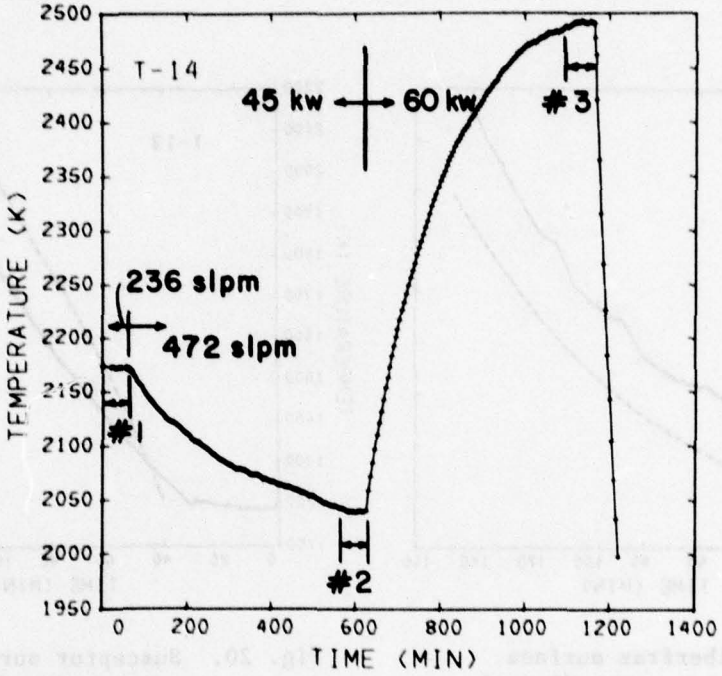

Fig. 23. Typical temperature plot during N_2 flow test.

During the 7- to 9-h interval between each 1-h hold, the furnace was gradually reaching an equilibrium temperature. Figure 23 is a typical temperature plot. The temperatures for these tests are perhaps better presented in a tabular form than they are graphically.

Tables II-IV include, respectively, the measured and calculated data for each of the three steady holds listed above. The input data for the calculation are the same as those for the transient heatup test. Two measured temperatures are given for each total radiation pyrometer, T-1, T-3, T-8, T-13, and T-14. The first is an effective black-body temperature that is equal to the true surface temperature when the surface emissivity is equal to 1. The second (in parenthesis) is a "true" surface temperature* obtained from the Wein approxomation to the Planck equation, with a surface emissivity of 0.85.** Because the pyrometers are

*In this report, all plots for these instruments are the corrected "true" surface temperature.

**The "true surface temperature is $T = 1/(4.5 \times 10^{-5} \ln 0.85 + 1/T_b)$, where T_b is the observed effective black-body temperature (K).

TABLE II

MEASURED AND CALCUALATED PARAMETERS AT STEADY HOLD NUMBER 1

Parameter	Measured	
F-1, Process N_2 (std ℓ/min)	218	Input to calculation
F-2, Annulus N_2 (std ℓ/min)	6.0	Input to calculation
W-1, EI cos Θ (kW)	35.8	--------
Water heat pickup (kW)	7.8	--------
Net susceptor power, (kW)	28.0	Input to calculation
		Calculated
T-1 (K)	1590. ± 6.8 (1609.)	1690
T-2[a] (K)	2162	2465
T-3 (K)	2255 (2293)	2659
T-5[b] (K)	2095	2444
T-6 (K)	2066	2722
T-7 (K)	2058	2418
T-8 (K)	2054. ± 5.1 (2085)	2659
T-9[a] (K)	1163	1566
T-10 (K)	431	474
T-11 (K)	429	429
T-12 (K)	401	401
T-13 (K)	2066 (2098)	2669
T-14 (K)	2139 (2173)	2669
T-15 (K)	1314	1821

[a] From hand-recorded data.

[b] T-4 and T-16 omitted because of over range.

TABLE III

MEASURED AND CALCULATED PARAMETERS AT STEADY HOLD NUMBER 2

Parameter	Measured	
F-1, Process N_2 (std ℓ/min)	430	Input to calculation
F-2, Annulus N_2 (std ℓ/min)	6.0	Input to calculation
W-1, EI cos θ (kW)	36.5	--------
Water heat pickup (kW)	8.4	--------
Net susceptor power (kW)	28.1	Input to calculation
		Calculated
T-1 (K)	1513 ± 8.35 (1530)	1493
T-2[a] (K)	1922	1888
T-3 (K)	2115 ± 2.93 (2148)	2223
T-5 (K)	1947 ± 5.6	1886
T-6 (K)	1924 ± 3.37	2256
T-7 (K)	1925 ± 5.1	1850
T-8 (K)	1909 ± 2.1 (1936)	2191
T-9 (K)	1314 ± 39.2	1339
T-10 (K)	430 ± 5.5	442
T-11 (K)	430 ± 1.5	444
T-12 (K)	405 ± 0.97	412
T-13 (K)	1958 ± 2 (1986)	2247
T-14 (K)	2013 ± 2 (2043)	2211
T-15 (K)	1218 ± 1.57	1511

[a]From hand-recorded data.

TABLE IV

MEASURED AND CALCULATED PARAMETERS AT STEADY HOLD NUMBER 3

Parameter	Measured	
F-1, Process N_2 (std ℓ/min)	420	Input to calculation
F-2, Annulus N_2 (std ℓ/min)	6.1	Input to calculation
W-1, EI cos θ (kW)	48.7	---------
Water Heat Pickup (kW)	11.7	---------
Net susceptor power (kW)	37.0	Input to calculation
		Calculated
T-1 (K)	≈ 1820 (1845) (off-scale)	1810
T-2[a](K)	2279	2576
T-3 (K)	≈ 2604 (≈ 2654)	2896
T-5 (K)	2304 ± 1.8	2507
T-6 (K)	2363 ± 6.1	2970
T-7 (K)	2271 ± 2.1	2454
T-8 (K)	2331 ± 6.3 (2371)	2897
T-9[a](K)	1443	1706
T-10 (K)	448	495
T-11 (K)	467	504
T-12 (K)	434	465
T-13 (K)	≈ 2325 (2365) (off-scale)	2916
T-14 (K)	2447 ± 1.4	2909
T-15 (K)	≈ 1485	1945

[a] From hand-recorded data.

looking through a long graphite tube, with the end of the tube at nearly the same temperature as the surface, the effective emissivity of the tube/surface approaches 1.0, and the correction may not be necessary. This will depend on the relative diameter of the "spot" focused on by the pyrometer to the diameter of the tube and the temperature gradient along the tube. Because the T-3 and T-8 pyrometers look across the annular gap between the susceptor and cansiter, the correction is probably needed for them. It is debatable whether it is needed for the others, but in any case the two values given place limits on the correct temperature.

C. Coating Tests.

1. Characterization of pyrolytic graphite/silicon carbide deposits.

a. General comments. The process conditions were chosen to lie within the range that ARC used for recent PG/SiC work to have a direct comparison with work done before the instrumented runs. Table V summarizes the process conditions used. These conditions correspond to 1.2 vol % of CH_4 for all three layers, and 0.235, 0.155, and 0.125 vol % of MTS for layers 1, 2, and 3, respectively.

Near the start of the third deposition layer, a hole, caused by oxidation, broke into the deposition canister at the joint between the upper spacer and the cansiter extension. The hole was at 50° from the angular reference line. Figure 24 shows the extent of oxidation. Subsequent examination of the coat from that layer indicated that the deposition chemistry was radically different, so it was not used in the analysis. To minimize possible effects of the breech on layers 1 and 2, samples were cut from the upper spacer, substrate, and exit spacer at 230° from the angular reference line, 180° from the breech. Figure 25 shows the sooty, nonadherent type of deposit that typically occurs at the upper end of the deposition cansiter near the coating gas inlet orifice. To a degree, the sooty deposit was enhanced by the air leak. Figures 26-28 show the surface texture of the coat in the upper spacer, substrate, and exit spacer regions. The third layer cracked and separated from the underlying coat near the bottom of the exit spacer.

b. Microstructure. Figures 29 and 30 show the microstructures of the three layers at 248 mm from the orifice. The microstrucutral code type appears to be Group 21 for both layers:[9] "SiC phase medium sized with a tendency to cluster in the PG cone boundaries, acicular needles 0.9-5.2 μm dia with a L/D ratio greater than 3/1." Figure 33 is a photomicrograph of layer 1 at 306 mm

TABLE V

SUMMARY OF PROCESS CONDITIONS

Layer	N_2(std ℓ/min)	CH_4(std ℓ/min)	MTS(gpm)	Surface Temperature Midpoint Subs., (K)	Time (h)
1	405.0 ± 0.7	4.90 ± 0.05	6.44±0.04	2020 ± 4	4
2	405.1 ± 0.7	4.90 ± 0.05	4.26±0.01	2020 ± 7	4
3	545.1 ± 3.8	7.72 ± 0.08	5.37±0.15	2020 ± 15	4

TABLE VI

COAT CHARACTERIZATION DATA

Canister Part	Distance from Orifice (cm)	Coat Thickness (mils) LASL Layer 1	LASL Layer 2	ANC Layer 1	ANC Layer 2	Coat Density (g/cm³) LASL(a) Layer 1	LASL(a) Layer 2	ANC(b) Layer 1	ANC(b) Layer 2	SiC Content of Coat (w/o) LASL(c) Layer 1	LASL(c) Layer 2	ANC(d) Layer 1	ANC(d) Layer 2
Entrance Spacer	193	16.5	15.7	-	-	2.28	2.22	2.21	2.185	6.7±0.2	2.6±0.1	-	-
"	224	20.2	19.0	-	-	2.20	2.28	2.215	2.190	6.3±0.1	2.9±0.1	-	-
"	268	27.3	25.8	22-32	25-35	2.23	2.22	2.25	2.24	9.3±0.1	5.5±0.9	12±1	8±1
Substrate	290	32.3	31.1	-	-	2.30	2.24	2.25	2.25	16.9±0.2	10.7±0.2	-	-
"	306	34.2	34.4	35-38	35	2.28	2.25	2.29	2.25	18.7±0.1	11.9±0.1	17±1	12±1
"	331	35.0	34.3	-	-	2.43	2.23	2.29	2.25	21.2±0.2	12.9±0.1	-	-
Exit Spacer	361	37.1	34.2	-	-	2.29	2.20	2.265	2.25	18.9±0.4	12.6±0.1	-	-
"	357	35.1	33.7	-	-	2.30	2.15	-	-	19.7±0.1	12.4±0.1	-	-
"	436	32.7	31.6	-	-	2.28	2.23	2.275	2.25	20.9±0.1	13.5±0.1	-	-
"	447	30.6	28.1	-	-	2.34	2.22	-	-	21.5±0.1	13.6±0.1	-	-
"	472	27.0	26.0	-	-	2.33	2.23	2.275	2.25	22.8±0.1	14.4±0.1	-	-

[a] Density determination by mercury porosimetry.
[b] Density determination by sink or float technique.
[c] SiC content by ashing technique.
[d] SiC content by microprobe analysis.

TABLE VII

ANALYSIS OF VARIANCE RESULTS

CH_4 switched from 3.29 ℓ/min to zero at 02.37.24 (1597.4) N_2 = 940 SCFH
Time of switch = 1597.40000 Number of Data Points = 30

T-15 Gas Average Before = 1364.020 K, Average After = 1364.193 K

Source of Variation	Degrees of Freedom	Sums of Squares	Mean Squares	F-Ratio
Between Flows	1	0.2253	0.2253	4.73
Within Data	28	1.3333	0.0476	
Total	29	1.559		

T-7 Substrate Average Before = 2016.473 K, Average After = 2021.433 K

Source of Variation	Degrees of Freedom	Sums of Squares	Mean Squares	F-Ratio
Between Flows	1	184.5120	184.5120	99.00
Within Data	28	52.1827	1.8637	
Total	29	236.69		

T-5 Backside Average Before = 2147.260 K, Average After = 2147.460 K

Source of Variation	Degrees of Freedom	Sums of Squares	Mean Squares	F-Ratio
Between Flows	1	0.3000	0.3000	0.54
Within Data	28	15.6120	0.5576	
Total	29	15.912		

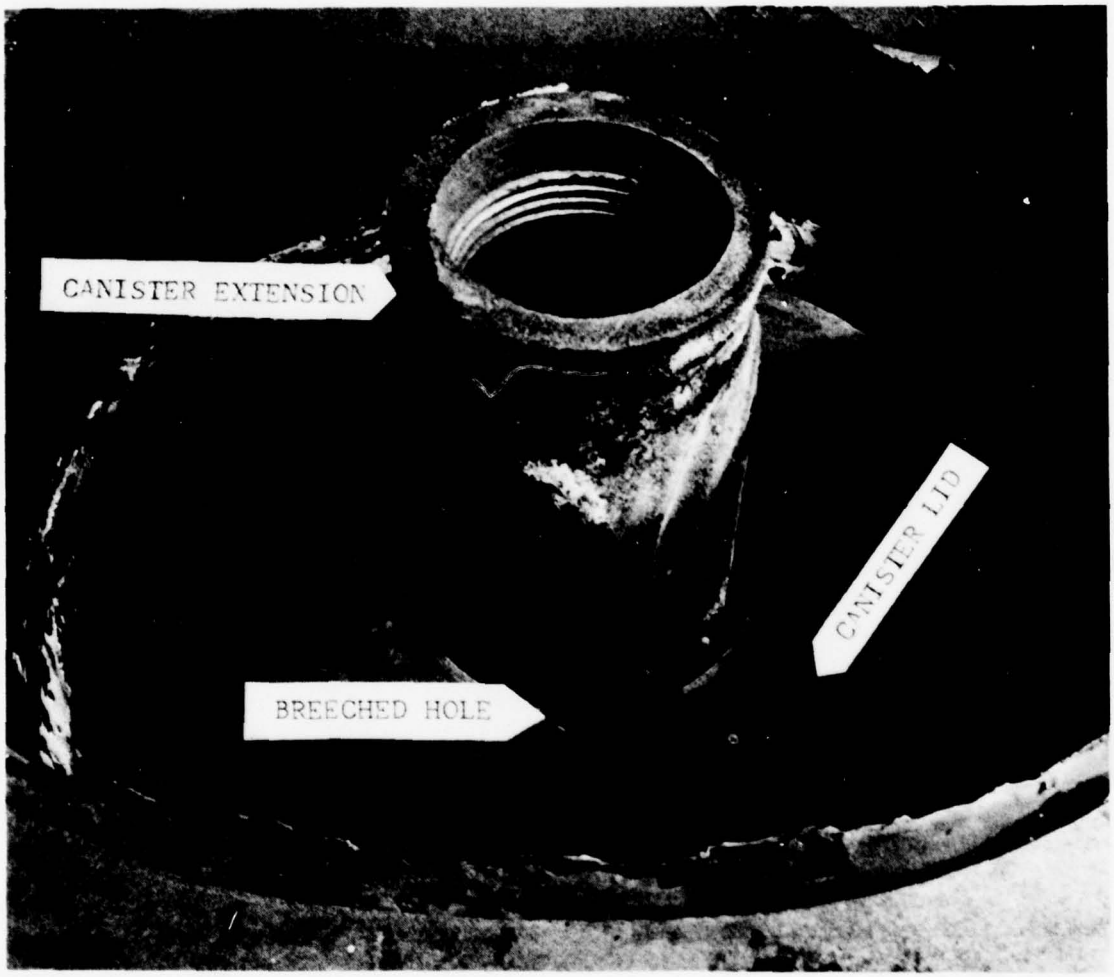

Fig. 24. Area where a hole was formed by oxidation which allowed gases in the furnace body to enter the deposition canister.

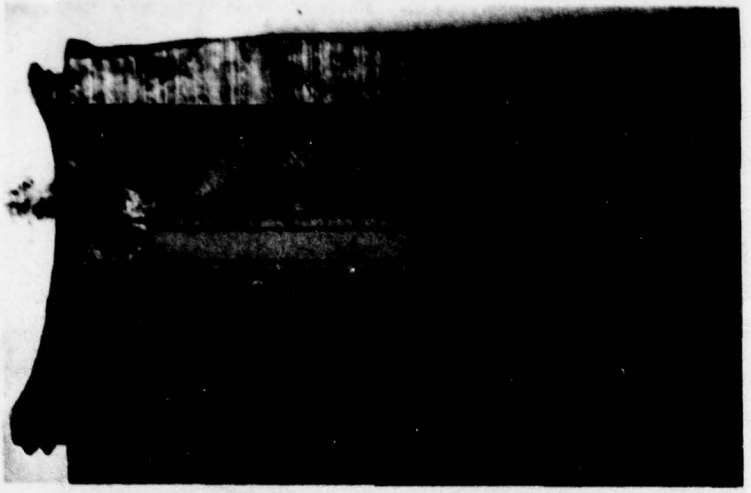

Fig. 25. Interior of the canister extension showing the characteristic sooty, deposit that forms near the orifice.

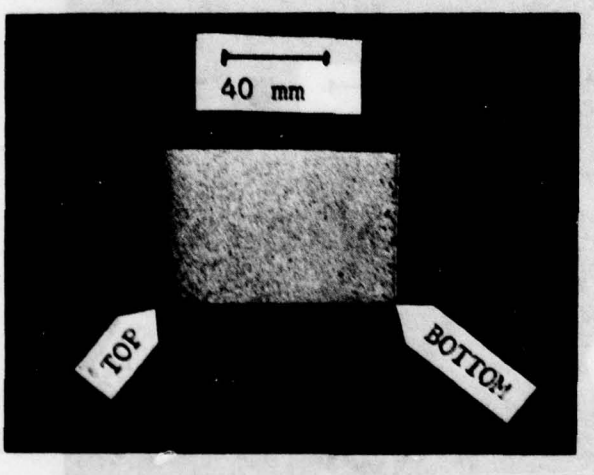

Fig. 26. Surface of the deposited coat on the entrance spacer.

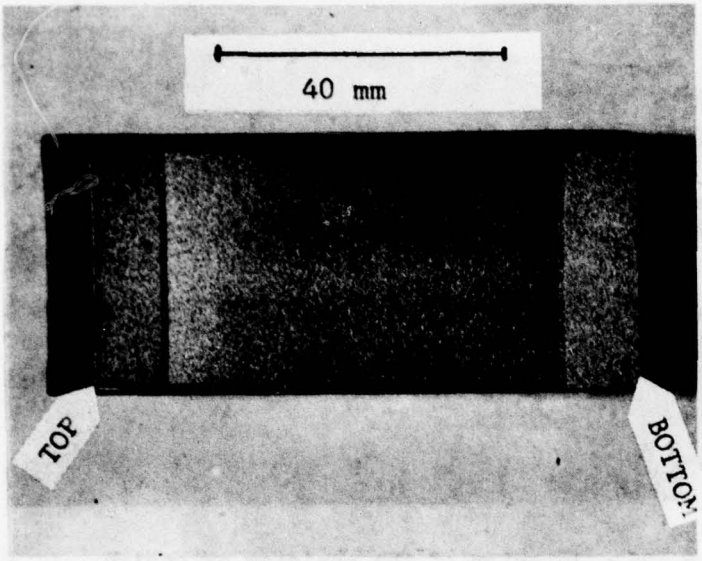

Fig. 27. A section of the substrate showing the surface of the deposited coat.

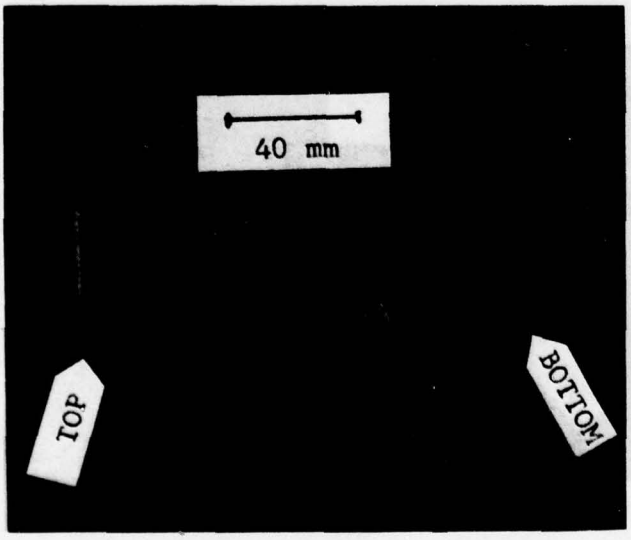

Fig. 28. A section of the exit spacer showing the surface of the deposited coat.

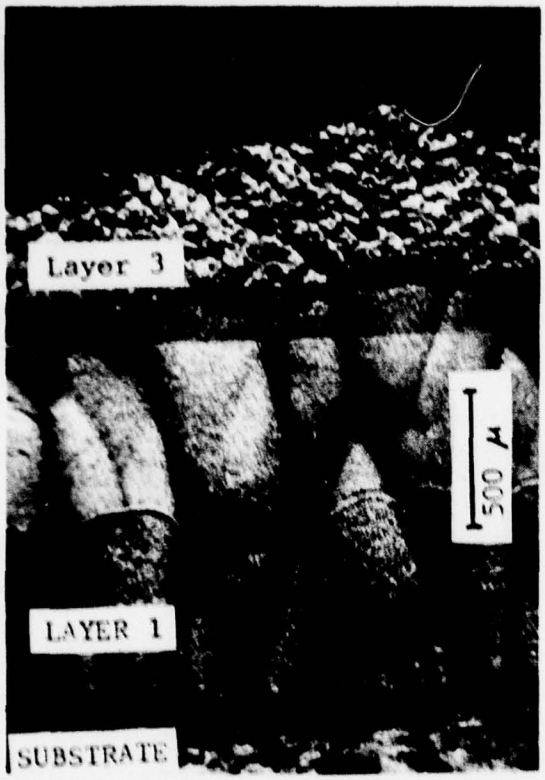

Fig. 29. Photomicrograph (40X) of the microstructure of the deposited layers 248 mm from the orifice and 25 mm above the bottom of the entrance spacer.

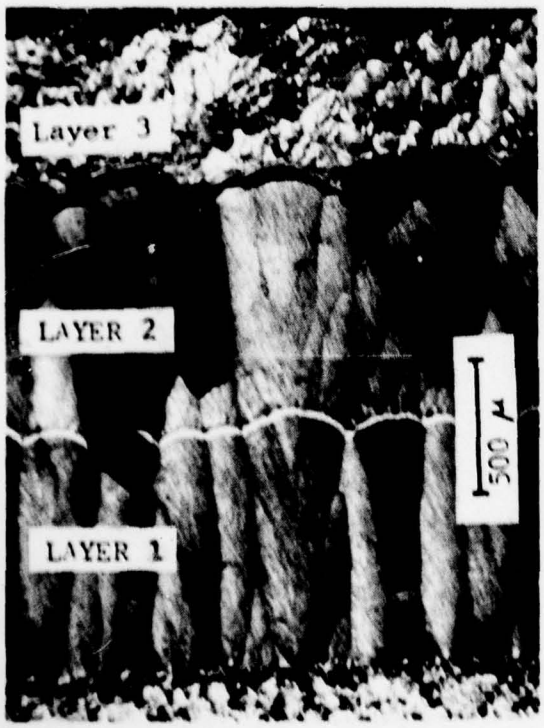

Fig. 30. Photomicrograph (40X) of the microstructure of the deposited layers 306 mm from the orifice at the midpoint of the substrate.

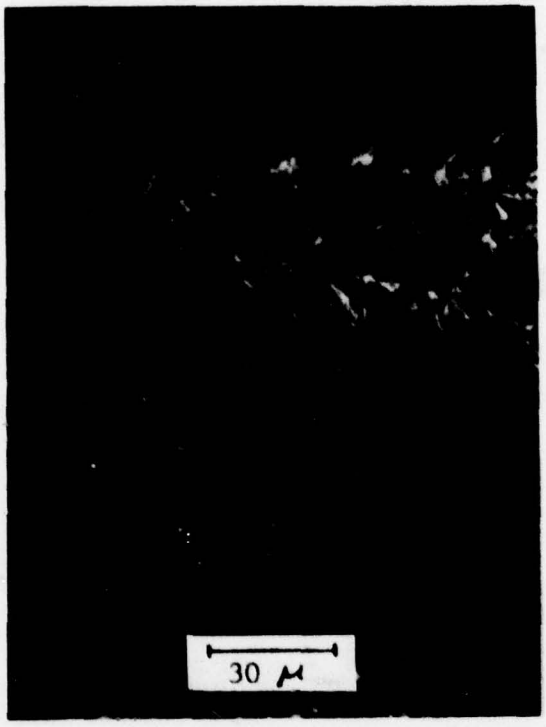

Fig. 31. Photomicrograph (630X) of the microstructure of layer 1 248 mm from the orifice.

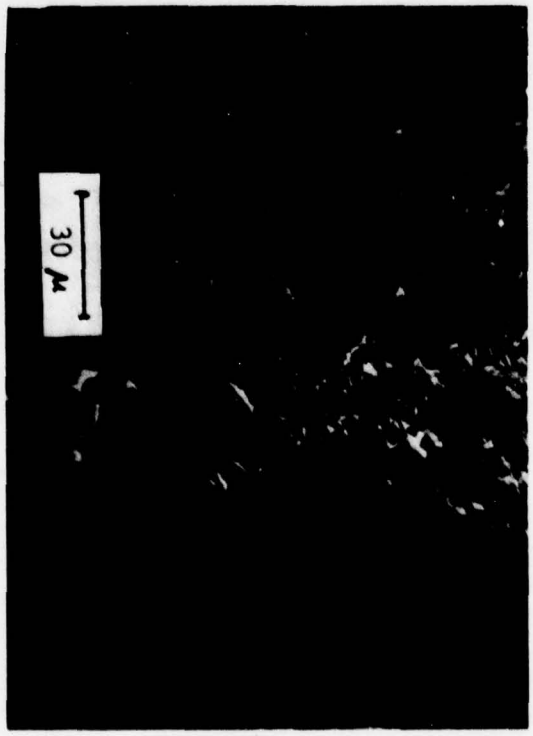

Fig. 32. Photomicrograph (630X) of the microstructure of layer 2 248 mm from the orifice.

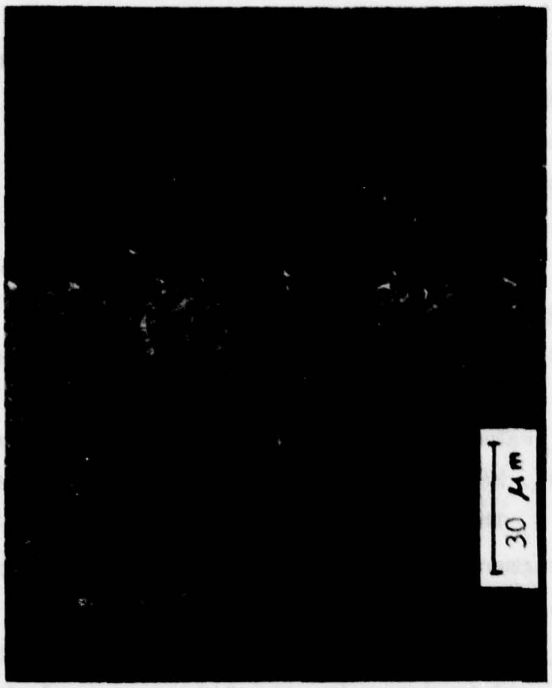

Fig. 33. Photomicrograph (630X) of the microstructure of layer 1 306 mm from the orifice.

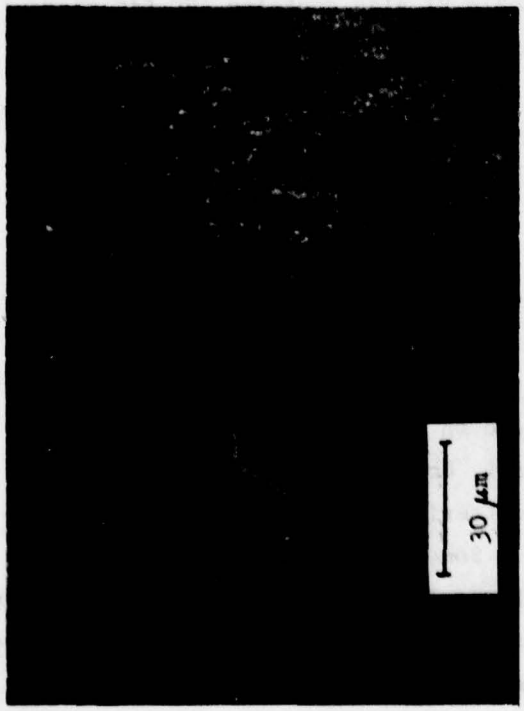

Fig. 34. Photomicrograph (630X) of the microstructure of layer 2 306 mm from the orifice.

from the orifice. The microstructural code type appears to be Group 5: "SiC phase very fine, evenly dispersed, acicular needles less than 0.25 μm dia with a L/D ratio greater than 3/1." There is a tendency for clustering at the PG cone boundaries where the structure approaches Group 21.

c. Coat thickness measurements. The thicknesses of layers 1 and 2 were measured in 25-mm steps from 193 to 472 mm from the inlet. The results are given in Table VI.

d. Coat density measurements. A 25-mm-wide strip was cut from the upper spacer, substrate, and exit spacer; separated into the individual layers; cut into segments 25 mm long; and then crushed to < 1.5-mm diam particle size. The density of the material from each segment was determined by mercury porosimetry at pressures of 0.5, 21., and 103. MPa. The values determined at 103 MPa are tabulated in Table VI. The distances from the inlet correspond to the mid point of the analyzed segment. The table also contains densities determined at ARC by a sink-or-float technique.

e. Determination of the SiC content. The rest of the crushed material from the coat density measurements was used to determine the SiC content of the individual layers. Duplicate 0.2-g samples were fired in a muffle furnace at 1373 K for 24 h. The weight percent of SiC was calculated gravimetrically and the results are presented in Table VI. Table VI also contains ARC SiC microprobe analyses. The SiC content of the 3rd layer on the upper spacer and substrate was 1 wt %.

f. Correlation between sample density and wt % of contained SiC. A least-squares fit to the data in Table VI gave the following relationship.

$$\frac{1}{\rho} = \frac{1 - W}{2.195} + \frac{W}{2.689} \quad ,$$

where W is the SiC weight fraction in the coat, and ρ is the density. Figure 35 shows the calculated and observed results.

2. Coating gas effect on substrate temperature measurement. Control of the coating process has generally been based on the optically measured temperature on the substrate (T-7 in these tests). Concern had arisen because the readings might be affected by radiation scattering and absorption in the coating gases and/or their pyrolysis products. Some preliminary calculations had indicated that the effect, if any, would be small, but these were not conclusive because of a lack of property data and information about elemental (solid) carbon particle size, shape, and distribution.

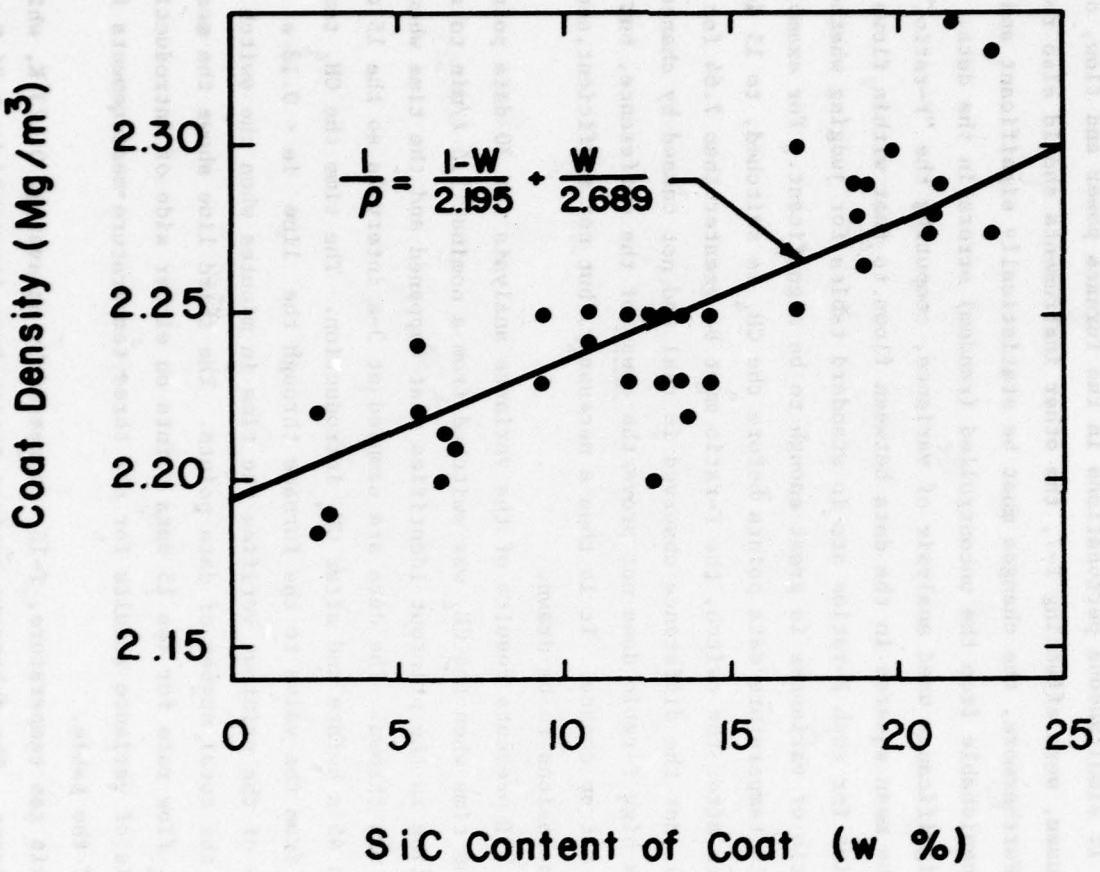

Fig. 35. Coat density vs weight percent of contained SiC.

The tests involved measuring the temperatures at the coating surface (T-7) and behind the substrate (T-5), and that of the exit gas (T-15) with continuous scans of the DAS while the coating gases were switched on and off. If the opacity of the coating gases was affecting the pyrometer at T-7, it should record nearly instantaneous changes in temperature while the others were unaffected. If simultaneous pertubations in the furnace power and flow, or unknown causes, were affecting T-7, the other instruments should also record the changes. Furthermore, the changes must be statistically significant and therefore distinguishable from the uncontrolled (random) errors in the data. The test for significance used analysis of variance, computing the "F-ratio," or ratio of the mean squares in the data between flows to that within flows. Probabilities for such F-ratios are in standard tables for judging whether or not the ratio of variances is great enough to be significant. For example, comparing 15 temperature data points before the CH_4 is switched, to 15 data points taken after the switch, the F-ratio must be greater than 7.64 for 99% probability that the difference observed is real and not caused by chance alone. Note that a high F-ratio does not prove the cause of the difference, but only that it is not by chance. It is thus a necessary, but not sufficient, condition for the conclusions to be drawn.

Table VII presents results of the variance analysis for 30 data points spanning the time when the CH_4 was switched from a nominal 3.5 ℓ/min to zero. The first line in the printout identifies what happened and the time when the CH_4 switch was thrown. The data are sampled at 3-s intervals so the 15 data points span 45 s before and after CH_4 introduction. The time the CH_4 took to travel 8 m from the valve to the furnace through the line is < 0.13 s. The second line of the printout verifies the time in minutes when the switch was thrown and the total number of data points. The third line shows the measured average CH_4 flow rate for the 15 data points on either side of introduction. The analysis of variance results for the three temperature measurements fill the rest of the table.

The exit gas temperature, T-15, increased by an average 0.173 K, which is not significant. The substrate surface temperature increased by 4.96 K which is statistically significant. The backside temperature of the substrate, T-5, increased by 0.2 K, which is not significant. The increase in indicated temperature for T-7 is in the direction that would be expected from clearing the opaque gas from between the substrate and sight port when CH_4 is switched off.

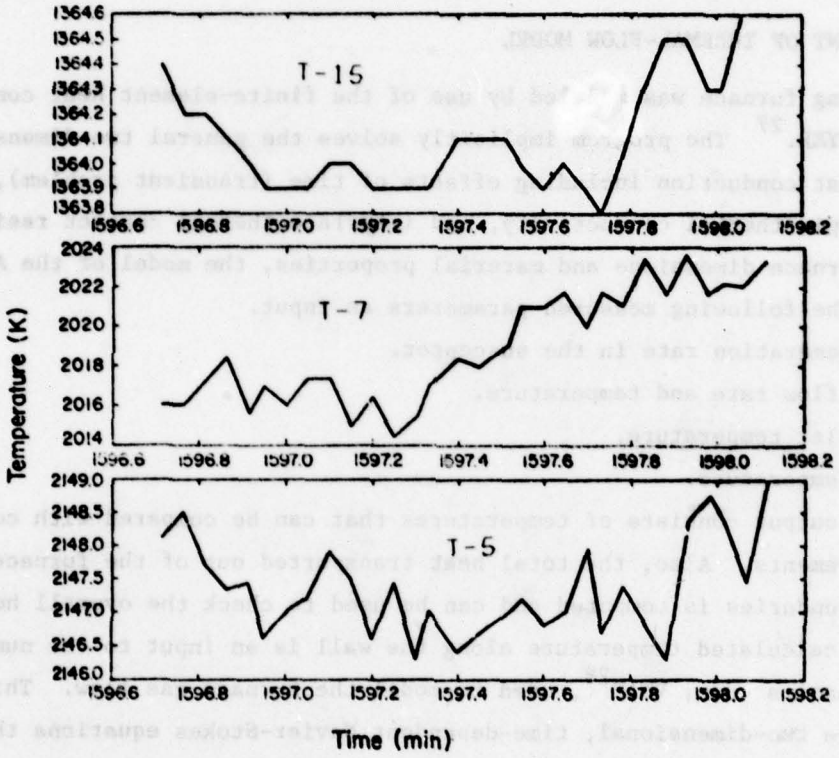

Fig. 36. Effect of coating gas on temperatures.

Figure 36 is a plot of the temperature data used in the analysis shown in Table VII. The temperature scales for T-15 and T-5 are greatly expanded over that used for T-7.

Similar analyses were carried out for each time during the coating runs when coating gases were switched on and off. The conclusions are that the apparent temperature measured by the Milletron two-color pyrometer at T-7 is affected by an average of 4.3 K by CH_4, but the MTS caused a statistically significant effect in only 3 out of 10 cases.

IV DEVELOPMENT OF THERMAL-FLOW MODEL

The coating furnace was modeled by use of the finite-element heat conduction program, AYER.[27] The program implicitly solves the general two-dimensional equation of heat conduction including effects of time (transient problem), in-plane anisotropic thermal conductivity, and interface thermal contact resistance. Besides the furnace dimensions and material properties, the model of the ARC furnace used the following measured parameters as input.

- Heat generation rate in the susceptor.
- Water flow rate and temperature.
- Gas inlet temperature.
- Room temperature.

The code output consists of temperatures that can be compared with corresponding measurements. Also, the total heat transported out of the furnace at the various boundaries is computed and can be used to check the overall heat balance. The calculated temperature along the wall is an input to the numerical fluid dynamics code, VNAP[28], used to model the furnace gas flow. This code solves the two-dimensional, time-dependent Navier-Stokes equations through use of an explicit finite-difference procedure. VNAP requires the measured gas-flow rate, pressure, and temperature as input data. The output includes fluid velocity components in the radial and axial directions, temperature, pressure, and density at each mesh point. The axial distribution of heat transferred from the wall is calculated and used as an input to AYER. The first part of this section discusses AYER; the second part discusses VNAP.

A. Heat Conduction Model.

The coating furnace shown in Fig. A-6 was idealized as a series of finite elements, shown in Fig. 37. The various materials used to assemble the furnace are identified by shading. At lateral interfaces between component parts, a

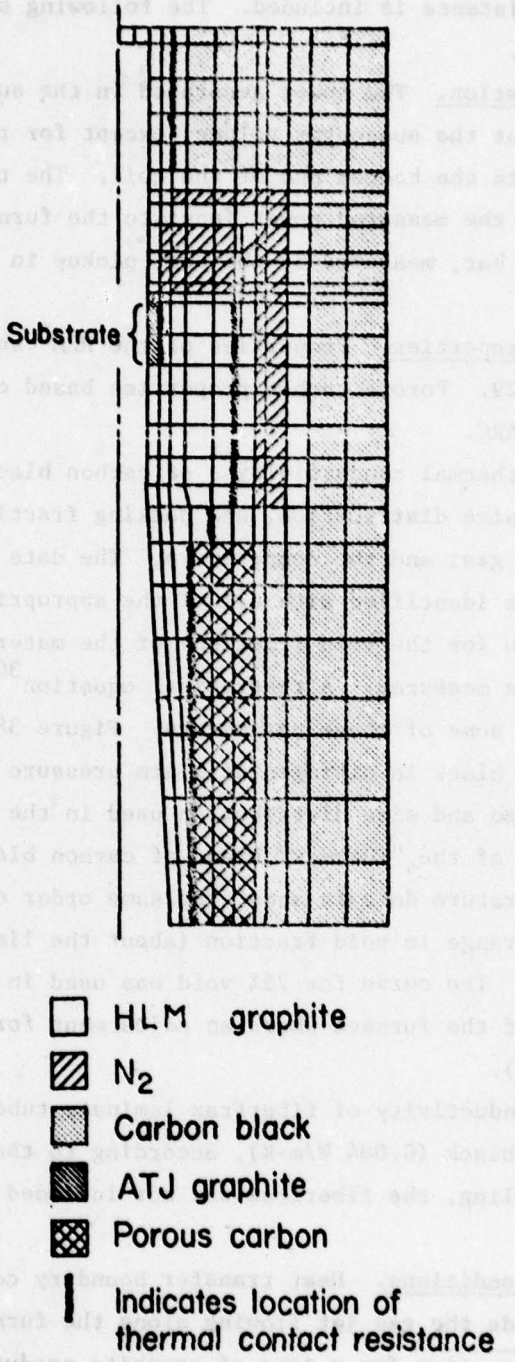

Fig. 37. AYER model of coating furnace.

thermal contact resistance is included. The following subsections describe the modeling parameters.

1. Heat generation. The power generated in the susceptor is distributed uniformily throughout the susceptor volume, except for reduced power in the finite element opposite the bottom end of the coil. The total power in the susceptor is obtained from the measured power input to the furnace, minus the I^2R loss in the coil and bus bar, measured by the heat pickup in the coil cooling water (see Tables II-IV).

2. Material properties. Properties of the HLM* and the ATJ graphite were obtained from Ref. 29. Porous carbon properties based on supplier's literature were obtained from ARC.

The effective thermal conductivity** of carbon black depends on the particle size, shape, size distriubtion, and packing fraction, the properties of the interstitial gas; and the temperature, The data available in the literature are not always identified with all of the appropriate parameters. Also the packing fraction (or the void fraction) of the material as-loaded in the ARC furnace could not be measured. A theoretical equation[30] was used to evaluate the significance of some of these parameters. Figure 38 shows the thermal conductivity of carbon black in nitrogen at 1-atm pressure vs temperature. The average particle size and size distribution used in the theoretical equation correspond to those of the "Thermax" brand of carbon black used at ARC. The scatter in the literature data is about the same order of magnitude as the effect of a 50-90% range in void fraction (about the limits of the range expected in the furnace). The curve for 75% void was used in the calculations, except in the upper part of the furnace where an adjustment for the sight ports was included (dotted line).

The thermal conductivity of fiberfrax laminate tubes is about the same as that of the carbon black (0.084 W/m·K), according to the supplier's literature. For economy in modeling, the fiberfrax was not included explicitly in the finite element mesh.

3. Boundary conditions. Heat transfer boundary conditions to the finite element model include the gas jet flowing along the furnace centerline, water

*Manufacture's designation for a type of graphite produced by Great Lakes Carbon Corp.

**Consisting of contributions from conduction through the solid and gaseous phases, plus radiation.

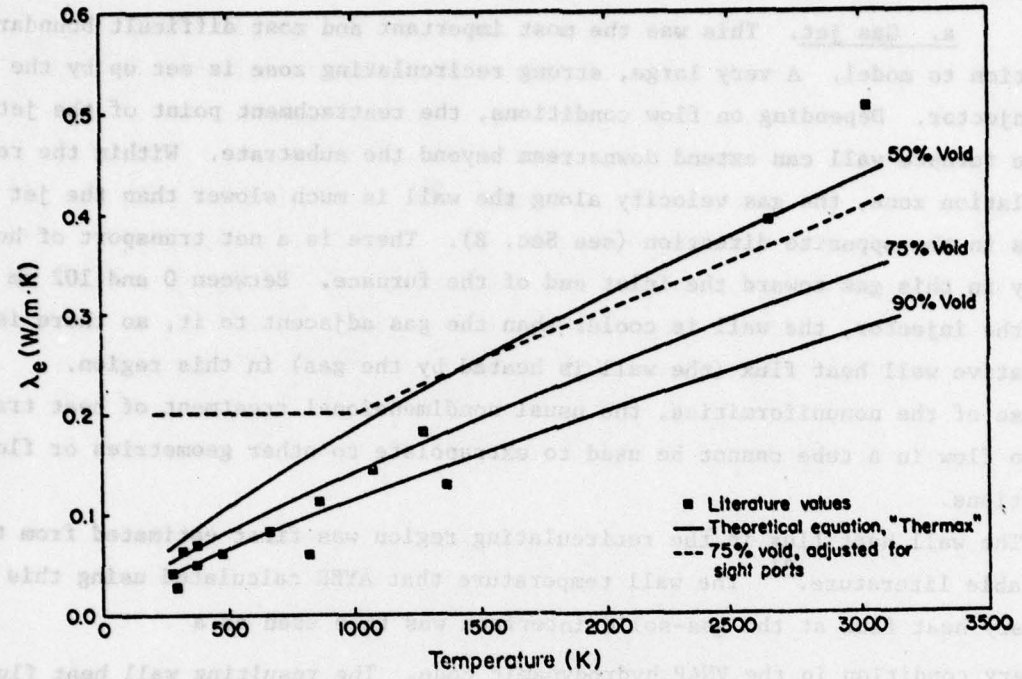

Fig. 38. Effective thermal conductivity of carbon black in nitrogen.

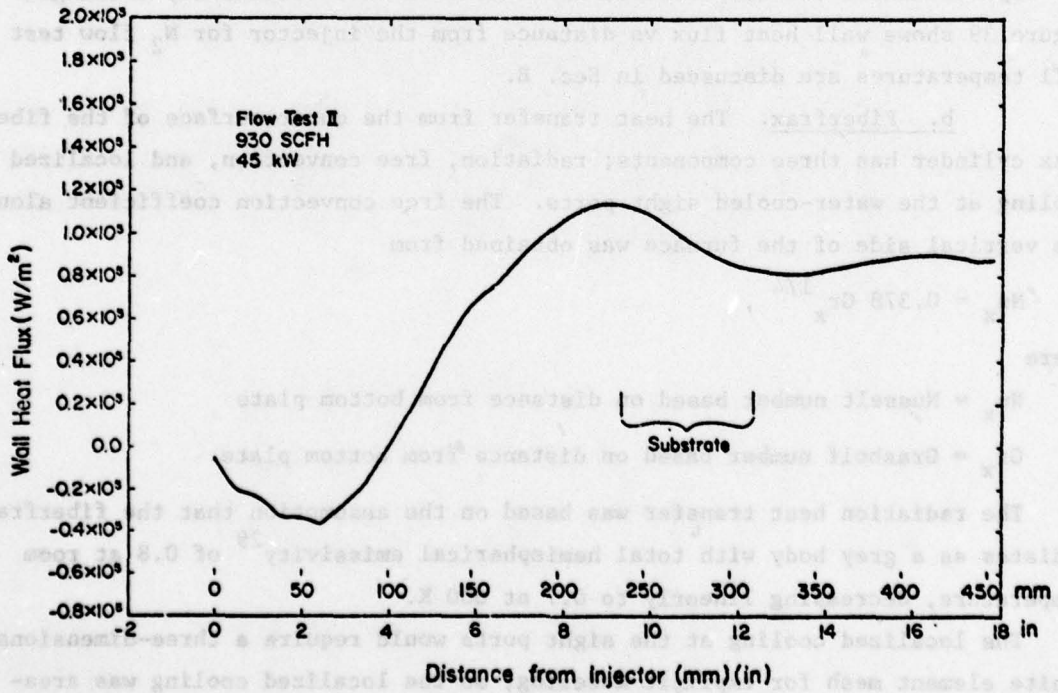

Fig. 39. Wall heat flux.

cooling of the top and bottom plates, and the combined radiation with natural convection to the room air and surroundings.

a. Gas jet. This was the most important and most difficult boundary condition to model. A very large, strong recirculating zone is set up by the jet injector. Depending on flow conditions, the reattachment point of the jet to the furnace wall can extend downstream beyond the substrate. Within the recirculation zone, the gas velocity along the wall is much slower than the jet and is in the opposite direction (see Sec. B). There is a net transport of heat energy in this gas toward the inlet end of the furnace. Between 0 and 102 mm from the injector, the wall is cooler than the gas adjacent to it, so there is a negative wall heat flux (the wall is heated by the gas) in this region. Because of the nonuniformities, the usual nondimensional treatment of heat transfer to flow in a tube cannot be used to extrapolate to other geometries or flow conditions.

The wall heat flux in the recirculating region was first estimated from the available literature.[31] The wall temperature that AYER calculated using this boundary heat flux at the gas-solid interface was then used as a boundary condition in the VNAP hydrodynamic code. The resulting wall heat flux calculated by VNAP was then substituted for the original estimate and the process was repeated until the temperatures and heat flux were essentially unchanged. Figure 39 shows wall heat flux vs distance from the injector for N_2 flow test II. Wall temperatures are discussed in Sec. B.

b. Fiberfrax. The heat transfer from the outer surface of the fiberfrax cylinder has three components; radiation, free convection, and localized cooling at the water-cooled sight ports. The free convection coefficient along the vertical side of the furnace was obtained from

$$Nu_x = 0.378\ Gr_x^{1/4} ,$$

where

Nu_x = Nusselt number based on distance from bottom plate

Gr_x = Grasholf number based on distance from bottom plate.

The radiation heat transfer was based on the assumption that the fiberfrax radiates as a grey body with total hemispherical emissivity[29] of 0.8 at room temperature, decreasing linearly to 0.7 at 600 K.

The localized cooling at the sight ports would require a three-dimensional finite element mesh for explicit modeling, so the localized cooling was area-weighted and averaged with the combined radiation-free convection described above.

The overall heat loss from sight ports was about 26% of the total loss from the fiberfrax.

c. Top and bottom plates. The water-cooled furnace base plate and furnace lid (part Nos. 3 and 29, respectively, in Fig. A-6) are stainless steel with internal flow passages. The water heat-transfer coefficient was calculated by use of standard correlations based on the flow passage dimensions and measured water flow rates. An adjustment was made to account for the thickness of stainless steel surrounding the coolant, as it was not explicitly modeled.

d. Internal boundaries. At interfaces between the internal parts of the furnace, there are contact resistances or actual gaps between the parts. Also, there are large internal cavities in some locations (Fig. A-6).

The effective heat transfer conductance at the interfaces was calculated from the following relation for parallel paths;

$$h_e = h_r + h_c ,$$

where h_e is the effective conductance used in the model. The quantity h_r, the conductance from thermal radiation, is given by the relation

$$h_r = F_{1-2}\, \varepsilon'\, \sigma\, (T_1^4 - T_2^4)/(T_1 - T_2) , \qquad (15)$$

where

$\varepsilon' = [1/\varepsilon_1 + 1/\varepsilon_2 - 1]^{-1}$

σ = Stefan-Boltzman constant

$\varepsilon_1, \varepsilon_2$ = total hemispherical emissivity of surfaces, 0.85 for graphite

T_1, T_2 = temperature of surfaces.

Because the gaps are small, the radiation view factor, F_{1-2}, is unity.

The quantity h_c, the conductance through stagnant N_2 at the joints, is given by

$$h_c = \lambda/\delta ,$$

where

λ = thermal conductivity of nitrogen = $0.000321\, \bar{T}^{0.771}$

$\bar{T}$ = average temperature of gas in the gap

δ = gap thickness = $\delta_0 + \alpha_1 \cdot r_1\, (\bar{T}_1 - T_0) - \alpha_2\, r_2\, (\bar{T}_2 - T_0)$,

where

δ_0 = nominal gap at assembly

α_1, α_2 = thermal expansion coefficients for parts on either side of the gap

r_1, r_2 = nominal radius of the parts on either side of the gap, $r_1 > r_2$

$\bar{T}_1$, $\bar{T}_2$ = average temperature of the parts

T_0 = room temperature.

For the large cavities, radiation is the dominant mode of heat transfer. Approximatey 70% of the susceptor power is transported to the canister o.d. by radiation. Calculation of the diffuse reflection and absorption in the toroidal cavity beneath the canister lid could become complicated because the temperature varies along the surface. After several alternative schemes were tried, the best results were obtained by assuming that the incremental areas defined by the finite elements radiate only to the incremental areas directly opposite. The appropriate view factors for each surface were obtained from standard references. Interior cavities in the furnace greatly complicate the thermal analysis.

Heat can radiate axially along the furnace centerline from the hotter region near the substrate to the cooler regions near the injector and the furnace exit. Fortunately, the view factor is small, and a small correction (~ 10%) was made to the wall heat flux supplied by VNAP.

Because much heat is transferred by radiation, free convection in the cavities is negligible in comparison.

4. Overall heat balance. As a check on the heat transfer model, the summary in Table VIII lists the measured heat pickup in the furnace cooling water. The heat convected to the gas jet and that lost from the fiberfrax to the room are also listed, as calculated by AYER. The total of these three quantities should equal the susceptor power, except for measurement and modeling errors.

B. Flow Model.

The inner part, or coating region, of the furnace is shown in Fig. 40. The injector is assumed to be mounted flush with the upstream end of the furnace. The flow enters from the left and leaves at the right. The bottom line is the axis of symmetry; the upper line is the furnace and gas interface.

1. Numerical method. The flow region in Fig. 40 is divided into 40 axial and 16 radial computational cells. The fluid properties at the cell edges or mesh points are computed by use of a second-order, explicit, finite-difference scheme. The boundary conditions consist of specification of the density, the axial and radial velocity components at the inlet, the temperature (AYER code)

TABLE VIII

OVERALL HEAT BALANCE

Parameter	Unit	Flow Tests			Coating Tests	
		I	II	III	I	II
1. F-5 water flow	std l/min	74.5[a]	74.5[a]	74.5[a]	90.0 ± 3	92.0 ± 4
2. T_{19}-T_{17} water ΔT	K	2.83	2.99	4.00	3.05	2.90
3. Q_w water heat pickup	kW	14.7	15.5	20.7	19.1	18.6
4. Q_{gas} gas heat pickup[b]	kW	8.7	9.4	12.5	8.4	8.4
5. Q_{side} free-convection + radiation from fiberfrax[b,c]	kW	3.6	3.3	5.0	3.2	3.2
6. TOTAL	kW	27.0	28.2	38.2	30.7	30.2
7. Susceptor input power	kW	28.1	28.0	37.0	26.6	27.6
8. Difference	kW	1.1	0.2	1.2	4.1	2.6

[a] Average of measurements at 3:45 and 9:00 p.m. with power off.

[b] Calculated

[c] Represents total loss from model o.d. less 26% estimate picked up in sight port cooling water, which is included in item 1.

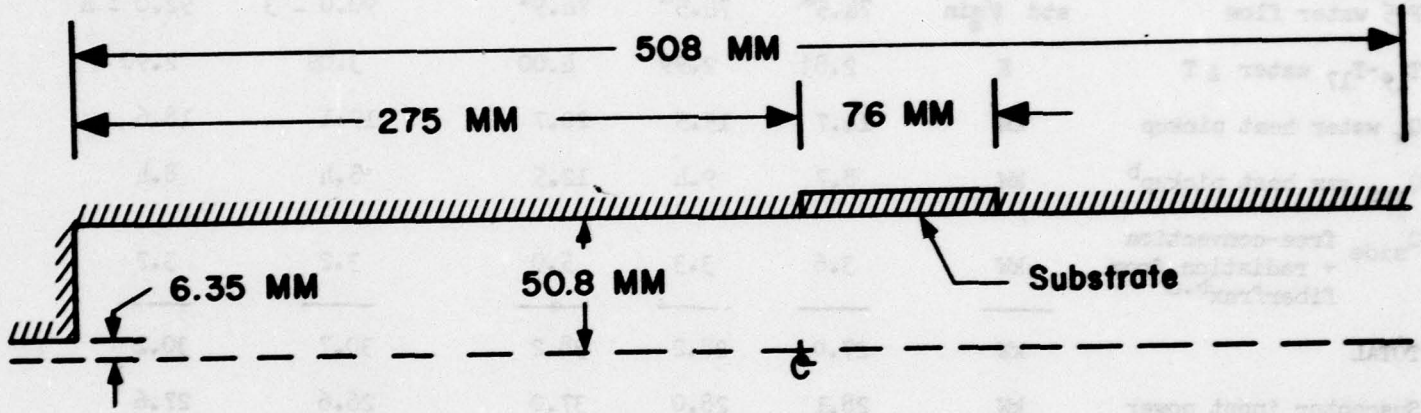

Fig. 40. Furnace coating region considered in the calculations.

and zero velocity components at the furnace wall, and the pressure at the furnace exit. The steady-state solutions presented here are obtained by allowing the flow to relax in time from an arbitrary initial guess to the final, two-dimensional, steady-state solution. Typical cases required ~1 h of computational time on a CDC-7600 computer with the VNAP code using the bulk of the time.

2. Turbulence model. The turbulence was modeled by using a mixing-length approximation. A more advanced kinetic-energy model is in progress. However, because present kinetic-energy models neglect density variations and generally do not predict flows with large density variatiions very well,[32] it is not obvious that these more advanced models will offer significant improvement for the sevenfold density variations considered here.

3. Results. The results for one cold wall flow test with N_2 gas, three hot wall flow tests with N_2 gas, and one coating run are presented below.

a. Cold wall flow tests. The 472 ℓ/min (1000 SCFH) case was calculated and compared with experiment. Figure 41 shows the velocity vector plot and contour plots of temperature and Mach number. Again, the bottom line is the axis of symmetry, the upper line is the furnace-gas interface, and the flow is from left to right. The high and low contour lines are labeled H and L, respectively. The flow remains separated from the furnace wall well past the substrate. The axis of symmetry, or centerline, velocity decay with axial distance is shown in Fig. 42, and the velocity as a function of radius at an axial station 152 mm from the injector is given in Fig. 43. Figures 42 and 43 show that while the calculated velocity decay lags behind these experimental data, the agreement is reasonably good for the present calculations. Although a kinetic-energy turbulence model would improve these results,[32] again it is not obvious that such models would significantly improve the heated wall cases.

b. Heated wall flow tests. Figure 44 shows the velocity vector plot along with contour plots of temperature and Mach numbers for Flow Test II. Again, the flow remains separated from the furnace wall past the substrate. This recirculating flow causes gas to flow upstream from a hotter to cooler region, thereby forming a hot spot near the furnace inlet. This causes heat to flow from the gas to the furnace. Figure 45 shows the calculated gas temperature at the furnace wall as a function of axial distance for the three flow tests.

c. Coating run. The velocity vector plot and contour plots of temperature and Mach number for the coating run are shown in Fig. 46. The calculated gas temperature at the furnace wall is given in Fig. 47.

VELOCITY VECTORS

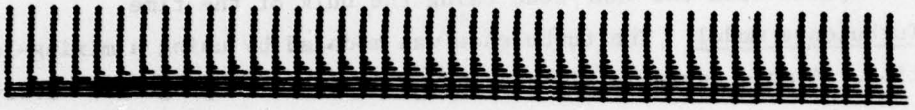

TEMPERATURE

H/L = 1.03

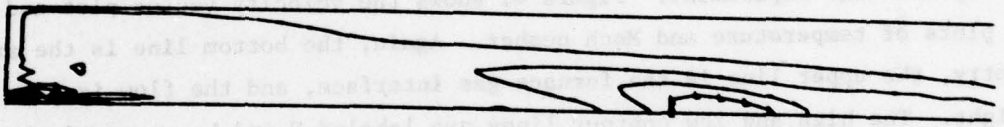

MACH NUMBER

H = 0.16, L = 0.02

Fig. 41. Velocity vectors, temperature and Mach number plots for the cold wall case.

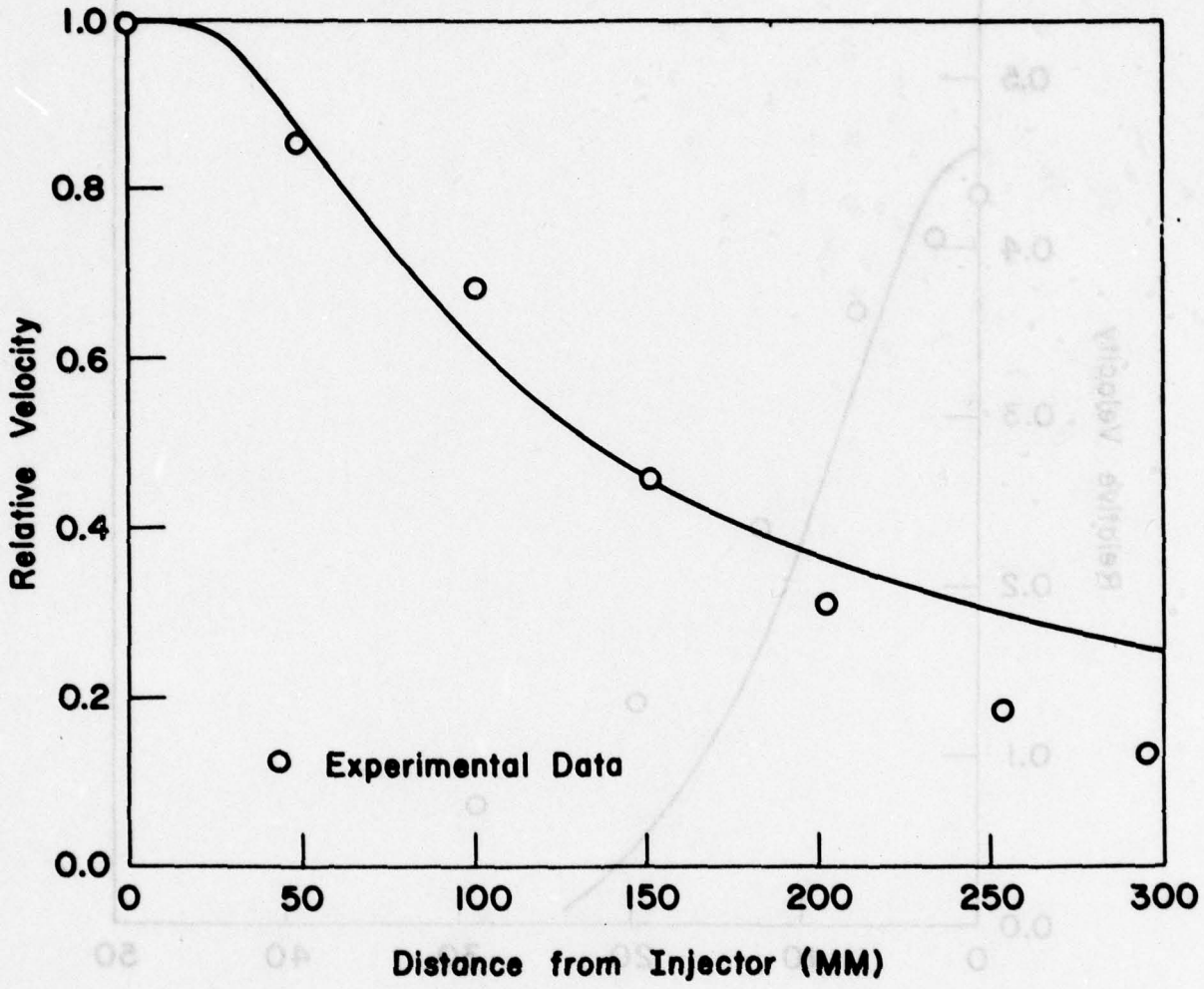

Fig. 42. Centerline velocity decay with axial distance from the injector for the cold wall case.

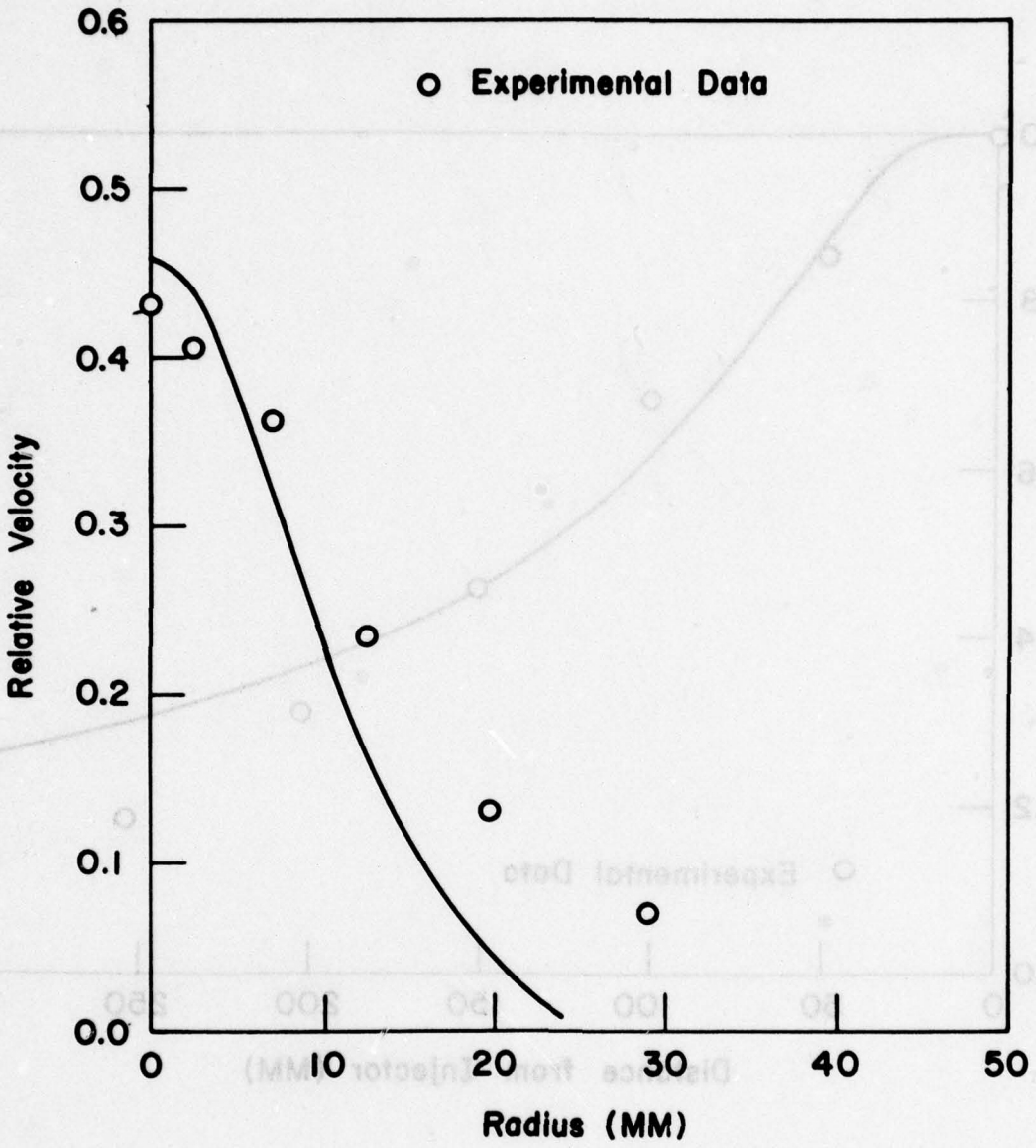

Fig. 43. Velocity profile at 152 mm (6 in) from the injector for the cold wall case.

VELOCITY VECTORS

TEMPERATURE H/L = 4.0

MACH NUMBER H = 0.15, L = 0.02

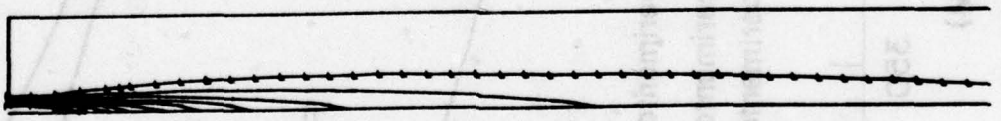

Fig. 44. Velocity vectors, temperature, and Mach number plots for Flow Test II.

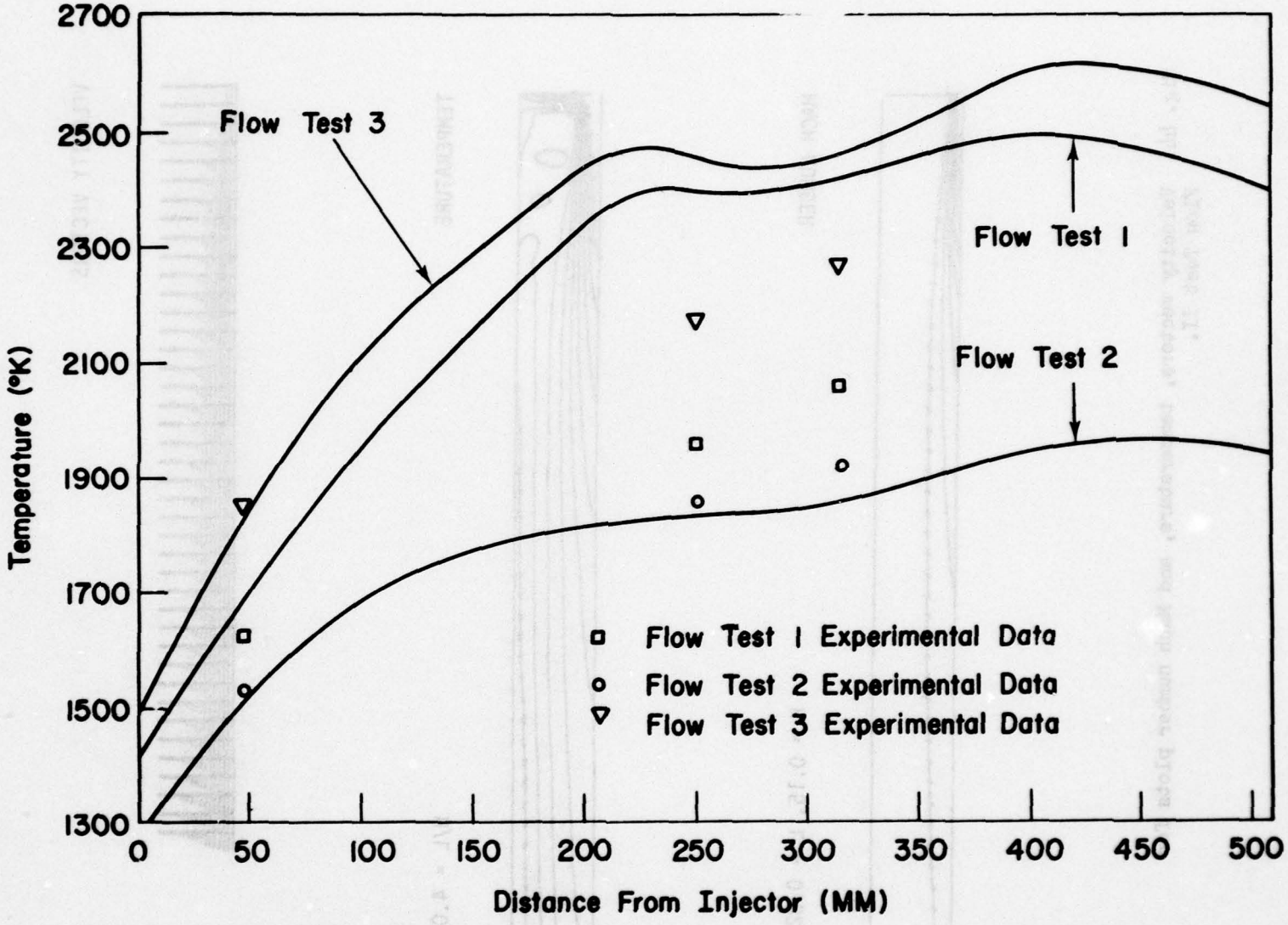

Fig. 45. Wall temperature vs axial distance from the injector for the three flow tests.

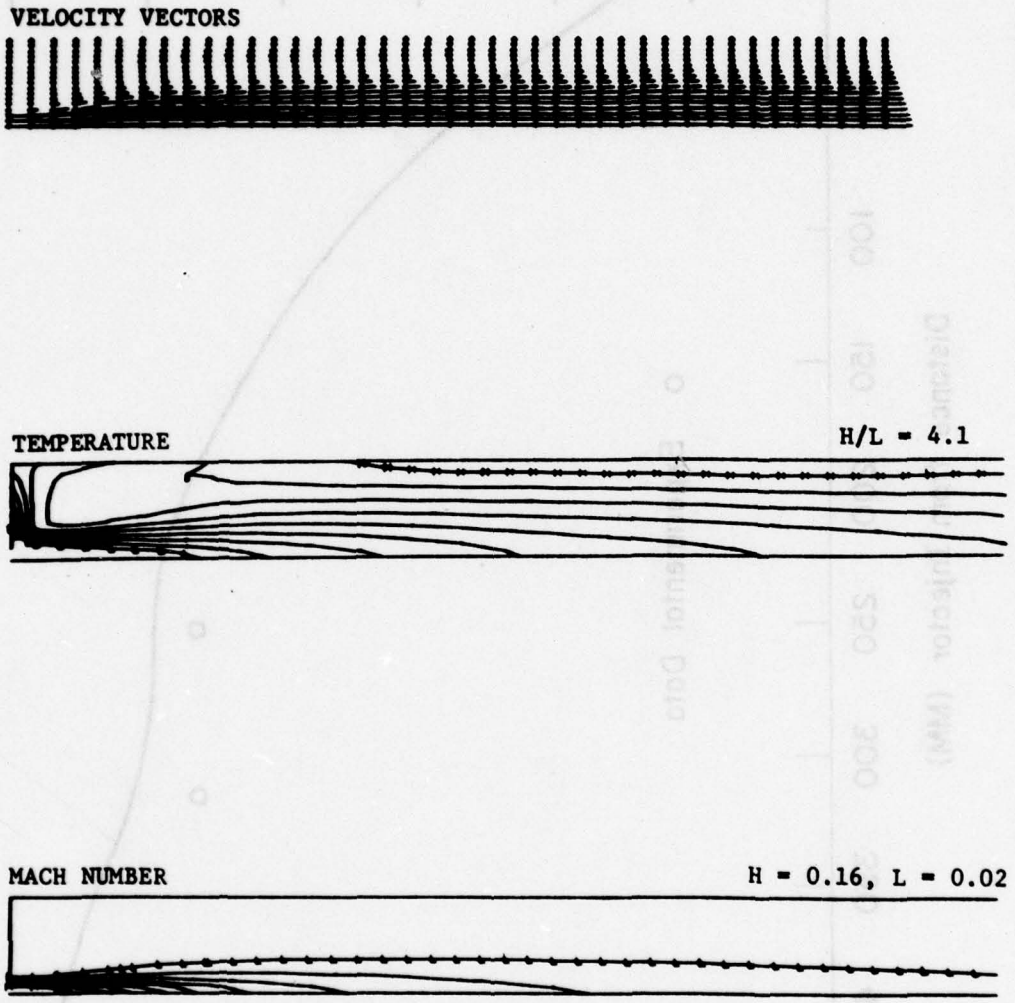

Fig. 46. Velocity vectors, temperature and Mach number plots for the coating run.

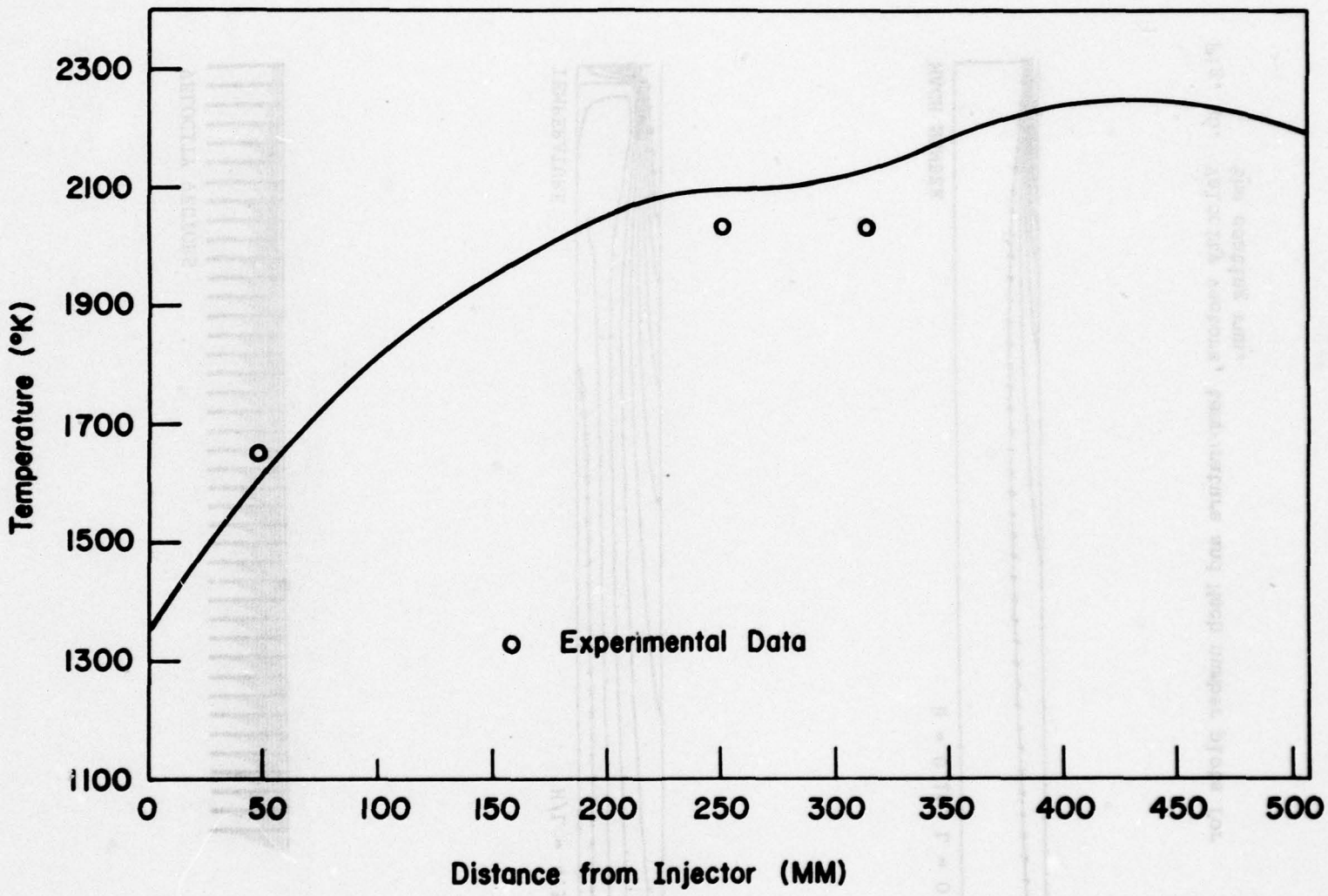

Fig. 47. Gas temperature at the wall vs axial distance from the injector for the coating run.

d. Discussion of results. The calculated wall temperature profiles for Flow Test II and the coating run agree fairly well with the experimental data. However, Flow Test I and III do not agree. It is not clear whether the problem lies in the furnace modeling, flow and turbulence modeling, or the AYER and VNAP code interfacing. Because the part of the experiment that was to produce velocity profiles for the heated wall case failed, the entire experimental flow data consist of three wall temperature measurements. Such data are not adequate to evaluate the performance of the flow and turbulence models. Because the turbulence modeling for such large density variations of a compressible fluid in a duct with an abrupt area increase is largely unknown, these data were very necessary.

Therefore, the determination of the performance and subsequent improvement of the flow and turbulence models will require additional flow data. Also, experiments with a simplified furnace geometry as well as ones with a simplier flow passage would be very helpful in locating problem areas.

4. Conclusions. The gas flow in injector furnaces is characterized by a large separated flow region with associated hot spot and a high level of turbulince. When the substrate is in the separated region, the amount of new material convected over the substrate is reduced. However, the high level of turbulence increased the diffusion of new material through the separated region. Also, high levels of turbulence may have a pronounced effect on the uniformity of coating. Finally, the wall temperature distribution upstream of the substrate seems difficult to control.

The injector furnace contains many complex physical phenomena occuring, simultaneously, so its design is a complicated task. The combined experimental and theorectical approach taken here does appear to be very promising.

V DEPOSITION KINETICS

We were not able to develop an analytical deposition kinetics model for the injector deposition furnace because of the complex computational problems encountered. (An analytical deposition kinetics model was developed for the channel flow furnace and is described in Volume II.) The following discussion characterizes the deposition process.

A. Characterization of the deposition process.

1. Deposition rate. The experimental deposition rate of PG and SiC as a function of axial position were calculated from the relations,

$$R_c = \frac{\Delta \ell \rho (1 - W)}{t\ 12.01} \quad (\text{moles/cm}^2\text{-s}) \qquad (17)$$

and

$$R_{SiC} = \frac{\Delta \ell \, \rho \, W}{t \; 40.10} \quad (\text{moles/cm}^2\text{-s}) \tag{18}$$

where

$\Delta \ell$ = the layer thickness deposited in time t

t = time that deposition for the layer occurs

ρ = density of the layer

W = weight fraction of SiC in layer

12.01 = molecular weight of C

40.01 = molecular weight of SiC.

Smooth curve plots of the data from Table VI were used to interpolate values of $\Delta \ell$, ρ , and W at 20-mm intervals. Figure 48 shows the calculated deposition rates as a function of distance from the injector. The deposition rate data for carbon are essentially the same for layers 1 and 2, in agreement with the constant CH_4/N_2 ratio used for both runs. The SiC deposition rate is proportional to the MTS concentration in the process gas stream.

The carbon deposition rate is constant (± 5%) from 295 to 375 mm from the injector. This interval adequately spans the substrate surface. The SiC deposition rate for both layers 1 and 2 was constant (± 5%) over the interval 315 to 395 mm from the injector. At about 260 mm, the deposition rates of both components drop off sharply.

2. Characterization of temperature and N_2 flow field. Figure 49 shows the characteristic N_2 gas flow for the coating run. The separated flow region (recirculation region) is characterized by two intersecting surfaces. On one surface, V_R, the radial velocity component is zero; on the other, V_X, the axial velocity component is zero. The line at which V_X and V_R intersect is the axis of rotation of the recirculation region. The line at which V_X intersects the deposition canister wall (attachment point) separates the deposition process into two domains. Upstream from the attachment point, deposition is from a separated flow region and downstream from the attachment point, the deposition is from an attached flow region. Because the mass flow in the attached flow region must equal the mass flow introduced through the injector, one can define the surface of separation between the recirculation region and the flow that forms the attached flow region beyond the attachment point by the relation

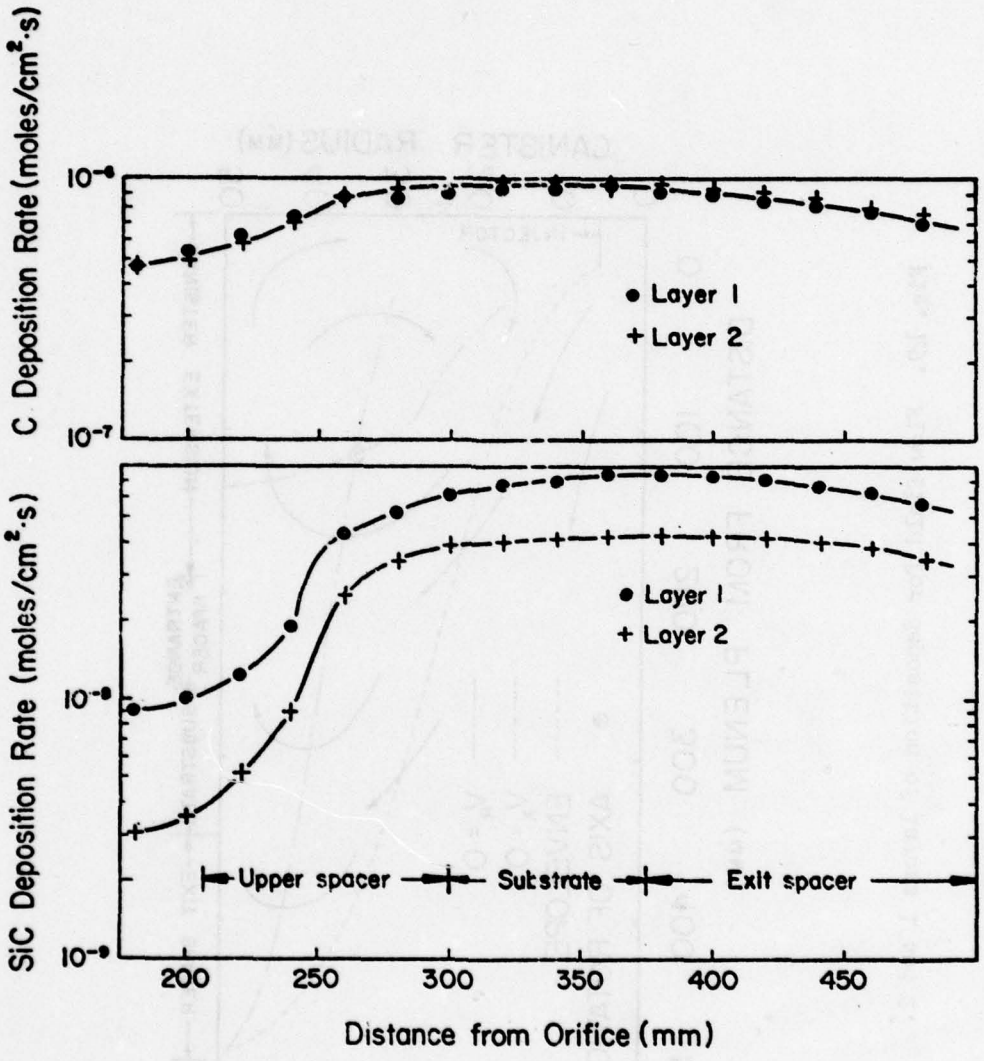

Fig. 48. Depostion rates as a function of distance from injector.

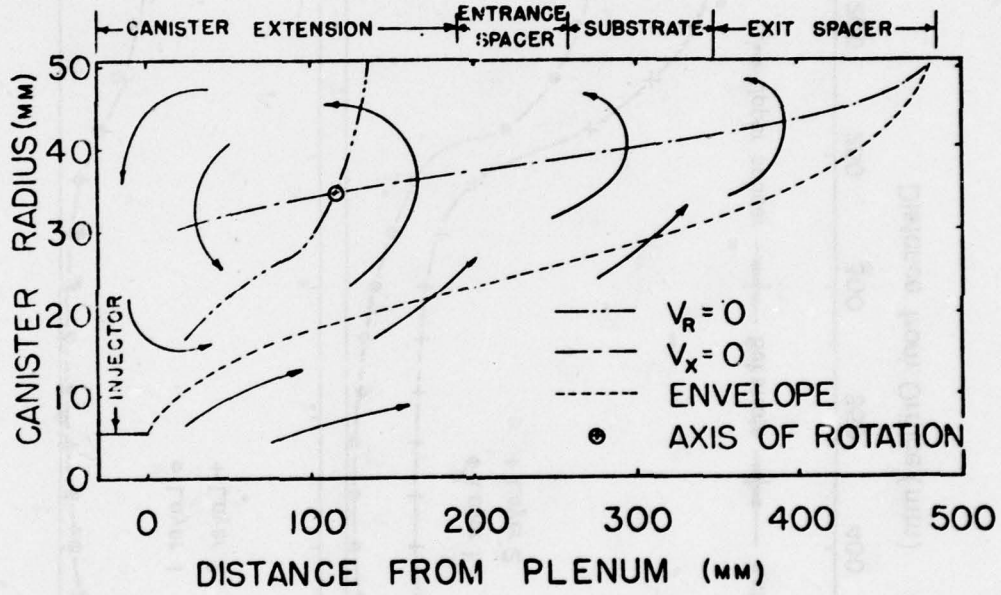

Fig. 49. Flow field for deposition of layers 1 and 2.

$$\dot{m} = 2\pi \int_0^R r \rho v \, dr \,, \tag{19}$$

where

r = radius

ρ = gas density

v = gas velocity

R = radius at which equality is satisfied

$\dot{m}$ = mass flow rate,

for a fixed axial distance from the injector. Values of R that satisfy this relation have been plotted in Fig. 50 and denoted as the envelope surface. To determine the ratio of the mass flow in the recirculating region to $\dot{m}$, the following integrations were preformed.

$$\dot{m}_x = 2\pi \int r \rho v_x \, dr \tag{20}$$

along V_R from the axis of rotation to the wall, and

$$\dot{m}_r = 2\pi \int r \rho v_r \, dr \tag{21}$$

along V_X from the axis of rotation to the wall. As expected, $\dot{m}_x = \dot{m}_r$, and the ratios, $\dot{m}_r / \dot{m} = \dot{m}_x / \dot{m} = 0.28$.

To compare flux rates near the substrate, axial plots of the radial component of nitrogen flux ($v_r \rho / 28.01$) at R = 44.5 and 47.6 mm from the wall are presented in Fig. 50A and 50B. If the N_2 flux is multiplied by the initial volume percent of methane in the process gas stream, one has an upper approximation of the flux of carbon (as CH_4) moving by the substrate. For example, at 300 mm (approximate center of substrate) the axial component of the flux past the surface at 1.5 mm is $1.8 \cdot 10^{-5}$ moles/cm^2-s; whereas the radial component of the flux toward the surface is $6 \cdot 10^{-7}$ and $3 \cdot 10^{-7}$ moles/cm^2-s at R=44.5 and 47.6 mm, respectively. These values may be compared with the experimentally determined carbon flux of $1 \cdot 10^{-6}$ moles/cm^2-s at this point. The canister wall temperature is shown in Fig. 50C.

From the information presented, the following characteristics of the temperature and flow field were identified.

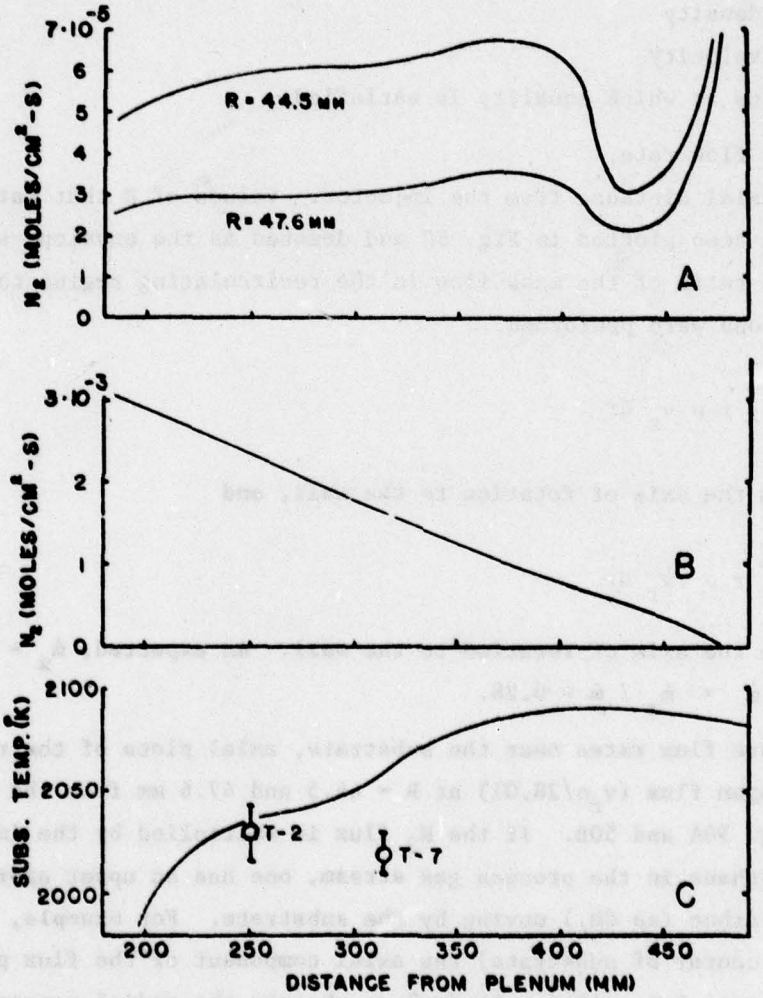

Fig. 50. Flow rates and wall temperatures in canister during deposition of Layers 1 and 2. A - Radial component of N_2 flow toward wall at R = 47.6 and 44.5 mm. B - Mean axial component (1.5 mm from wall) of N_2 flow back up wall. C - calculated wall temperature. T-7 measured on substrate surface. T-2 calculated surface substrate temperature based on wall temperature measurement.

- Deposition on the substrate occured from a recirculation region (separated flow region). The coating gas was flowing back toward the inlet end of the canister when it moved over the substrate.
- The substrate surface temperature and the gas temperature near the substrate decrease as the coating gas moves across the substrate surface.
- Fresh CH_4 and MTS are introduced into the recirculation region by turbulent mixing along the envelope surface. The amount of new material convected to the substrate in a recirculation region is less than that in the attached flow region.

B. Comparison of Present and Prior Work.

Figure 51 summarizes prior ARC work with a depositon furnace similar to the one used now. The inside diameter of the deposition canister and injector, and the coating gas compositions were the same. The internal configuration was similiar to that shown in Fig. 1-C. The distance to the center of the substrate was ~ 300 mm, and the deposition apparently took place from an attached flow region. The temperature corresponds to the surface temperature at the center of the substrate.

The carbon deposition rate at 2033 K (calculated surface temperature at center of substrate) in the prior work was 1.5 times greater than that in the current work. This can be explained by a larger convective transfer near the point of attachment. Figure 52 compares the SiC deposition rates as a function of MTS concentration at 2033 K. At 0.1 vol % MTS, the prior ARC deposition rate is approximately 1.5 times that of the present owrk.

The most striking feature of Fig. 51 is the increased SiC deposition rate with decreasing temperature. This trend suggests that there is a lower range of temperatures where the SiC deposition rate would be independent of temperature and hence gas diffusion limited.

The loss of layer 3 data kept us from getting data on the effects of the coating gas velocity over the substrate surface. Generally the coating gas velocity over the substrate and the substrate surface temperature strongly influence the SiC microstructure and the surface roughness of the coat. For example, if the deposition temperature gets too high or the coating gas velocity too low, the SiC forms at the PG cone boundaries as large equiaxed crystals that degrade the mechanical properties of the material. The coat surface becomes rougher with the same changes in temperature and velocity.

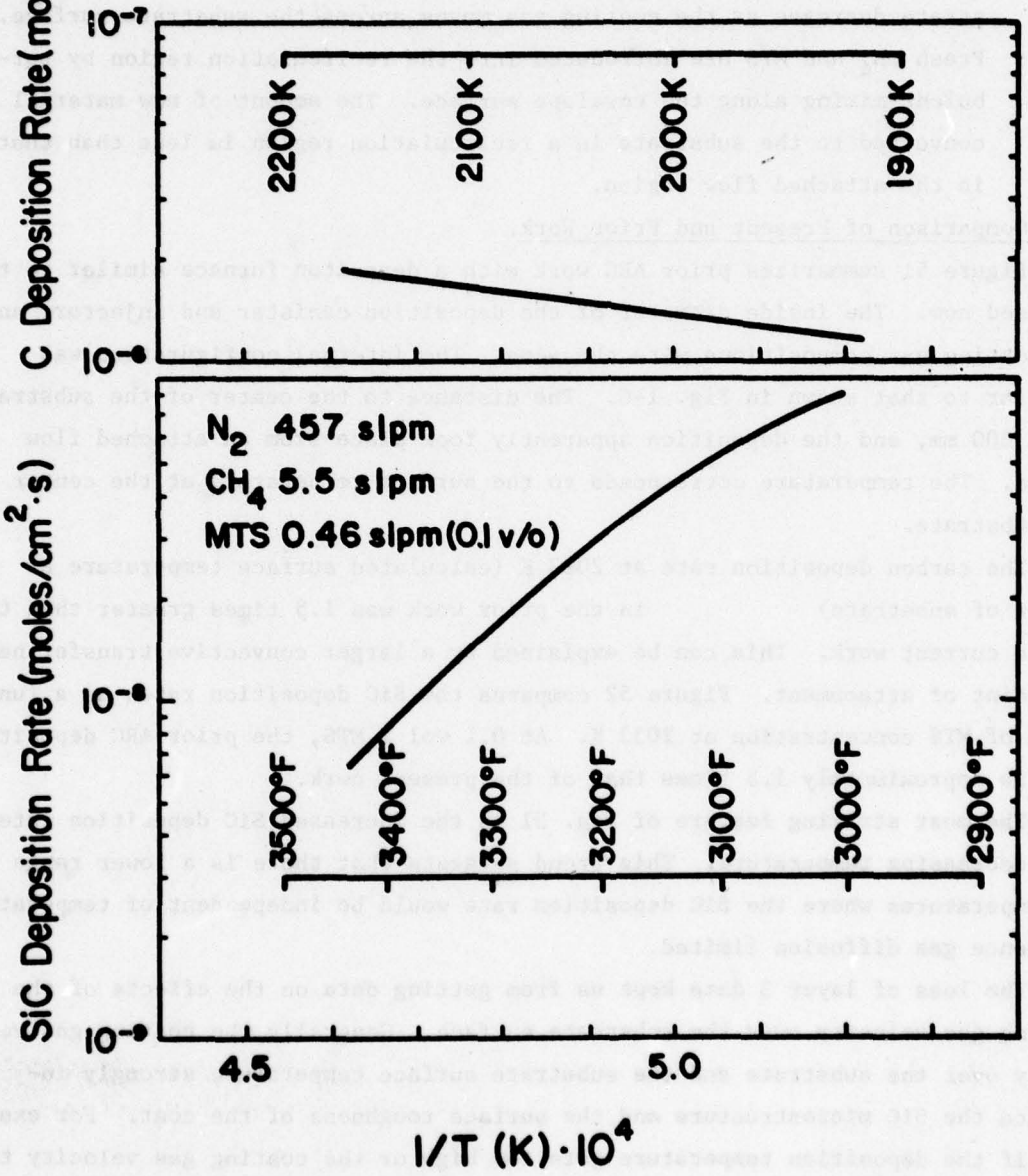

Fig. 51. Deposition rate data from prior ARC coating runs.

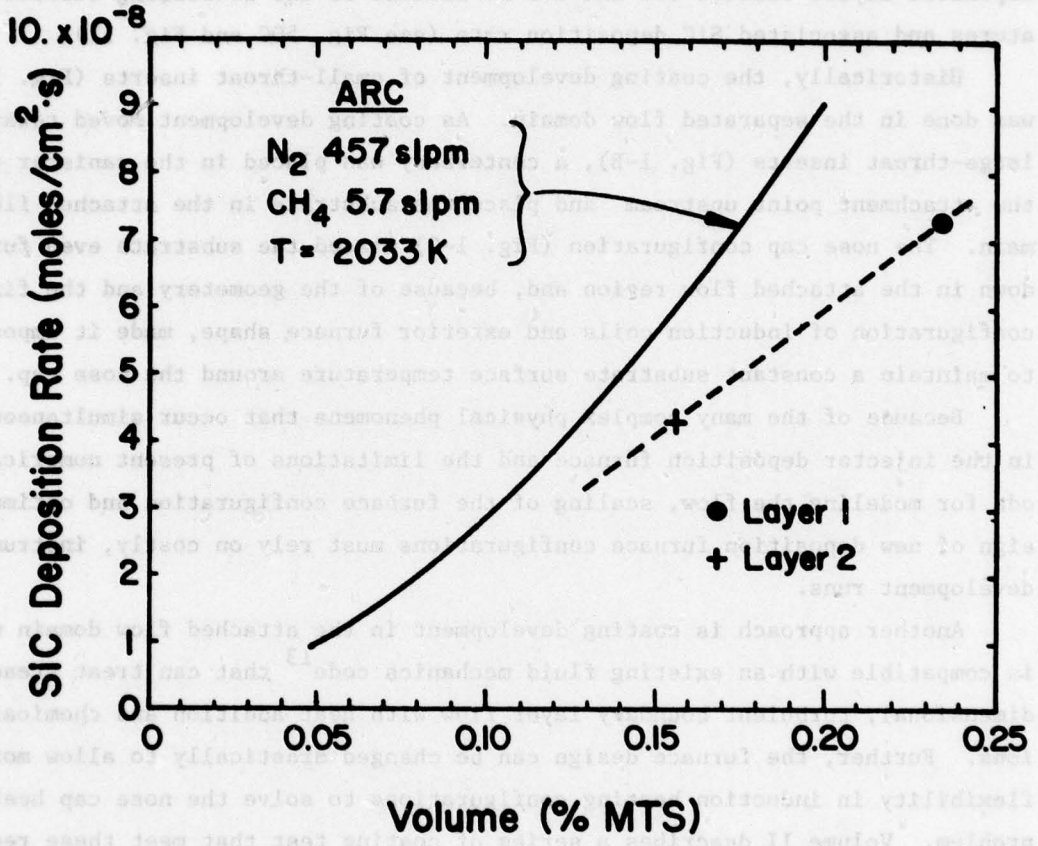

Fig. 52. SiC deposition rate vs MTS concentration.

Unfortunately there was no prior work with which to compare axial variations of deposition rates. In the present work, the sharp decrease at ~260 mm must be caused by deposition depletion of the freshly introduced CH_4 and MTS in the recirculation region as the gas flows back upstream over the canister wall. If this were not so, one would expect the weight percent of SiC to increase in the deposited layers between 350 and 200 mm because of the decreasing surface temperatures and associated SiC deposition rate (see Fig. 50C and Fig. 51).

Historically, the coating development of small-throat inserts (Fig. 1-A) was done in the separated flow domain. As coating development moved toward the large-throat inserts (Fig. 1-B), a centerbody was placed in the canister to move the attachment point upstream and place the substrate in the attached flow domain. The nose cap configuration (Fig. 1-C) placed the substrate even further down in the attached flow region and, because of the geometery and the fixed configuration of induction coils and exterior furnace shape, made it impossible to maintain a constant substrate surface temperature around the nose cap.

Because of the many complex physical phenomena that occur simultaneously in in the injector deposition furnace and the limitations of present numerical methods for modeling the flow, scaling of the furnace configuration and optimum design of new deposition furnace configurations must rely on costly, instrumented development runs.

Another approach is coating development in the attached flow domain which is compatible with an existing fluid mechanics code[13] that can treat steady, two-dimensional, turbulent boundary layer flow with heat addition and chemical reactions. Further, the furnace design can be changed drastically to allow more flexibility in induction heating configurations to solve the nose cap heating problem. Volume II describes a series of coating test that meet these requirements.

VI SUMMARY

A. Data Base.

Methods of instrumenting and collecting data (Sec. IIC and App. B) for defining the furnace and process characteristics (Sec. IIB and App. A), test procedures (App. D), and recorded and reduced data (App. D) were documented.

B. Instrumentation.

A data acquisition system was designed and implemented to measure and record 37 furnace parameters to ± 2% maximum overall inaccuracy. These measurements included seven flow rate parameters, two furnace power parameters, two linear

parameters, one angular position parameter, and time of day. Controllers to provide stable and accurate control of the mass flow rates of the process gases were specified and installed. The design and performance of the furnace instrumentation permitted assembly of a data base than greatly enhanced the ability to understand and model the characteristics of the chemical vapor deposition furnace.

C. Analytical Modeling.

1. Heat transfer. The general-purpose heat transfer code, AYER (Sec. IV.A) was proved capable of modeling the complex injector depostion furnace in transient and steady state operation (Sec. III). The thermal properties of the materials (Sec. IV.A.2) and the boundary conditions (Sec. IV.A.3), particulary at the coating gas boundary, are the most difficult inputs to supply accurately. Internal cavities in the furnace add complexities caused by radiation scattering and reflection (Sec. IV.A.3.d). The computer program is not too large and running times on a CDC 7600 are about 30 s per case.

2. Flow. The modified numerical fluid dynamics code, VNAP (Sec. IV.B.1) showed fair ability to model the coating runs and the flow in the cold wall and heated wall (Sec. IV.B.3). Problems arose because (a) the only code available had been developed to handle inviscid supersonic flows without recirculation, so it was less versatile than was desirable and difficult to use in this specific application; and (b) the modeling of turbulent, separated flows with heat addition, chemical reaction, and mass transfer is in an early stage of development world-wide so very little information was available to guide a timely development. Given the time and resources, the combined experimental and theoretical approach developed here is a promising way to advance modeling of this phenomenon. The computer program is large, and the running times on a CDC 7600 are about 1 h per case.

3. Kinetics. No analytical deposition kinetics models was developed. Such development required a numerical fluid dynamics code that could model turbulent, separated flows with heat addition, chemical reactions, and mass transfer. We thought that VNAP would serve, but difficulties in validating the code through the heat addition stage left inssuficient time to develop the kinetics model. However, VNAP proved capable of modeling the gas stream lines and thermal histories in injection deposition furnaces with configuration similar to those shown in Figs. 1-A and 1-B. In principle, this capability should provide a basis for making qualitative chemical kinetic calculations. The data from the coating runs were analyzed (Sec. III.C.) and the deposition process was characterized (Sec. V).

4. Simple scaling laws. No simple scaling laws were developed, because of the complex relationships between the variation of the axial heat transfer to the gas at the wall as a function of process variable, and the extreme sensitivity of the calculated temperatures to this heat transfer. Even so simple a change as a shift in the gas flow rate for a fixed geometry and power input caused unexpected shifts in the modeled wall heat-flux distribution. If the effects of changes in the furnace design are to be fully understood, use of the costly iterative instrumented engineering tests and modeling approach developed here would be required.

D. Alternative Approach.

During the early part of this work, it became apparent that some complex computational problems would have to be solved if the turbulent, separated flow were to be modeled adequately. Preliminary analysis of the flow fields encountered in the injection deposition furnace suggested that codeposited PG/SiC material with the requisite mechancial properties had been obtained from both separated and attached flow regions. On the basis of information developed to this point and the availability of a qualified computational fluid mechanics code that could treat steady, two-dimensional, turbulent boundary flow with heat addition, chemical reactions, and mass transfer (but not recirculation flow) an alternative approach was developed. A coating furnace was designed to operate in the attached flow region and be compatible with the data input required by the flow code and the AYER code. A further consideration was easy modification of substrate and induction coil configurations. The furnace was built, tested, and analyzed. The results are presented in Volume II.

ACKNOWLEDGMENTS

We appreciate the interest and advice of Major John G. Dean, the Air Force Rocket Propulsion Laboratory Technical Project Officer for this program. We also appreciate the cooperation given by Atlantic Research Corporation in the performance of the engineering tests at their facilities in Alexandria, Virginia and, in particular, in the individual efforts of Dr. Joseph P. Copeland, Mr. Kenneth E. Undercoffer, and Mr. Charles Newquist.

REFERENCES

1. William F. Payne, "Pyrolytic Graphite Coated Throat Inserts," Air Force Rocket Propulsion Laboratory report AFRPL-TR-74-42 (August 1974).
2. E. Olcott, "Study of Pyrolytic Graphite/Silicon Carbide Codeposited Coattings," Air Force Rocket Propulsion Laboratory report AFRPL-TR-71-132 (October 1971).
3. Richard H. Singleton, "Development and Evaluation of PG/SiC Codeposit Coatings for Rocket Nozzle Inserts, Vol. I, Thermal and Mechanical Properties of Pyrolytic Graphite/Silicon Carbide Codeposits," Air Force Rocket Propulsion Laboratory report AFRPL-TR-73-70 (October 1973).
4. Kenneth E. Undercoffer, ibid., Vol. II, "Vapor Deposition of Pyrolytic Graphite/Silicon Carbide Codeposited Coatings."
5. Cedric Bielawski, ibid., Vol. III, "Substrate Rocket Motor Testing of PG/SiC Lined Throat Inserts."
6. Richard H. Singleton, "Development and Evaluation of PG/SiC Codeposit Coatings for Rocket Nozzle Inserts, Vol. I, Insert Test and Evaluation in High Performance Propellant Environments," Air Force Rocket Propulsion Laboratory report AFRPL-TR-73-107 (February 1973).
7. James W. Murray, ibid., Vol. II, "Thermostructural Analysis of Selected Nozzle Test Firings."
8. Martin C. Hughes, "Codeposited PG/SiC Nozzle Liners for Advanced ICBM Systems, Vol. I, Deposition Process Development," Air Force Rockt Propulsion Laboratory report AFRPL-74-15 (August 1974).
9. Martin C. Hughes and Richard H. Singleton, ibid., Vol. II, "Coating Characterization."
10. Martin C. Hughes, ibid., Vol. III, "Small Nozzle Test Firings."
11. Martin C. Hughes, ibid., Vol. IV, "Thermostructual Analysis Using a Simplified Model."
12. Joseph P. Copeland, R. J. Diefendorf, Charles B. Henderson, Martin C. Hughes, Merril K. King, James R. MacPherson, Bruno J. Marci, James W. Murray, Richard H. Singleton, Kenneth E. Undercoffer, and Ralph S. Valentine, "Evaluation of the PG/SiC Nosecap Deposition Process," Atlantic Research Corporation report ARC 10216 (August 1974).
13. S. V. Patankar and D. B. Spalding, "Heat and Mass Transfer in Boundary Layers," London Intertext Books, London (1970).

14. Eugene L. Olcott, "Pyrolytic Graphite-Silicon Carbide Microcomposites," U. S. Patent No. 3,738,906, June 1973.
15. M. D. Gordon, K. P. Lavrovskii, and A. N. Rumyantsev, "Formation of the Solid Phase During Thermal Decomposition of Methane in an Atmosphere of Hydrogen," Doklady Akad. Nauk SSSR 191, 1289 (April 1970).
16. G. I. Kozlov and V. G. Knoore, "Single-pulse Shock Tube Studies on the Kinetics of the Thermal Decomposition of Methane," Combust. Flame 6, 253 (1962).
17. H. B. Palmer and T. H. Hirt, "The Activation Energy for the Pyrolysis of Methane," J. Phys. Chem. 67, 709 (1963).
18. J. L. Hudson and Julian Heicklen, "Theory of Carbon Formation in Vapor-Phase Pyrolysis - I. Constant Concentration of Active Species," Carbon 6, 405 (1969).
19. H. Luhlecih, D. Seeberger, K. Koizlick, and H. Nickel, "Two-Component Model of Pyrocarbon and its Effect on Material Parameter Analysis." J. Vac. Sci. Technol. 12, 750 (1975).
20. H. Luhlecih, K. Koizlik, P. Pflaum, D. Seeberger, J. Linke, and H. Nickel, "New Conceptions of the Deposition Mechanism of Pyrocarbon," KFA (Juelich) report JUL-1092-RW, August 1974, translated by USAEC Technical Information Center, Oak Ridge, Tennessee, GERHTR-137.
21. L. M. Ivanova and Al A. Pletysushkin, "Thermal Decomposition of Methyltrichlorosilane Vapor," Izv. Akad. Nauk SSSR, Neorganicheskie Mater. 4,1089 (1968).
22. John H. D'Azzo and Constantine H. Hoapis, Feedback Control System Analysis and Synthesis (McGraw-Hill Inc., New York, 1966).
23. Harry L. Stiltz, Aerospace Telemetry (Prentice Hall Inc., Englewood Cliffs, NJ, 1961).
24. F. White, Viscous Fluid Flow (McGraw Hill, NY, 1974), p. 510.
25. F. Durst A. Melling, and J. H. Whitelaw, "Low Reynolds Number Flow over a Plane Symmetric Sudden Expansion," J. Fluid Mech. 64, 111 (1974).
26. E. O. Macagno and T. K. Hung, "Computational and Experimental Study of a Capative Annular Eddy, "J. Fluid Mech. 28, 43 (1967).
27. R. G. Lawton, "The AYER Heat Conduction Program," Los Alamos Scientific Laboratory report LA-5613-MS (May 1974).
28. M. C. Cline, "Computation of Two-Dimensional, Viscous Nozzle Flow," AIAA Journal 14, 295 (1976)

29. Y. S. Toulockian, Ed., Thermophysical Properties of High Temperature Solid Materials, Thermophysical Properties Research Center, Purdue University (MacMillian Company, NY, 1957).

30. H. W. Godbee and W. T. Ziegler, "Thermal Conductivity of Magnesia, Alumina and Zirconia Powders in Air at Atmospheric Pressure from 200° to 1500°F," J. Appl. Phys. 37, 56 (1966).

31. P. P. Zemanick and R. S. Dougall, "Local Heat Transfer Downstream of Abrupt Circular Channel Expansion," ASME J. of Heat Transfer, February 1970, p. 53.

32. B. E. Launder, A. Morse, W. Rodi, and D. B. Spalding, "The Prediction of Free Shear Flows -- A comparison of the Performance of Six Turbulence Models," Imperial College of Science and Technology report, TM/TN/B/19 (1972).

APPENDIX A

COATING FURNACE AND PROCESS EQUIPMENT

TABLE OF CONTENTS

LIST OF ILLUSTRATIONS

I. WATER AND ELECTRICAL SERVICE

The furnace cooling water was taken from a house service line. Pressure fluctuations from the varying demands on the line caused some problems. Moderate decreases in the line pressure caused lowered flow rates of cooling water through the induction coil, support plate, furnace lid, water-cooled injector, and water-cooled sight ports. If the situation continued for 10-15 min. the temperature in the deposition canister rose. The supply water pressure in the induction coil was interlocked with the motor generator set so that a major pressure drop would turn it off. Problems from water pressure fluctuations could be minimized if the water came directly from a large water main or a closed loop process water cooling system.

The induction coil power was provided by a 10-kHz, 100-kW, motor generator set. Figure A-1 shows the control panel.

II. PROCESS GASES

A. Nitrogen (N_2).

The nitrogen was supplied from a large liquid nitrogen dewar. The main supply line from the dewar was connected to the distribution panel shown in Fig. A-2. Figure A-3 shows the configuration of the distribution panel. The process nitrogen line passes from the manifold through a shutoff valve, pressure regulator, process nitrogen transducer (F-1, see Fig. B-14), process nitrogen flowmeter, metering valve, a manifold for mixing with CH_4 and CH_3SiCl_3, to the water-cooled process gas injector on the top of the furnace, Fig. A-4. The process flow rate was set with the metering valve, and with the configuration used, direct comparison could be made with the process nitrogen flow meter used in the past and the data acquisition system readout from the newly installed process nitrogen transducer.

The other line from the manifold passed through a shutoff valve and a pressure regulator, and then divided into lines for sight port purge, case purge, and annulus purge. The case purge supplied a nitrogen atmosphere to the lamp black-containing parts of the furnace. The annulus nitrogen line passed through a flow meter and nitrogen transducer and then to the injector seal on top of the furnace, Fig. A-4. The annulus nitrogen forms a gas seal around the process gas injector. Again the configuration used permitted a direct comparison with the annulus nitrogen flow meter used in the past and the data acquisition system readout from the newly installed annulus nitrogen transducer.

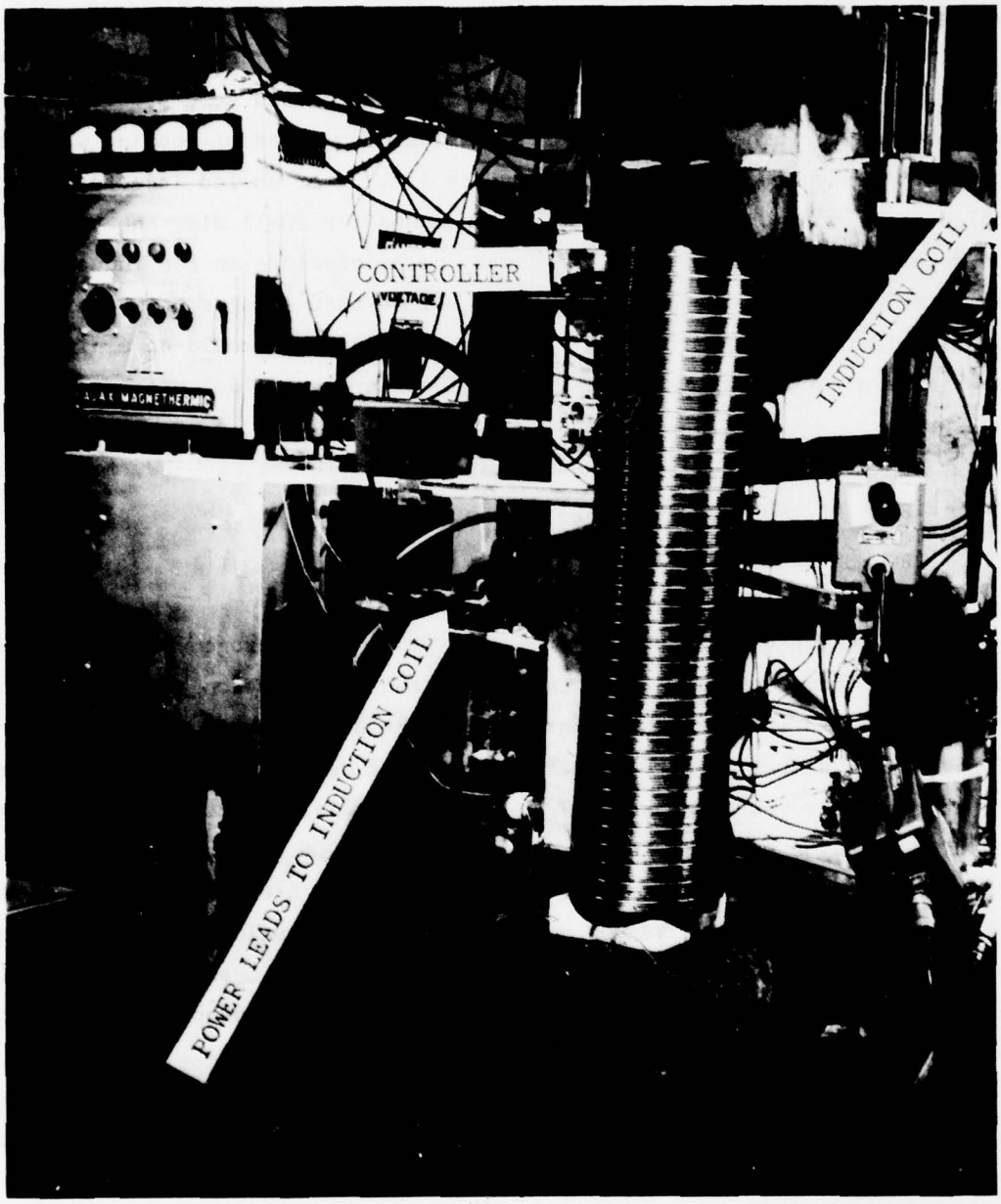

Fig. A-1. Motor generator set controller.

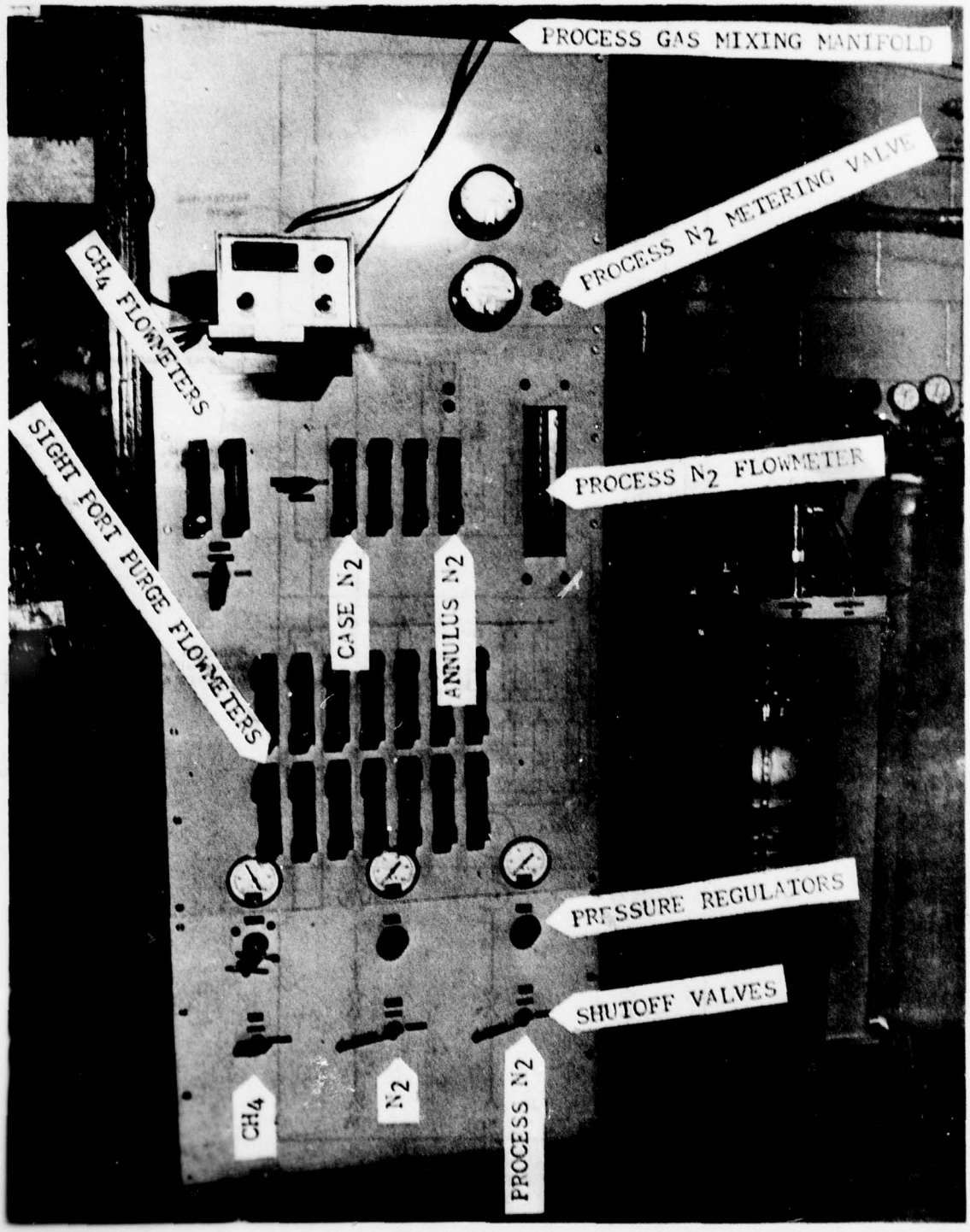

Fig. A-2. Process gas distribution panel.

THIS PAGE IS BEST QUALITY PRACTICABLE
FROM COPY FURNISHED TO DDC

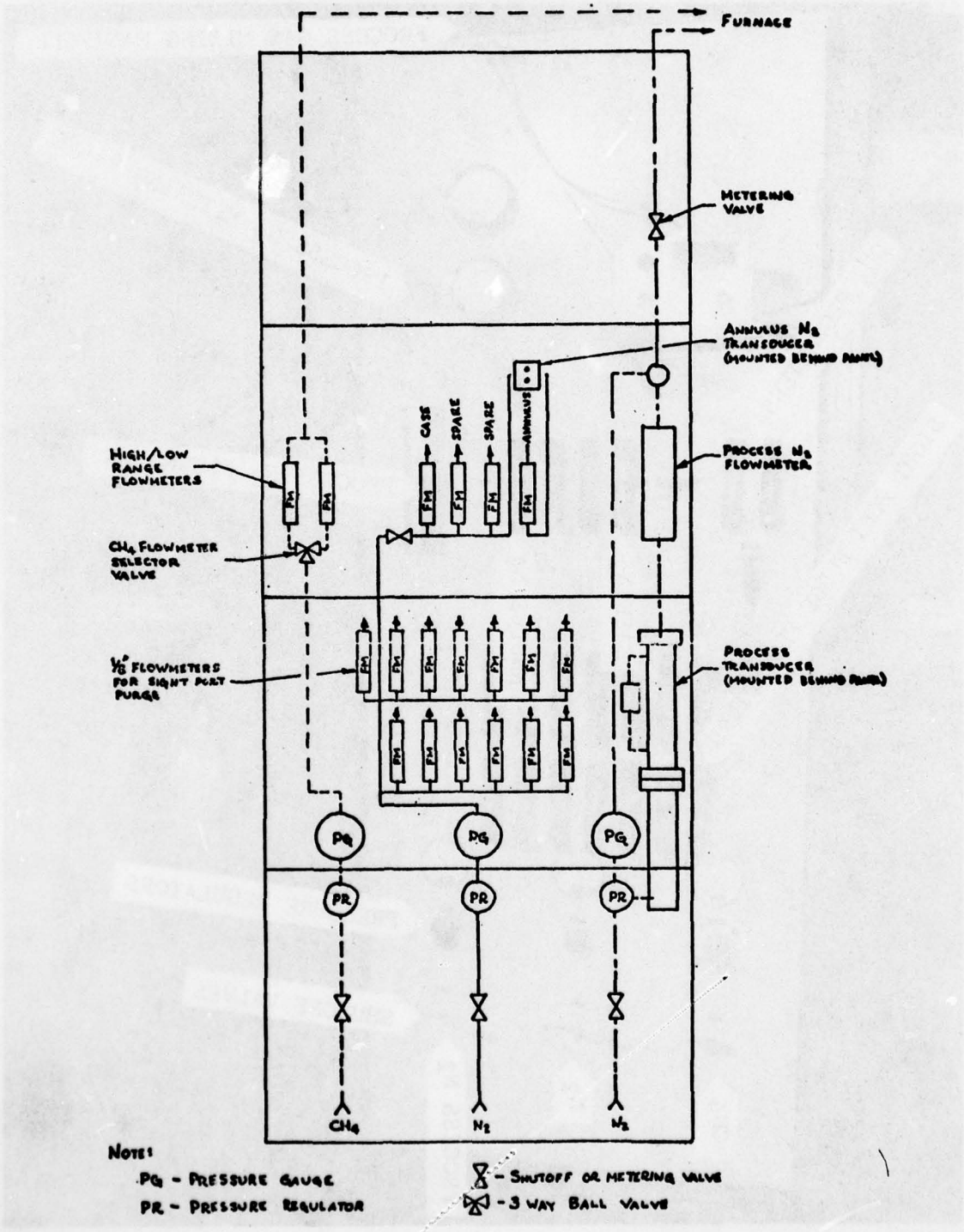

Fig. A-3. Schematic of process gas distribution panel.

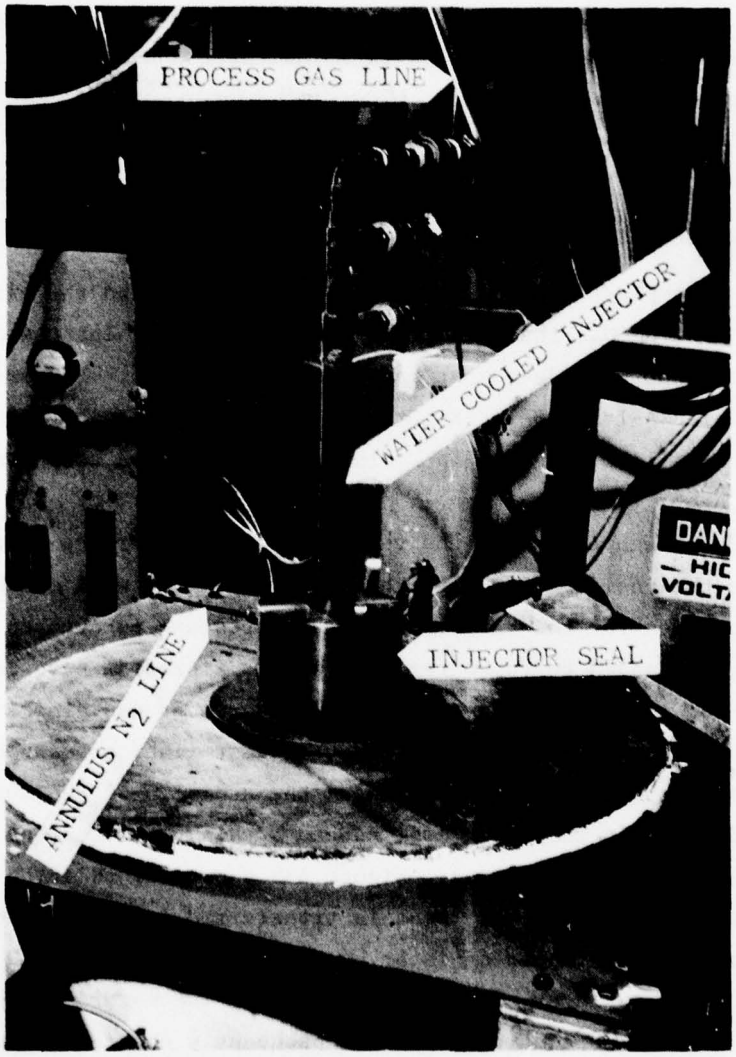

Fig. A-4. Furnace top details.

B. Methane (CH_4).

The methane was taken from the house natural gas lines. Analysis showed that it contained 95% CH_4 and 5% C_2H_6. The CH_4 line entered the distribution panel through a shutoff valve, passed through a pressure regulator and a CH_4 controller, and then tied into the mixing manifold on the process gas line. Comparison could be made with the CH_4 flow rate indicator and the CH_4 flow meter.

C. Methyl trichlorosilane (CH_3SiCl_3, MTS).

The MTS delivery system is described in App. B, Sec. II.B.3. A line ran from the MTS controller to the mixing manifold on the process gas line.

III. COATING FURNACE ASSEMBLY

Figure A-5 is a plan view of the deposition furnace and the circumferential location of the instruments that penetrate its outer wall. Instrument types are coded, i.e., T-1, and the code number is shown in a hexagon. For specific descriptions see Tables A-I and B-I. Figure A-6 is an elevation of the deposition furnace, and a parts list is given in Table A-II. The parts code numbers are circled on Fig. A-6.

Figures A-7 through A-14 show the various stages of furnace assembly. Figure A-7 shows the inside surface of the outer fibrefrax wall of the furnace with penetration holes for the various sight and pressure port tubes. These graphite tubes were sealed to the outer wall with a fibrefrax base cement. On the outside surface of the wall, a seal of silicon rubber was placed over the base cement. The susceptor support and lower exhaust liner are supported by the water-cooled support plate. Figure A-8 shows the addition of the susceptor. The electrical field from the induction coil suscepts this piece thereby setting up eddy currents that cause I^2R heating. Figure A-9 shows the addition of the canister base and the lower canister. Heat is transferred from the susceptor to the lower and upper canister by radiation. Figure A-10 shows the addition of the upper canister and the exit spacer. The material deposited on the exit spacer during the coating run was subsequently characterized.

Figure A-11 shows the addition of the substrate ring that simulated a rocket-nozzle throat liner. The deposited coat on this component was also characterized. Figure A-12 shows the addiition of the entrance spacer and the canister lid. The coat deposited on the entrance spacer also was characterized. Figure A-13 shows the addition of the canister extension and the lampblack shield. The outer furnace wall is sealed to the furnace top with a fibrefrax

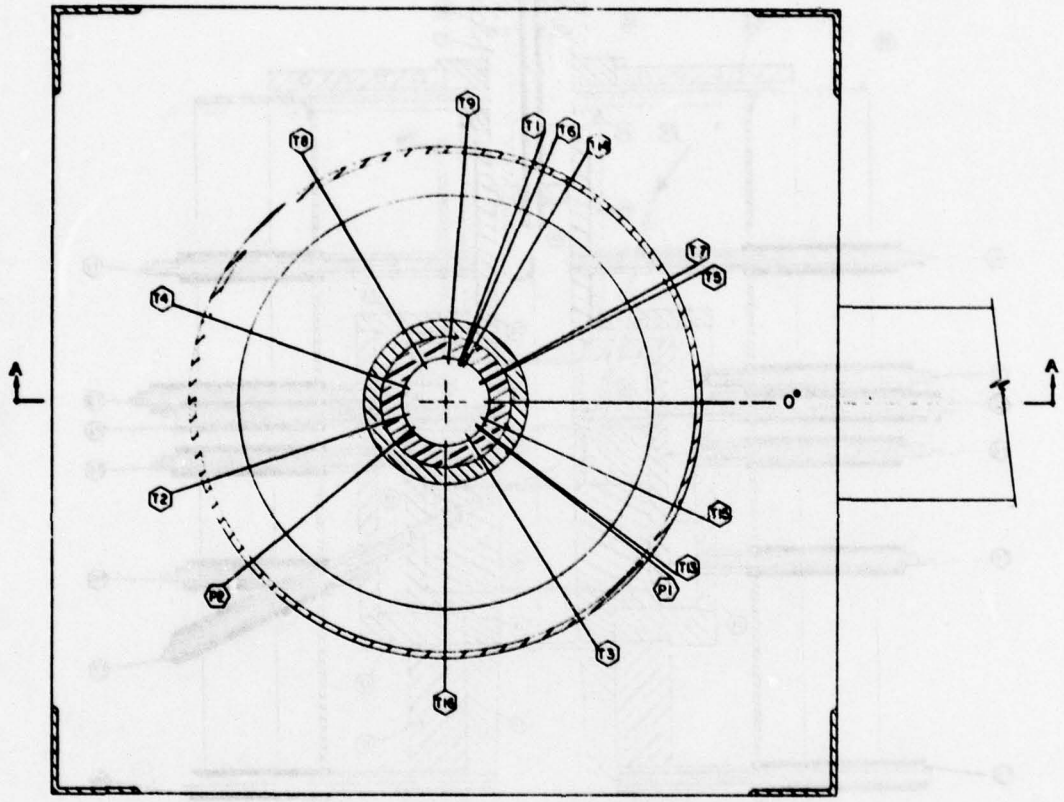

Fig. A-5. Plane view of instrument locations for deposition furnace.

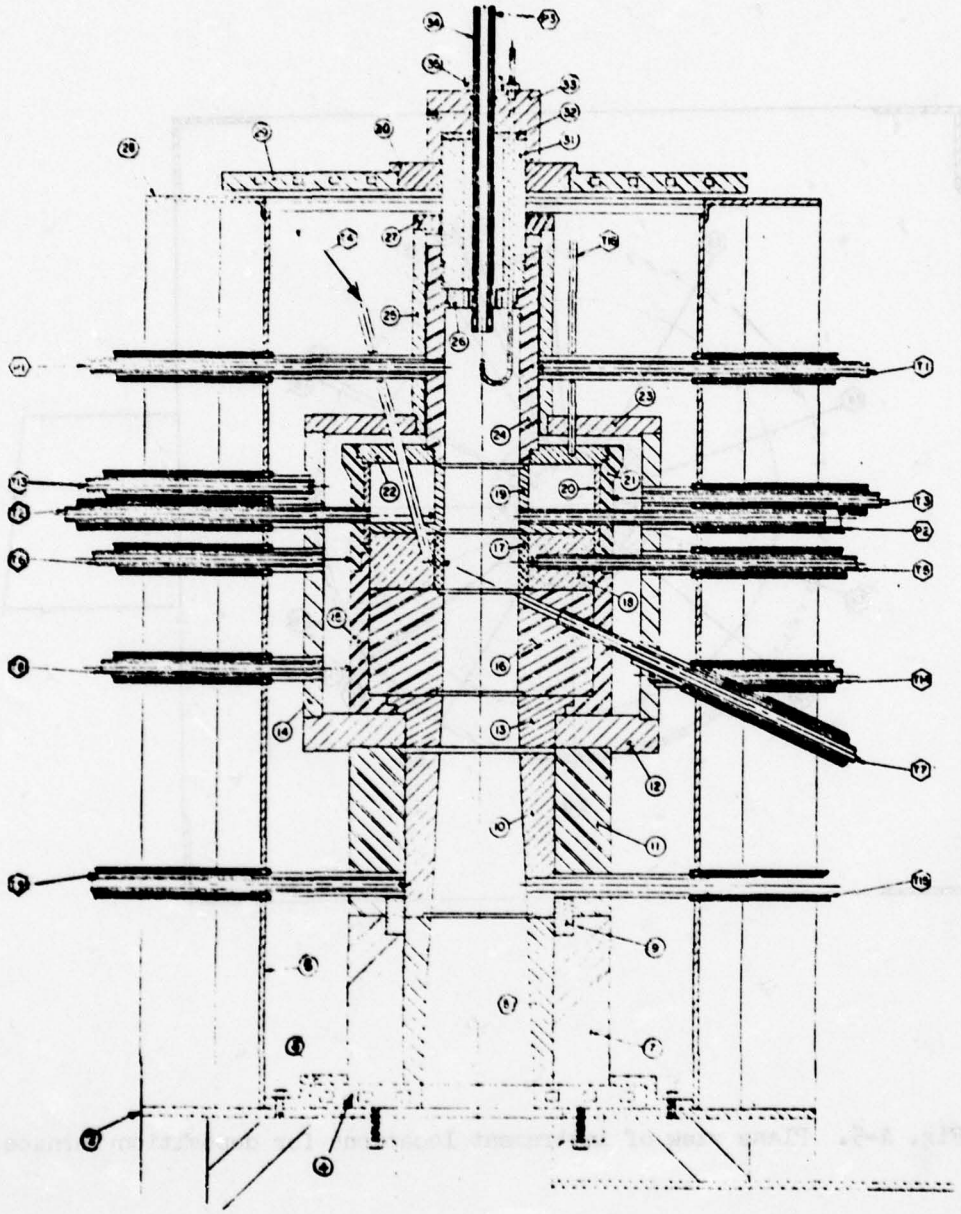

Fig. A-6 . Elevation of deposition furnace.

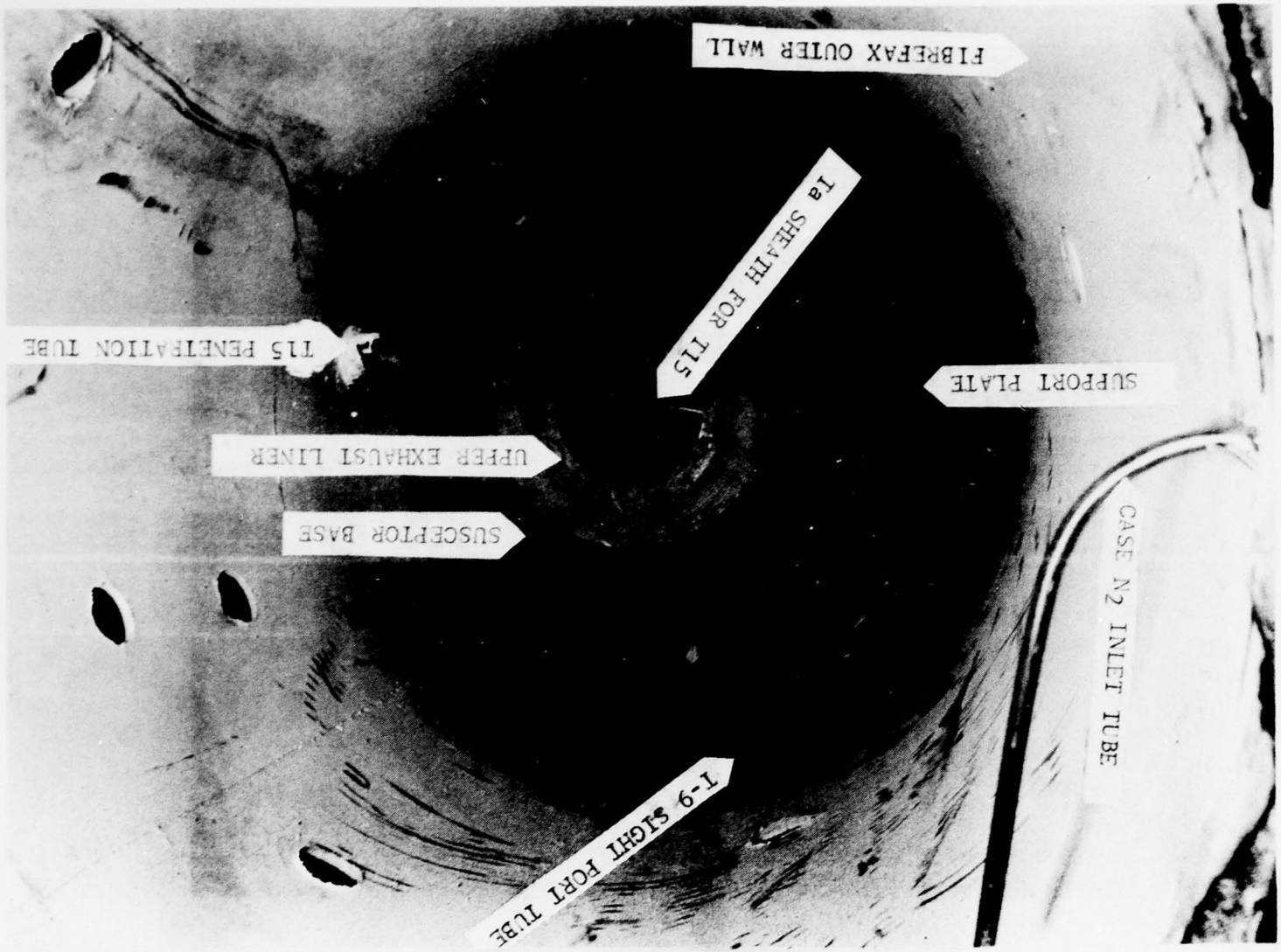

Fig. A-7. Furnace assembly at susceptor support level.

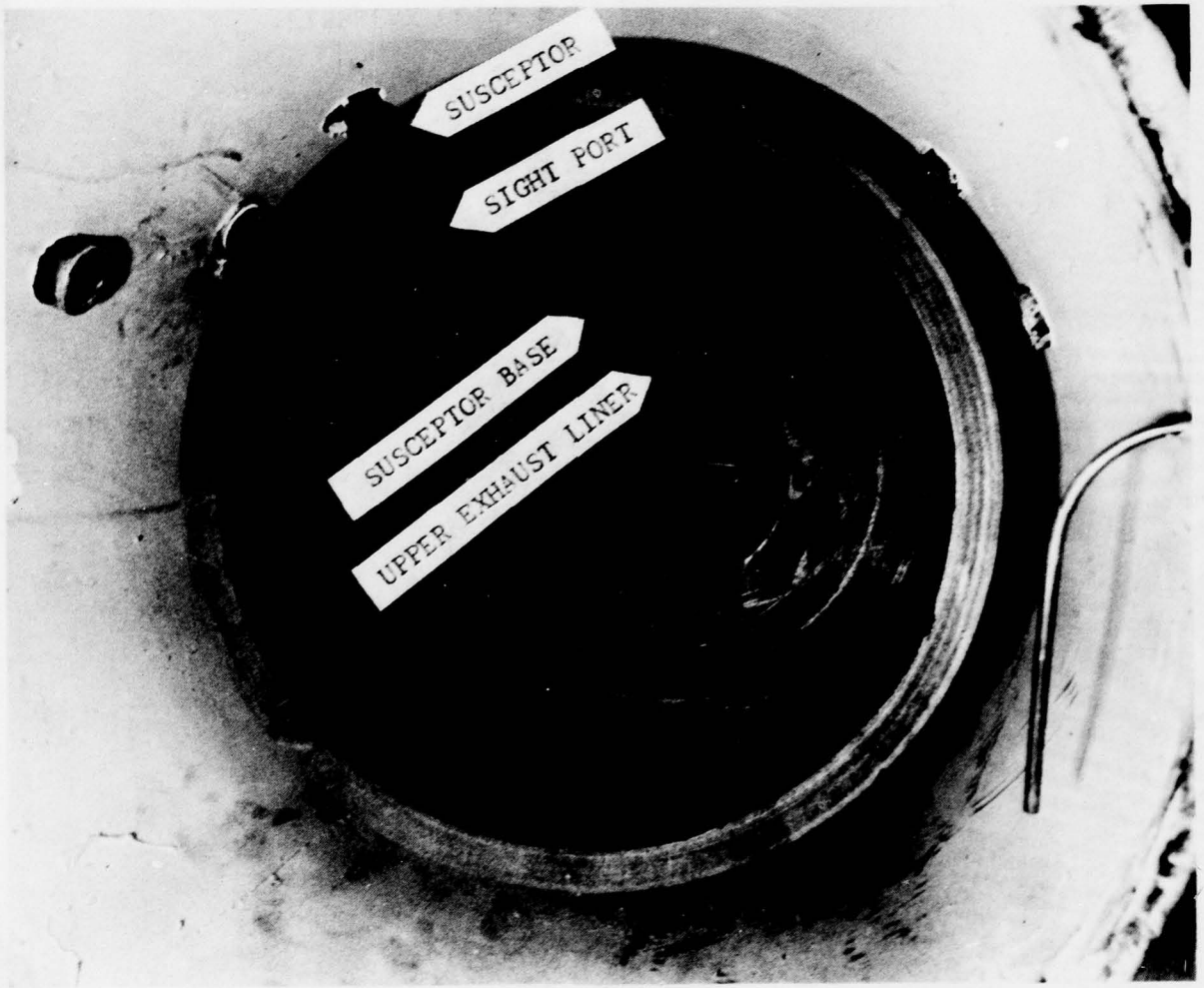

Fig. A-8. Furnace with the addition of susceptor and sight port tubes.

Fig. A-9. Furnace assembly to the lower canister base level.

Fig. A-10. Furnace assembly to the upper canister level.

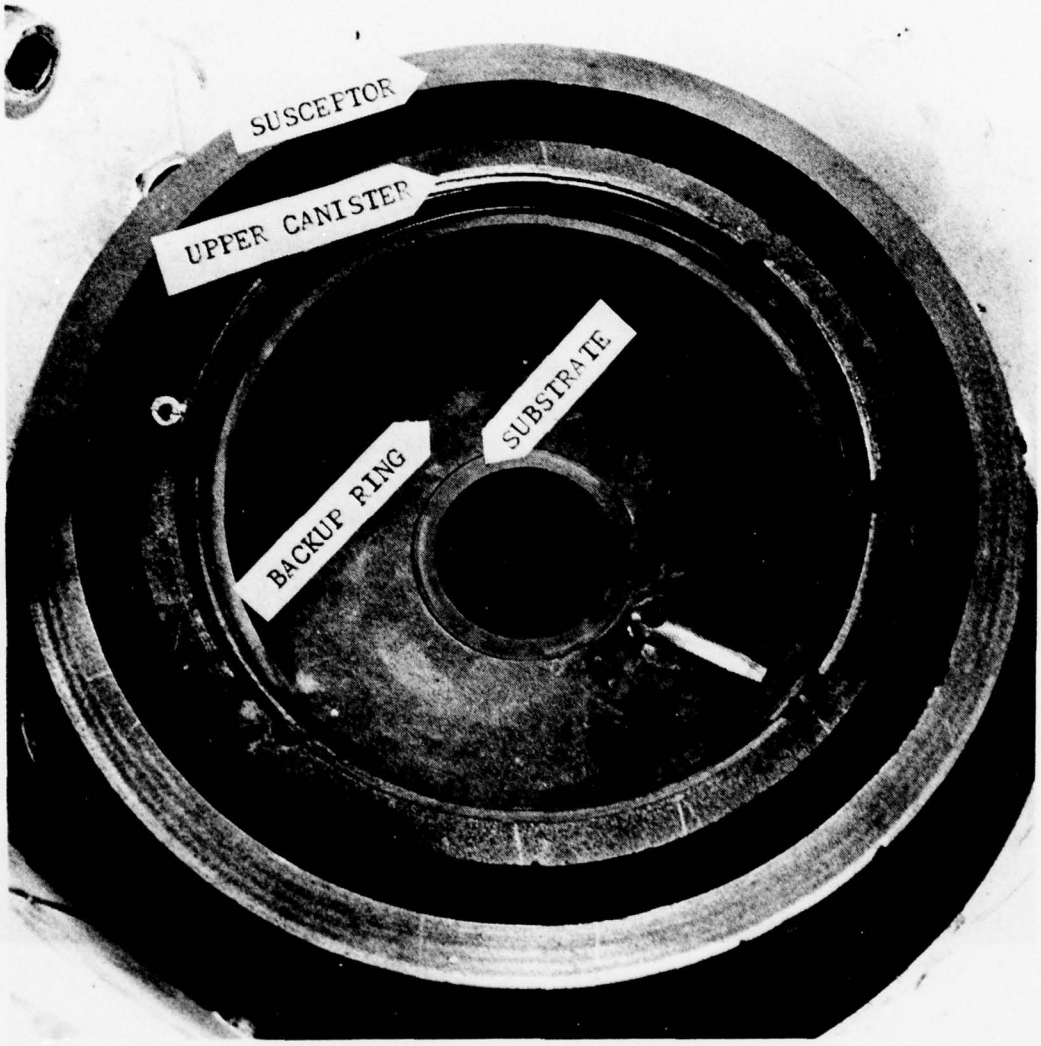

Fig. A-11. Furnace assembly to the backup ring level.

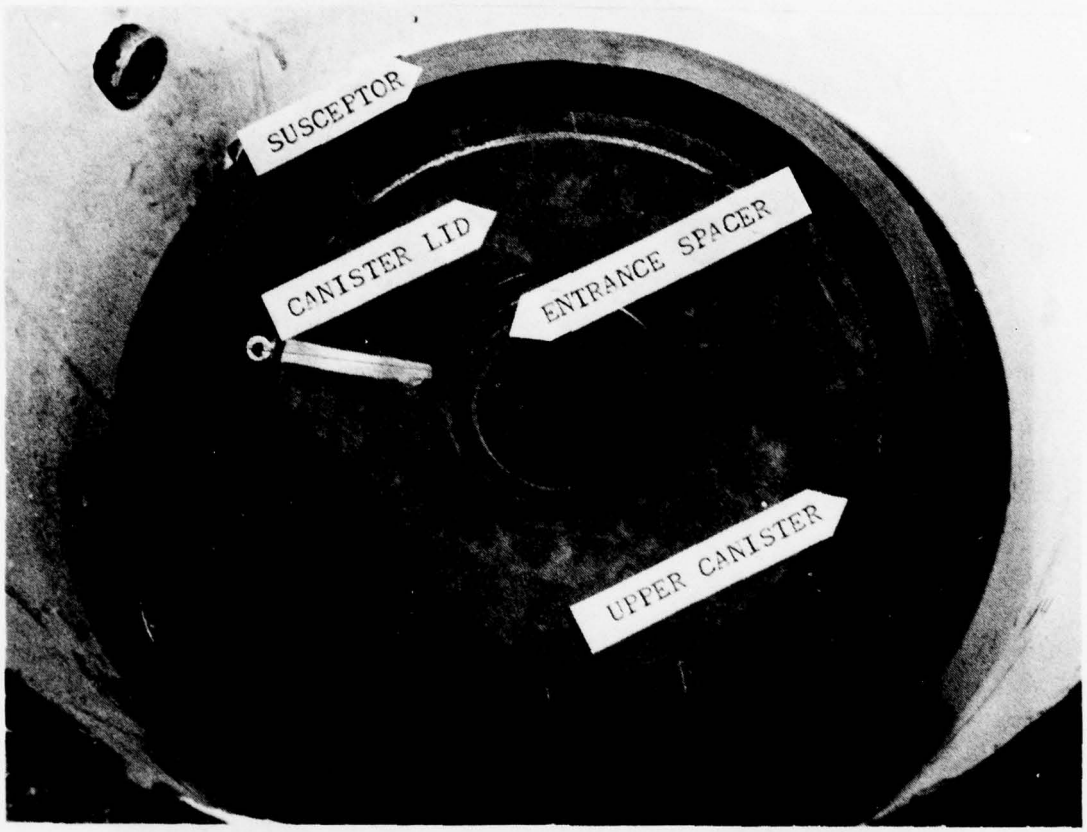

Fig. A-12. Furnace assembly to the canister lid level.

Fig. A-13. Furnace assembly to the lampblack shield level.

TABLE A-I

INSTRUMENTATION LOCATION

Parameter	Circumferential Location (CW)	Distance from Base Plate (mm)	Notes
P-1	37° 35'	1010	
P-2	140° 00'	806	
T-1	289° 42'	1010	
T-2	161° 13'	797	
T-3	58° 11'	832	
T-4	200° 00'	746	Thermocouple measuring location, leads exit between Items 28 and 29.
T-5	332° 43'	745	
T-6	292° 07'	745	
T-7	330° 55'	581	Angled sight port, distance from base plate is at point of penetration of Item 6, furnace case.
T-8	241° 13'	597	
T-9	273° 56'	305	
T-13	36° 22'	845	
T-14	299° 23'	591	
T-15	24° 14'	305	
T-16	90° 00'	895	Thermocouple measuring location, leads exit between Items 28 and 29.

TABLE A-II

MATERIALS OR PARTS

Part Number	Name	Material
1	Furnace exhaust tube assembly	Stainless steel
2	Furnace stand	Aluminum

AD-A058 115 LOS ALAMOS SCIENTIFIC LAB N MEX F/G 11/2
DEVELOPMENT OF PYROLYTIC GRAPHITE/SILICON CARBIDE COMPOSITE MAT--ETC(U)
JUN 78 T C WALLACE, G E CORT, J J DAMRAN W-7405-ENG-36
UNCLASSIFIED AFRPL-TR-78-46-VOL-1 NL

2 OF 3
AD
A058 115

TABLE A-II (continued)

Part Number	Name	Material
3	Furnace base plate	Stainless steel
4	Support plate	Stainless steel
5	Alignment collar	Stainless steel
6	Furnace case	Fibrefrax
7	Susceptor support	Porous carbon
8	Lower exhaust line	HLM graphite
9	Susceptor support ring	Porous carbon
10	Upper exhaust liner	HLM graphite
11	Susceptor support	Porous carbon
12	Susceptor base	HLM graphite
13	Canister base	HLM graphite
14	Susceptor	HLM graphite
15	Lower canister	HLM graphite
16	Exit spacer	HLM graphite
17	Substrate	ATJ graphite
18	Backup ring	HLM graphite
19	Entrance spacer	HLM graphite
20	Canister filler ring	HLM graphite
21	Upper canister	HLM graphite
22	Canister lid	HLM graphite
23	Susceptor lid	HLM graphite
24	Canister extension	HLM graphite
25	Lampblack shield	HLM graphite
26	Spider	HLM graphite
27	Lampblack shield lid	HLM graphite

TABLE A-II (continued)

Part Number	Name	Material
28	Furnace top	Stainless steel
29	Furnace lid	Stainless steel
30	Drive shaft bearing	HLM graphite
31	Drive shaft	HLM graphite
32	Drive shaft extension	HLM graphite
33	Injector seal	303 stainless steel
34	Injector	Copper
35	Injector collar	Stainless steel

base cement. Figure A-14 shows the addiition of the drive shaft and the lamp-black shield. After the last thermocouple was inserted through the susceptor lid, the space between the susceptor and wall was filled with lampblack to within 5-6 in. of the furnace top. The water-cooled furnace lid and the injector seal, added last, were shown in Fig. A-4.

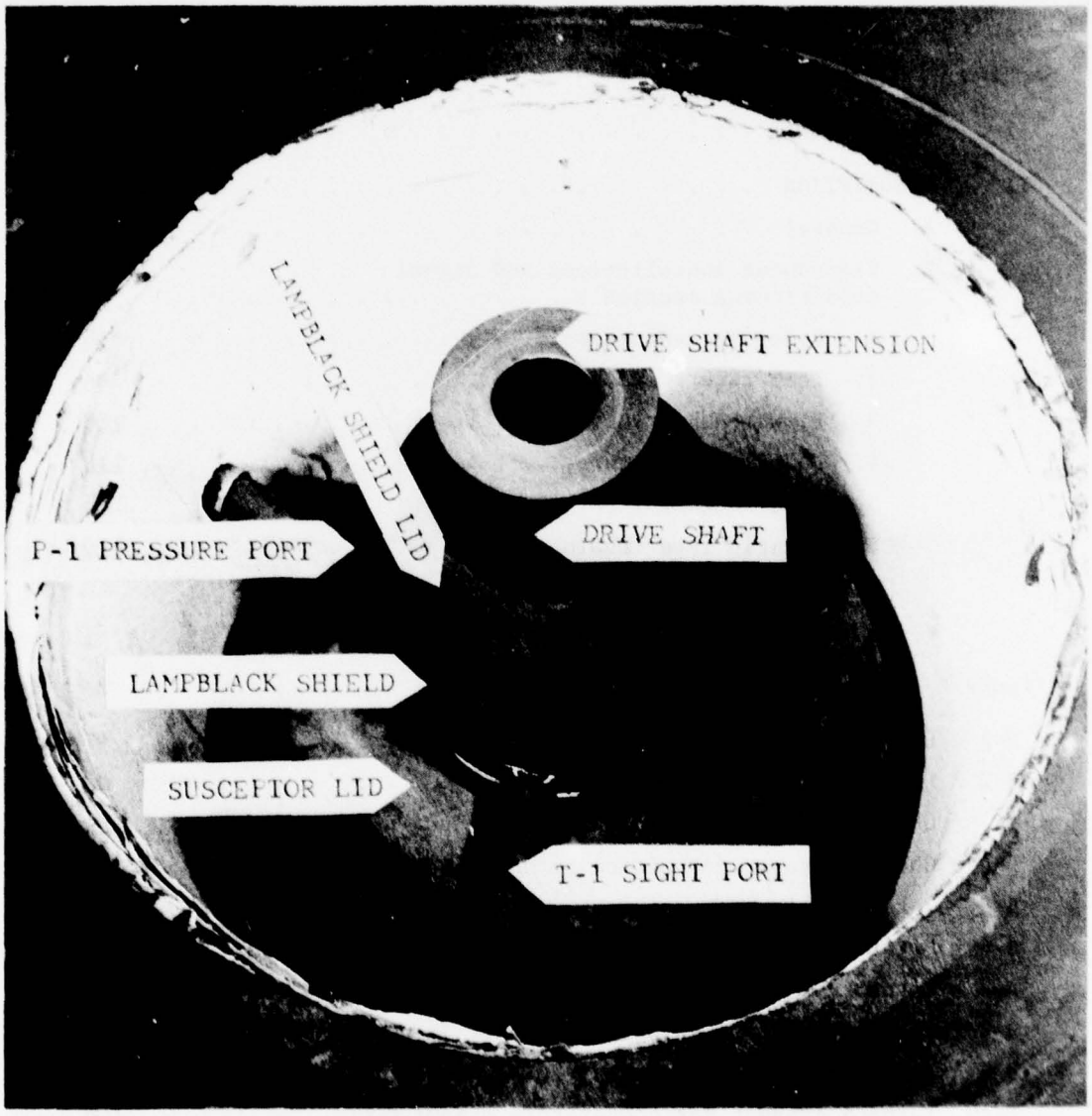

Fig. A-14. Furnace assembly to the drive shaft level.

APPENDIX B

INSTRUMENTATION REQUIREMENTS AND DESCRIPTION

TABLE OF CONTENTS

LIST OF ILLUSTRATIONS

LIST OF ILLUSTRATIONS (continued)

I. REQUIREMENTS

The data acquisition system (DAS) had to measure and record approximately 35 channels of analog data. The end-to-end inaccuracy of each channel was to be ± 2% maximum. The frequency response of each parameter was < 1 Hz, and the resolution had to be at least one part in 1000. The Measurement List (Table B-I) specifies the parameters to be measured, their ranges, and the transducer or method used.

II. DESCRIPTION

A. General.

The DAS consisted of a data logger that multiplexed the 35 analog channels and formatted the data. These data were then recorded on magnetic tape by a seven-track incremental tape recorder. Twenty temperature measurements, five pressure measurements, seven flow measurements, two power measurements and the time of the day were recorded. Two linear distances and one angular position were recorded manually. Figure B-1 shows the measurement locations on the furnace. Figure B-2 is a block diagram of the DAS. Figures B-3 and B-4 show the furnace room and the completly instrumented furnace.

B. Transducer Installations and Signal Conditioning Section.

1. Pressure measurements. Total and static pressures were measured using conventional bonded strain gauge and variable reluctance type pressure transducers. Parameter P-3 was measured just upstream of the injection nozzle by a bonded strain-guage type pressure transducer. Its output was 5 Vdc for 138 kPa full-scale input. The output was connected to a voltage divider to reduce the 5 Vdc to 3 Vdc to be compatible with the 3 Vdc full-scale range of the data logger.

P-1 and P-2 are static pressure measurements made at the wall in the upper section of the coating canister, 51 and 254 mm from the injector, respectively. The pressure inside the furnace was transferred through impulse lines to the pressure transducers mounted about a meter from the furnace. The impulse lines consisted of a 19-mm-dia carbon tube threaded on one end and screwed into the wall of the coating canister. A 6-mm line then connected one of the transducer pressure ports to the carbon tube extending through the furnace wall. The connection between the line and the carbon tube was water-cooled, Fig. B-5. The other transducer pressure port was left open to the atmosphere which made this a gauge-pressure measurement, as the furnace exhaust also was open to the atmos-

TABLE B-I

MEASUREMENT LIST

PARAMETER	PARAMETER DESCRIPTION	RANGE	RESOLUTION	ACCURACY	TRANSDUCER TYPE	TRANSDUCER MANUFACTURER AND PART NUMBER	TRANSDUCER S/N
T-1	Temperature of the OD wall of the coating canister	1310 to 1910K	0.5 K	± 2	Optical pyrometer	R^{2} Thermodot, TD-7B	1121
T-2	Temperature of the OD wall of the coating canister just upstream of the substrate	1435 to 2015K	0.5 K	± 2	Optical pyrometer	Millitron, Therm-O-Scope	177
T-3	Temperature of outside surface of canister	1250 to 2590K	0.5 K	± 2	Optical pyrometer	Micro-Optical	744
T-4	Temperature of backside of substrate	273 to 2200K	0.1 K	± 2	W/WRe T/C	ARI, T-9)8J2D(AE)9)360	---
T-5	Temperature of backside of substrate	1279 to 3592K	0.5 K	± 2	Optical pyrometer	Millitron, Therm-O-Scope	522
T-6	Temperature of outside surface of canister	1834 to 3000K	0.5 K	± 2	Optical pyrometer	Millitron, Therm-O-Scope	568
T-7	Temperature of coating side of substrate	1300 to 2582K	0.5 K	± 2	Optical pyrometer	Millitron, Therm-O-Scope	463
T-8	Temperature of outside surface of canister	1620 to 2480K	0.5 K	± 2	Optical pyrometer	R^{2} Thermodot TD-9FH	132
T-9	Temperature of wall, exhaust duct	1325 to 2780K	0.5 K	± 2	Optical pyrometer	Millitron, Therm-O-Scope	174
T-10	Temperature of outside surface of furnace	273 to 673K	0.06 K	± 2	Type T T/C	---	---
T-11	Temperature of outside surface of furnace	273 to 673K	0.06 K	± 2	Type T T/C	---	---
T-12	Temperature of outside surface of furnace	273 to 673K	0.06 K	± 2	Type T T/C	---	---
T-13	Temperature of outside surface of susceptor	1157 to 4710K	0.5 K	± 2	Optical pyrometer	IRCON, 300	3343
T-14	Temperature of outside surface of susceptor	1200 to 3310K	0.5 K	± 2	Optical pyrometer	Micro-Optical	745
T-15	Temperature of exhaust gas	273 to 2200K	0.1 K	± 2	W/WRe T/C	ARI, T-9)8 18D(AE) 9)360	---
T-16	Temperature of top of coating canister	273 to 673K	0.06 K	± 2	Type T T/C	ARI, T-91R-32 FT9C	---
T-17	Temperature Inlet cooling water	273 to 310K	0.06 K	± 2	Type T T/C	Thermo Electric, T18U-304-0-12-0L	---
T-18	Temperature, room ambient	273 to 325K	0.06 K	± 2	Type T T/C	Thermo Electric, T18U-304-0-12-0L	---
T-19	Temperature cooling water discharge	273 to 373K	0.06 K	± 2	Type T T/C	Thermo Electric, T18U-304-0-12-0L	---
T-20	Temperature cooling water, coil discharge	273 to 373K	0.06 K	± 2	Type T T/C	Thermo Electric, T18U-304-0-12-0L	---
P-1	Pressure of gas in upper section of coating canister	-25 to +25psfd	0.01psf	± 1.5	Variable reluctance	Tavis, P-1088	2348
P-2	Pressure of gas in upper section of coating canister	-25 to +25psfd	0.01psf	± 1.5	Variable reluctance	Tavis, P-1088	2349
P-3	Pressure upstream of injector	0 to 20psig	0.01psi	± 1.5	Bonded strain gage	Std.Controls 212-25-010-03	23525
P-4	Pressure, Static, Profile between injector and substrate	-25 to +25psfd	0.01psf	± 1.5	Variable reluctance	Tavis, P-1088	2366
P-5	Pressure, Total, Profile between injector and substrate	-75 to +75psfd	0.01psf	± 1.5	Variable reluctance	Tavis, P-1088	2365
F-1	Mass flow rate of process N_2	0 to 1416 SLPM	0.1SLPM	± 2	Thermal	Hastings Raydist ANL-50G(L-50F W/H-3M)	361
F-2	Mass flow rate of annulus N_2	0 to 20,000sccm	5.0sccm	± 2	Thermal	Hastings Raydist ALL-50KGX	2172
F-3	Mass flow rate of CH_4	0 to 10 SLPM	0.001SLPM	± 2	Thermal	Tylan GF-348	---
F-4	Mass flow rate of MTS	0 to 9gpm	0.001gpm	± 4	Thermal	Tylan GF-348	---
F-5	Mass flow rate of cooling H_2O	0 to 340.6SLPM	0.01SLPM	± 1	Turbine	Flow Technology, FT-80MFO-LB	80034

TABLE B-I (contd.)

PARAMETER	PARAMETER DESCRIPTION	RANGE	RESOLUTION	ACCURACY	TRANSDUCER TYPE	TRANSDUCER MANUFACTURER AND PART NUMBER	S/N
F-6	Mass flow rate, $\dot{m}$	0 to 68LPM	0.0018LPM	± 2	Thermal	Tylan, GF-348	---
F-7	Flow rate ratio, $\dot{m}_f/\dot{m}$	0 to 30%	0.001	-	Calculated	Tylan, GF-348	---
W-1	Total 10KHz power to furnace	0 to 125KW	0.1KW	± 1.5	Transformer	LASL	---
W-2	Apparent power (EXI)	0 to 125KW	0.1KW	± 1.5	Transformer	LASL	---
Time	Test Time	0 to 365 days	1 Sec.	± 0.01 Sec.	DAS clock	Doric Scientific	---
D-1	Distance of P-4 & P-5 from injector	0 to 11.55 inches	0.01 inch	± 0.05 inch	Linear Rule	---	---
D-2	Distance of T-15 from inner wall	0 to 5 inches	0.01 inch	± 0.05 inch	Linear Rule	---	---
ϕ-1	Angle of P-4 & P-5 from furnace center line	80 degrees	0.85 degree	± 0.5 degree	Protractor	---	---

phere. A 5:3 voltage divider was used on the transducer output signal, to scale its output to the full-scale input that the data logger required.

The static and total pressure measurements, P-4 and P-5, respectively, were measured axially from 25 to 289 mm from the injector face. At each 102-mm increment from the injector, the Pitot tube was swung through an arc of ± 80 degrees, dwelling at every 5 degrees to obtain data. The configuration of the tantalum tubing Pitot tube is depicted in Fig. B-6. Figure B-7 shows the connections of the impulse lines from the pressure transducers to the Pitot tube. It also depicts the measurement setup for parameters D-1 and ϕ-1. The 12-mm-thick clear plastic sheet had a line scribed on both sides to eliminate errors associated with parallax when measuring the angular position of the Pitot tube. The pressure transducers' reference pressure ports were left open to the atmosphere to yield the same results as those described above for P-1 and P-2. Again, the 5-Vdc full-scale output signal was connected to a 5:3 voltage divider before being connected to the data logger.

2. Temperature measurements. Temperature was measured using copper versus Constantan (Type T) and W-5% Re vs W-26% Re thermocouples, total radiation pyrometers, and two-color pyrometers.

The low-temperature measurements (273-673 K) were measured using Type T thermocouples (TC) with ungrounded junctions. The TCs were 3 mm dia with a stainless steel sheath. Parameters measured with this TC configuration were T-17, T-18, T-19, and T-20. Figure B-8 shows a typical installation.

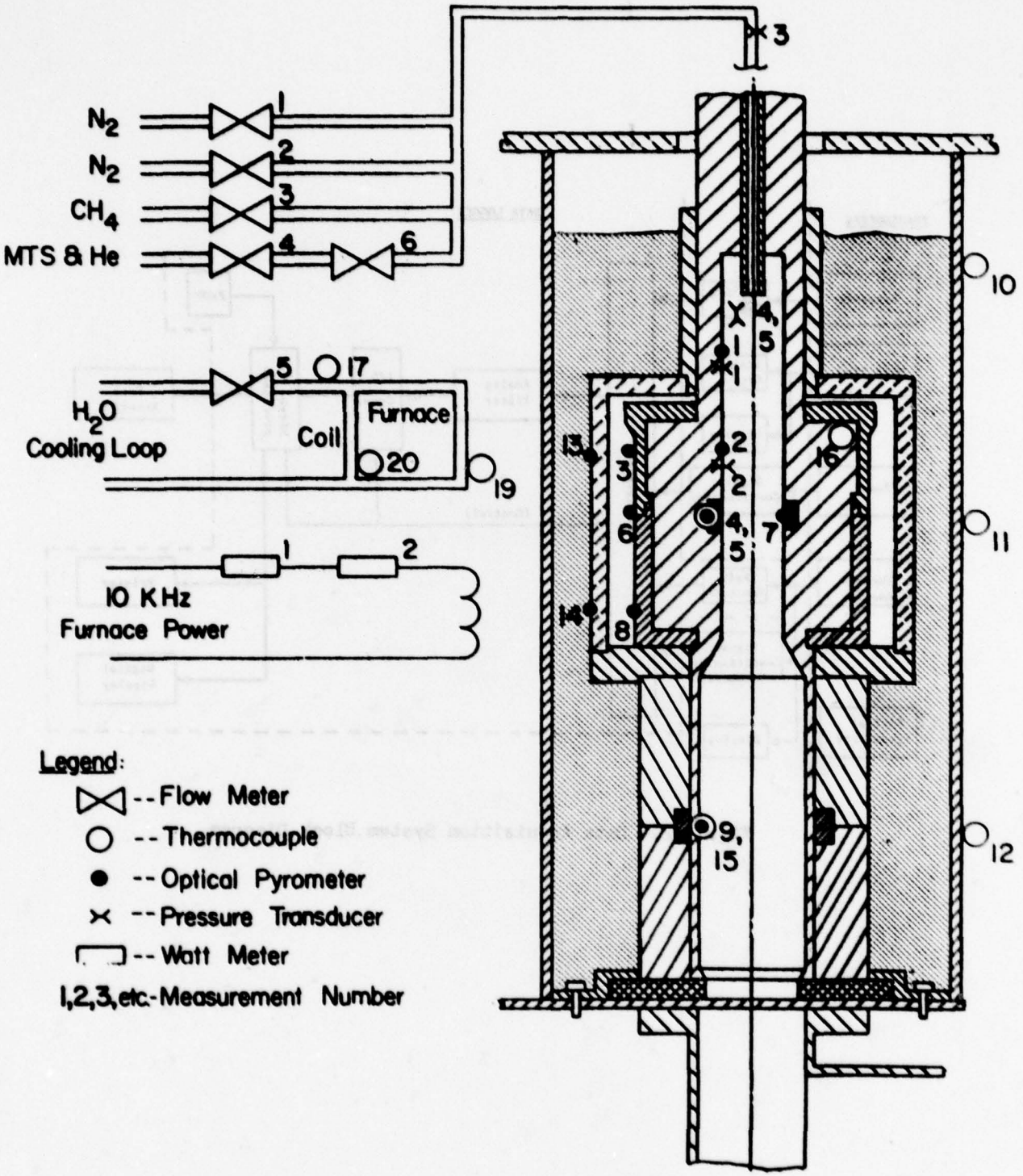

Fig. B-1. Parameter location.

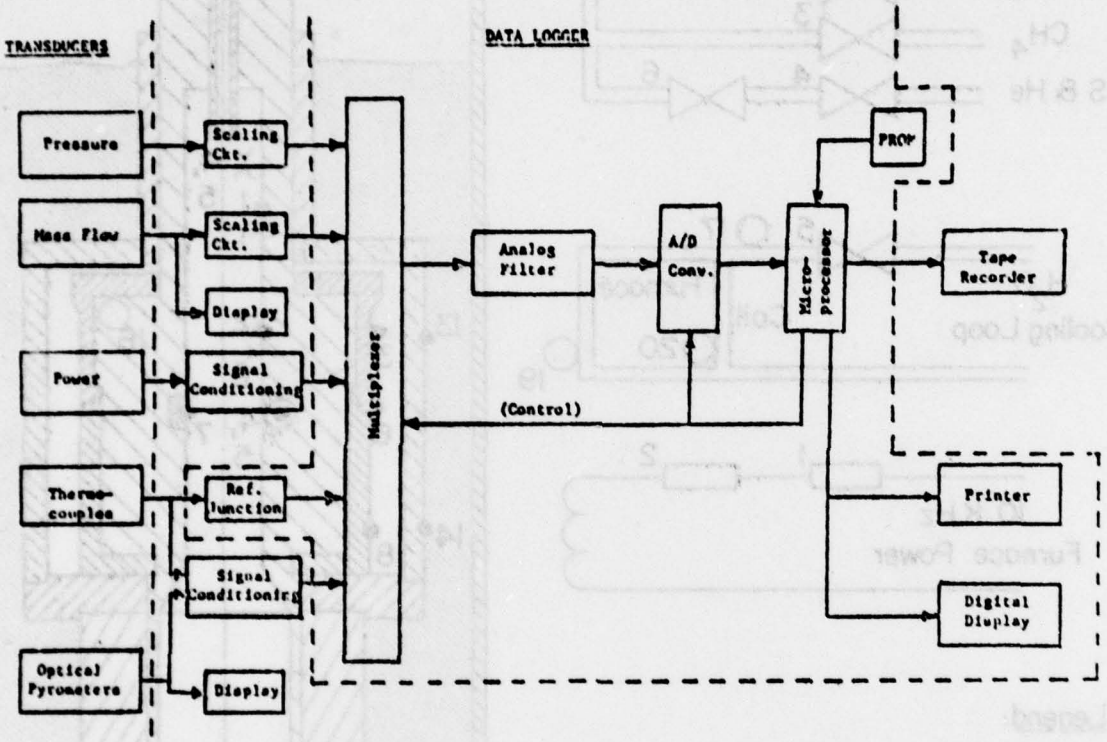

Fig. B-2. Data Acquisition System Block Diagram.

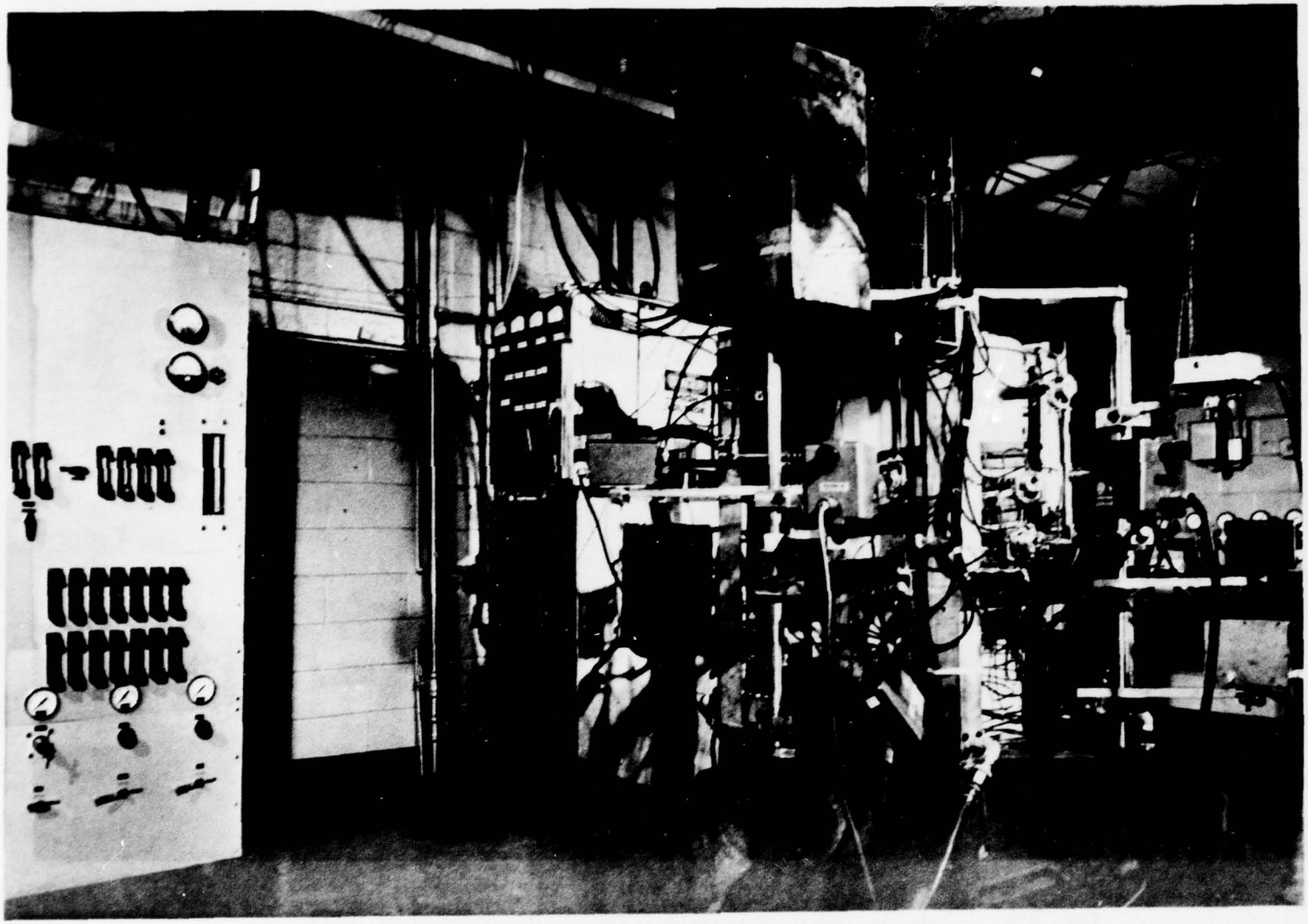

Fig. B-3. Chemical vapor deposition furnace instrumentation (I).

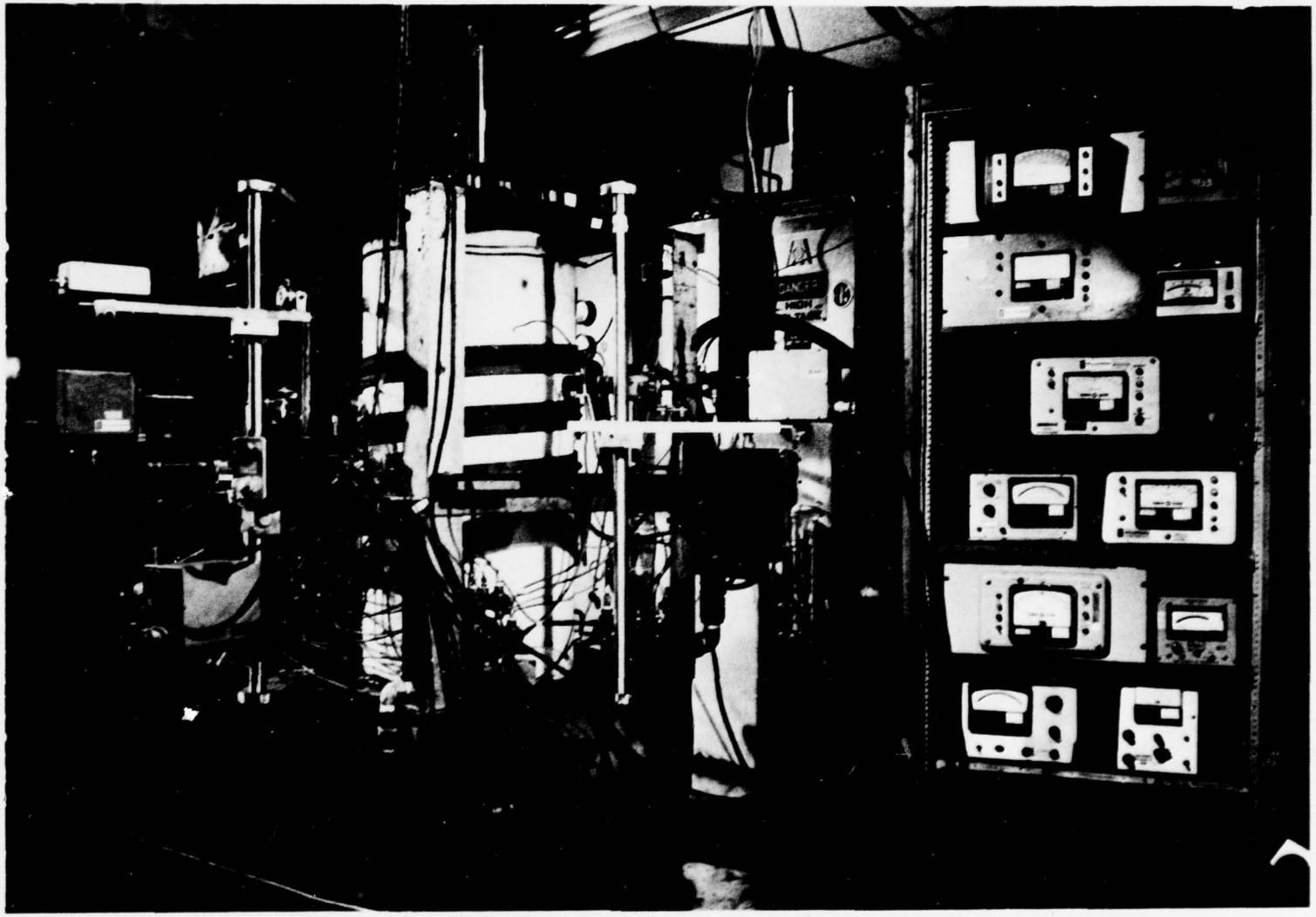

Fig. B-4. Chemical vapor deposition furnace instrumentation (II).

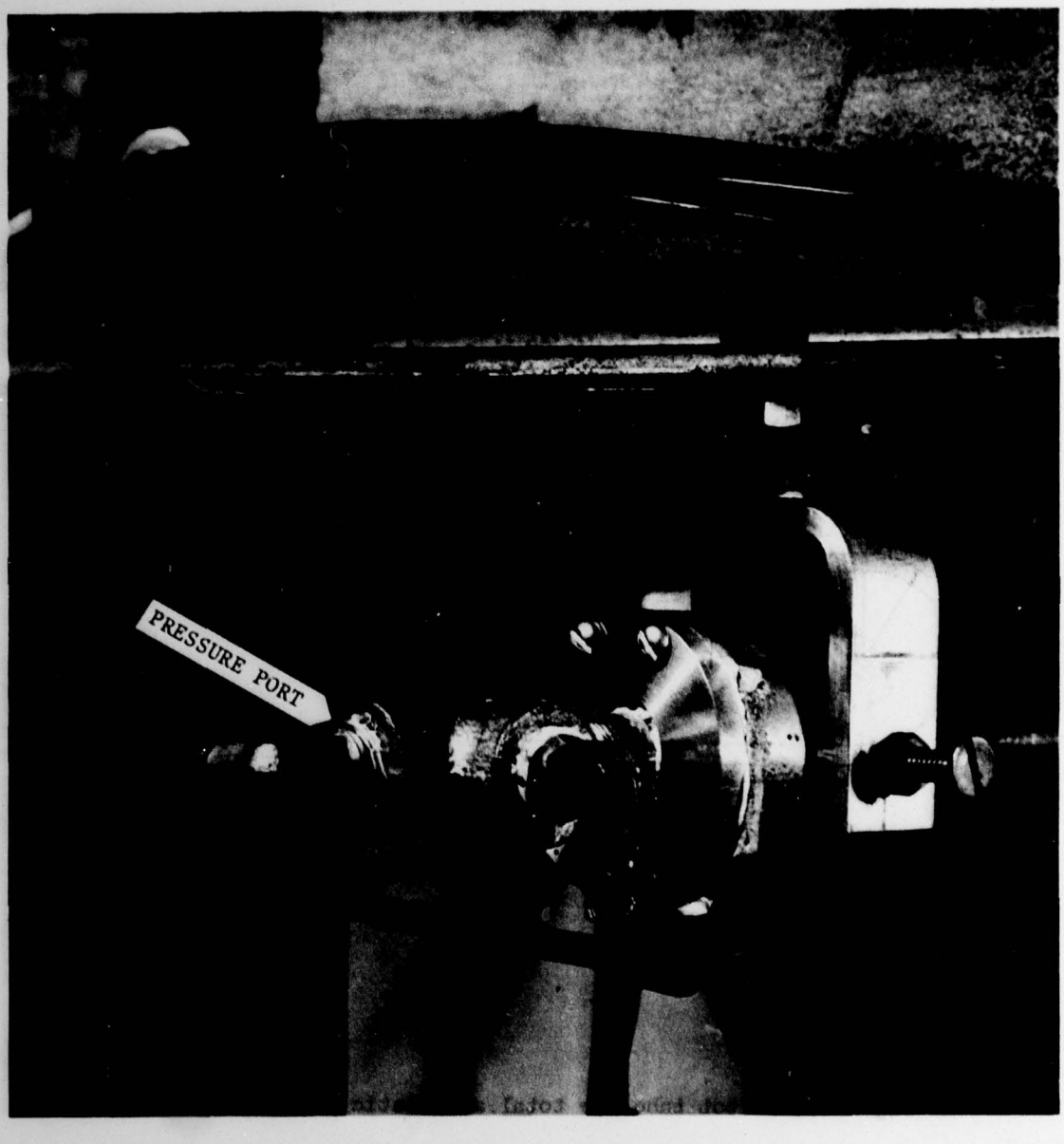

Fig. B-5. Water-cooled pressure port.

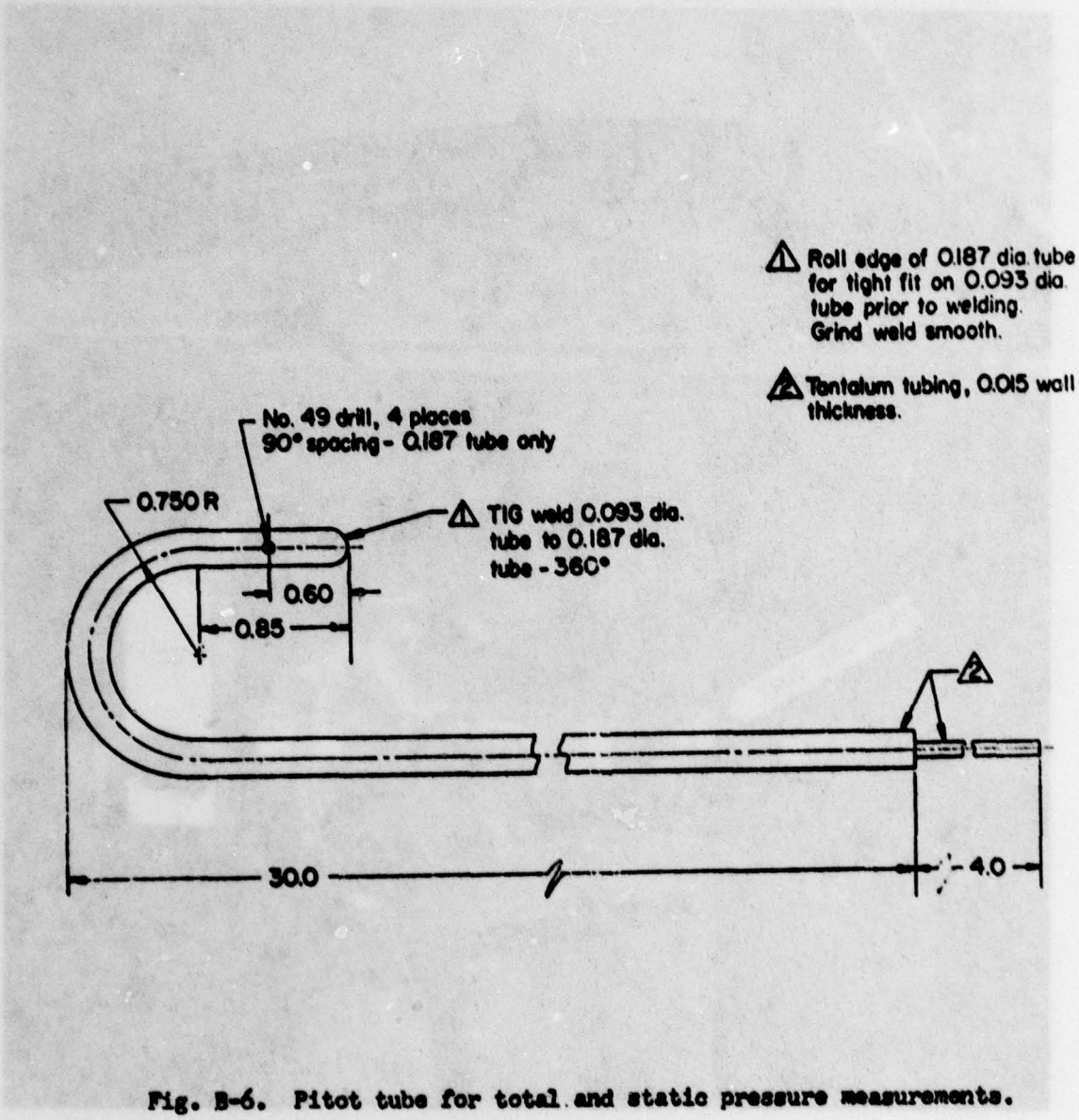

Fig. B-6. Pitot tube for total and static pressure measurements.

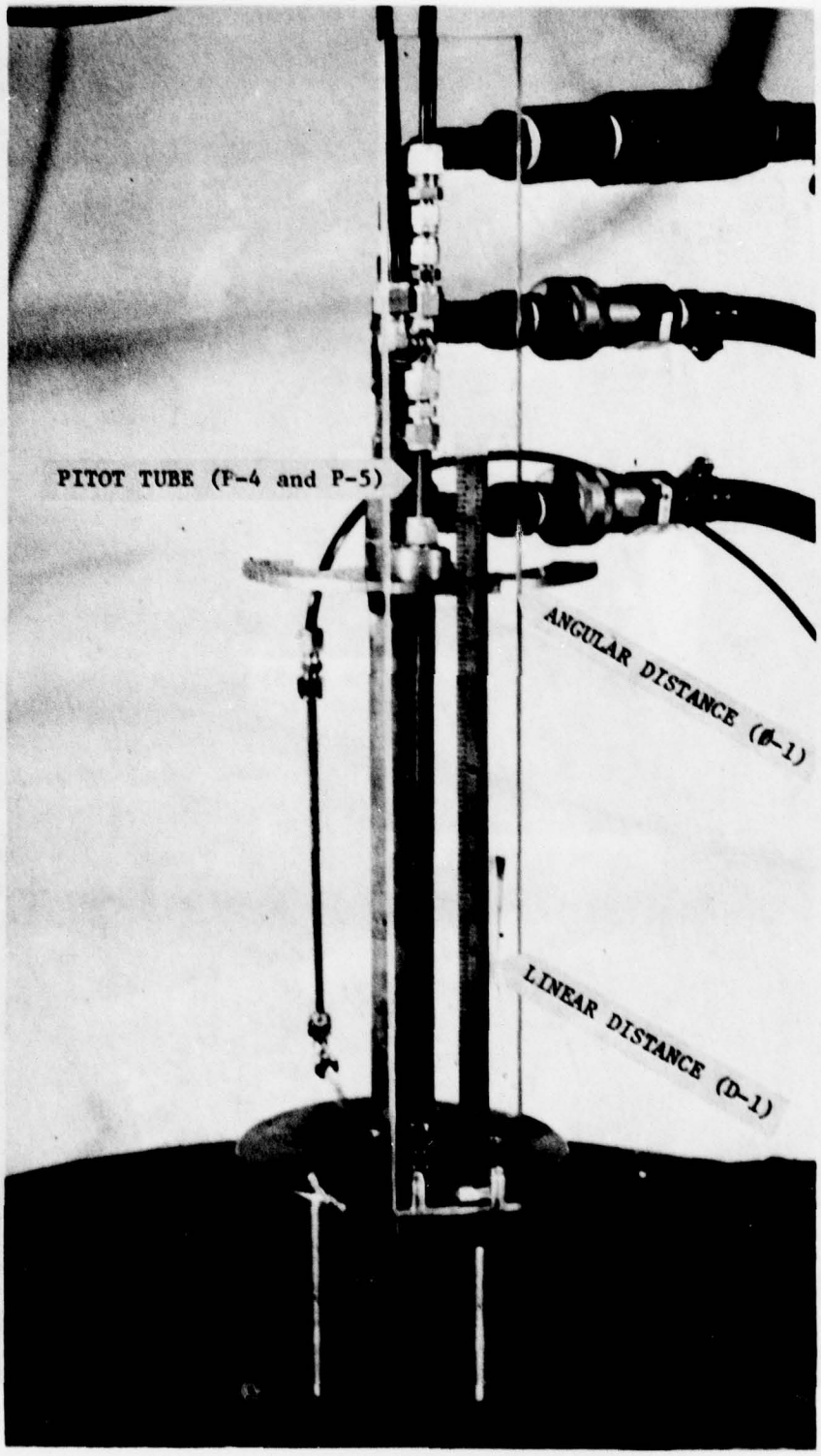

Fig. B-7. Pitot tube position measurement technique.

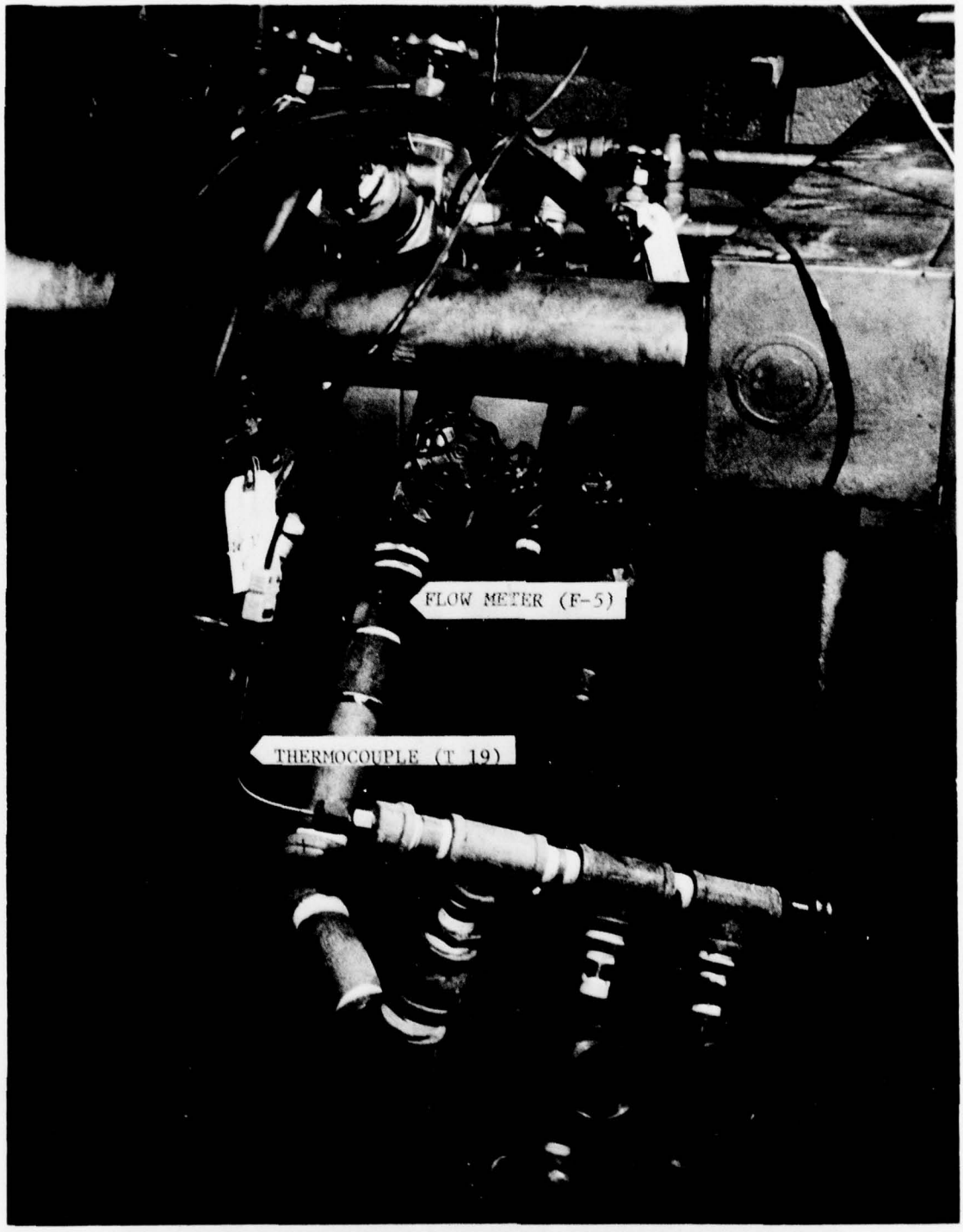

Fig. 3-8. Thermocouple and turbine flowmeter installation.

Parameters T-10, T-11, and T-12 were measured by use of a bare wire junction placed on the surface of the Fiberfax insulation. This junction was bonded to the surface with a Fiberfrax base cement and insulated from the atmospheric cooling and heating affects by silicon rubber. Each measurement device consisted of three junctions wired in parallel and placed in a horizontal plane around the furnace. The three junctions were spaced approximately 120 degrees apart. This configuration was used to obtain an approximate average of the furnace surface temperature in three parallel planes. Figure B-9 shows a typical junction installation.

The remaining type-T TC measurement was T-16. This unit was a 6.35-mm-dia stainless steel sheath TC inserted into a tantalum thermowell. This TC was used to extend the range of T-4 to room ambient. The tantalum thermowell was used to capture and contain the stainless steel and MgO insulation when it melted, as the temperature at this location was expected to exceed 1800 K.

The reference junction for the Type-T TCs was contained within the data logger. Premium grade, shielded TC extension wire was used to connect the TCs to the data logger.

The parameters T-4 and T-15 were measured using ungrounded, W-5% Re vs W-26% Re TCs. The TC sheath was 3-mm dia tantalum, and compacted beryllia (BeO) was used to connect the units to a room temperature reference junction. The TC that measured T-4 was wrapped in 42 turns of a 0.025-mm-thick tantalum foil, and this assembly was inserted into a tantalum thermowell, 12.7 mm in diameter and 0.38 mm thick. This completed assembly was to protect the TC from being contaminated with carbon for approximately 100 h at 2035 K.

The TC that measured T-15 was inserted into a 0.38-mm-thick tantalum sheath that had been installed in the furnace. Pressure fittings were used on the furnace exterior to seal the installation from an exhaust gas leak. Figure B-10 shows the water-cooled port and TC installation. A shield was installed inside the furnace to minimize thermal radiation errors. The TC was inserted inside the 12.7-mm-diam tantalum tube shown in Fig. B-11. During installation, the shield was rotated and locked in place so that the slots in it were placed at approximately 45 degrees to facilitate gas flow through the shield.

The total radiation pyrometers were used to measure parameters T-1, T-3, T-8, T-13, and T-14. These pyrometers respond to a particular band or "window" within the radiation spectrum resulting from the thermal excitation of matter.

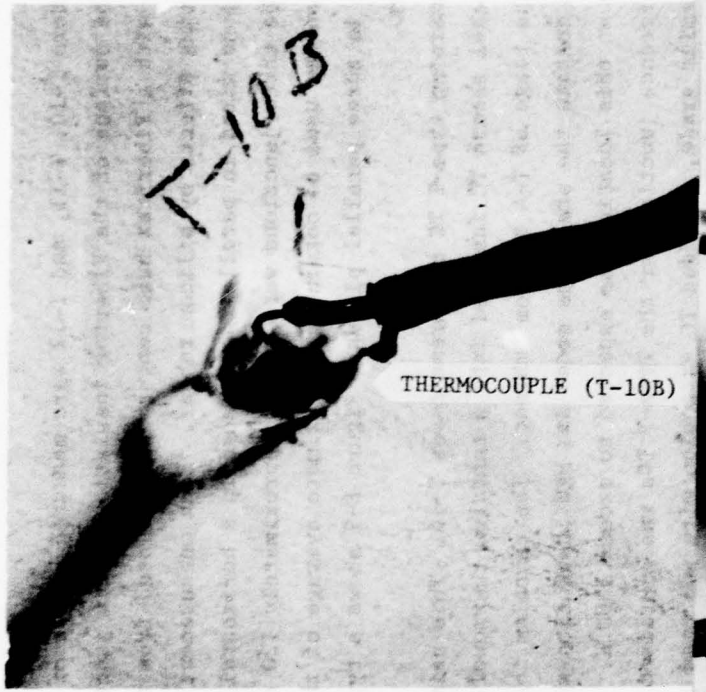

Fig. B-9. Furnace surface temperature measurement.

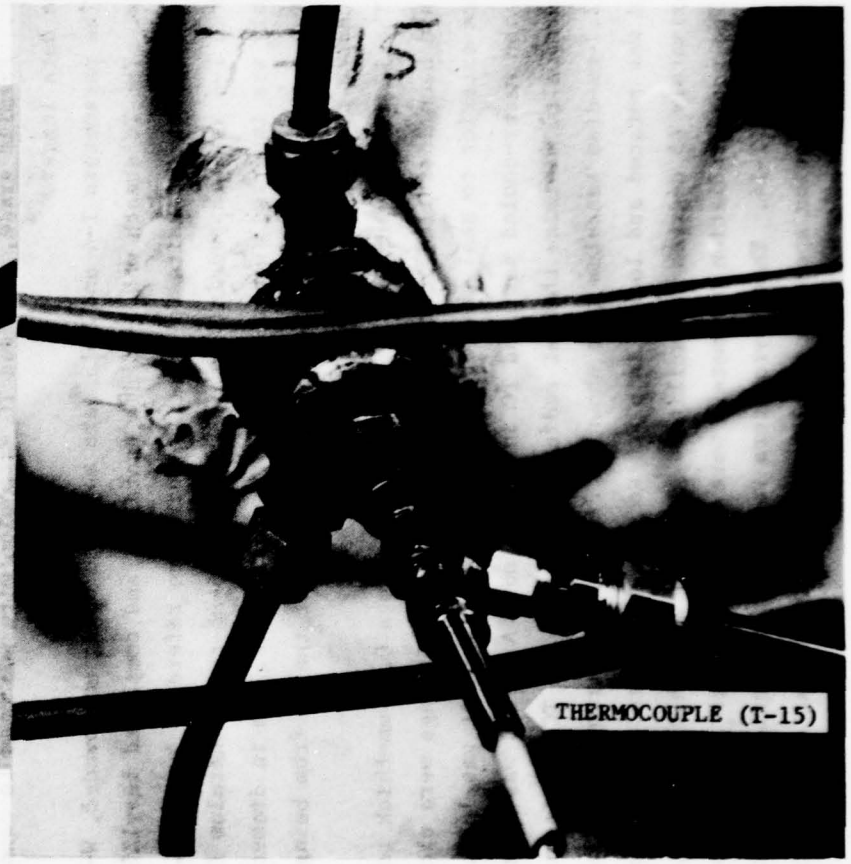

Fig. B-10. Furnace exhaust gas temperature measurement.

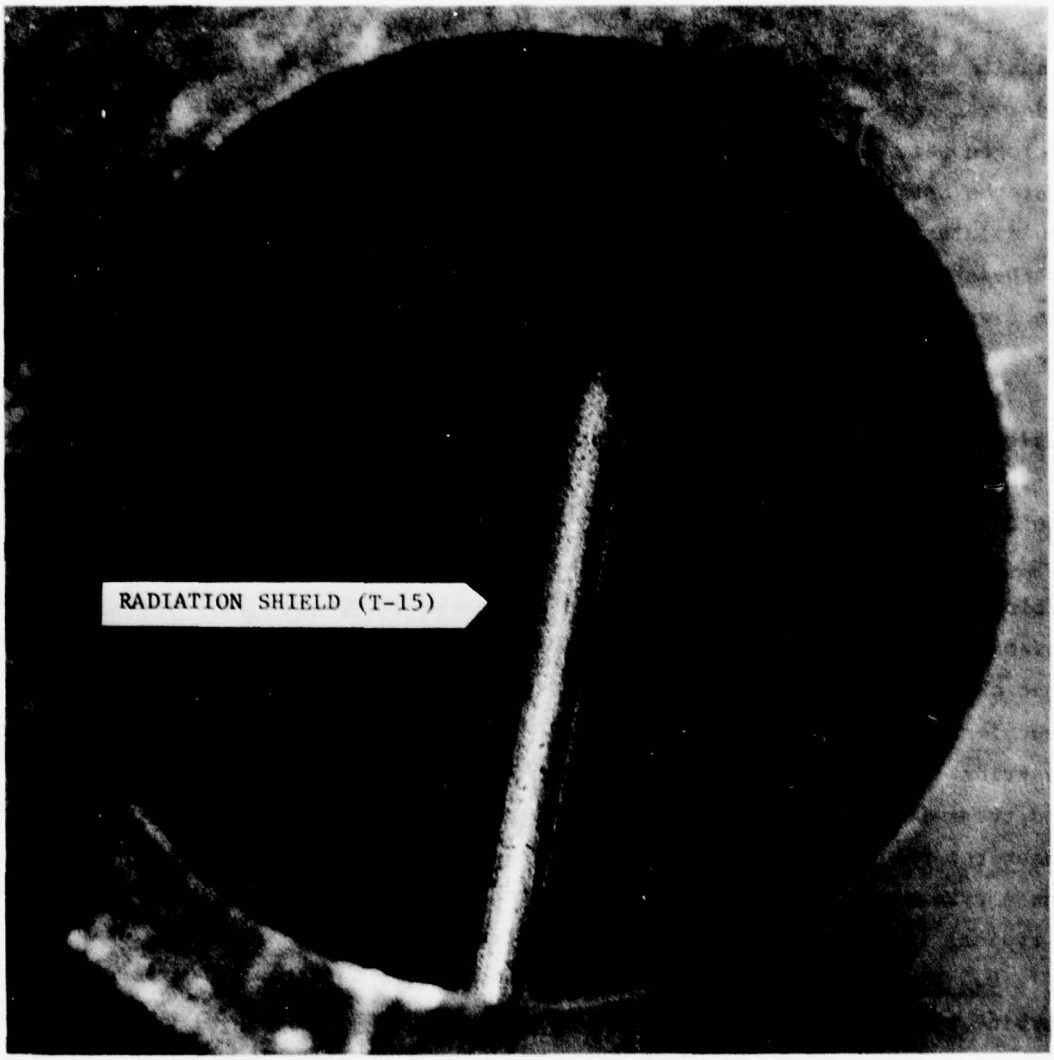

Fig. B-11. Thermocouple thermal radiation shield.

Most of the units used responded to a relatively narrow bandwidth within the ir spectrum; the particular wavelength depended upon the temperature range of the instrument.

Each pyrometer "looked" through a clear fused quartz window, and into a graphite tube to the surface whose temperatue was to be measured. The window mount was water-cooled, and the graphite tube was constantly purged with dry nitrogen gas. The purging was necessary to keep the window clean and to insure that the optical path to the target was free of solid and gaseous matter that would interfere with an accurate temperature measurement (nitrogen is transparent at these wavelengths). Typical installations are shown in Figs. B-12 and B-13. The signals from several of the instruments had to be amplified before being presented to the data logger for range matching..

Two-color pyrometers were used to "look" through a gas with varying composition to the surface to be measured. As mentioned earlier, any radiation-attenuating material in the optical path between the radiant source and detector would affect the readings.

It is theoretically possible to eliminate these errors by using the principle of ratio pyrometry. In this type of measurement, the ratio of the radiant powers in two wavebands is measured. Wein's Law may be operated on to demonstrate that the ratio of the power in two wavebands emmited by a heated object is a function of the temperature only. Such a ratio characterizes the temperature distribution regardless of geometry, emmittance (if the material is a gray body), and transmittance. If the two wavebands are suitable, a linear relationship between the ratio and temperature over a wide range of temperatures can be obtained. These pyrometers were mounted like the total radiation units. Figure B-12 shows a typical installation for measurements T-2, T-5, T-6, T-7, and T-9.

3. Flow measurements. Flow rates and mass flow rates were measured using turbine type type flowmeters, respectively. The parameters encompass a range extending from 3 g/min to 10 ft^3/min. All the flowmeters were installed so that a minimal length of straight pipe with constant diameter was connected to the inlet and outlet of the flowmeters. The length of this straight section was at least five times and three times the flowmeter diameter for the flowmeter inlet and outlet, respectively. All the output signals were 5 Vdc full scale. They were reduced to 3 Vdc full scale by a 5:3 voltage divider before being applied to the data logger's input.

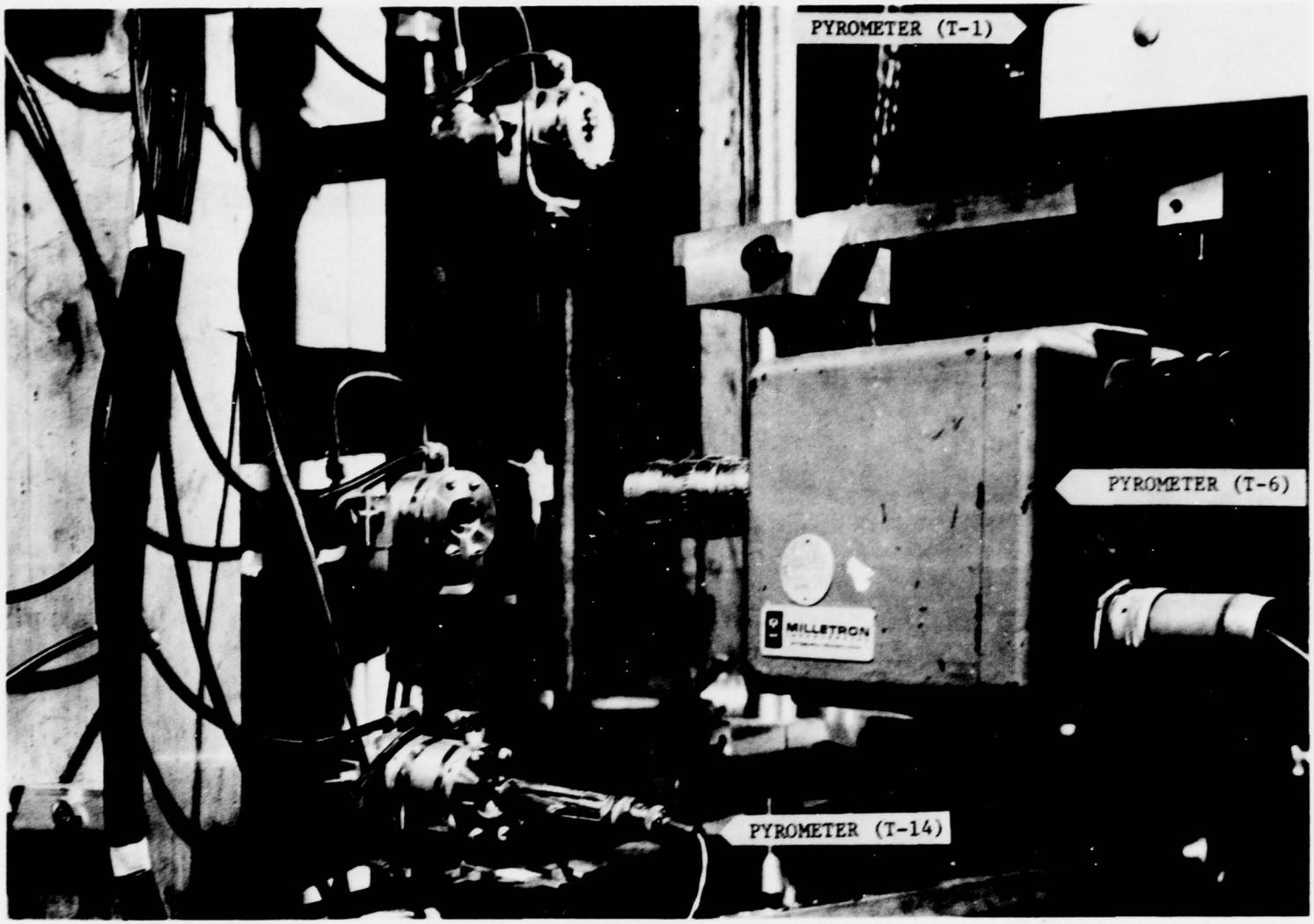

Fig. B-12. Typical optical pyrometer installation.

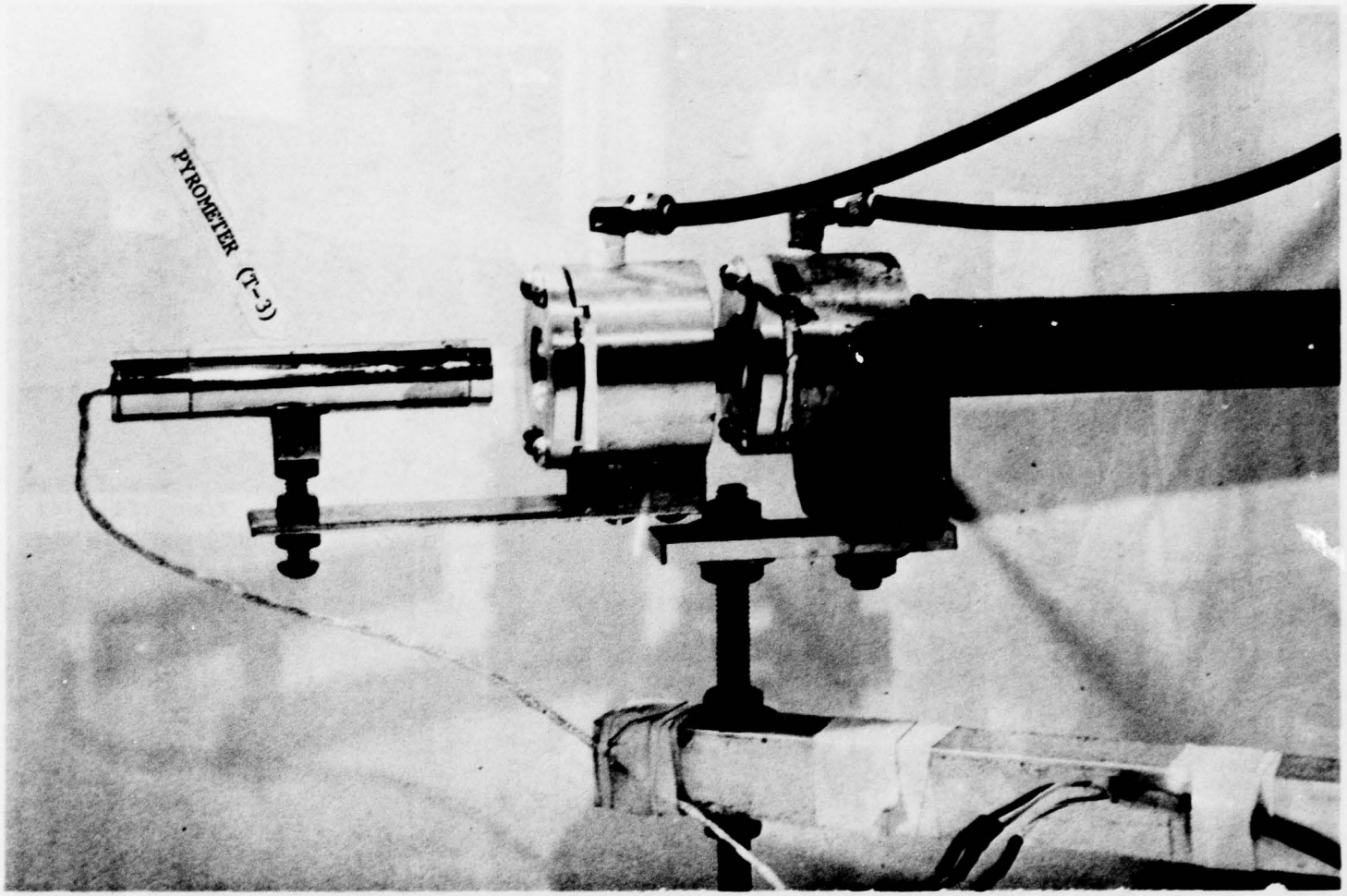

Fig. B-13. Optical pyrometer and sight tube installation.

Parameters F-1 and F-2 were measured by a thermal-type mass flow-meter. The units measured true mass flow without corrections or compensations for the temperature and pressure of the gas. They operate on the thermal principle which depends on the mass flow of the gas and its heat capacity to change the temperature along a heated conduit. This temperature change is measured by a built-in arrangement of thermocouples and does not require any sensing elements or projections into the flow stream. Figures B-14 and B-15 show the F-1 and F-2 installation, respectively.

The parameters F-3, F-4, and F-6 were measured by use of a similiar principle. As stated earlier, the temperature rise of a gas is a function of the amount of heat added, the mass-flow rate, and gas properties. These mass-flow meters incorporate two resistance type temperature sensors wound adjacent to each other on the outside of a sensor tube. They form part of a bridge circuit and have 40-mW power dissipation each. When there is no flow in the tube, both sensors are at the same temperature, the bridge is balanced, and the output signal is zero. When there is flow in the tube, the upstream sensor is cooled and the downstream sensor is heated, which produces a signal from the bridge proportional to flow. This signal is then amplified and linearized.

To facilitate accurate control of these parameters, controllers were used to set and regulate their mass flow rate. The controller for the methane (CH_4) was a standard proportional controller, whereas that for the methyl trichlorosilane (MTS) was unique. The MTS mass flow rate is controlled by controlling the mass flow rate of gaseous helium. This is accomplished as follows: helium carrier gas is injected into the bottom of a tank of liquid MTS. A controller using the above thermal principle measures and controls the helium mass flow rate as a function of the demand for MTS. As the carrier gas bubbles through the liquid MTS, it vaporizes the liquid and the combination (He and MTS) passes through a second thermal flowmeter. This second unit has one self-heated element positioned in a cavity through which the carrier gas flows and another in a cavity through which the mix flows. These elements conduct heat through the gases to the base. The temperature difference between the element and the base is proportional to the thermal conductivity of the gas. The thermal conductivity of the mixed gases depends on the ratio of source to carrier. By comparing the temperature of the element on the carrier side to that of the element of the mixture side, and with proper amplification and linerazation, a 0- to 5-Vdc output signal is obtained for zero to full-scale ratio. Another circuit electron-

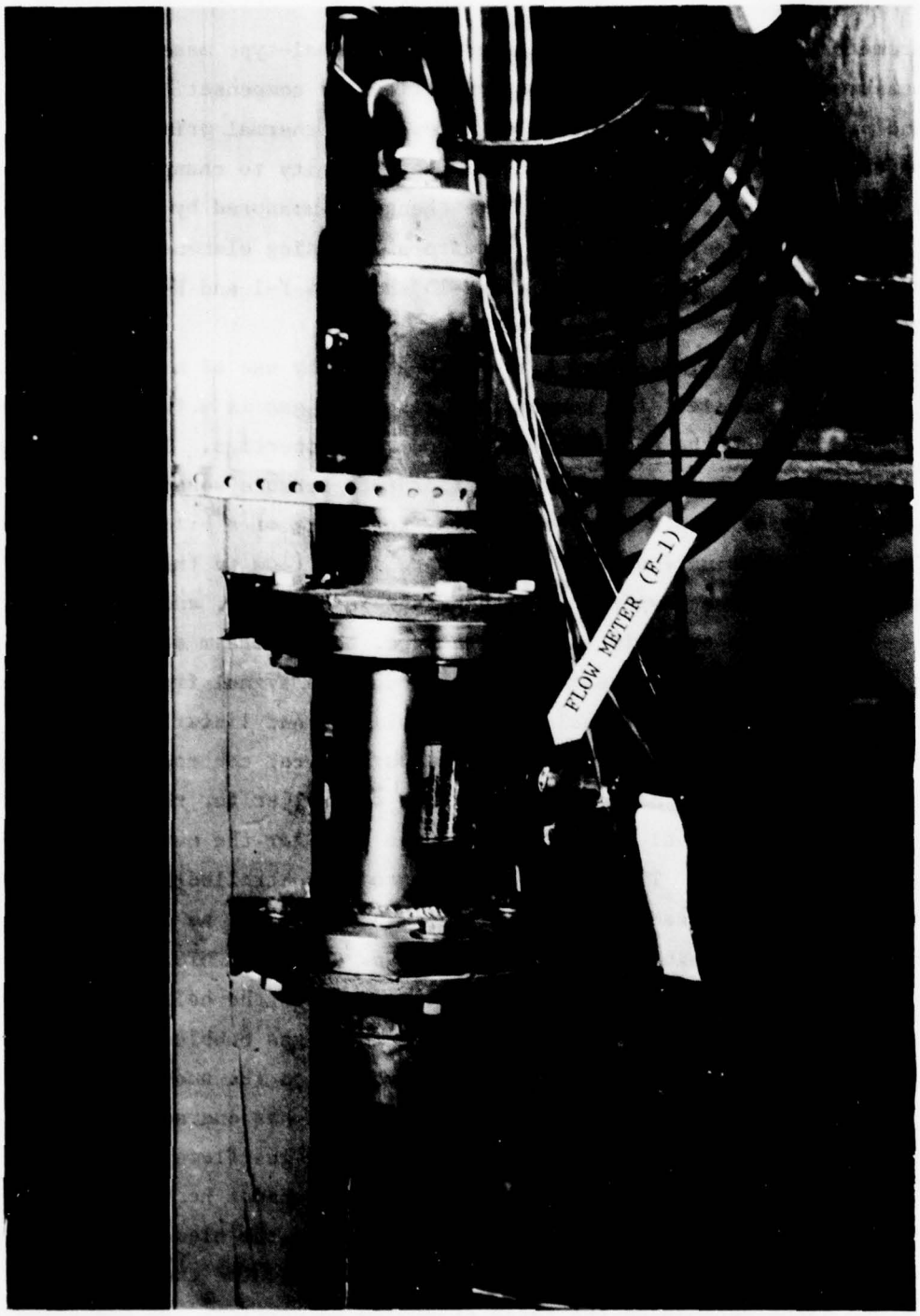

Fig. B-14. Process N_2 flowmeter installation.

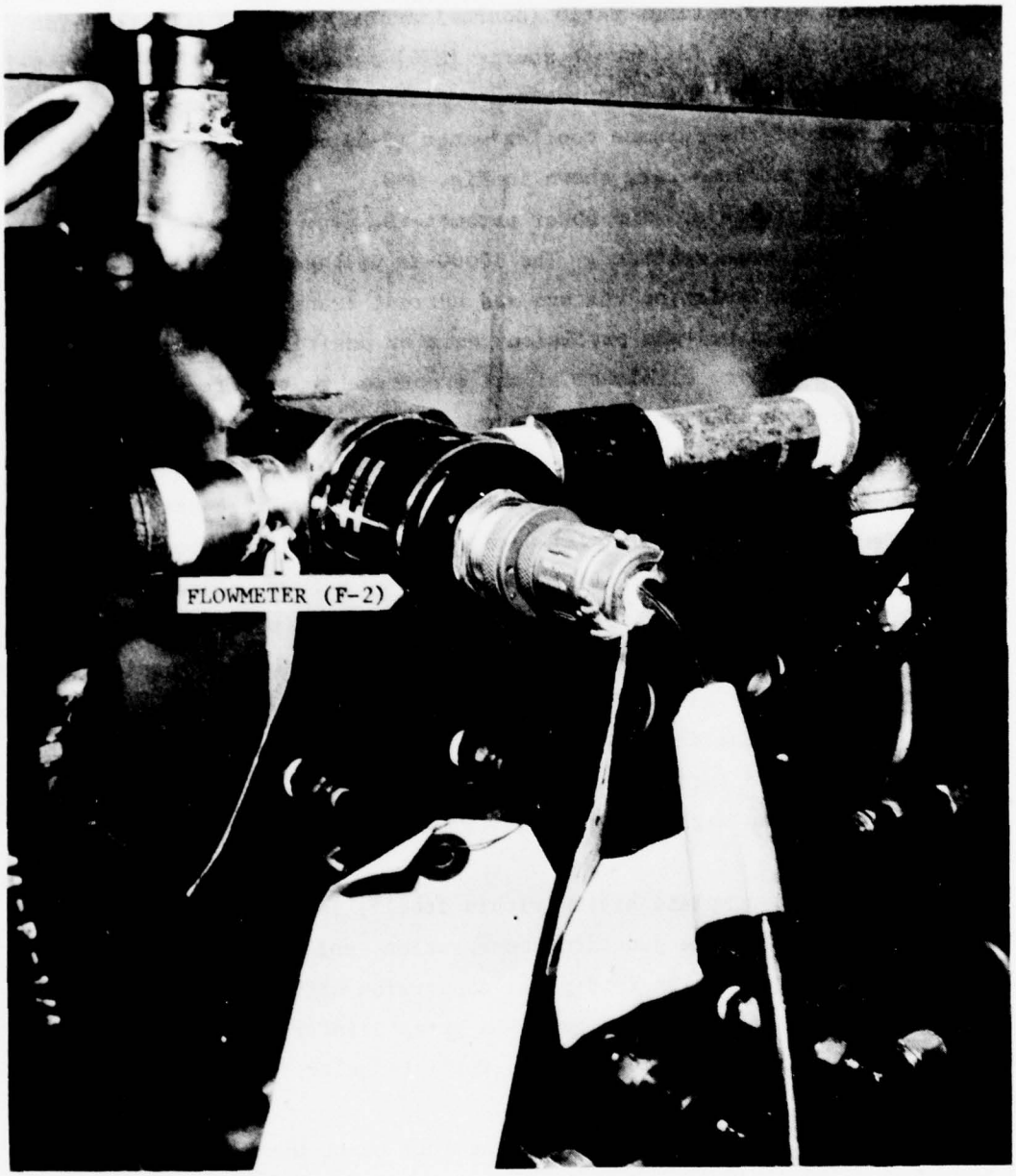

Fig. B-15. Annulus N_2 flowmeter installation.

ically multiplies carrier times ratio (source/carrier) to give a 0- to 5-Vdc source output for zero to full-scale source (MTS) mass flow rate. Figures B-16 and B-17 show the system that measures and controls these parameters.

The flow rate of the furnace cooling water (F-5) was measured using a standard turbine type flowmeter, shown in Fig. B-8.

4. Power measurements. Two power parameters, true power (EI cos Ø) and apparent power (EI), were recorded. The 10000-Hz voltage and current signals were obtained through isolation voltage and current transformers. The current signal was applied to a 0.1-ohm precision resistor positioned adjacent to the transformer (Fig. B-18) to eliminate signal error due to transformer loading and a drop associated with lead wire resistance. The resulting voltage signal was then applied to a signal conditioner located approximately 30 m away adjacent to the data logger. The two voltage signals (one from the voltage transformer and the other from the precision resistor) were scaled using high-input impedance amplifiers and electronically multiplied together by a four quadrant multiplier. The resulting dc signal was scaled, filtered, and applied to the data logger as power (EI cos Ø). The signal out of the multiplier was also ac coupled to a RMS dc converter whose output was scaled to achieve the apparent power signal.

5. Data logger. The data logger used was a digital multipoint recorder, capable of measuring and formatting 40 channels of analog data. System operation is controlled by an eight-bit parallel microprocessor with ROM and PROM microprograms.

The basic unit, a complete system within itself, included 40 points of input terminations, reference junction compensation, solid state (FET) multiplexing, microvolt-level analog to digital conversion with a digital display in engineering units, printout on a built-in strip printer, an internal alarm system, and a built-in electronic timer to initiate selective periodic logging cycles for unattended operation.

Front panel controls are provided in the form of pushbuttons and thumbwheel switches as shown in Fig. B-19. The upper series of six pushbuttons operates the time-of-day clock, peripheral devices, the alarm system, and the internal printer. The lower series of eight pushbuttons provides the mode selection and scan interval controls. FIRST POINT and LAST POINT thumbwheel switches, each with three decades, select the low and high scan points and set the time-of-day clock.

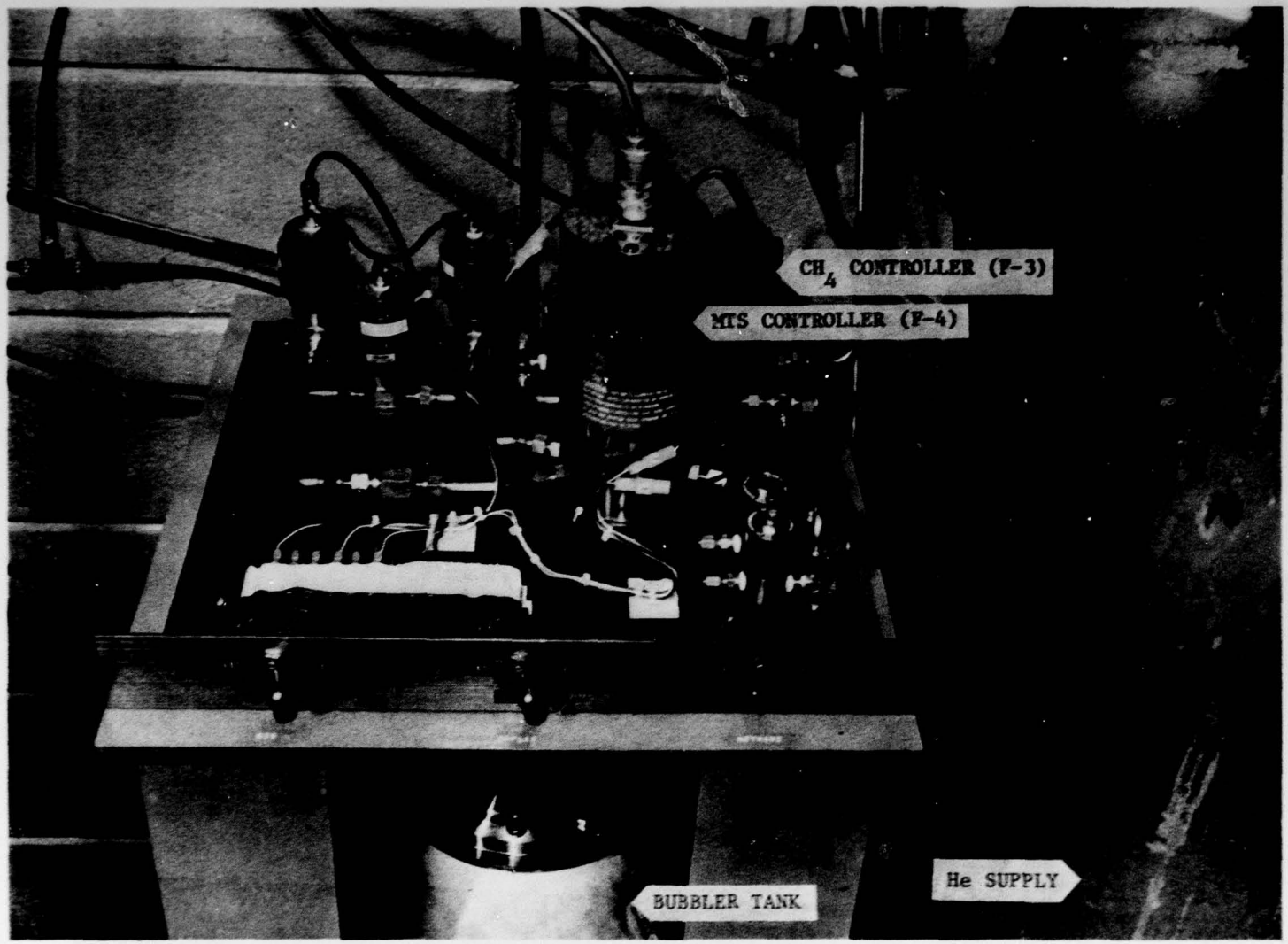

Fig. B-14. Process gas control system.

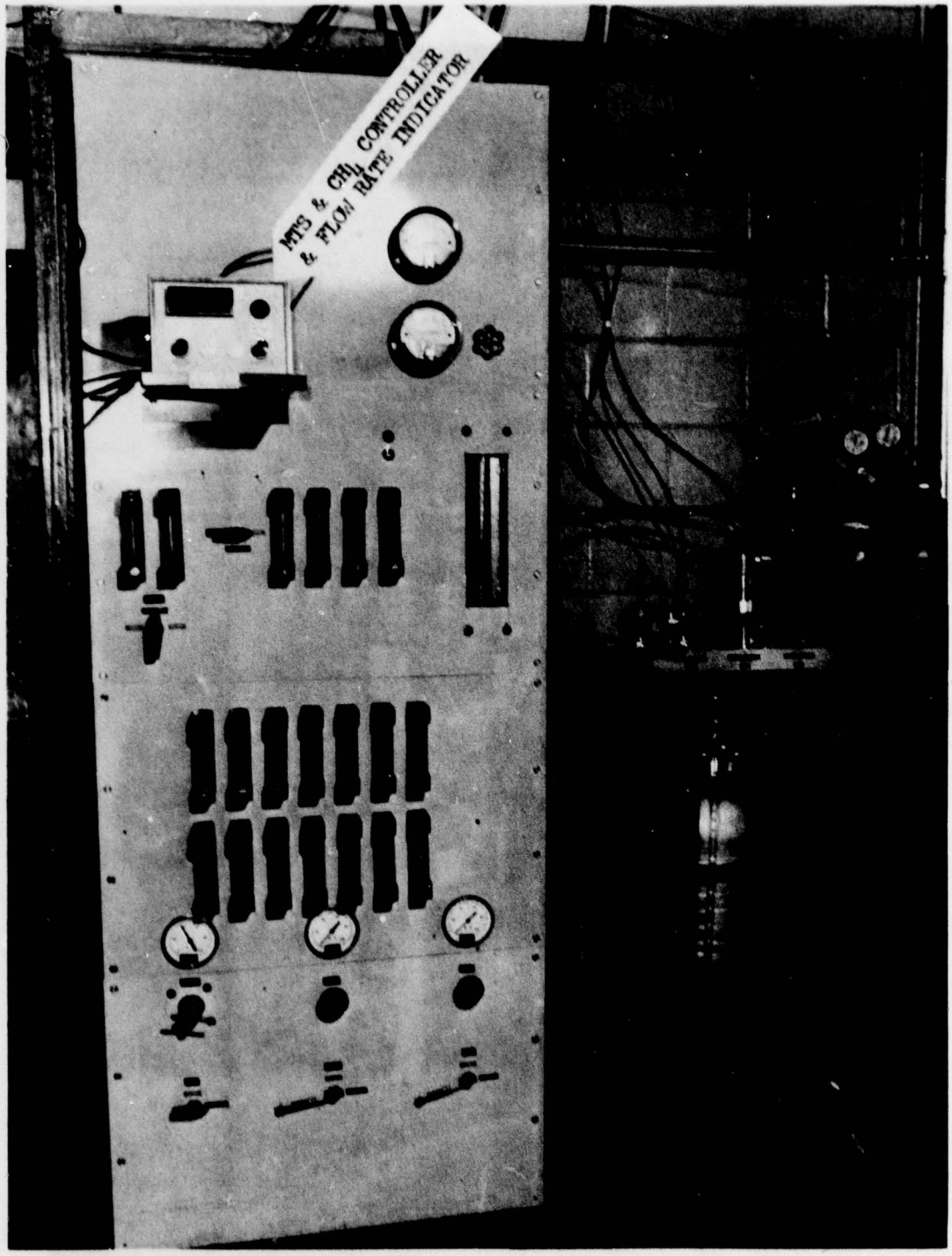

Fig. B-17. Process and purge gas control system.

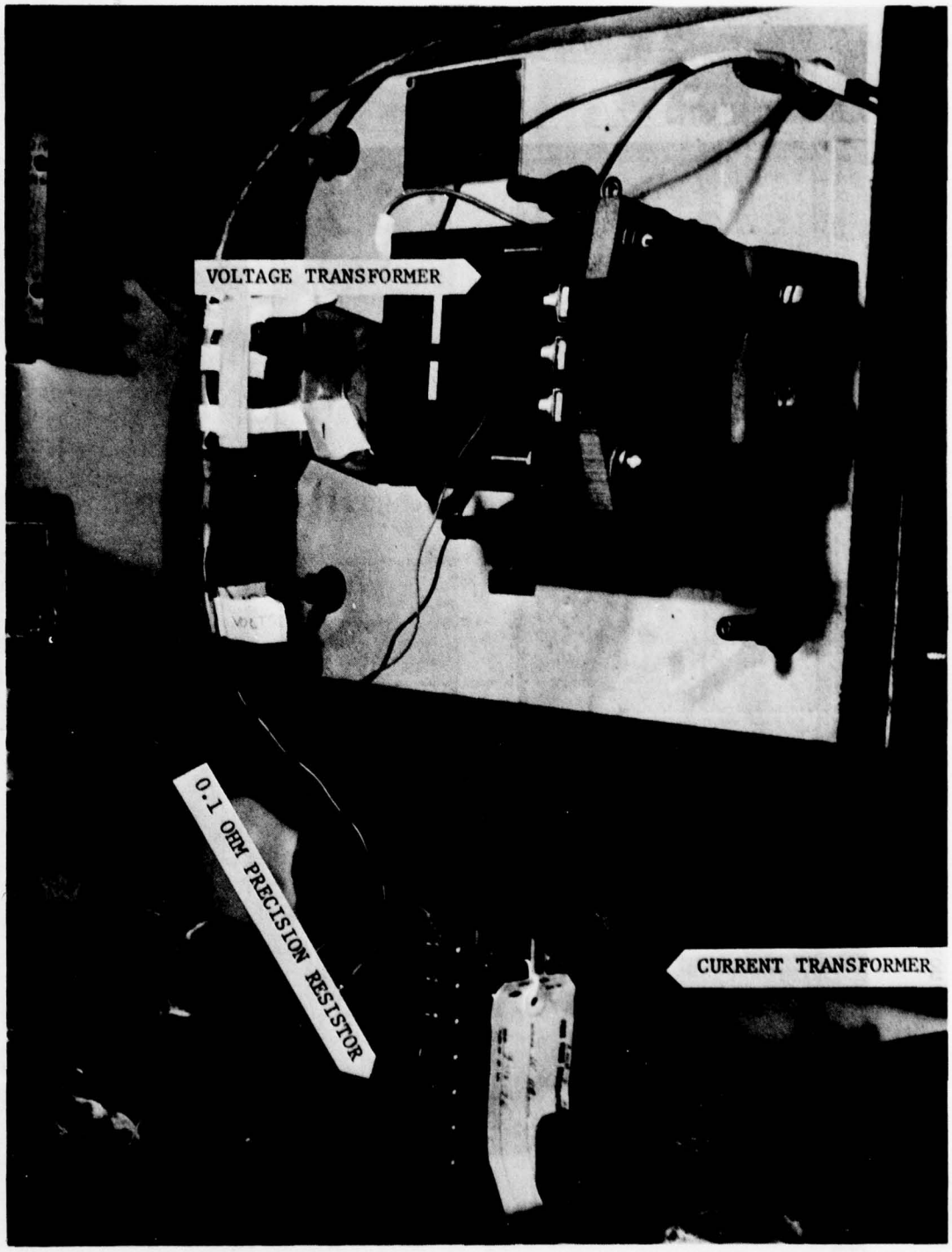

Fig. B-18. Furnace power measurement transducer installation.

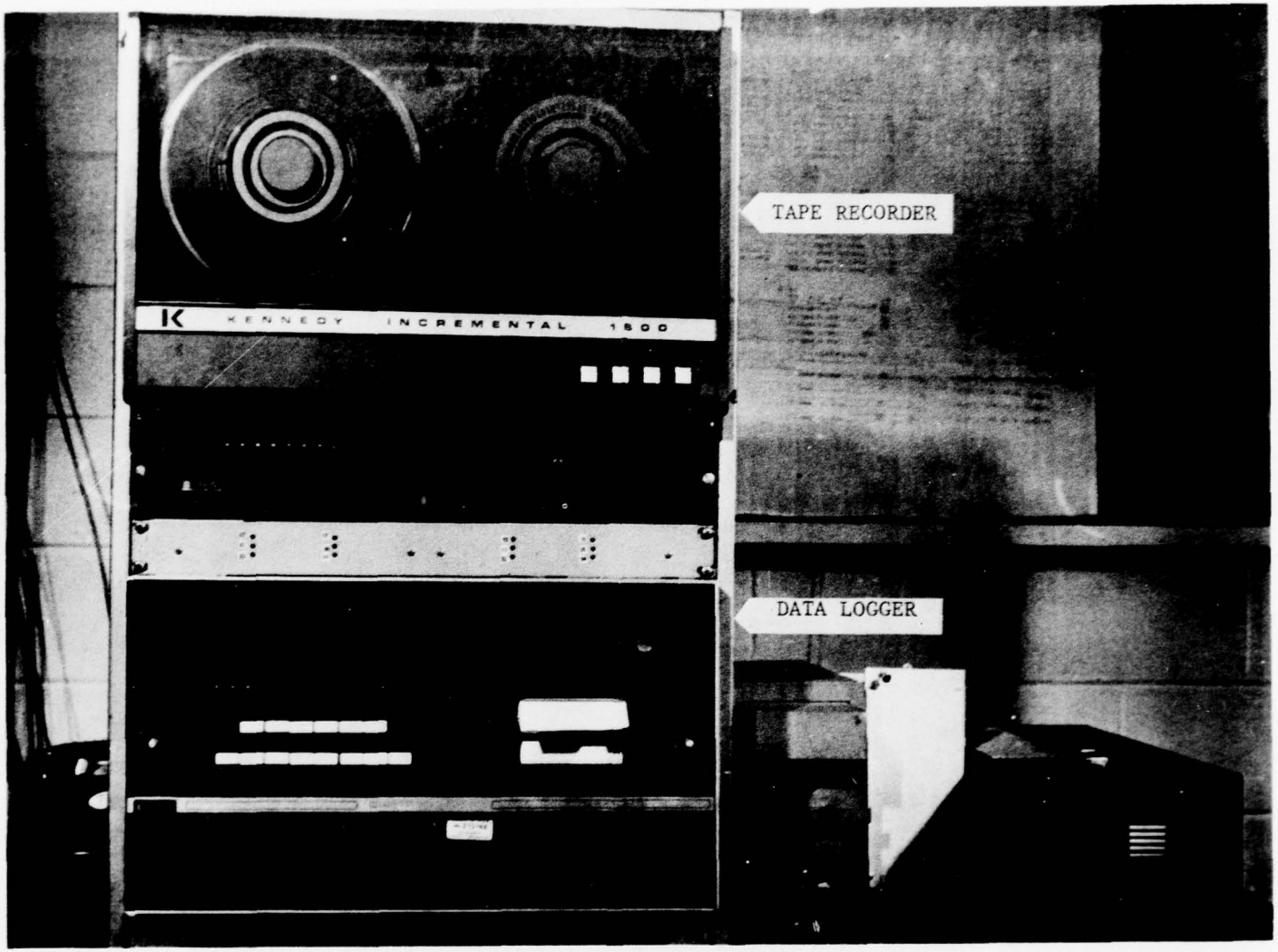

Fig. B-19. Data logger and tape recorder installation.

The unit has a full 16-bit digitizer capable of 10- or 100-μV resolution or 0.2 K thermocouple resolution, depending on the range the operator selects. An all-digital method of linearization for near perfect match to NBS thermocouple tables eliminates analog shaping circuit drift.

The digital display provides point address, magnitude (with negative polarity indication), time-of-day (hours, minutes and seconds), and units of measurement readout. In addition, an "I/O" neon light shines to indicate that an error has been detected in a peripheral instrument. The display lights when the power switch is activated and flashes to inform the operator of power on or power interrupt, alarm, I/O failure, or low tape conditions.

An internal interface circuit card is used to couple the data logger to peripheral equipment such as the seven-track incremental magnetic tape recorder.

The output of this card includes the digitized data, an operator-selected test number, time-of-day (days, hours, minutes, seconds), and peripheral control signals.

The internal printer has a typical recording rate of two points per second. It prints out the same information that is provided to the other peripheral equipment.

6. Magnetic tape recorder. The digital data from the data logger were recorded on magnetic tape by the incremental magnetic tape recorder. The unit uses half-inch-wide tape and records in an IBM seven-channel BCD code. In a seven-track system, six of the tracks are data channels and the seventh is the parity channel. Even parity was used for the BCD coding.

APPENDIX C

CALIBRATION DOCUMENTATION

TABLE OF CONTENTS

LIST OF ILLUSTRATIONS

I. PYROMETERS

A. Configuration

The pyrometers were calibrated with a radiation source whose temperature could be changed readily and measured independently.

The temperature of the radiation source was accurately determined with a Micro Optical Pyrometer, M-5399, that had been calibrated by National Bureau of Standards Test No. 182836.

The radiation source was an inductively heated graphite crucible mounted in an eddy current concentrator. Figure C-1 shows the configuration of the calibration system. The graphite crucible and eddy current concentratior are mounted in a quartz mantle connected to a vacuum system. This arrangement permits operation of the radiation source in either a vacuum or inert gas.

The thin-walled graphite crucible (38 mm o.d., 5 mm thick, and 57 mm high) and lid were machined from ATJ graphite. The interior of the crucible was lined with Carbocel, a porous graphite, to minimize temperature gradients and to increase the surface area of the blackbody cavity in the bottom section of the crucible. The maximum target diameter required for the various pyrometers calibrated was 8 mm. Correspondingly, the sight hole into the blackbody cavity was 9.5 mm and the hole in the crucible lid was 10 mm.

The optical path from the blackbody cavity passes through a polished quartz window and is then reflected at a right angle by a polished quartz prism to the pyrometers. The intensity of the light beam is decreased slightly by reflection as it passes through each quartz surface. The decrease in light intensity may be treated as an absorbtion coefficient (independent of window or prism thickness) and is calculated from the relation

$$A = 1/T_o - 1/T_s \ (K^{-1}) \qquad (C\text{-}1)$$

where T_o is the temperature, K, observed through the window (or prism) and T_s, is the temperature, K, of the source. For the reference pyrometer, M-5399, A is $2.6 \cdot 10^{-6}\ K^{-1}$ for both the prism and window. If there is a series of windows or prisms in the optical path, i.e., n windows, the total absorption coefficient, A_t , is equal to nA. A will vary with the pyrometer's sensitivity at the wavelength absorbed by the quartz. Values determined for each pyrometer calibrated are given in Table C-I. Further, quartz windows for the ARC deposition furnace were fabricated from the same quartz stock used for the calibration.

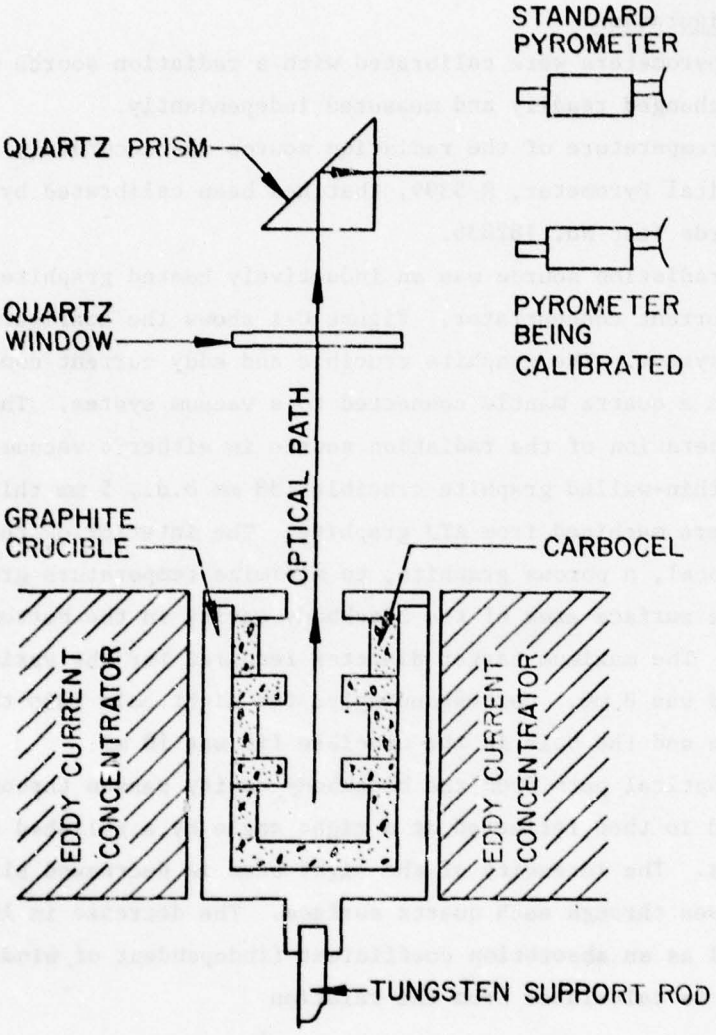

Fig. C-1. Configuration of calibration setup.

TABLE C-I

PYROMETER CALIBRATION DATA

Pyrometer	Serial Number	Range or Scale	$A \cdot 10^6$ (K^{-1})	Calibration Adjustment Voltage(mV)	Calibration Equation Temperature (K) vs Output(mV)	Std. Dev. $\pm\sigma_T$(K)	Calib. Range ($K \cdot 10^{-3}$)
Milletron, Two-color	174	5000°R	2.3	29.0	$T = 1156.3 + 27.746(mV) - 0.01378(mV)^2$	15	1.3-2.3
Milletron, Two-color	177	2000°C	2.4	100.2	$T = 1437.8 + 4.9802(mV) + 0.02765(mV)^2$	5	1.6-2.2
		3000°C	2.4	0.3	$T = 2205.6 + 9.3917(mV) + 0.06059(mV)^2$	8	2.2-2.4
Milletron, Two-color	322	2000°C	0.80	100.4	$T = 1294.9 + 9.6259(mV) + 0.00445(mV)^2$	19	1.6-2.3
		3000°C	0.80	0.6	$T = 2296.1 + 12.532(mV) + 0.02569(mV)^2$	14	2.3-2.5
Milletron, Two-color	368	5000°C	0.62	-	$T = 1833.9 + 2.3323(mV) + 0.00212(mV)^2$	9	1.8-2.4
Milletron, Two-color	463	3000°C	0.51	232.0	$T = 1317.3 + 4.0598(mV) + 0.00059(mV)^2$	13	1.6-2.4
Thermodot, TD-9FH	132	2600°F	4.0	8.32	$T = 1260.9 + 20.08(mV) + 3.462(mV)^2$	4	1.3-1.8
		4000°F	4.0	8.32	$T = 1523.0 + 129.18(mV) - 14.798(mV)^2 + 1.4661(mV)^3$	11	1.6-2.4
Thermodot, TD-7B	1121	4000°F	13.4	10.0	$T = 1310.1 + 19.783(mV)$	4	1.6-1.9
Thermodot, TD-6A	6751	2200°C	12.6	565.0	$T = 1320.3 + 1.6368(mV)$	14	1.6-2.2
Ircon, Model 300	3343	H	14.8	44.5	$T = 1202.8 + 17.828(mV) - 0.05936(mV)^2$	4	1.6-2.0
		I	12.6	44.5	$T = 1235.2 + 61.633(mV) - 0.59756(mV)^2$	5	1.6-2.4
Micro-Optical	744	w/o neut. filter	4.3	-	$T = 1.625 \cdot 10^4/[10.022 - \ln(mV)]$	6	1.5-2.2
		w/neut. filter	4.3	-	$T = 1.645 \cdot 10^4/[8.5189 - \ln(mV)]$	6	1.6-2.4
Micro-Optical	745	w/o neut. filter	4.3	-	$T = 1.627 \cdot 10^4/[11.072 - \ln(mV)]$	7	1.8-2.2
		w/neut. filter	4.3	-	$T = 1.721 \cdot 10^4/[9.6848 - \ln(mV)]$	7	1.8-2.4

B. Procedure

Specified preoperation, operation and focusing procedures for each pyrometer were followed before calibration. Pyrometer voltage outputs were measured with a Hewlett-Packard 3490 A multimeter. The black body crucible was brought up to temperature and allowed to equilibrate for ½ h, and the calibration was started. The voltage output and meter readings were recorded for the pyrometer being calibrated; the prism was then rotated to the reference pyrometer and the temperature of the radiation source was determined and recorded. The prism was then rotated back to the first pyrometer, and the voltage and meter readings were again recorded. The temperature was raised sequentially (20-40 K) allowing 10 min for thermal equilization before repeating the above calibration stemps, to approximately 2300 K and then sequenced back down to the starting temperature.

About every third calibration point, an additional quartz window was placed in the optical path to the pyrometer being calibrated and the change in meter reading and voltage output were recorded. This information permitted determination of the absorption for the window.

C. Calibration data

The data, mV output vs temperature for one quartz window in the optical path, was least-squares fitted for several of the pyrometers to an equation of the form

$$T(K) = A + B(mV) + C(mV)^2 + \ldots . \qquad (C\text{-}2)$$

and the standard deviation, σ_T, was used to determine what degree of polynomial adequately represented the data. For pyrometers, S/N 744 and S/N 745, the data was least-squares fitted to an equation of the form

$$T(K) = A/(B - \ln(mV)) \qquad (C\text{-}3)$$

The results are presented in Table C-I

II PRESSURE TRANSDUCERS

The pressure transducers were calibrated by their respective manufacturers. The calibration data were used for the end-to-end calibration of the data acquisition system (DAS). The calibration was accomplished by disconnecting the electrical connector at the transducer and substituting a short circuit and then a dc voltage for the transducer. The calibration equation for each pressure channel is given in Tables C-II and C-III for the nitrogen flow tests and coating tests, respectively.

TABLE C-II

DATA REDUCTION FORMULAS FOR TEST NUMBER SERIES 15600 - DATE 3-16-76

Ch.	Parameter	Range	Units	Data Reduction Formula	Instrument Range
00	Ref. Cal.	---	Volts	$Y = V$	
01	P-1	±25	psfd	$Y = 16.667(V) - 25$	
02	P-2	±25	psfd	$Y = 16.667(V) - 25$	
03	P-3	0/20	psig	$Y = 6.6667(V)$	
04	P-4	±25	psfd	$Y = 16.667(V) - 25$	
05	P-5	±75	psfd	$Y = 50(V) - 75$	
06	F-1	0/50	SCFM	$Y = 16.667(V)$	
07	F-2	0/20,000	SCCM	$Y = (20,000/3)V$	
08	---	---	---	---	
09	T-15	273/2200	°K	$Y = 303.5 + 6.7632 \times 10^2(V) - 1.0423 \times 10^2(V^2) + 3.0118 \times 10^1(V^3)$	
10	T-9	1163/2780	K	$Y = 1163.6 + 27.045 \times 10^3(V)$	
11	T-5	1279/2300	K	$Y = 1279.0 + 10.192 \times 10^3(V)$	Low
11	T-5	2295/3592	K	$Y = 2295.0 + 12.942 \times 10^3(V)$	High
12	T-7	1300/2582	K	$Y = 1299.7 + 4.2755 \times 10^3(V)$	
13	---	---	---	---	---
14	T-13	1235/2590	K	$Y = 1235.2 + 6.5241 \times 10^3(V) - 6.6957 \times 10^3(V^2)$	I
15	T-6	1834/3000	K	$Y = 1833.9 + 2.3323 \times 10^3(V) + 2.1196 \times 10^3(V^2)$	
16	T-1	1310/1910	K	$Y = 1310.1 + 39.783 \times 10^3(V)$	Mid
17	T-8	1260/1700	K	$Y = 1260.9 + 5.8412 \times 10^2(V) + 2.9308 \times 10^3(V^2)$	2600°F Full Scale

TABLE C-II (contd.)

Ch.	Parameter	Range	Units	Data Reduction Formula	Instrument Range
17	T-8	1620/2480	K	$Y = 1520.3 + 1.1015 \times 10^{3}(V) + 5.7107 \times 10^{3}(V^{2})$	4000°F Full Scale
18	T-3	1250/2590	K	$Y = 1.6446 \times 10^{4} / \left[8.5189 - \ln(V/3.428 \times 10^{-2}) \right]$	
19	---	---	---	---	
20	---	---	---	---	
21	---	---	---	---	
22	T-17	273/310	K	$Y = 0.5556(°F) + 255.22$	
23	T-19	273/373	K	"	
24	T-18	273/325	K	"	
25	T-10	273/673	K	"	
26	T-11	273/673	K	"	
27	T-12	273/673	K	"	
28	T-16	273/673	K	"	
29	T-20	273/373	K	$Y = 0.5556(°F) + 255.22$	
30	F-5	0/340.65	SLPM	$Y = 113.55(V)$	
31	W-1	0/117.18	KW	$Y = 39.06(V)$	
32	T-14	1200/3310	K	$Y = 1.7209 \times 10^{4} / [9.6848 - \ln(V/3.381 \times 10^{-2})]$	
33	T-4	273/2200	K	$Y = 303.5 + 6.7632 \times 10^{2}(V) - 1.0423 \times 10^{2}(V^{2}) + 3.0118 \times 10^{1}(V^{3})$	

TABLE C-III

DATA REDUCTION FORMULAS FOR TEST NUMBER SERIES 15800 - DATE 5-5-76

Ch.	Parameter	Range	Units	Data Reduction Formula	Instrument Range
00	Ref. Cal.	---	Volts	$Y = V$	
01	F-6	0/6	SLPM	$Y = 2(V)$	
02	F-7	0/30	% S/C	$Y = 10(V)$	
03	P-3	0/20	psig	$Y = 20/3(V)$	
04	T-14	1200/3310	K	$Y = 1.7209 \times 10^4/[9.6848 - \ln(V/3.381 \times 10^{-2})]$	
05	F-2	0/20,000	SCCM	$Y = 20{,}000(V)/3$	
06	F-1	0/1416	SLPM	$Y = 472(V)$	
07	F-4	0/9	GPM	$Y = -3(V)$	
08	F-3	0/10	SLPM	$Y = 3.3333(V)$	
09	T-15	273/2200	K	$Y = 303.5 + 6.7632 \times 10^2(V) - 1.0423 \times 10^2(V^2) + 3.0118 \times 10^1(V^3)$	
10	---	---	---	---	---
11	T-7	1300/2582	K	$Y = 4.2755 \times 10^3(V) + 1299.7$	
12	T-5	1279/2300	K	$Y = 10.192 \times 10^3(V) + 1279.0$	Low
13	T-2	1435/2015	K	$Y = 2.5328 \times 10^5(V^2) + 1.5073 \times 10^4(V) + 1437.8$	Low
14	T-13	1137/4710	K	$Y = -1.5475 \times 10^3(V^2) + 2.6232 \times 10^3(V) + 1137.32$	H
	T-13	1137/4710	K	$Y = -5.7271 \times 10^3(V^2) + 6.6981 \times 10^3(V) + 1298.5$	I
15	T-6	1834/3000	K	$Y = 2.1196 \times 10^3(V^2) + 2.3323 \times 10^3(V) + 1833.9$	

TABLE C-III(cont'd.)

Ch.	Parameter	Range	Units	Data Reduction Formula	Instrument Range
16	T-1		K	(Low range not calib. yet.)	Low
	T-1	1310/1910	K	$Y = 39.783 \times 10^3(V) + 1310.1$	Mid
17	T-8	1620/2480	K	$Y = 5.7107 \times 10^3(V^2) + 1.1015 \times 10^3(V) + 1620.3$	4000°F Full Scale
18	T-3	1250/2590	K	$Y = 1.6446 \times 10^4/[8.5189 - \ln(V/3.428 \times 10^{-2})]$	
19	T-9	1125/1880	K	$Y = 1.5157 \times 10^4(V) + 1125.48$	
20	---	---	---	---	
21	---	---	---	---	
22	T-17	273/310	K	$Y = 0.5556(°F) + 255.22$	
23	T-19	273/373	K	"	
24	T-18	273/325	K	"	
25	T-10	273/673	K	"	
26	T-11	273/673	K	"	
27	T-12	273/673	K	$Y = 0.5556(°F) + 255.22$	
28	---	---	---	---	
29	T-20	273/373	K	$Y = 0.5556(°F) + 255.22$	
30	F-5	0/340.65	SLPM	$Y = 113.55(V)$	
31	W-1	0/125	KW	$Y = 41.667(V)$	
32	W-2	0/125	KW	$Y = 41.550(V)$	

III THERMOCOUPLES

The thermocouples (TCs) were calibrated by their respective manufacturers. The calibration data were used to calibrate the signal conditioners and, subsequently, for the end-to-end calibration of the DAS. The DAS for the W-5% Re vs W-26% Re channels was calibrated by the boltage substitution method described above. Voltage substitution was used for the type-T TCs also, but only as an end-to-end wiring check. Ambient temperature readings of the units were compared for a single-point calibrtion check. The calibration equation (data reduction equation) for each TC is listed in Tables C-II and C-III for the test series 15600 and 15800, respectively.

IV POWER TRANSDUCER

The voltage and current transformers were calibrated at LASL to verify their accuracy. The signal conditioning was calibrated at LASL by varying the input voltage, current, and phase angle. No end-to-end calibration was performed on these channels (W-1 and W-2) at ARC owing to the lack of test equipment. The data reduction equations are shown in Tables C-Il and C-lll.

V DATA ACQUISITION SYSTEM

An end-to-end pretest calibration was conducted on the DAS as described above. In addition, the calibrate switches on the pyrometers were activated and these channels were verified. The above calibration data were recorded on magnetic tape for the first tests (mitrogen flow tests), and the data were reduced and verified before we proceeded with the test. The calibration data were hand-recorded but not recorded on magnetic tape for the deposition tests. A post-test calibration was performed on the DAS to the degree possible, limited only by test and hardware constraints. Tables C-IV and C-V outline the pre- and post-test calibration data dor the two series of tests.

In addition to the calibration performed above, a pseudo pre- and post-test calibration was conducted just before and after the tests. This calibration consisted of recording on magnetic tape the calibration point for the pyrometers, zeros for some channels and ambient conditions for others. A minimimum of 10 data points per channel was recorded. Becaused of the need to maintain gas and cooling water flow rates on the furnace for approximately 24 h subsequent to the test, no pot-test calibration data were obtained for some channels.

THIS PAGE IS BEST QUALITY PRACTICABLE
FROM COPY FURNISHED TO DDC

TABLE C-IV

DAS CALIBRATION FOR TEST NUMBER SERIES 13600 - DATE 3-16, 3-17, 3-18-76

		Pre-Test Calibration				Post-Test Calibration					
Parameter	DAS Ch.	Cal. Voltage Input	DAS Input	Simulated Input	Meter Reading	Cal. Voltage Input	DAS Input	Simulated Input	Meter Reading	Instr. Range	Remarks
Ref. Ch.	00	---	0.5002 V	---	---	---	0.5002	---	---	---	DAS Ref. Cal. Voltage
P-1	06	4.000 V	2.3996 V	1132.8 SLPM	---	---	---				
P-2	07	4.000 V	2.4001 V	16000 SCCM	---	---	---				
P-3	30	4.001 V	2.3998 V	272.48 SLPM	---	---	---				
P-1	01	4.000 V	2.3994 V	20.0 psf	---	---	---	---	---	---	
P-2	02	5.000 V	3.0000 V	25.0 psf	---	---	---				
P-3	03	4.000 V	2.3997 V	16.0 psi	---	---	---				
P-4	04	4.000 V	2.4000 V	20.0 psf	---	---	---				
P-5	05	4.000 V	2.4000 V	60.0 psf	---	---	---				
T-1	16	*10.01 mV	10.01 mV	---	783°C	*18.93 mV	18.93 mV	---	---	Low	Unit miscalibrated at 0950 hrs. 3/17/76
T-1	16	*10.01 mV	10.01 mV	1708.3 K	1385°C	*18.93 mV	18.93 mV	---	---	Mid	
T-1	16	*10.01 mV	10.01 mV	---	3275°C	*18.93 mV	18.93 mV	---	---	High	
T-2	13	*1.30 mV	1.30 mV	---	2020°C	*1.30 mV	1.30 mV	---	2020°C	Low	Parameter not recorded on DAS
T-2	13	*100.00 mV	100.00 mV	---	2000°C	*100.00 mV	100.00 mV	---	2000°C	High	
T-3	18	Ambient	0.91 mV	---	---	---	---				
T-5	16	6.74 mV	222.10 mV	2572.7 K	---	---	---				
T-4	33	Short	0.0046 V	296.89 K	---	---	---				
T-4	33	8.90 mV	0.8309 V	810.77 K	---	---	---				
T-5	11	*100.20 mV	100.20 mV	2300.2 K	2000°C	*100.5 mV	100.5 mV	2300.2 K	2005°C	Low	
T-5	11	*0.50 mV	0.50 mV	2301.5 K	2000°C	*0.4 mV	0.4 mV	2301.5 K	2005°C	High	
T-6	15	*150.2 mV	150.2 mV	2232.0 K	3980°F	*20 mV	20 mV	---	---	---	Cal. circuit anomally on Post Test Cal.
T-7	12	*231.0 mV	231.0 mV	2287.8 K	2000°C	*231.0 mV	231.0 mV	2287.8 K	2000°C		
T-8	17	*8.30 mV	287.4 mV	1670.9 K	2500°F	---	---	---	---	2600°F	
T-8	17	*8.30 mV	287.4 mV	2408.6 K	3750°F	*---	290.2 mV	2408.6 K	3750°F	4000°F	
T-8	17	Short	0.69 mV	1620.3 K	---	---	---	---	---	4000°F	
T-9	--	---	---	---	---	---	---	---	---	---	Parameter not recorded on DAS.
T-10	25	Ambient	64.8°F	---	---	Ambient	325.6°F	---	---		
T-11	26	Ambient	60.9°F	---	---	Ambient	331.2°F	---	---		
T-12	27	Ambient	59.2°F	---	---	Ambient	302.4°F	---	---		
T-13	14	---	---	---	---	---	---	---	---		Cal. Sw. Inoperative.
T-14	32	Ambient	0.0031 V	---	---						
T-14	32	7.06 mV	0.2336 V	2220 K	---						
T-15	09	Short	0.0030 V	296.9 K	---						
T-15	09	8.90 mV	0.8283 V	809.3 K	---						
T-16	28	Ambient	56.9°F	---	---	Ambient	383.7°F	---	---		
T-17	22	Ambient	48.4°F	---	---	Ambient	47.3°F	---	---		
T-18	24	Ambient	64.8°F	---	---	Ambient	67.4°F	---	---		
T-19	23	Ambient	48.6°F	---	---	Ambient	51.5°F	---	---		
T-20	29	Ambient	49.6°F	---	---	Ambient	54.7°F	---	---		
W-1	31	Ambient	0.0343 V	0.0 KW	---	Ambient	0.87283 V	0.0 KW	---		

*Calibration voltage from internal calibration standard of instrument.

THIS PAGE IS BEST QUALITY PRACTICABLE
FROM COPY FURNISHED TO DDC

TABLE C-V

DAS CALIBRATION FOR TEST NUMBER SERIES 5800 - DATE 5-5 & 5-6-76

		Pre-Test Calibration				Post-Test Calibration					
Parameter	DAS Ch.	Cal. Voltage Input	DAS Input	Simulated Input	Meter Reading	Cal. Voltage Input	DAS Input	Simulated Input	Meter Reading	Instr. Range	Remarks
Ref. Ch.	00	---	0.5003	---	---	---	0.5003	---	---	---	DAS Ref. Cal Voltage
F-1	06	Short	-0.0002 V	0.0 SLPM	---						
F-1	06	4.006 V	2.4006 V	1132.8 SLPM	---						
F-2	05	Short	-0.0001 V	0.0 SCCM	---						
F-2	05	4.002 V	2.3997 V	1600	---						
F-3	08	Short	-0.002 V	0.0 SLPM	---						
F-3	08	4.000 V	2.4009 V	8.0 SLPM	---						
F-4	07	Short	-0.0002 V	0.0 gpm	---						
F-4	07	4.000 V	2.4001 V	7.2 gpm	---						
F-5	30	Short	-0.0002 V	0.0 SLPM	---						
F-5	30	4.000 V	2.4004 V	372.48 SLPM	---						
F-6	01	Short	-0.0001 V	0.0 SLPM	---						
F-6	01	4.000 V	2.4000 V	4.8 SLPM	---						
F-7	02	Short	-0.0001 V	0.0%	---						
F-7	02	3.998 V	2.3992 V	24.0%	---						
F-3	03	Short	-0.00024	0.0 psi	---						
F-3	03	4.000 V	2.3984 V	16.0 psi	---						
T-1	16	*10.04 mV	10.04 mV	1709.5 K	1385°C	*9.939 mV	9.939 mV	1705.5 K	1385°C	Mid	
T-2	13	*33.04 mV	33.04 mV	2212.3 K	2000°C	*33.23 mV	33.23 mV	2212.3 K	2000°C	Low	
T-2	13	*0.60 mV	0.60 mV	---	2000°C	---	---	---	---	High	
T-3	18	Short	1.03 mV	1250.0 K	---						
T-3	18	5.00 mV	172.60 mV	2382.6 K	---						
T-5	12	*100.2 mV	100.2 mV	2500.2 K	2000°C	*100.37 mV	100.37 mV	2500.2 K	2000°C	Low	
T-6	15	*150.2 mV	150.2 mV	2232.0 K	3980°F	---	---	---	---	---	Cal. circuit anomaly on Post Test Cal.
T-7	11	*231.0 mV	231.0 mV	2287.8 K	2000°C	*231.62 mV	231.62 mV	2287.8 K	2000°C		
T-8	17	Short	1.20 mV	1620.0 K	---					4000°F	
T-8	17	8.0 mV	274.40 mV	2352.5 K	---	*8.44	290.0 mV	2420 K	3750°F	4000°F	
T-9	19	*-9.3 mV	-9.3 mV	984.5 K	2000°R						
T-9	19	*29.6 mV	29.6 mV	1574.1 K	3420°R	*42.49 mV	42.49 mV	1769.5 K	3420	---	
T-10	25	9.4 μV	426.0°F	**	---	---	---	---	---	---	
T-10	25	Ambient	66.9°F	---	---	Ambient	280.6°F				
T-11	26	9.4 μV	426.0°F	**	---						
T-11	26	Ambient	65.8°F	---	---	Ambient	293.6°F				
T-12	27	9.4 μV	426.0°F	**	---						
T-12	27	Ambient	65.1°F	---	---	Ambient	298.6°F	---			
T-12	27	Ambient	65.1°F	---	---	Ambient	298.6°F	---			
T-13	14	Short	0.43 mV	1137 K	---						
T-13	14	29.9 mV	282.74	1755.3 K		*44.5 mV	420.3 mV	---	90%	N	Cal. voltage of 420.3 mV over-ranged DAS

* Calibration voltage from internal calibration standard of instrument.
**System check only. Not accurate volts to °F calibration.

THIS PAGE IS BEST QUALITY PRACTICABLE
FROM COPY FURNISHED TO DDC

TABLE C-V (contd.)

Parameter	DAS Ch.	Pre-Test Calibration: Cal. Voltage Input	Pre-Test Calibration: DAS Input	Pre-Test Calibration: Simulated Input	Pre-Test Calibration: Meter Reading	Post-Test Calibration: Cal. Voltage Input	Post-Test Calibration: DAS Input	Post-Test Calibration: Simulated Input	Post-Test Calibration: Meter Reading	Instr. Error	Remarks
T-14	04	Short	0.0021 V	1200 K	---						
T-14	04	0.040 V	1.3546 V	2870.9 K							
T-15	09	Short	0.0024 V	296.9 K	---	---					
T-15	09	29.9 mV	2.7667 V	2014.7 K	---	----					
T-17	22	9.2 μV	423.4°F	**	---	---	---	---	---		
T-17	22	Ambient	60.5°F	---	---	Ambient	60.5°F	---	---		
T-18	24	9.4 μV	426.0°F	**	---	---	---	---	---		
T-18	24	Ambient	66.9°F	---	---	Ambient	74.4°F	---	---		
T-19	23	9.4 μV	426.0°F	**	---	---	---	---	---		
T-19	23	Ambient	60.7°F	---	---	Ambient	63.5°F	---	---		
T-20	29	9.4 μV	426.0°F	**	---	---	---	---	---		
T-20	29	Ambient	61.2°F	---	---	Ambient	65.5°F	---	---		
W-1	31	Short	0.000 V	0.0 KW	---	---	---	---	---		
W-1	31	Ambient	-0.0045 V	0.0 KW	---	Ambient	-0.0135 V	0.0 KW	---		
W-2	32	Short	0.000 V	0.0 KW	---	---	---	---	---		
W-2	32	Ambient	0.0004 V	0.0 KW	---	Ambient	0.0004 V	0.0 KW	---		

**System check only. Not accurate volts to °F calibration.

APPENDIX D

TEST PROCEDURE AND DATA DOCUMENTATION

TABLE OF CONTENTS

LIST OF ILLUSTRATIONS

I. GENERAL

This appendix contains the test procedures, the test logs, and graphs of reduced data from the nitrogen flow and deposition tests. Included also is a discussion of data anomalies.

II. NITROGEN FLOW TESTS

These tests commenced on March 16, 1976 at 1440 h after several hours of system configuration verification and pretest checkout. The test identification number is 15601. The test procedure, which is part of the data package, is given here. These tests were concluded on March 18, 1976 at 0300 h.

The procedure was modified as the test proceded and data were being analyzed and compared with the objectives. It was found unnecessary to perform paragraphs 5.3, 5.4, 7.2, and 8.2 of the test procedure.

A. Procedure for Nitrogen Flow Tests

The procedure for the nitrogen flow tests is presented in Table D-I. The procedure is that on file at LASL.

B. Nitrogen Flow Test Log.

The enclosed test log for test 15601 (Table D-II) is a typewritten copy of the original on file at LASL. It is included because it outlines pertinent events that occured during the test and their time of occurrence. It is included so that the reader may correlate these events with the data presented here.

C. Nitrogen Flow Test Data.

The data in Table D-III cover that part of the test in which power was applied to the furnace. It was not convenient to present the data on other parts of the test in this format; so parts of the data appear in Sec. III of this report. All data were recorded on magnetic tape which is on file at LASL.

D. Discussion of N_2 Flow Tests Data.

Part of the data from the flowmeter which measured cooling water flow rate (F-5) is erroneous. The data obtained before applying power to the furnace are accurate; however, power in excess of 25 kW applied to the furnace caused a signal-to-noise ratio of approximately 0.1. This problem was resolved before the deposition tests.

Parameters T-2 and T-9 were not recorded on the DAS because of excessive common mode voltage on their signals. These parameters were recorded manually at 15-min intervals throughout this test. The signal conditioner for these two parameters drifted approximately ± deg/h. A circuit was designed to reduce the

THIS PAGE IS BEST QUALITY PRACTICABLE
FROM COPY FURNISHED TO DDC

TABLE D-I

COPY OF TEST PROCEDURE-N_2 FLOW TESTS

ATLANTIC RESEARCH CORPORATION
ALEXANDRIA, VIRGINIA

Furnace operator

LASL Procedures

Test 15601.

This is copy 2 of 6 copies.

			Checked by	Checked by
1.0	Assembly			
1.1	Fixtures assembled as per SK6944-001A. Check following items for proper location, alignment, and assure that correct transducers are in place.			
1.1.1		T-1	CWR	
.2		T-2		
.3		T-3		
.4		T-4		
.5		T-5		
.6		T-6		
.7		T-7		
.8		T-8		
.9		T-9		
.10		T-10		
.11		T-11		
.12		T-12		
.13		T-13		
.14		T-14		
.15		T-15		
.16		T-16		
.17		T-17		
.18		T-18		
.19		T-19		
.20		T-20		
.21		P-1		
.22		P-2		
.23		P-3		
.24		P-4		
.25		P-5		
.26		F-1		
.27		F-2		
.28		F-3		
.29		F-4		

1/2" from top wall (Full insertion)
19 15/32" from fitting to wall
T.C /T-15 Length = 19.0" call it 1/2" from wall
(spare is 18 1/8")

Distribution: #1, DAS operator
#2, Furnace Operator
#3 & 4, LASL
#5 & 6, spare

THIS PAGE IS BEST QUALITY PRACTICABLE
FROM COPY FURNISHED TO DDC

TABLE D-I (continued)

LASL Procedures (continued)

			Checked by	Checked by
	.30	F-5	CWM	EOP
	.31	W-1		
	.32	Furnace Case Pressure Gage		
1.2		Injector location (10.8 inches from subs.)		
1.3		Lampblack approx. 8 inches above susc. Slope upwards towards fiberfrax to compensate for settling. Measured depth (3 places)_____.		
1.4		Cooling water connections to:	5 5/16 ← NEXT TO L.A. SHIELD 5 5/16 ← center 6" ← outer edge of susc	
	1.4.1	T-1		
	.2	T-2		
	.3	T-3		
	.4	T-5		
	.5	T-6		
	.6	T-7		
	.7	T-8		
	.8	T-9		
	.9	T-13		
	.10	T-14		
	.11	T-15		
	.12	P-1		
	.13	P-2		
	.14	Coil		
	.15	Injector		
	.16	S.P. Outlet Manifold		
	.17	Furnace Exhaust Tube Assembly		
	.18	Bus Bar		
	.19	Support Plate		
	.20	S.P. Inlet Manifold		
	.21	Furnace Lid		
1.5		Drain lines to items 1.4.1 - 1.4.16 interconnected and monitored by T-19 & F-5		
1.6		Process gas connections for:		
	1.6.1	N_2 Process		
	.2	N_2 Annulus		
	.3	~~CH_4 (to Tylan Panel)~~		
	.4	~~He (to Tylan Panel)~~		

THIS PAGE IS BEST QUALITY PRACTICABLE
FROM COPY FURNISHED TO DDC

TABLE D-I (continued)

ATLANTIC RESEARCH CORPORATION
ALEXANDRIA, VIRGINIA

LASL Procedures (continued)

	Checked by	Checked by
1.7 Purge gas connections to:		
1.7.1 T-1	CWR	EE
.2 T-2		
.3 T-3		
.4 T-5		
.5 T-6		
.6 T-7		
.7 T-8		
.8 T-9		
.9 T-13		
.10 T-14		
.11 T-15		
.12 P-1		
.13 P-2		
.14 P-1 & P-2 Annulus		
.15 Furnace Case		
1.8 Furnace power connections		
1.9 Capacitor connections made and recorded		
2.0 Pre-Heatup Check Out (1.10 Turn on instruments requiring a warm up "CAL" mode. All Label and mount tape. 1.12 after ½ Hr perform 10 complete data scans)		
2.1 N_2 Supply		
2.2 ~~CH_4 Supply~~		
2.3 ~~MTS Supply~~		
2.4 All Cooling Water Valves Open	CWR	
2.4.1 WV-1		
.2 WV-2		
.3 WV-3		
.4 WV-4		
.5 WV-5		
.6 WV-6		
.7 WV-7		
.8 WV-8		
2.5 Check cooling water sight flow indicators		
2.5.1 T-1	CWR	
.2 T-2		

THIS PAGE IS BEST QUALITY PRACTICABLE
FROM COPY FURNISHED TO DDC

TABLE D-I (continued)

ATLANTIC RESEARCH CORPORATION
ALEXANDRIA, VIRGINIA

LASL Procedures (continued)

		Checked by	Checked by
2.5.3	T-3	CM	
.4	T-5		
.5	T-6		
.6	T-7		
.7	T-8		
.8	T-9		
.9	T-13		
.10	T-14		
.11	T-15		
.12	P-1		
.13	P-2		
.14	Bus Bar		
.15	Support Plate		
.16	Coil		
.17	Exhaust Tube		
.18	Furnace Lid		
repeat at 7.00 PM .19	Injector		
2.6	Coil water flow rate measurement		
2.6.0	Take continuous scans, all channels. Note time and F-5 flow. 23		
23.0 2PM 2.6.1	Close NV-8		
19.3 .2	Manually record flow rate of F-5 (DAS channel #20) 19.5 GPM		
.3	Note DAS time - Take 10 continuous scans, all channels		
23.0 .4	Open NV-8		
23.0 .5	Manually record flow rate of F-5 - 23 GPM		
.6	Note DAS time - Take 10 continuous scans, all channels		
2.7	ARC instrument panel should be set up as follows:		
2.7.1	All flowrator valves closed		
.2	NV-1 open		
.3	NP-1 set at 50 psig		
.4	NV-2 open		
.5	NV-3 open		
.6	NP-2 set at 50 psig		
.7	~~NV-1 open~~		
.8	NV-2 open to desired rotometer		
.9	NP-1 set at 50 psig		

THIS PAGE IS BEST QUALITY PRACTICABLE
FROM COPY FURNISHED TO DDC

TABLE D-I (continued)

ATLANTIC RESEARCH CORPORATION
ALEXANDRIA, VIRGINIA

LASL Procedures (continued)

		Checked by	Checked by
2.8	Initiate heatup gas flow rates at gas panel by adjusting flowrator valves to achieve following indicated rates:		
2.8.1	N_2 Case - 150 SCFH (4002)		
.2	N_2 Annulus 24% (4001) F_2		
.3	N_2 Process - 200 SCFH F_1		
.4	N_2 P-1 - ~~35%~~ 0		
.5	N_2 P-2 - ~~35%~~ 0		
.6	N_2 P-1 & P-2 Annulus - ~~10%~~		
.7	N_2 T-1 - ~~5%~~ 20%		
.8	N_2 T-2 - ~~10%~~ 50		
.9	N_2 T-3 - ~~35%~~ 100		
.10	N_2 T-5 - ~~10%~~ 50		
.11	N_2 T-6 - ~~35%~~ 100		
.12	N_2 T-7 - 100%		
.13	N_2 T-8 - ~~35%~~ 100		
.14	N_2 T-9 - ~~5%~~ 20		
.15	N_2 T-13 - ~~5%~~ 20		
.16	N_2 T-14 - ~~5%~~ 20		
.17	N_2 T-15 - 100%		
~~.18~~	~~CH_4 - 0~~		

15 SCFH = full scale on Fisher-Porter units

Note: Items 2.8.4 through 2.8.17 require flowmeter tube No. 1/8 - 20 - p - 3/37 with SS float.

THIS PAGE IS BEST QUALITY PRACTICABLE
FROM COPY FURNISHED TO DDC

TABLE D-I (continued)

3.0 Cold Flow Profile Tests

3.1 Adjust N_2 process rate to 500 SCFH (ARC flowmeter). ~~Note: Compare F-1 with ARC flowmeter. If F-1 rate is greater, set flow using F-1.~~

3.1.1 Start reading with probe at 0° position and 2 inches below injector tip.

.2 Rotate probe from side to side stopping to take pressure readings every 5 degrees. This may be accomplished by stopping the DAS as the probe is rotated and starting it whenever the desired position is reached. Take ~~each~~ continuous readings of P1, P2, P3, P4, P5, and for approximately 30 seconds. Record DAS time, rotational position, axial position of each reading, and ~~both~~ pressure transducer outputs of P4 & P5.

(DAS channels 01-06)

(DAS channels 04 & 05)

.3 Repeat this procedure at 2 inch increments from the injector to full extent of probe.

.4 Record left and right extent (degrees) of travel at each axial position to determine location of canister extension inside wall and as an indication of the amount of eccentricity of the probe from the centerline position.

3.2 Adjust N_2 process rate to 1000 SCFH (ARC flowmeter) and duplicate procedure of 3.1.

3.3 Adjust N_2 process rate to ~~1500~~ 1400 SCFH (ARC flowmeter) and duplicate procedure of 3.1.

9:00PM - set up Heise Gauge

1000 SCFH P_2 = 1.14

1400 SCFH P_3 = 2.13

500 SCFH P_2 =

Heise 1.4 = 2.3 Psi

THIS PAGE IS BEST QUALITY PRACTICABLE
FROM COPY FURNISHED TO DDC

TABLE D-I (continued)

4.0 Transient Heating Tests

4.1 During heatup hand record all available data in run logs A and B at 15 minute intervals. (Continue this procedure throughout remainder of run.) DAS Record on 1 min. intervals of all channels (00 through 33)

4.1.1 All gas flow rates same as in Section 2.8.

4.2 Heat furnace at 50 kW for 30 minutes. Start at 9:31

Water pressure 26 psi ↑ 26 psi 10:10

4.3 After 30 minutes adjust power to 90 kW.

4.3.1 Adjust settings on control panel as smoothly and rapidly as possible, within limitations of equipment.

.2 If an intended power setting is overshot, do not readjust--in other words, do not juggle the controls in attempting to exactly duplicate a printed test condition.

.3 The number of changes in power are to be minimized.

.4 Except in cases where a safety hazard is involved, do not adjust power settings in response to measured parameters (temperatures) which might have been established for normal coating runs.

(DAS channel 12 should be 171.6 ± 2.4 mv) (Minetron SN-463 ±10 T)

4.4 After substrate inner surface temperature has reached 1738°C (F-7):

4.4.1 Record DAS time and elapsed time. ← Discontinue DAS record

.2 Adjust N_2 process rate to 500 SCFH.

.3 Adjust power level to maintain 1738°C.

4.5 ARC pyrometer calibration (to be conducted after temperature has stabilized).

4.5.1 Remove 2-color pyrometer head from SP-7. 1740°

.2 Read temperature with ARC optical pyrometer S/N 1792643 with sight port cover in place. Indicated: 3123 H, 3120 xH

.3 Repeat 4.5.2 with sight port cover off. 3150 H, 3145 xH

.4 Reinstall 2-color pyrometer head, and record temperature with sight port cover removed. 1742°

.5 Replace sight port cover and record temperature with 2-color pyrometer. 1750°

THIS PAGE IS BEST QUALITY PRACTICABLE
FROM COPY FURNISHED TO DDC

TABLE D-I (continued)

ATLANTIC RESEARCH CORPORATION
ALEXANDRIA, VIRGINIA

5 6.0 N_2 Flow Tests

6.1 N_2 Flow Test 1

5 6.1.1 Adjust N_2 process rate to 500 SCFH.

.2 Stabilize substrate inner surface temperature at 1738 $\pm$ 10 °C for at least one hour with no power adjustment required greater than $\pm$ 2 kW/15 minutes.

.3 Record time stabilization is achieved and start DAS, -5 min interval.

.4 Maintain power level for 1 hour with no changes to allow temperature to stabilize. If substrate inner surface temperature drifts more than 25°C, repeat steps 6.1.2, 6.1.3, and 6.1.4. *

5 6.2 N_2 Flow Test 2.

6.2.1 Adjust N_2 process rate to 1000 SCFH.

.2 Maintain all other parameters including power level.

.3 Maintain 1000 SCFH for 1 hour or longer to achieve stable temperature. *

5 6.3 N_2 Flow Test 3

6.3.1 Adjust N_2 process rate to 1400 SCFH. Note T-8 meter. Switch to lower range if necessary. Note time

.2 Maintain all other parameters including power level.

.3 Maintain 1400 SCFH for 1 hour or longer to achieve stable temperature. *

5 6.4 N_2 Flow Test 4

6.4.1 Adjust N_2 process rate to 1000 SCFH. Reset T-8 meter to higher range if changed in 6.. Note time

.2 Maintain all other parameters including power level.

.3 Maintain these parameters for 1 hour or longer to achieve stable temperature and then proceed to power-level Test 1.

*

* Exit gas temperature Profile. Procedure on next page.

THIS PAGE IS BEST QUALITY PRACTICABLE
FROM COPY FURNISHED TO DDC

TABLE D-I (continued)

* Exit 6a Temperature Profile

Verify T-15 thermocouple at maximum insertion. (This is where it should normally be "parked".) Set DAS for continuous scan of Channels 09 through 12. (T-15, T-9, T-5, and T-7). Take continuous scans on DAS for 30 seconds (approx 10 sets of data) Hand Record DAS time, thermocouple T-15 position and T-15 output millivolts (DAS channel 09). Withdraw the T-15 thermocouple $\frac{1}{2}$ inch and repeat the 30 second DAS scan and the hand recording of time, position and millivolts. Discontinue recording on the DAS while the probe is being moved. Continue the process, each time moving the T-15 thermocouple in $\frac{1}{2}$ inch increments until the diameter of the exit tube (~ 5 inches) has been traversed. At the end of the traverse, return the T-15 thermocouple to its fully inserted "parking" position and re-set the DAS for 5 min. scans of all channels (00 through 33.

THIS PAGE IS BEST QUALITY PRACTICABLE
FROM COPY FURNISHED TO DDC

TABLE D-I (continued)

7.0 Power Level Tests (Maintain N_2 Flow Test 4 Gas Flow Rates)

7.1 Power Level Test 1.

7.1.1 Increase coil power level by 15 kW.

.2 * Maintain this power level for 1 hour or longer to achieve stable temperature. *

7.2 Power Level Test 2.

7.2.1 Decrease coil power level by 15 kW.

.2 * Maintain this power level for 1 hour or longer to achieve stable temperature. *

* Exit Gas Temperature Profile, Procedure on Pg 9.

THIS PAGE IS BEST QUALITY PRACTICABLE
FROM COPY FURNISHED TO DDC

TABLE D-I (continued)

8.0 Test Termination

8.1 Turn off furnace power.

8.1.1 Record DAS time and elapsed time in run logs.

.2 Maintain gas flow rates of previous test (Section 7.0).

.3 Continue hand recording of data at 15 min intervals and continue DAS recording of data, at 5 min. intervals all channels (00 – 33)

8.2 After 1 hour, adjust process gas flow rate to 200 SCFH.

8.2.1 Record DAS time and elapsed time in run logs.

.2 Continue hand recording of data and continue DAS recording of data.

8.3 After 1 hour, terminate run.

8.3.1 Discontinue hand recording of data, ~~and turn off DAS~~.

8.3.2 set all applicable pyrometers to "calibrate" mode. Take 10 scans on DAS of all channels (0-33). Using the tape recorder control, add a file gap, & rewind the tape. Verify that it has been labled with the date, test number 15601, and tape sequence number. Turn off the DAS and tape deck.

8.3.2. Cover all sight ports with cardboard

8.3.3 Turn off all instruments

8.3.4. Cover all pyrometer heads with plastic bags.

TABLE D-II

TEST LOG - N_2 FLOW TESTS, I.D. 15601

DAS Time	Remarks
22:04:50	F-5 disconnected.
22:05 25	F-5 reconnected.
22:38:00	Water pressure dropped suddenly to approximately 12 psi, then returned to 26.
23:18:34	T-1 (Channel 16); switch from low to medium scale.
23:18:15	Water pressure fluctuation 27 to 20 to 27 psi in 5 seconds.
23:34:20	Switched range from low to medium; T-8, ch. 17. DAS showed momentary overrange. Shut furnace power off to check F-5 meter effect.
23:54:50	At end of transient heat test, increased N_2 process to 500 SCFH. F-5 decreased from 52 to 22 when power off. When power reapplied, F-5 increased to 33 again.
24:00:00	Low intensity light on T-7. Glass clouded. Slid glass to clear. Low intensity light out. T-7 = 1720°C/DAS off.
24:10:00	Low intensity light back on T-7; readjusted focus; light out. Temperature reading did not change.
02:00:00	Prior to temperature recording, adjusted T-9 pyrometer head. Temperature reading now seems reasonable and low intensity light not on. Small adjustments in head alignment no longer cause gross indicated temperature changes.
03:15:00	Paragraph 4.5 of the Test Procedures: ARC pyrometer calibration. Temperature using 2 color with glass cover in place - 1740°C Temperature using ARC optical pyrometer with glass cover in place - 3123°F (H) - 3123°F (XH) Temperature using ARC optical pyrometer without glass cover in place - 3150°F (H) - 3145°F (XH) Temperature using 2 color optical pyrometer without glass cover in place - 1742°C Temperature using 2 color optical pyrometer with glass cover in place - 1750°C Pressure determination at P-1 while sight port glass removed: pressure 0 or less (-.2 psi).
04:15:00	While taking exhaust temperature scans cannot maintain T-15 N_2 flow rate. Thermocouple seems to be blocking flow. After shoving T/C back in, maximum achievable rate is 65%.

TABLE D-II (continued)

DAS Time	Remarks
04:53:45	Tried to make traverse of exit gas temperatures with T-15. Wouldn't budge. Left in place approximately ½" from wall for remainder of run.
05:04:30	Increased process N_2 flow to 1000 SCFH.
09:38:35	Calibrated T-2; was reading about 30°C low.
09:50:00	Calibrated remaining instruments.
14:29:45	Increased power from 45 Kw to 60 Kw in 5 seconds.
17:00:00	Hot spot in fiberfrax - 180 position- center of furnace.
17:20:00	Tapped with wood stick to cause carbon block to fall into void.
17:40:00	Hot spot near T-3 and T-11A (0°).
18:45:00	Intermittant low intensity indication on T-7.
19:00:00	Power circuit back on line.
19:10:00	T-5 in calibrate position for this scan. Next scan it will be switched to high scale (19:15:00 scan).
20:15:00	Shielding F-5 with dustpan, aluminum foil, foil in place for 20:15:00 scan.
20:25:00	Low intensity signal (intermittant) on T-5.
21:10:00	F-5 disconnected to check mag. pickup signal.
22:05:00	Dismounted T-13 pyrometer head (IRCON). Read temperature using L&N pyrometer 3715°F (2319 K). (Conversion from scale reading on Range I is 2093 K.)
22:17:00	T-1 switched to high scale.
23:04:00	Read T-13 with L&N pyrometer - 3745°F (2336 K).
23:30:30	Turned power off.
23:32:00	F-5: 21 GPM, water pressure 27 ½ psig.
23:35:20	T-5 switched to low scale.
23:36:25	T-2 switched to low scale.

TABLE D-III

REDUCED DATA FOR THE NITROGEN FLOW TESTS

The reduced test data are plotted versus normalized time in minutes. A second reference scale at the bottom of each page gives the corresponding DAS or real time in hours. The label on each figure identifies the parameter plotted (see Figs. A-6 and B-1). The parameters are arranged in alphabetical and numerical order.

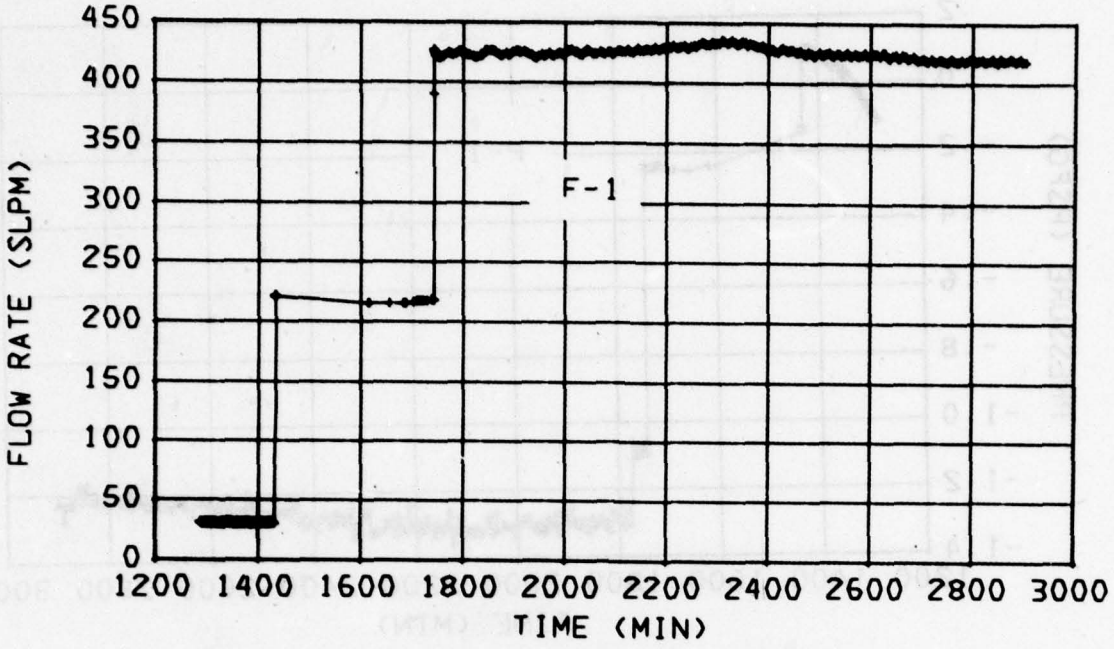

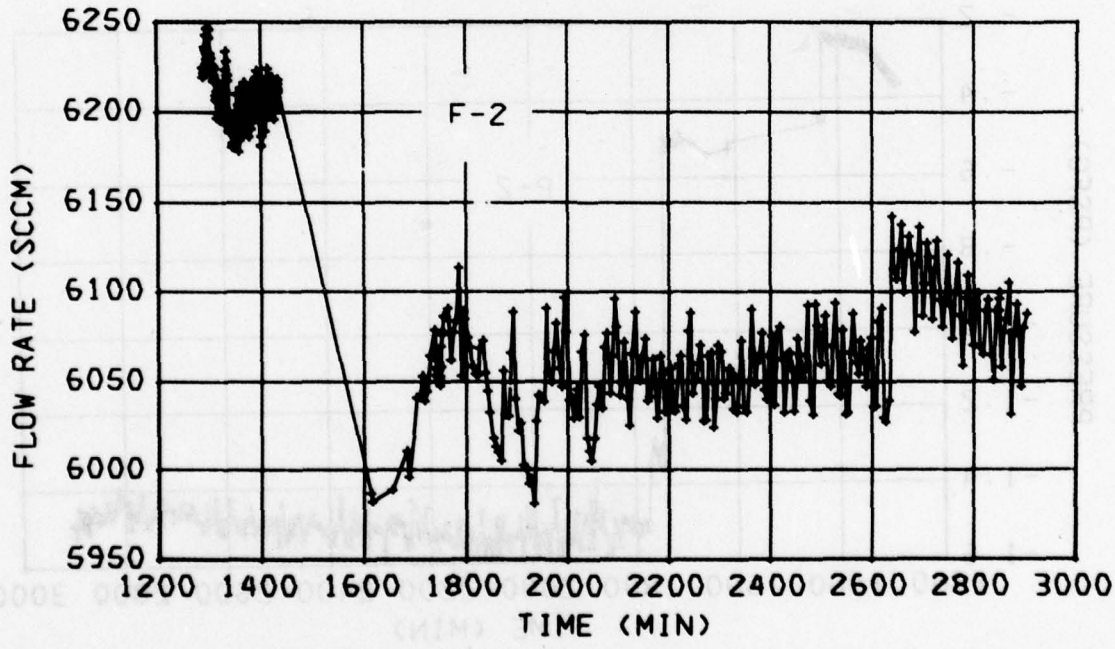

2000 2320 0240 0600 0920 1240 1600 1920 2240 0200

DAS TIME OR REAL TIME (HRS)

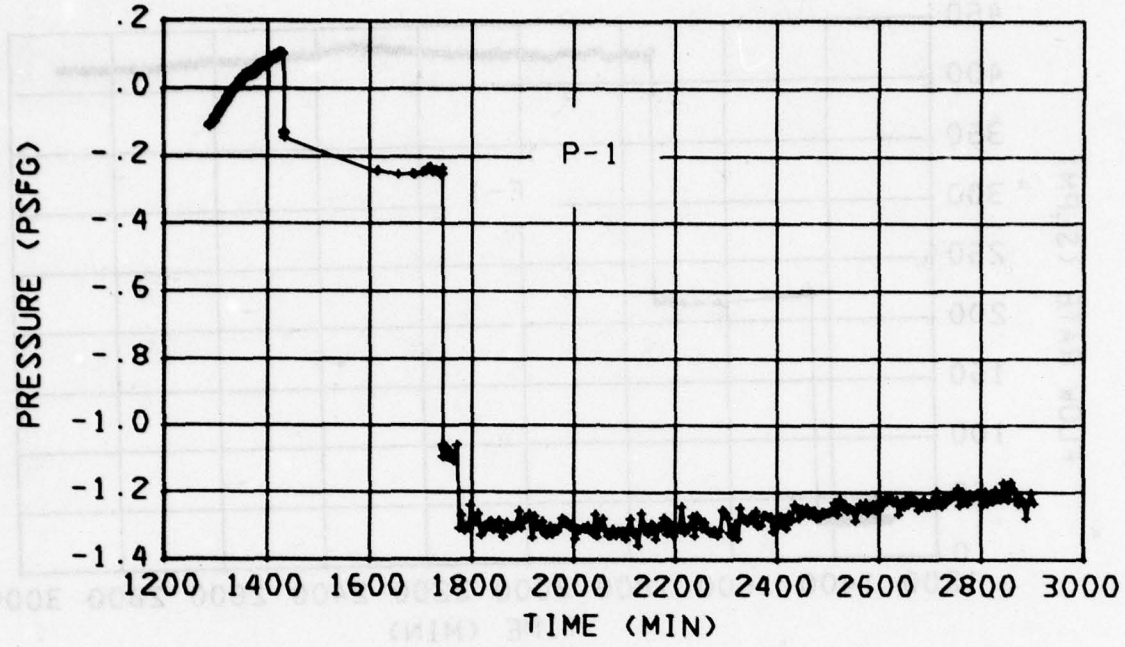

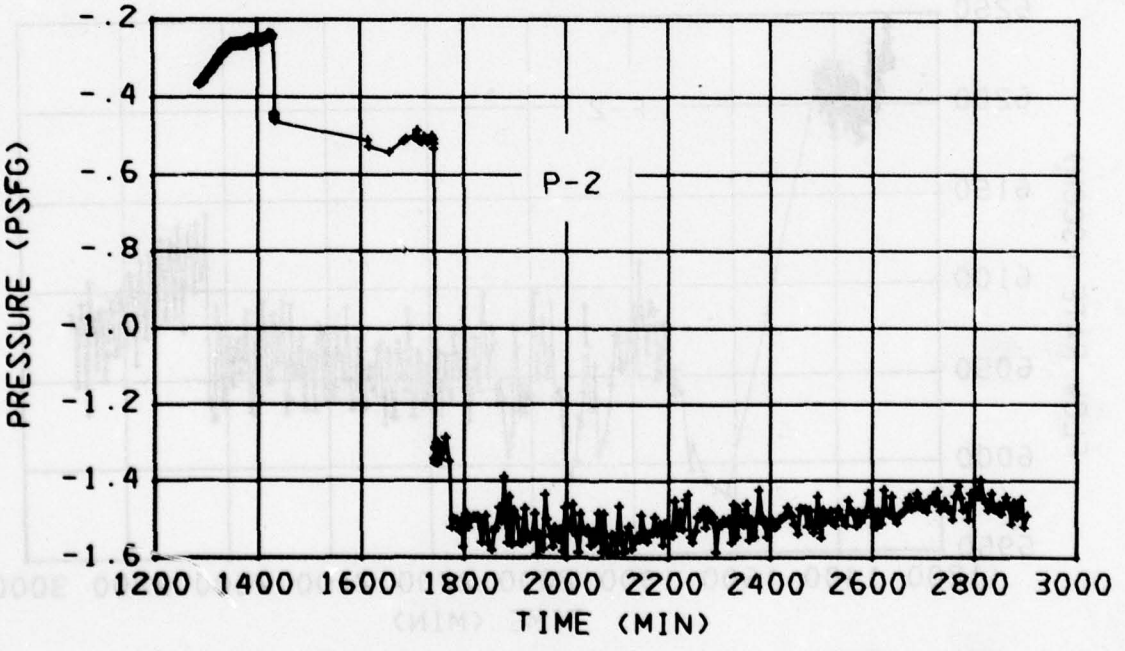

2000 2320 0240 0600 0920 1240 1600 1920 2240 0200

DAS TIME OR REAL TIME (HRS)

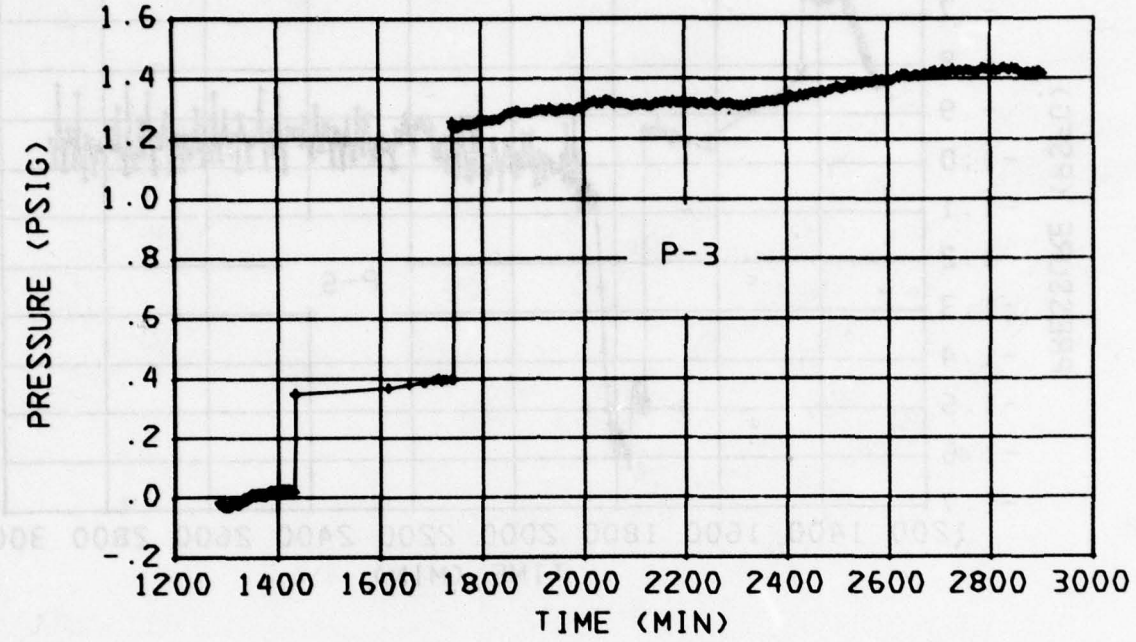

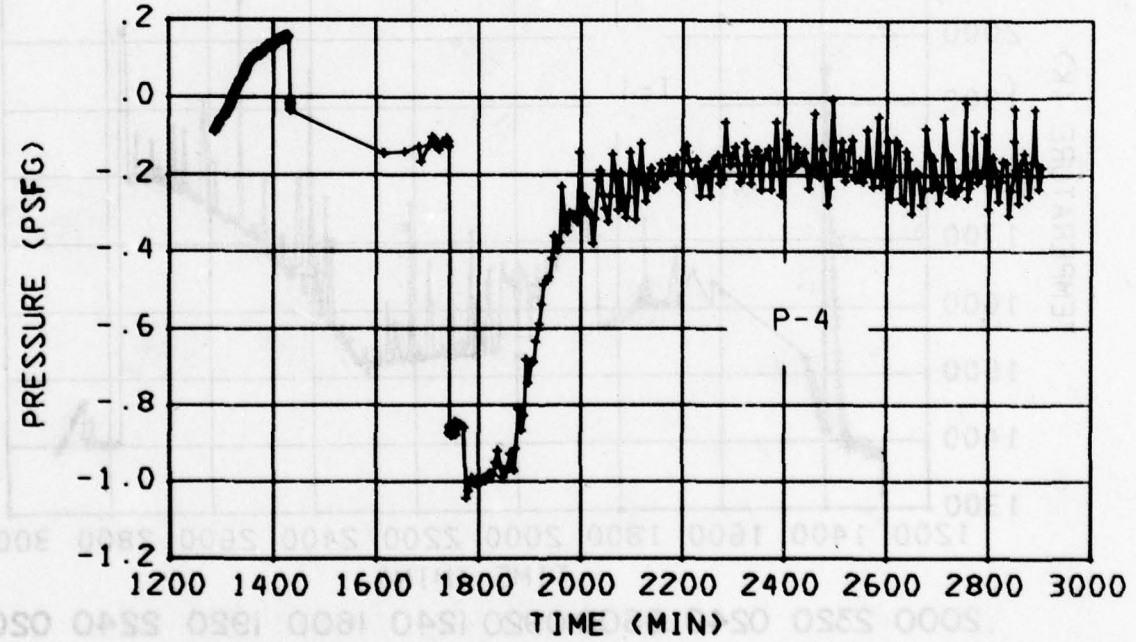

2000 2320 0240 0600 0920 1240 1600 1920 2240 0200

DAS TIME OR REAL TIME (HRS)

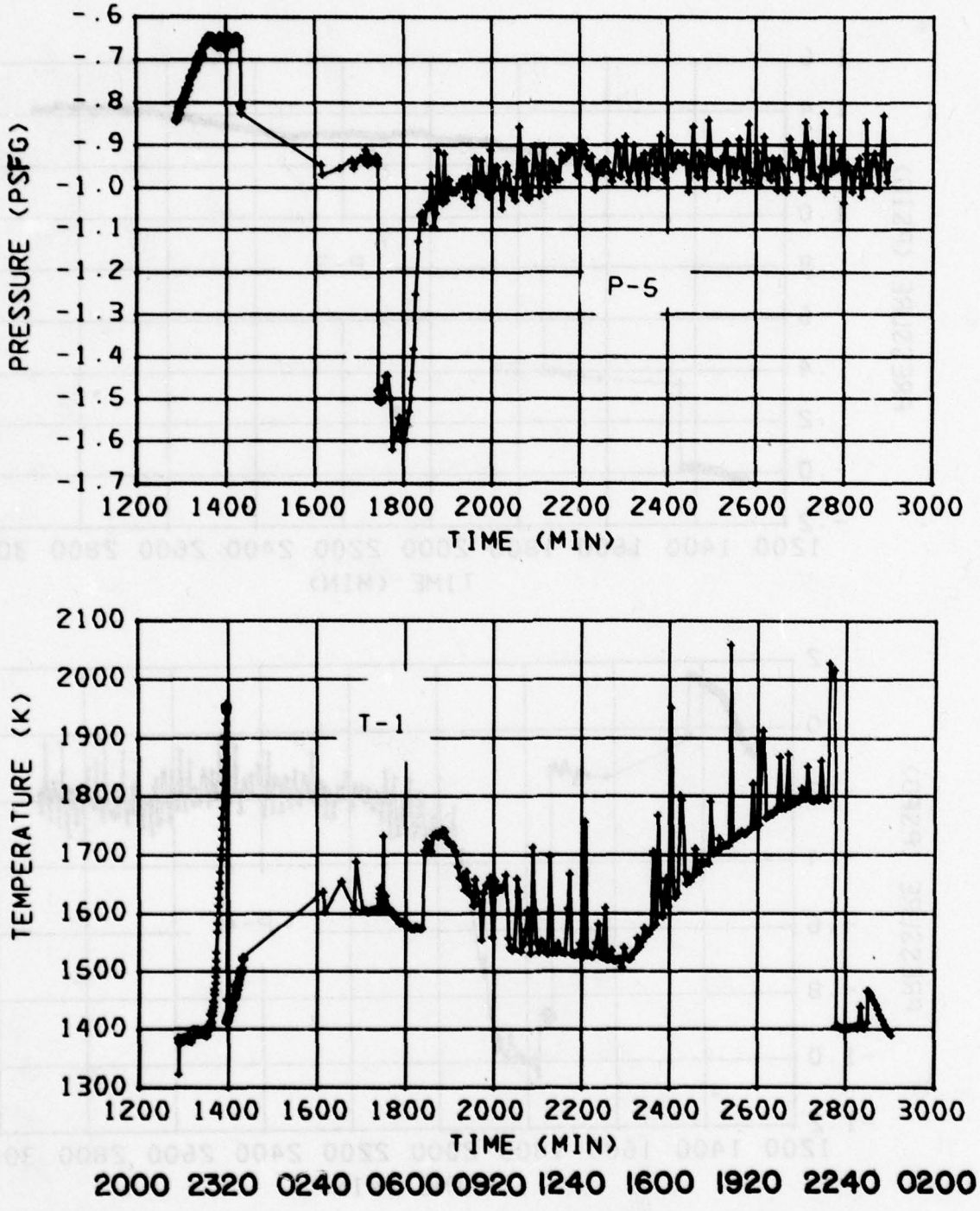
PRESSURE (PSFG)
-.6
-.7
-.8
-.9
-1.0
-1.1
-1.2
-1.3
-1.4
-1.5
-1.6
-1.7
P-5
1200 1400 1600 1800 2000 2200 2400 2600 2800 3000
TIME (MIN)
TEMPERATURE (K)
2100
2000
1900
1800
1700
1600
1500
1400
1300
T-1
1200 1400 1600 1800 2000 2200 2400 2600 2800 3000
TIME (MIN)
2000 2320 0240 0600 0920 1240 1600 1920 2240 0200
DAS TIME OR REAL TIME (HRS)

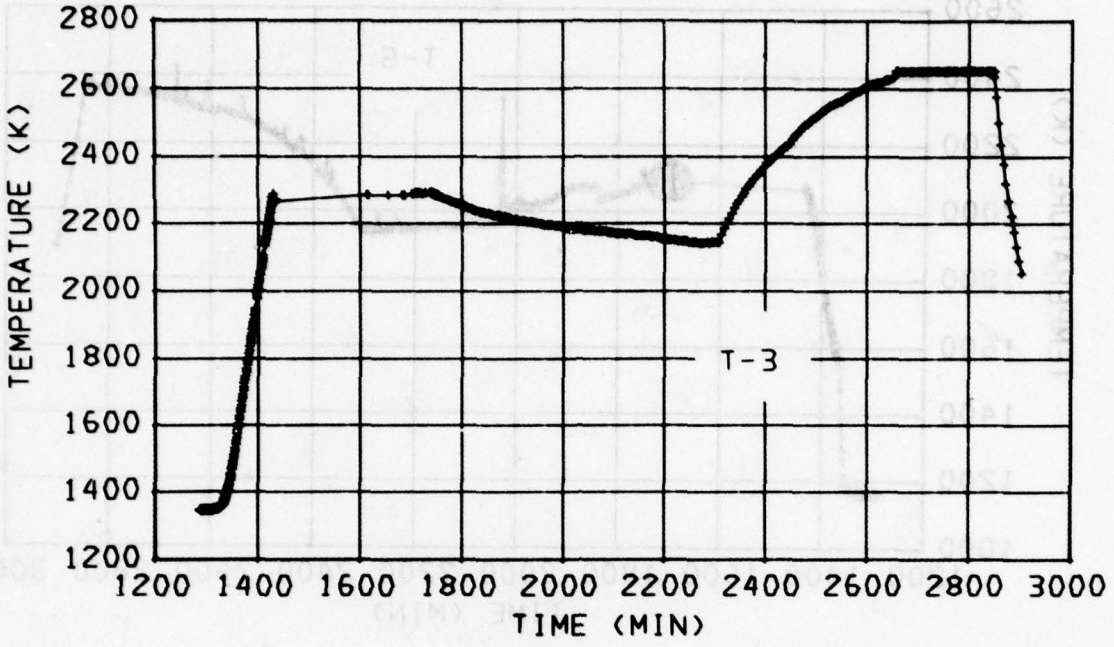

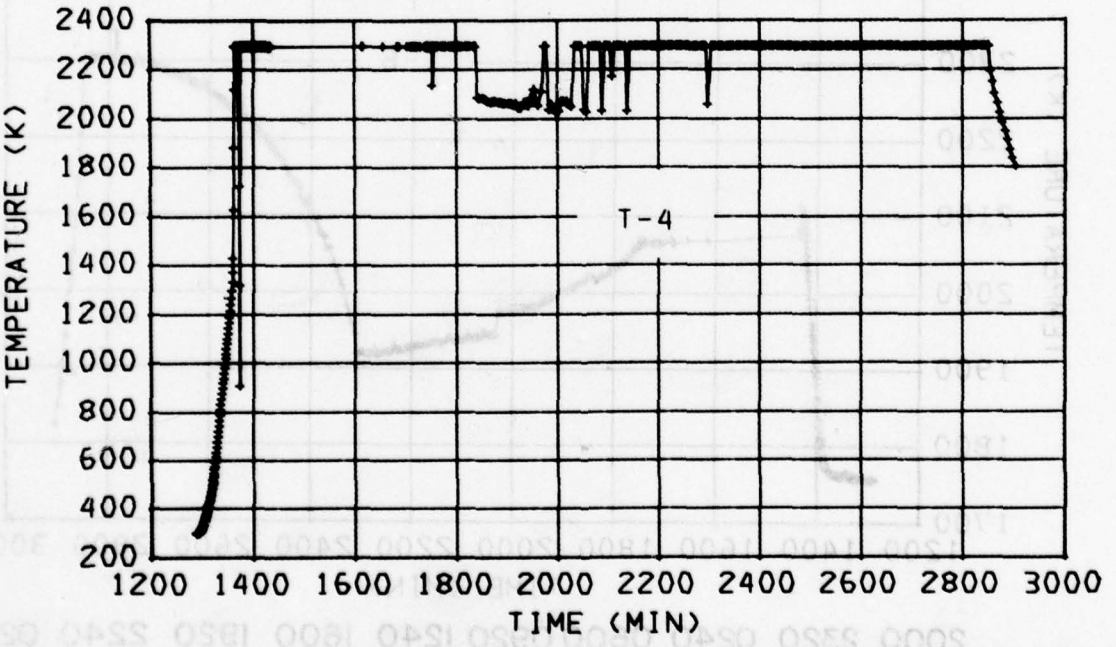

2000 2320 0240 0600 0920 1240 1600 1920 2240 0200

DAS TIME OR REAL TIME (HRS)

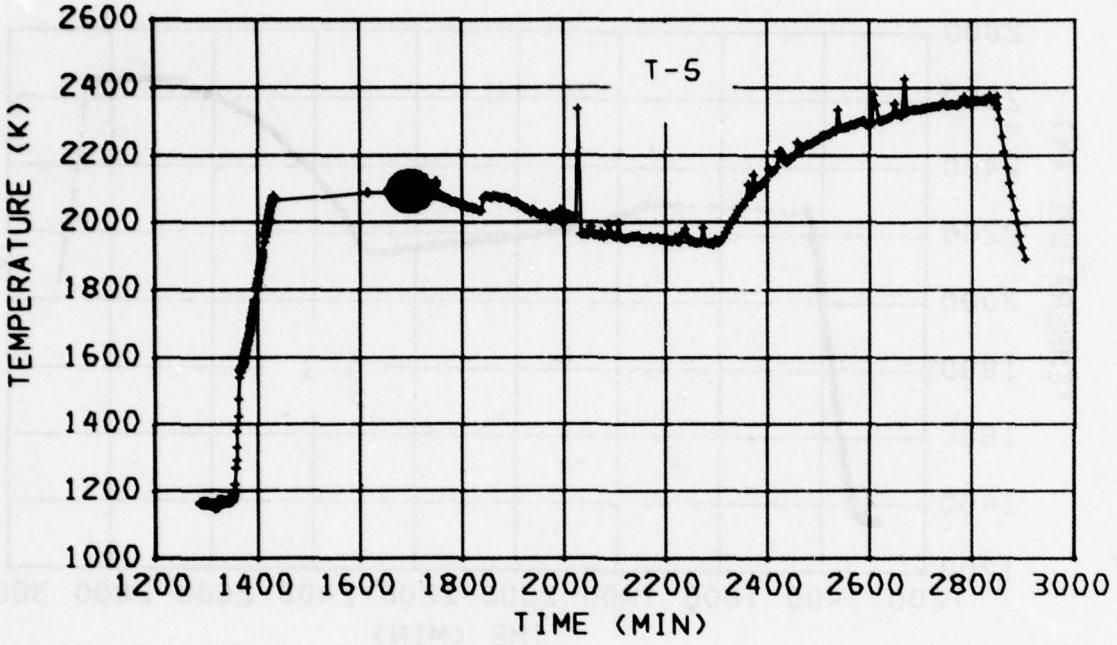

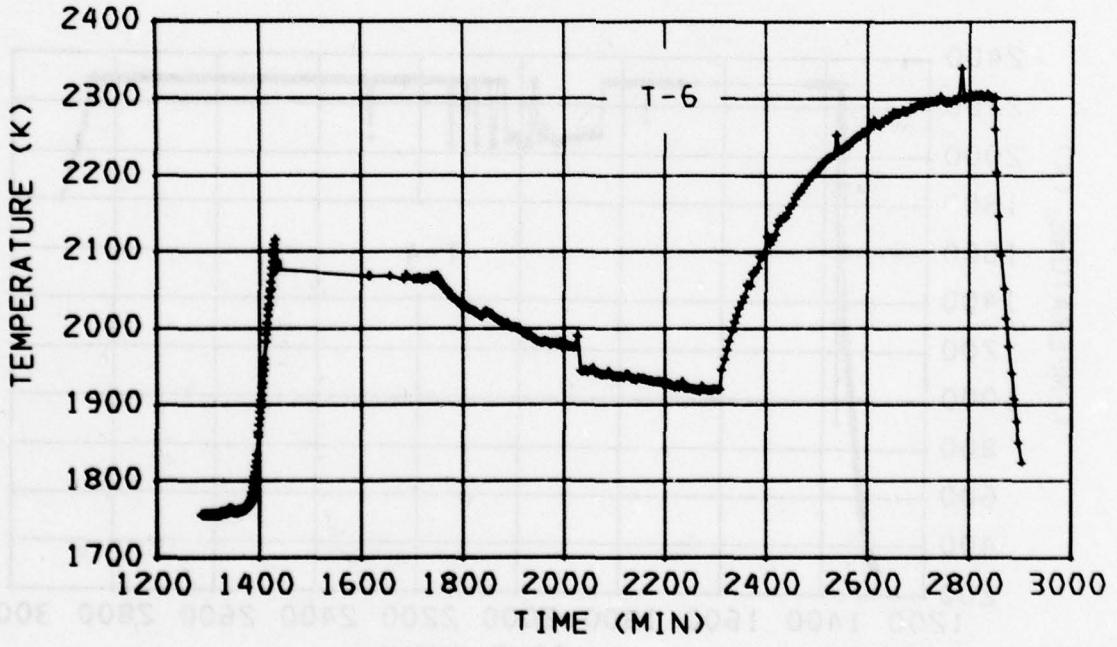

2000 2320 0240 0600 0920 1240 1600 1920 2240 0200

DAS TIME OR REAL TIME (HRS)

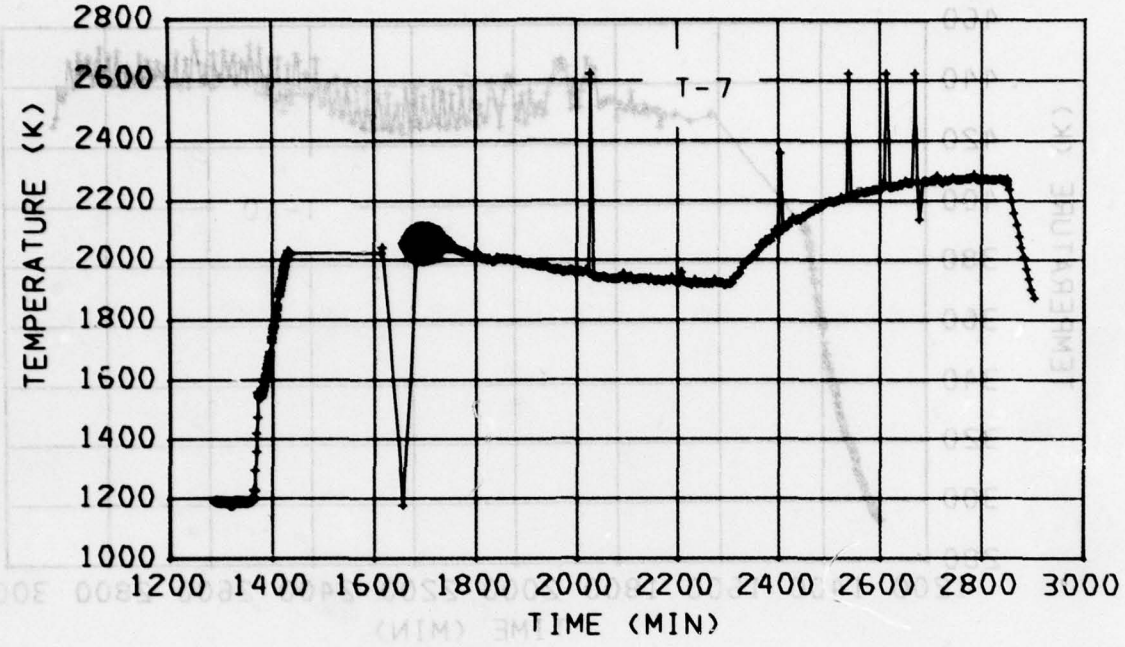

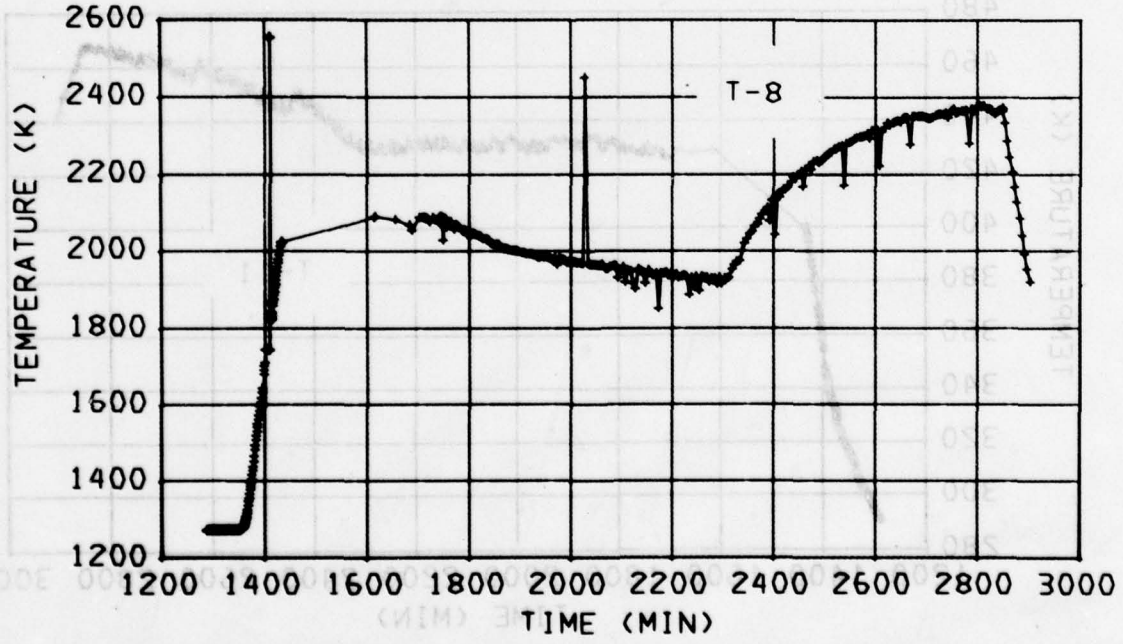

2000 2320 0240 0600 0920 1240 1600 1920 2240 0200

DAS TIME OR REAL TIME (HRS)

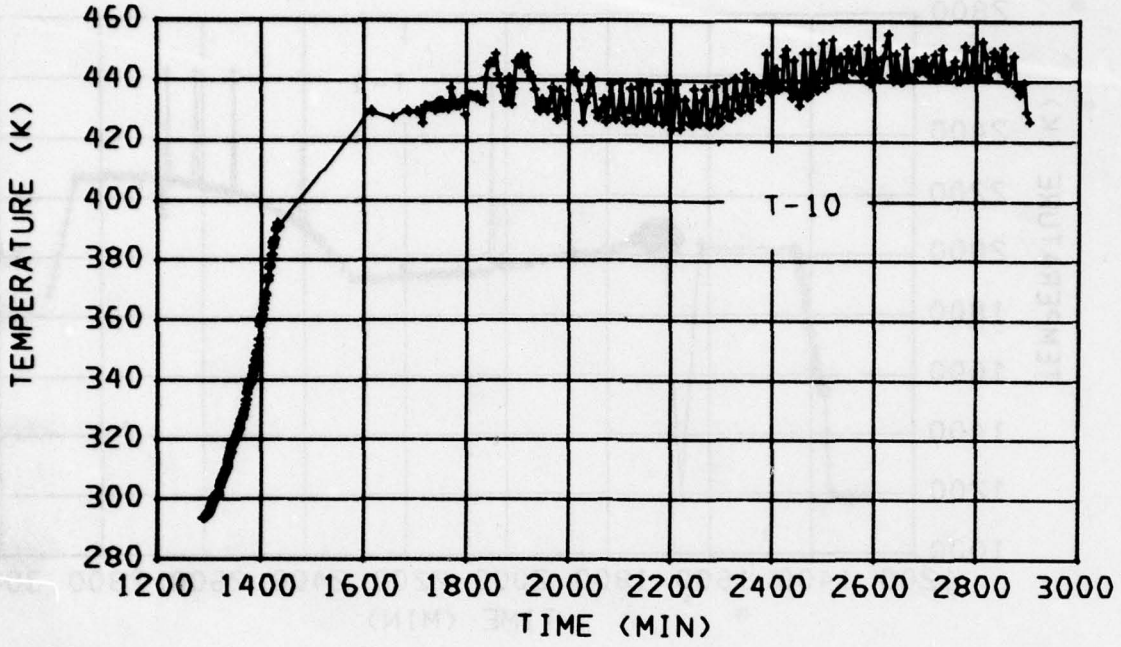

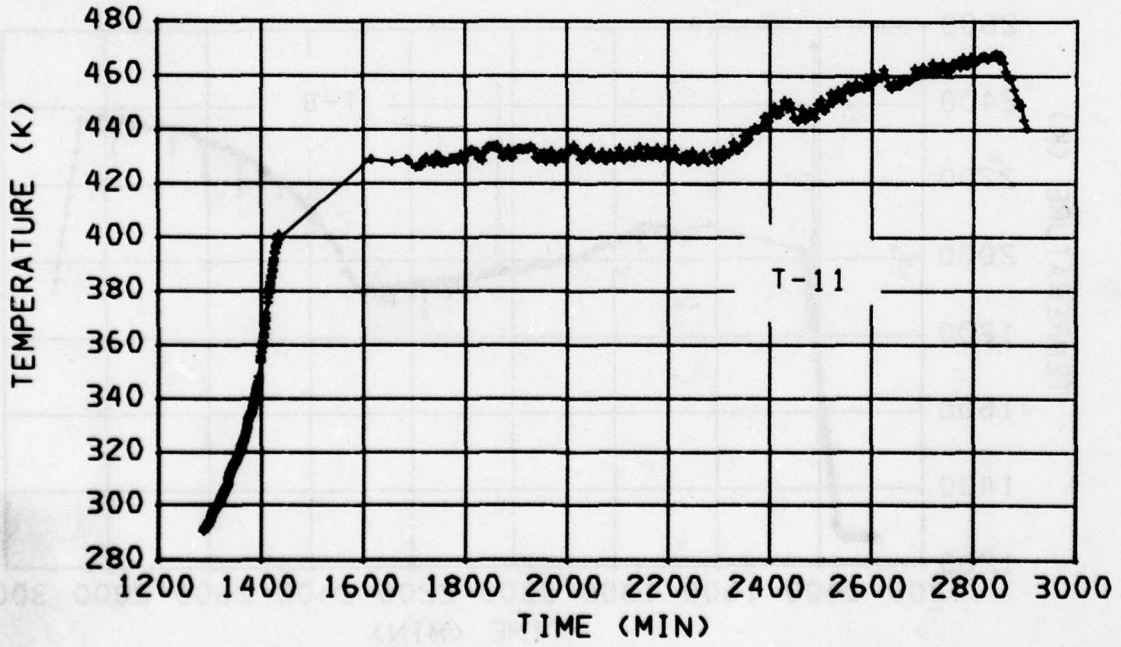

2000 2320 0240 0600 0920 1240 1600 1920 2240 0200

DAS TIME OR REAL TIME (HRS)

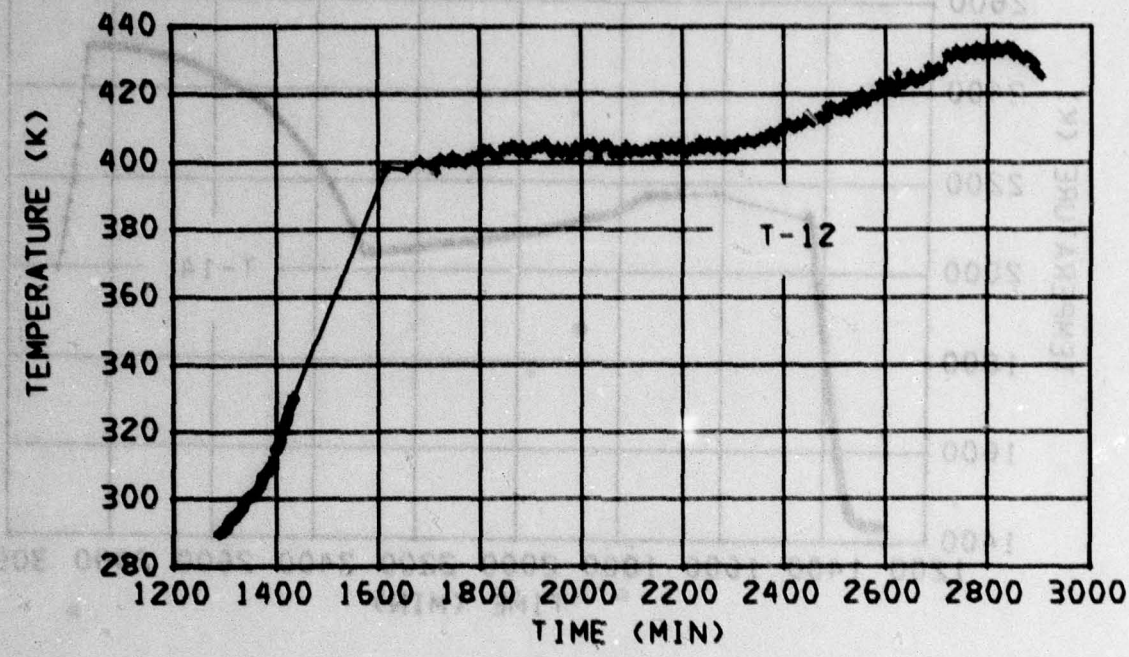

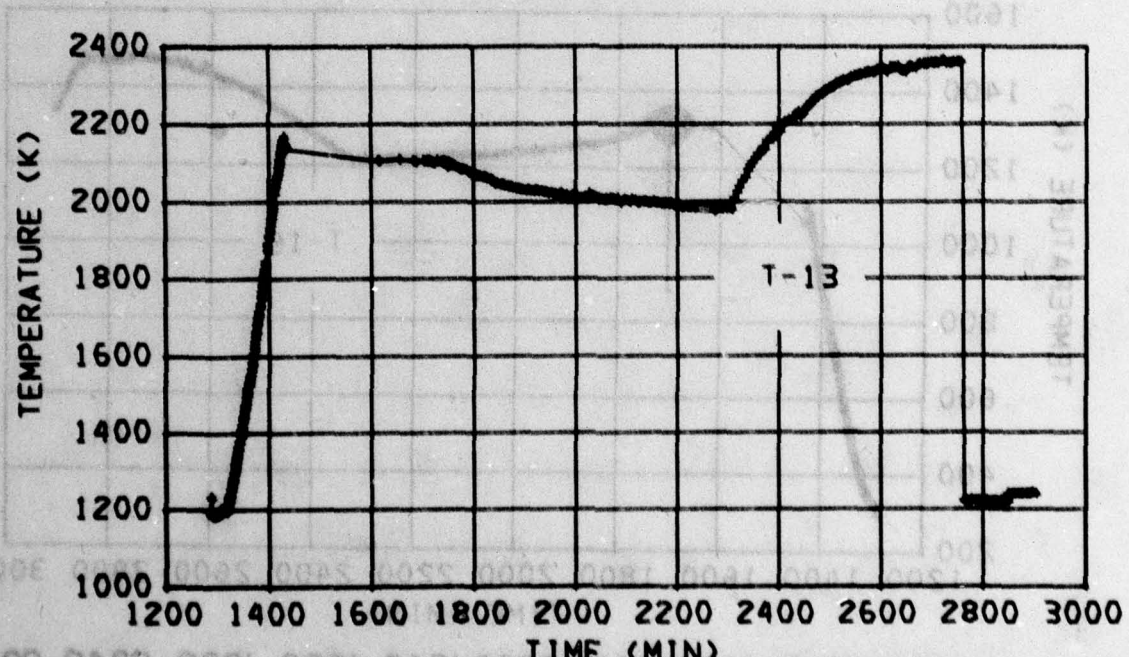

2000 2320 0240 0600 0920 1240 1600 1920 2240 0200

DAS TIME OR REAL TIME (HRS)

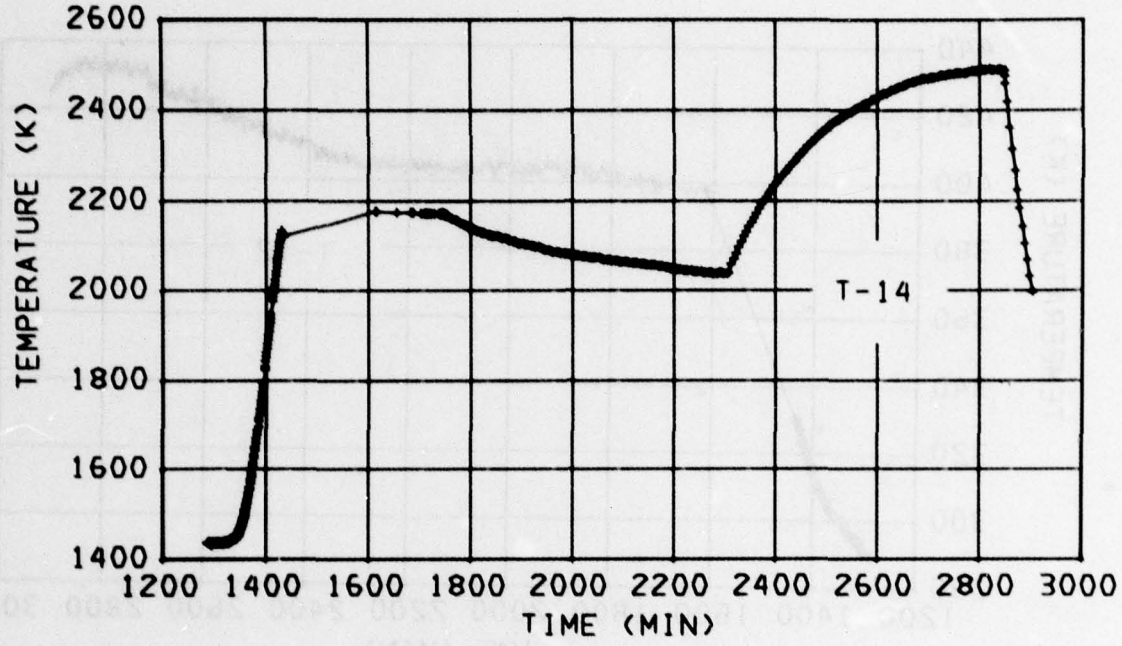

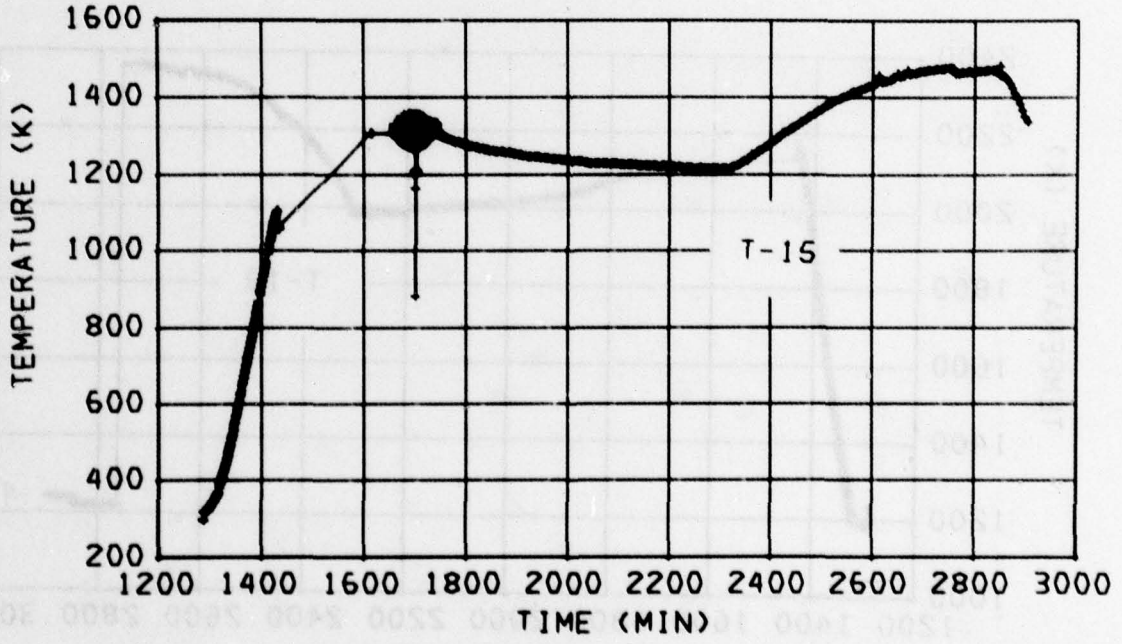

2000 2320 0240 0600 0920 1240 1600 1920 2240 0200

DAS TIME OR REAL TIME (HRS)

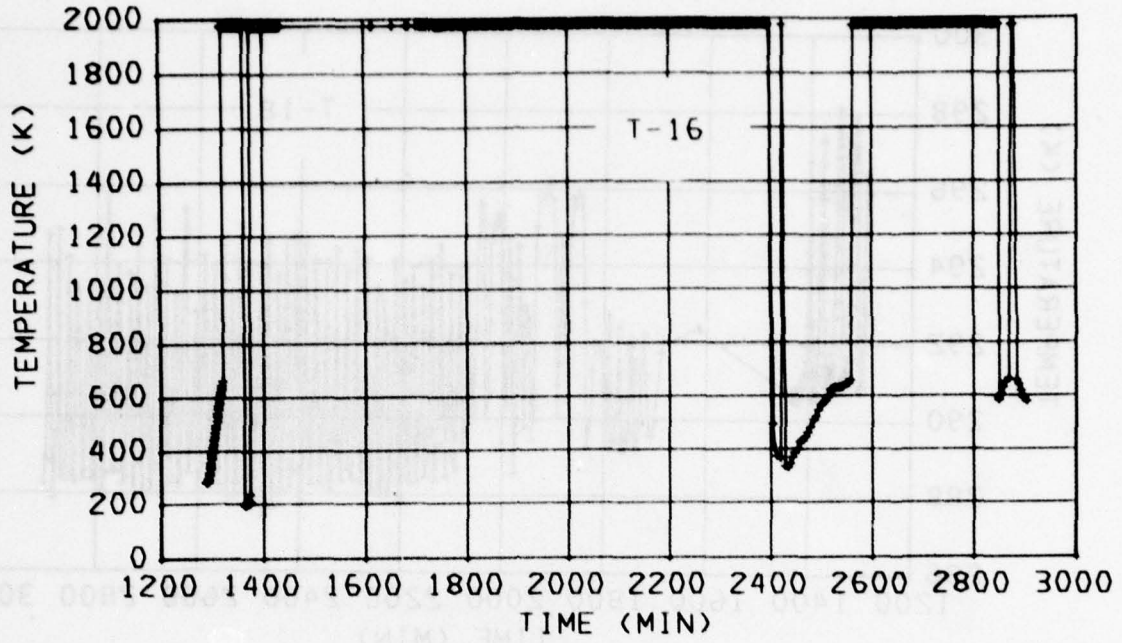

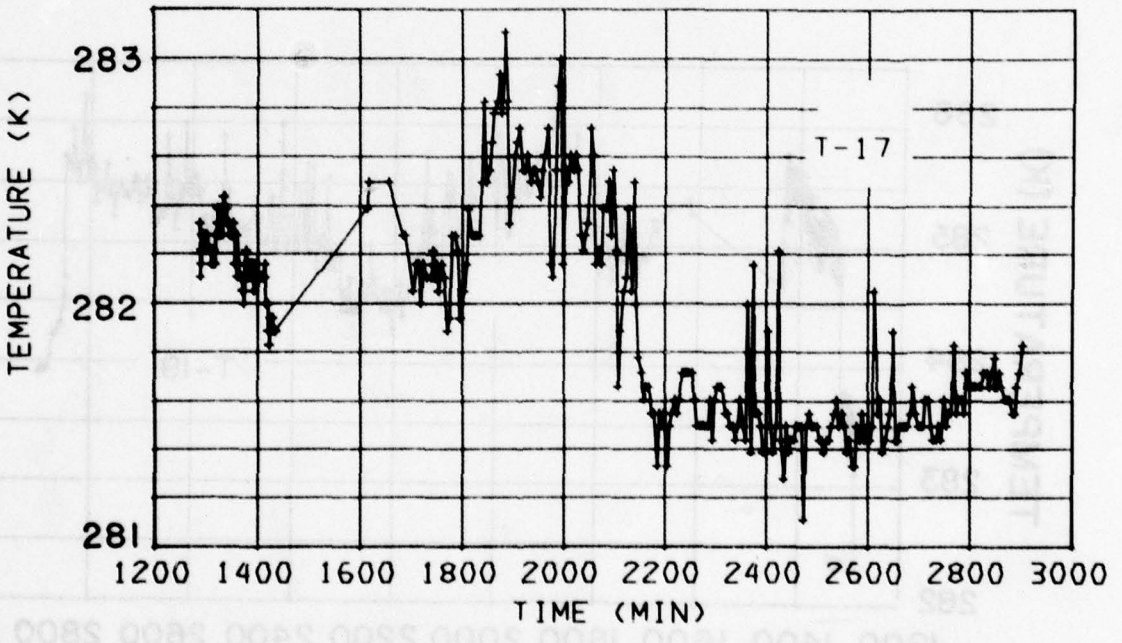

2000 2320 0240 0600 0920 1240 1600 1920 2240 0200

DAS TIME OR REAL TIME (HRS)

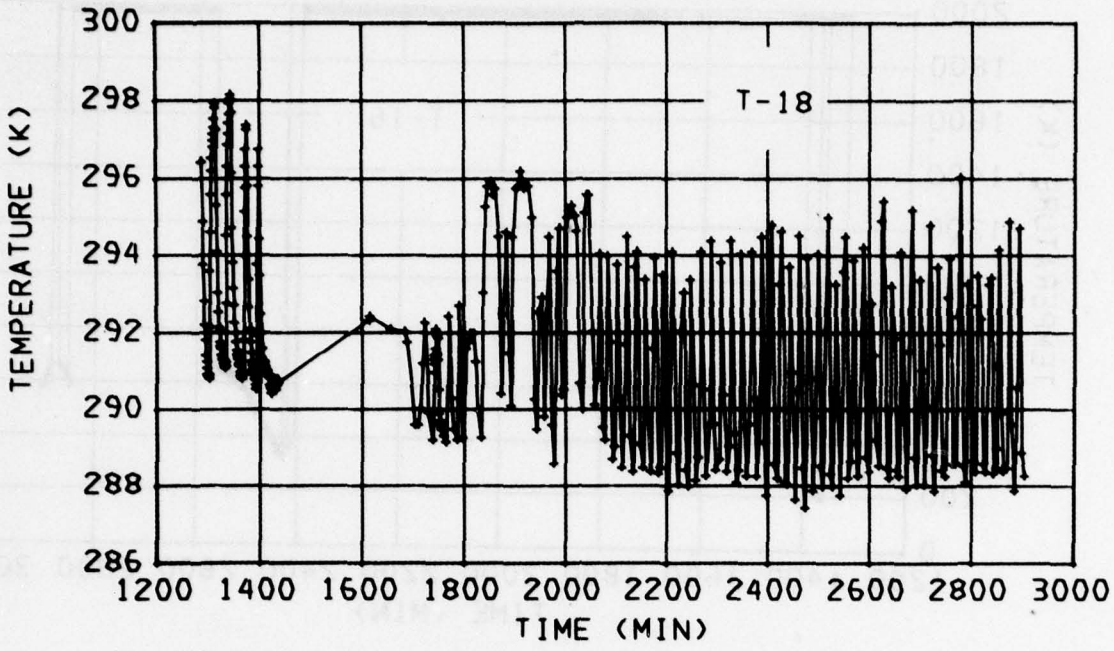
T-18
TEMPERATURE (K)
300
298
296
294
292
290
288
286
1200 1400 1600 1800 2000 2200 2400 2600 2800 3000
TIME (MIN)

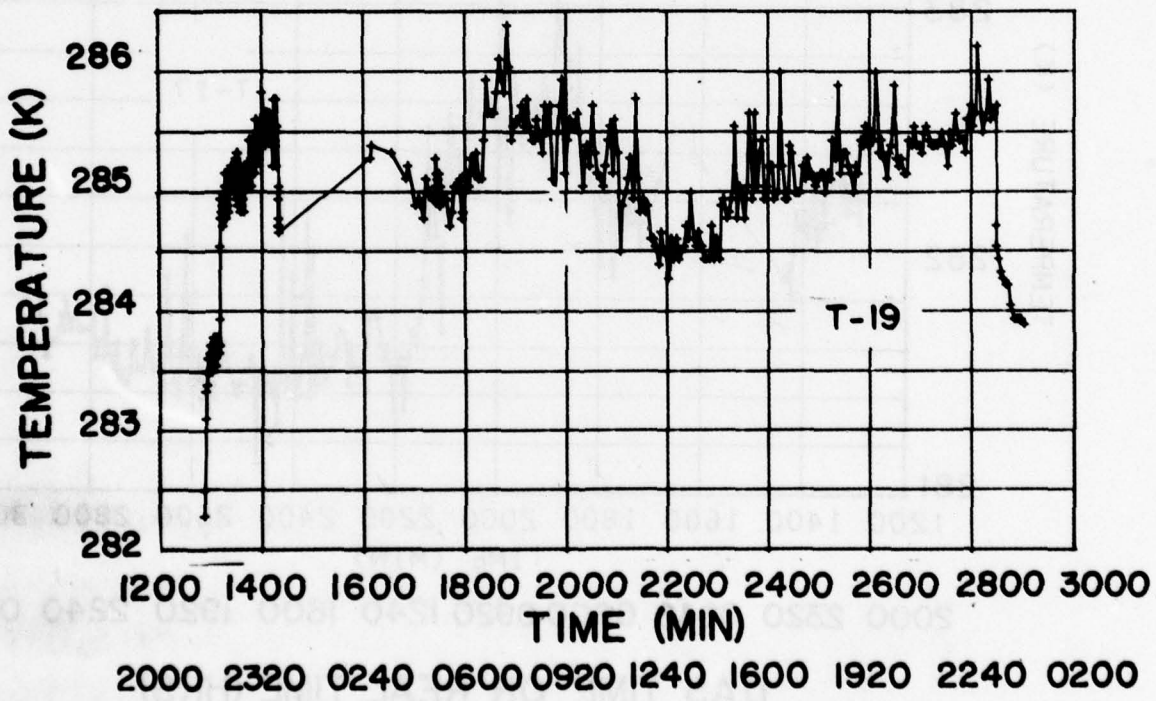
T-19
TEMPERATURE (K)
286
285
284
283
282
1200 1400 1600 1800 2000 2200 2400 2600 2800 3000
TIME (MIN)
2000 2320 0240 0600 0920 1240 1600 1920 2240 0200
DAS TIME OR REAL TIME (HRS)

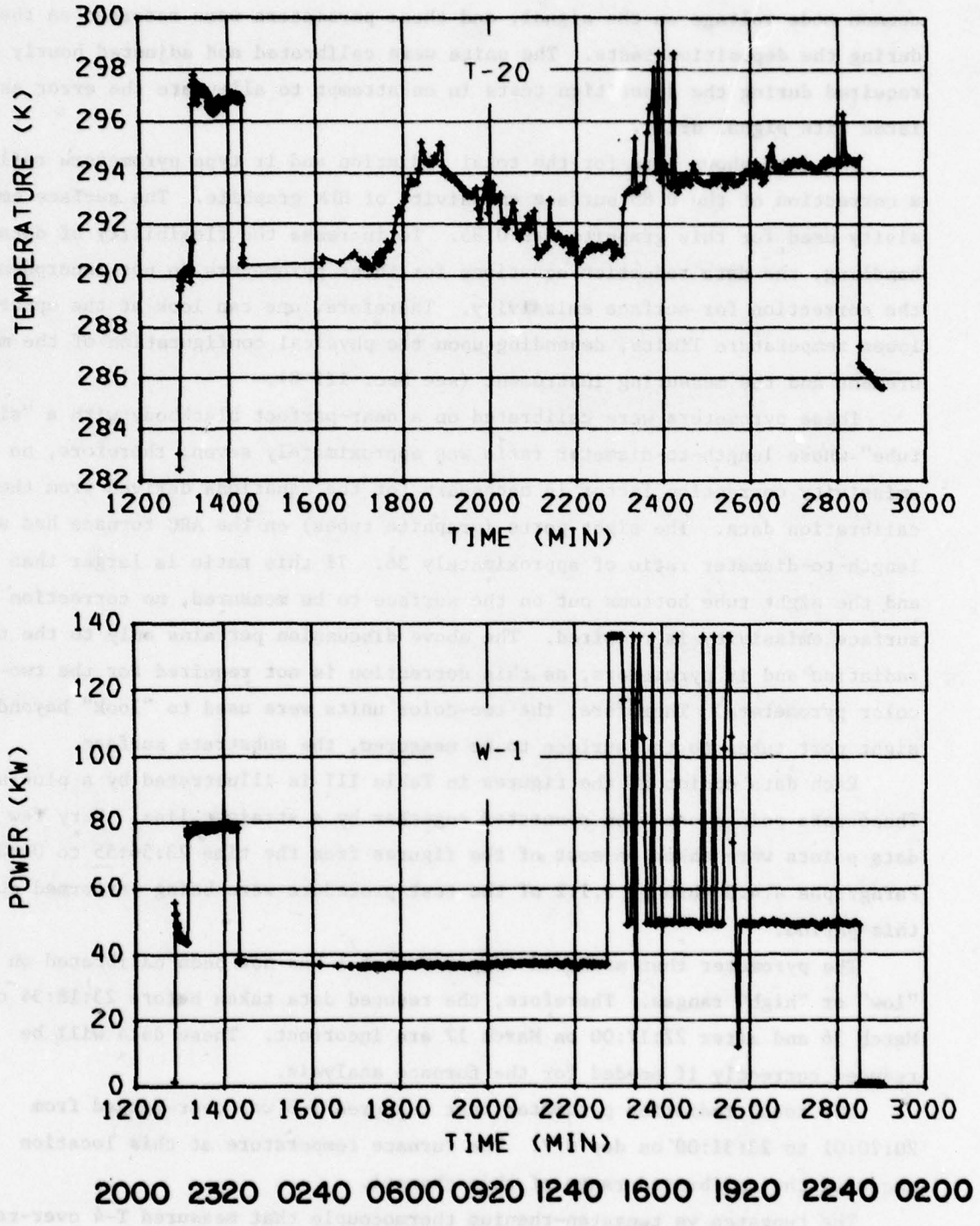
T-20
TEMPERATURE (K)
300
298
296
294
292
290
288
286
284
282
1200 1400 1600 1800 2000 2200 2400 2600 2800 3000
TIME (MIN)
W-1
POWER (KW)
140
120
100
80
60
40
20
0
1200 1400 1600 1800 2000 2200 2400 2600 2800 3000
TIME (MIN)
2000 2320 0240 0600 0920 1240 1600 1920 2240 0200
DAS TIME OR REAL TIME (HRS)

common mode voltage on the signal, and these parameters were recorded on the DAS during the deposition tests. The units were calibrated and adjusted hourly as required during the deposition tests in an attempt to alleviate the error associated with signal drift.

The data shown here for the total radiation and ir type pyrometers reflect a correction of the 0.85 surface emissivity of HLM graphite. The surface emissivity used for this graphite was 0.85. To increase the flexibility of data handling, the data reduction equations for these pyrometers do not incorporate the correction for surface emissivity. Therefore, one can look at the upper and lower temperature limits, depending upon the physical configuration of the measurement and the measuring instrument (see Sec. III B).

These pyrometers were calibrated on a near-perfect blackbody with a "sight tube" whose length-to-diameter ratio was approximately seven; therefore, no emissivity correction factor is necessary for the equations derived from the calibration data. The sight ports (graphite tubes) on the ARC furnace had a length-to-diameter ratio of approximately 36. If this ratio is larger than five and the sight tube bottoms out on the surface to be measured, no correction for surface emissivity is required. The above discussion pertains only to the total radiation and ir pyrometers, as this correction is not required for the two-color pyrometers. Therefore, the two-color units were used to "look" beyond the sight port tubes to the surface to be measured, the substrate surface.

Each data dpoint of the figures in Table III is illustrated by a plus sign. These data points are then connected together by a straight line. Very few data points were taken on most of the figures from the time 23:56:55 to 04:05:00. Paragraphs 4.4.3 through 5.1.2 of the test procedure were being performed during this period.

The pyrometer that measured temperature T-1 has not been calibrated on the "low" or "high" ranges. Therefore, the reduced data taken before 23:18:34 on March 16 and after 22:17:00 on March 17 are incorrect. These data will be reduced correctly if needed for the furnace analysis.

The total radiation pyrometer that measured T-3 was over-ranged from 20:20:01 to 23:31:00 on day 077. The furnace temperature at this location exceeded the calibrated range of this channel.

The tungsten vs tungsten-rhenium thermocouple that measured T-4 over-ranged at 22:47:00 on day 076 and ultimately failed. At 06:45 on day 077, the output signal from T-4 came back on scale, and at 09:55 it over-ranged again. Also,

at these exact times the recorded output of T-1, T-5, T-6, and T-7 changed. These output signals increased when T-4's signal was within the DAS range and decreased again as T-4 over-ranged.

The errors associated with T-5, T-6, and T-7 during this period are plus 40, 30, and 15 K respectively. The T-1 data are completely erroneous during this period, except, possibly, for the points at 08:55:00 and 09:20:00 h.

As indicated above, the T-1 data were affected during this same period. The negative-going spike at 08:55 on T-1 corresponds to the time when T-4 momentarily over-ranged. The temperature recorded for T-1 at this time was 1537 K. The parameters T-5, T-6, T-7, and T-8 also were affected at this time. Their data showed temperature drops of 16, 3. 7, and 16 K, respectively.

These data indicate that T-4 was intermittently shorted to the furnace. This short circuit was either providing a ground loop or connecting the voltage on the furnace (substrate) to the DAS, exceeding its common mode voltage specification. The data on almost all of the channels are noisier than normal which suggests the existance of such a system problem.

The positive-going spike in the data plots of parameters T-5, T-6, T-7, and T-8 at 09:50 h on day 077 occurs because the pyrometers that measured these parameters were placed in the "CAL" position for a single DAS scan. The pyrometer measuring T-5 showed a "34 K calibration error." However, when this pyrometer was placed in the "CAL" position at 19:10:01 on day 077, it repeated its original calibration of 2304 K. This fact gives weight to the argument that the data offset between 06:45 h and 09:50 h is approximately 4 K in error.

During the above calibration check of the pyrometers, we found that the calibration circuit for T-6 had failed. The calibration signal for T-7 over-ranged, indicating a positive shift in its output signal. The pyrometer measuring T-8 repeated its calibration point within 1 K.

After the test, the pyrometer heads for parameters T-5 and T-6 were found to be reversed. The pyrometers were connected to the respective signal conditioners and DAS channels correctly. However, the units were "looking" at the wrong parameter. The reduced data show his discrepancy but the correct data were used for the computer model study.

The data for furnace power, W-1, are sporadic after approximately 14:00 on day 077. The signal conditioning for the power measurement was being trouble shot and repaired at this time. The data are correct except for the large deviations away from the 50-kW level.

III DEPOSITION TESTS

The test identification numbers for the deposition test are in the series 15800. These tests started at 13:32:08 on day 126 (May 5, 1976) and concluded at 19:24:28 on day 127 (May 6, 1976). The procedures for these tests are included because they are part of the data package.

A. Deposition Test Procedure.

The deposition test procedure is presented in Table D-IV. It is a copy of that on file at LASL.

B. Deposition Test Log.

The enclosed test log (Table D-V) for test series 15800 is a typed copy of the original which is on file at LASL. It is included as part of the data package since it outlines pertinent events which occurred during the test and their time occurrence. It is enclosed so that the reader may correlate these events with the data graphs presented in this appendix.

C. Deposition Test Data.

The data in the following figures (Table VI) depict that portion of the test in which power was applied to the furnace. It was not convenient to present the data taken during other parts of the test in this format; therefore, portions of the data appear in Sec. III of this report. All of the data was recorded on magnetic tape which is on file at LASL.

D. Discussion of Deposition Tests Data.

Each data point on the figures is illustrated by a plus sign. These data points are then connected together by a straight line. The small arrows on the abscissa depict a different test number. To facilitate the interpretation of the data, the test I. D. numbers are identified below.

	Test I.D. Number	Test Description
1.	15800	Furnace Heat Up
2.	15801	Effect of MTS on Substrate Temp T-7
3.	15802	Coating Run Number 1
4.	15803	Effect of CH_4 on Substrate Temp T-7
5.	15804	Coating Run Number 2
6.	15805	Coating Run Number 3 Setup
7.	15818	Effect of MTS on Substrate Temp T-7

THIS PAGE IS BEST QUALITY PRACTICABLE
FROM COPY FURNISHED TO DDC

TABLE D-IV
COPY OF TEST PROCEDURE - DEPOSITION TESTS

LASL PROCEDURES — LAB COPY

		Checked by	Checked by
1.0 Assembly			
1.1 Fixtures assembled as per SK6944-001A. Check following items for proper location, alignment, and assure that correct transducers are in place.			
1.1.1	T-1	CN	CN
.2	T-2	CN	CN
.3	T-3	CN	CN
.4	T-5	CN	CN
.5	T-6	CN	CN
.6	T-7	CN	CN
.7	T-8	CN	CN
.8	T-9	CN	CN
.9	T-10	CN	CN
.10	T-11	CN	CN
.11	T-12	CN	
.12	T-13	CN	
.13	T-14	CN	
.14	T-15	CN	
.15	T-17	CN	CN
.16	T-18	CN	CN
.17	T-19	CN	CN
.18	T-20	CN	CN
.19	P-3	CN	CN
.20	F-1	CN	CN
.21	F-2	CN	CN
.22	F-3		

THIS PAGE IS BEST QUALITY PRACTICABLE
FROM COPY FURNISHED TO DDC

TABLE D-IV (continued)

1.1.23	F-4	—	NA
.24	F-5	en	KU
.25	W-1	en	KU
.26	Furnace Case Pressure Gages.	en	KU
1.2	Injector location (10.8 inches from subs.)	en	KU
1.3	Lampblack approx. 8 inches above susc. Slope upwards towards fiberfrax to compensate for settling. Measure depth (3 places) 6½ 6½ 7½	en	KU
1.4	Cooling water connections to:		
1.4.1	T-1	en	KU
.2	T-2	en	KU
.3	T-3	en	KU
.4	T-5	en	KU
.5	T-6	en	KU
.6	T-7	en	KU
.7	T-8	en	KU
.8	T-9	en	KU
.9	T-13	en	KU
.10	T-14	en	KU
.11	T-15	en	KU
.12	P-1	en	KU
.13	P-2	en	KU
.14	Coil	en	KU
.15	Injector	en	KU
.16	S. P. Outlet Manifold	en	KU
.17	Furnace Exhaust Tube Assembly	en	KU
.18	Bus Bar	en	KU
.19	Support Plate	en	KU

THIS PAGE IS BEST QUALITY PRACTICABLE
FROM COPY FURNISHED TO DDC

TABLE D-IV (continued)

1.4.20	S. P. Inlet Manifold		en	KU
.21	Furnace Lid		en	KU
1.5	Drain lines to items 1.4.1 - 1.4.16 interconnected and monitored by T-19 and F-5.		en	KU
1.6	Process gas connections for:			KU
1.6.1	N_2 Process		en	
.2	N_2 Annulus		en	KU
.3	CH_4 (to Tylan Panel)		en	KU
.4	He (to Tylan Panel)		en	KU
.5	MTS		en	KU
.6	Pressure to pneumatic valves on Tylan unit		en	KU
1.7	Initial MTS System Purge:			
1.7.1	All valves closed (SV-1 through SV-11)		en	KU
.2	Adjust N_2 pressure to 25 psi to Valve # SV-10		en	KU
.3	Disconnect MTS fill line at MTS Valve E		en	KU
.4	Set Valve # SV-7 to "PURGE" Valve # SV-11 to "OPEN" Valve # SV-10 to "OPEN" MTS purge rotameter to "FULL SCALE"		en	
.5	Purge with N_2 for 15 minutes		en	KU
.6	Set Valve # SV-7 to "OFF" Valve # SV-8 to "PURGE" Valve # SV-9 to "PURGE"		en	KU
.7	Purge with N_2 for 15 minutes		en	KU
.8	Set Valve # SV-11 to "CLOSED" Valve # SV-8 to "FILL"		en	KU
.9	Purge with N_2 for 15 minutes		en	KU
.10	Connect MTS fill line to MTS Valve E while N_2 is flowing. Tighten fitting with wrench and leak test.		en	KU

THIS PAGE IS BEST QUALITY PRACTICABLE
FROM COPY FURNISHED TO DDC

TABLE D-IV (continued)

1.7.11	Set Valve # SV-9 to "FILL" Valve # SV-8 to "PURGE" Valve # SV-7 to "OVERFLOW"	en	KU
.12	Connect vacuum pump to overflow line	en	KU
.13	Set Valve # SV-11 to "OPEN"	en	KU
.14	Pump until tank is evacuated	en	KU
.15	Set Valve # SV-11 to "CLOSED" Valve # SV-9 to "PURGE"	en	KU
.16	Flow N_2 until tank is pressurized	en	KU
.17	Set Valve # SV-9 to "FILL"	en	KU
.18	Return to Step 1.7.13 until Steps 1.7.13 through 1.7.18 have been repeated 10 times	en	KU
.19	Disconnect vacuum pump	en	KU
.20	Depressurize bubbler tank. Set Valve # SV-7 to "OFF" and Valve # SV-11 to "OPEN"	en	KU
.21	After tank has depressurized, set Valve # SV-11 to "CLOSED" Valve # SV-9 to "OFF" Valve # SV-8 to "OFF" Valve # SV-10 to "CLOSED"	en	KU
.22	Adjust He pressure to 25 psig to Valve # SV-4. Adjust N_2 pressure to 25 psig to Valve # SV-4. Adjust CH_4 pressure to ~~25~~ 40 psig.	en	KU
.23	Set Valve # SV-4 to "HELIUM" Valve # SV-1A & SV-1B to "OPEN" Valve # SV-2 to "OPEN" Valve # SV-6 to "BYPASS" Valve # SV-5 to "BYPASS"	en	KU
.24	Flow Helium for 5 minutes	en	KU
.25	Set Valve # SV-4 to "NITROGEN" and set process N_2 bleed to 100 SCFH	en	KU
.26	Set Valve # SV-3 to "OPEN"	en	KU
.27	Purge with CH_4 for 5 minutes	en	KU
.28	Set Valve # SV-3 to "CLOSED"	en	KU

THIS PAGE IS BEST QUALITY PRACTICABLE
FROM COPY FURNISHED TO DDC

TABLE D-IV (continued)

1.7.29	Continue Nitrogen purge for 15 minutes	en	KV
.30	Set Valve # SV-4 to "OFF" Valve # SV-2 to "CLOSED" Valve # SV-5 to "OFF" Valve # SV-6 to "OFF" Valve # SV-1A & SV-1B to "CLOSED" Process N_2 bleed to 0 SCFH	en	KV
1.8	Fill MTS bubbler tank		
1.8.1	Set Valve E to "OFF"	en	KV
.2	Close all valves on MTS drum (on porch)	en	KV
.3	Open Helium tank valve (on porch)	en	KV
.4	Adjust the pressure to 8 psi maximum OPEN Helium valve	en	KV
.5	Set Valve A to "HELIUM"	en	KV
.6	Set Valve B to "OPEN"	en	KV
.7	Set Valve C down toward MTS drum	en	KV
.8	Set Valve D to "MTS FILL"	en	KV
.9	Adjust N_2 pressure to SV-10 to 10 psi	en	KV
.10	Set Valve # SV-10 to "OPEN" Valve # SV-7 to "OVERFLOW" Valve # SV-9 to "PURGE" Valve # SV-8 to "PURGE" MTS purge rotameter to "FULL SCALE"	en	KV
.11	After bubbler has pressurized to 10 psi: Set Valve # SV-10 to "CLOSED" Valve # SV-9 to "OFF" Valve # SV-8 to "OFF" Valve # SV-11 to "OPEN" Hood blower to "ON" Close MTS purge rotameter valve	en	KV
.12	After bubbler has depressurized: Set Valve # SV-9 to "FILL" Valve # SV-8 to "FILL" Valve E to "BUBBLER"	en	KV
.13	When MTS liquid flows from overflow tube: Set Valve C to "OFF" ← CLOSE ALL VALVES ON MTS DRUM ← CLOSE VALVE E Valve # SV-8 to "PURGE" Valve # SV-9 to "PURGE" Valve # SV-7 to "PURGE" Valve # SV-10 to "OPEN" MTS purge rotameter to minimum flow required for purge	en	KV

THIS PAGE IS BEST QUALITY PRACTICABLE
FROM COPY FURNISHED TO DDC

TABLE D-IV (continued)

1.8.14	Continue purging overflow line until free of MTS	cn	KU
.15	Set Valve # SV-10 to "CLOSED" Valve # SV-9 to "OFF" Valve # SV-8 to "OFF" Valve # SV-7 to "OFF" Valve # SV-11 to "CLOSED"	___	___
1.9	Purge gas connections to:		
1.9.1	T-1	cn	KU
.2	T-2	cn	KU
.3	T-3	cn	KU
.4	T-5	cn	KU
.5	T-6	cn	KU
.6	T-7	cn	KU
.7	T-8	cn	KU
.8	T-9	cn	KU
.9	T-13	cn	KU
.10	T-14	cn	KU
.11	T-15	cn	KU
.12	Furnace Case	cn	KU
1.10	Furnace power connections	cn	KU
1.11	Capacitor connections made and recorded	cn	KU
1.12	Turn on all instrumentation and power supplies. Place pyrometers in "Cal" mode. (DAS procedure 1.1)	cn	KU
1.13	Label and mount tape. (See DAS procedures 2.1 and 1.2.) Set run number to ~~15700~~ 15500	KWF	___
1.14	After one hour perform 10 complete data scans. (See DAS procedure 1.4.) Insert one file gap on mag tape (Das procedure 2.2.1).	KWF	___

Capacitor connection
Y = connected
O = Not connected

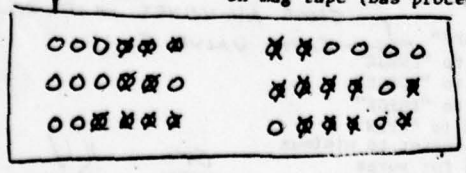

THIS PAGE IS BEST QUALITY PRACTICABLE
FROM COPY FURNISHED TO DDC

TABLE D-IV (continued)

2.0	Pre-Heatup Check Out		
	2.1 N_2 Supply 59.5 in H_2O = 111,270 cu ft	on	KU
	2.2 CH_4 Supply 4 bottles @ 200 psi = 323 cu ft	on	KU
	2.3 MTS Supply - bubbler filled	on	KU
	2.4 All Cooling Water Valves Open		
	2.4.1 WV-1	on	KU
	.2 WV-2	on	KU
	.3 WV-3	on	KU
	.4 WV-4	on	
	.5 WV-5	on	
	.6 WV-6	on	
	.7 WV-7	on	
	.8 WV-8	—	
	2.5 Check cooling water sight flow indicators		
	2.5.1 T-1	on	KU
	.2 T-2	on	KU
	.3 T-3	on	
	.4 T-5	on	
	.5 T-6	on	
	.6 T-7	on	
	.7 T-8	on	
	.8 T-9	on	Indicator Stuck
	.9 T-13	on	KU
	.10 T-14	on	KU
	.11 T-15	on	
	.12 P-1	on	
	.13 P-2	on	

THIS PAGE IS BEST QUALITY PRACTICABLE
FROM COPY FURNISHED TO DDC

TABLE D-IV (continued)

2.5.14	Bus Bar (INDICATOR BROKEN)	cn	KU
.15	Support Plate	cn	KU
.16	Coil	cn	KU
.17	Exhaust Tube	cn	KU
.18	Furnace Lid	cn	KU
.19	Injector	cn	KU
2.6	Coil water flow rate measurement		
2.6.1	Ten continuous scans, all channels; (DAS procedure 1.4) and manually record DAS time and F-5. F-5 = 26 ±1	cn	KU
.2	Close WV-8 14:10:03	cn	KU
.3	Manually record flow rate of F-5 F-5=22 ±.5	cn	KU
.4	Note DAS time. Take 10 continuous scans all channels. (DAS procedure 1.4)	cn	KU
.5	Open WV-8 14:13:55	cn	KU
.6	Manually record flow rate of F-5 F-5 = 26.5 ±.5	cn	KU
.7	Note DAS time. Take 10 continuous scans, all channels. (DAS procedure 1.4) Insert one file gap on mag tape (DAS procedure 2.2.1).	cn	KU
2.7	ARC instrument panel should be set up as follows:		
2.7.1	All rotameter valves closed	cn	KU
.2	NV-1 open	cn	KU
.3	NP-1 set at 50 psig	cn	KU
.4	NV-2 open	cn	KU
.5	NV-3 open	cn	KU
.6	NP-2 set at 50 psig	cn	KU
.7	MV-1 open	cn	KU
.8	MV-2 open to desired rotameter	cn	KU
.9	MP-1 set at ~~25~~ 40 psig	cn	KU

THIS PAGE IS BEST QUALITY PRACTICABLE
FROM COPY FURNISHED TO DDC

TABLE D-IV (continued)

2.7.10	Tylan control switches SV-1, SV-2 and SV-3 to "OFF"	CN	KU
.11	Open valve to N_2 supply for Tylan unit. Set regulator to 75 psig.	CN	KU
.12	Open valve to He supply for Tylan unit. Set regulator to 25 psig.	CN	KU
.13	VALVE SV-4 = HELIUM	CN	KU
2.8	Initiate heatup gas flow rates at gas panel by adjusting rotameter valves to achieve the following indicated rates:		
2.8.1	N_2 Case - 150 SCFH (4002)	CN	KU
.2	N_2 Annulus 24% (4001) (Parameter F2).	CN	KU
.3	N_2 Process Bleed - 50 SCFH	CN	KU
.4	N_2 Process - 200 SCFH (Parameter F1).	CN	KU
.5	N_2 T-1 - 20%	CN	KU
.6	N_2 T-2 - 50%	CN	KU
.7	N_2 T-3 - 100%	CN	KU
.8	N_2 T-5 - 50%	CN	KU
.9	N_2 T-6 - 100%	CN	KU
.10	N_2 T-7 - 100%	CN	KU
.11	N_2 T-8 - 100%	CN	KU
.12	N_2 T-9 - 20%	CN	KU
.13	N_2 T-13 - 20%	CN	KU
.14	N_2 T-14 - 20%	CN	KU
.15	N_2 T-15 - 100%	CN	KU
.16	CH_4 - 010 } Tylan Control Panel	CN	KU
.17	MTS - 010 } Tylan Control Panel	CN	KU
.18	Tylan switches SV-1, SV-2 and SV-3 to "OFF"	CN	KU
.19	Set Valves SV-5 and SV-6 to "BUBBLER"	CN	KU

THIS PAGE IS BEST QUALITY PRACTICABLE
FROM COPY FURNISHED TO DDC

TABLE D-IV (continued)

NOTE: Items 2.8.4 through 2.8.15 require flowmeter tube No. 1/8 - 20 - p 3/37 with SS float.

3.0	Furnace Heat Up:		
3.1	During heatup print-out and hand record all available data in run logs A & B at 15-minute intervals. DAS record on 1-minute intervals of channels 00-32. (DAS procedure 1.4). Insert one file gap on mag tape at each pyrometer range change (DAS procedure 2.2.1). Manually record DAS time.	RWF	KU
3.1.1	All gas flow rates same as in Section 2.8	CB	KU
3.2	Heat furnace at 50 KW for 30 minutes	CB	KU
3.3	After 30 minutes adjust power to 90 KW	CB	KU
3.3.1	Adjust settings on control panel as smoothly and rapidly as possible, within limitations of equipment.	____	KU
.2	If an intended power setting is overshot, do not readjust--in other words, do not juggle the controls in an attempt to exactly duplicate a printed test condition.	____	KU
3.4	After substrate inner surface temperature has reached 1738 ± 10° C (T-7):		
3.4.1	Record DAS time and elapsed time	16:52:00	KU
.2	Change DAS recording to 5 minute intervals (DAS procedure 1.4)	____	KU
.3	Adjust N_2 process rate to 940 SCFH	____	KU
.4	Adjust power level to maintain 1738 ± 10° C (T-7)	____	KU
.5	Stabilize substrate inner surface temperature at 1738 ± 10° C for at least one hour with no power adjustment required greater than ± 2 kW/15 minutes. During stabilization, measure exhaust temperature profile.	____	KU
.6	Record time stabilization is achieved	____	KU

DAS Time at Stab. - 20:15

4.0	Coating Runs:		
4.1	Effect of NTS on substrate temperature (T-7)		
4.1.1	Discontinue DAS scan (DAS procedure 1.4.1). Insert 1 file gap on mag tape (DAS procedure 2.2.1).	____	____

THIS PAGE IS BEST QUALITY PRACTICABLE
FROM COPY FURNISHED TO DDC

TABLE D-IV (continued)

4.1.1.1	Realign prism	____	____
4.1.2	Change Test ID number to 1501 (DAS procedure 1.2).	____	____
.3	Set DAS to scan channels 06 - 12 (DAS procedure 1.4) (T-5, T-7, F-3, F-4, F-1, T-15).	____	____
.4	Initiate DAS for continuous scan of above channels and take a minimum of 10 complete scans prior to proceeding to next step. Hand record parameters, T-5, T-7, F-3, F-4, F-1, T-15 (DAS procedure 1.4)	____	____
.5	Record substrate temperature (T-7) with ARC L&N Pyrometer and prism. Record DAS time. 21:38:11	____	____
.6	Remove prism 21:38:20	____	____
.7	Set MTS flow controller to 4 g/min. Tylan Vernier – 4H4 0	____	____
.8	Turn Tylan switch SV-1 to "ON". Record DAS time. 21:42:39	____	____
.9	After MTS flow rate is stable, hold for 2 min. Hand record parameters, T-5, T-7, F-3, F-4, F-1, T-15.	____	____
.10	Turn Tylan switch SV-1 to "OFF". Record DAS time. 21:45:42	____	KV
.11	After 2 min hand record parameters T-5, T-7, F-3, F-4, F-1, T-15	____	KV
.12	Set MTS flow at 6.5 g/min. Tylan vernier – 7.200	____	KV
.13	Turn Tylan switch SV-1 to "ON". Record DAS time 21:51:26	____	KV
.14	After flow rate is stable for 2 min, hand record parameters, T-5, T-7, F-3, F-4, F-1, T-15	____	____
.15	Set CH_4 flow at ~~5.664~~ lpm	____	____
	Tylan readout 3.46 FP ROTAMETER 12.5 SCFH Tylan vernier - 3.480 (11.3)		
.16	Turn Tylan switch SV-3 to "ON". Record DAS time 21:58:20	____	____
.17	After CH_4 flow rate is stable for 2 min, hand record parameters, T-5, T-7, F-3, F-4, F-1, T-15	____	____

THIS PAGE IS BEST QUALITY PRACTICABLE
FROM COPY FURNISHED TO DDC

TABLE D-IV (continued)

✓	4.1.18	Record substrate temperature (T-7) with ARC L&N Pyrometer and prism. Record DAS time. 22:07:27	____	____
✓	.19	Remove prism 22:08:09	____	____
	.20	Discontinue DAS scan (DAS procedure 1.4.1). Insert 1 file gap on mag tape (DAS procedure 2.2.1).	____	____
4.2		Coating Run No. 1 Control Temp established at 1725°C		
✓	4.2.1	Change Test ID number to 15802 (DAS procedure 1.2)	____	____
✓	.2	Set DAS to scan channels 00 - 32 (DAS procedure 1.4)	____	____
✓	.3	Set DAS to scan at 5-minute intervals. Record DAS time. (DAS procedure 1.4) 22:15:00		____
✓	.4	Hand record and print out all data at this time & at 15-min intervals over the next 4 hours. (DAS procedure 1.4.4)	____	____
✓	.5	Adjust power as required to maintain T-7 at value measured in 4.1.17. Record DAS time at each adjustment of power.	____	____
0215	.6	After 4 hours, discontinue DAS scan. (DAS procedure 1.4.1) Insert 1 file gap on mag tape (DAS procedure 2.2.1).	____	____
4.3		Effect of CH_4 on substrate temperature		
	4.3.1	Change Test ID number to 15803 (DAS procedure 1.2)	____	____
	.2	Set DAS to scan channels 06 - 12 (T-5, T-7, F-3, F-4, F-1, T-15) (DAS procedure 1.4).	____	____
	.3	Initiate DAS for continuous scan of above channels and take a minimum of 10 complete scans prior to proceeding to next step. Hand record parameters T-5, T-7, F-3, F-4, F-1, T-15. (DAS procedure 1.4).	____	____
0215	.4	Turn Tylan switch SV-1 to "OFF". Record DAS time. 02:22:52		____

02:22:52
02:26:44

THIS PAGE IS BEST QUALITY PRACTICABLE
FROM COPY FURNISHED TO DDC

TABLE D-IV (continued)

			Wait 2 minutes.		
✓ 0227	4.3.5		Record substrate temperature (T-7) with ARC L&N pyrometer and prism. Record DAS time. 3080 °F	~~02644~~	02:25:27 ↓
✓		.6	Remove prism.	____	02:27:15
✓ 0240		.7	After 15 minutes from 4.3.4, set Tylan switch SV-3 to "OFF". Record DAS time.	02:39:24	____
			Wait 2 minutes.		
✓ 0242		.8	Record substrate temperature (T-7) with ARC L&N pyrometer and prism. Record DAS time. 3082 °F	~~54007~~	02:39:46 ↓
✓		.9	Remove prism.	____	02:40:57
		.10	Discontinue DAS scan (DAS procedure 1.4.1). Insert 1 file gap on mag tape (DAS procedure 2.2.1).	____	____
	4.4		Coating Run No. 2		
✓		4.4.1	Change Test ID number to 1504 (DAS procedure 1.2)	____	____
✓		.2	Set DAS to scan channels 00 - 32 (DAS procedure 1.4)	____	____
✓		.3	Set DAS to scan ~~at 5-minute intervals~~ continuous. (DAS procedure 1.4.6) Record DAS time.	~~024744~~ 02:43:30	____
✓		.4	Set MTS flow at 4.3 g/min Tylan vernier 4.770	____	____
✓		.5	Set Tylan switch SV-1 to "ON" Record DAS time	02 45 14	____
✓		.6	After the MTS flow rate is stable for 2 minutes, hand record parameters T-5, T-7, F-3, F-4, F-1, T-15.	____	____
✓		.7	Set CH_4 flow at 5.664 lpm Tylan readout - 3.45 Tylan vernier - 3.480 FD Nominal 17.5 (113 Actual)	____	____
✓		.8	Set Tylan switch SV-3 to "ON". Record DAS time.	02:51:19.	____
✓		.9	After CH_4 is stable for 2 minutes, hand record parameters T-5, T-7, F-3, F-4, F-1, T-15.	025600	17:...
✓			Set DAS to scan at 5 Min. intervals	____	____
✓		.10	Hand record and print-out all data at 15-minute intervals over the next 4 hours (DAS procedure 1.4.4).	____	____

THIS PAGE IS BEST QUALITY PRACTICABLE
FROM COPY FURNISHED TO DDC

TABLE D-IV (continued)

4.4.11	Adjust power as required to maintain T-7 at value recorded in 4.4.9. Hand record DAS time at each adjustment of power. (1720°C)	____	____
0700 .12	After 4 hours set Tylan switch SV-1 to "OFF". Record DAS time.	0705.00	____
0715 .13	After 15 minutes from 4.4.12 set Tylan switch SV-3 to "OFF". Record DAS time.	0720.00	____
.14	Discontinue DAS scan.(DAS procedure 1.4.1). Insert 1 file gap on mag tape (DAS procedure 2.2.1).	____	____
4.5	Coating Run No. 3 set up.		
4.5.1	Change Test ID number to ~~15805~~ 15801 (DAS procedure 1.2)	____	____
.2	Set DAS to scan at ~~15~~ ? 5-minute intervals and initiate scan. Record DAS time. (DAS procedure 1.4)	07:25:00	____
.3	Set N_2 process flow rate to 1465 SCFH. Record DAS time.	0730:00	____
.4	Adjust power to maintain 1738 ± 10° C (T-7). Record DAS time at each adjustment of power .	____	____
.5	Stabilize substrate inner surface temperature at 1738 ± 10° C (T-7) for at least one hour with power adjustments required no greater than ± 2 kW/15 min	11:30:00	____
.6	Record time stabilization is ~~achieved~~ completed.	12:30:00	____
.7	Discontinue DAS scan (DAS procedure 1.4.1). Insert 1 file gap on mag tape (DAS procedure 2.2.1)	____	____
4.6	Repeat of 4.1 with increased flow:		
4.6.1	Change Test ID number to ~~15806~~ 15818 (DAS procedure 1.2).	____	____
.2	Set DAS to scan channels 06 - 12 (T-5, T-7, F-3, F-4, F-1, T-15) (DAS procedure 1.4).	____	____

THIS PAGE IS BEST QUALITY PRACTICABLE
FROM COPY FURNISHED TO DDC

TABLE D-IV (continued)

5	4.6.3	Initiate DAS for continuous Scan of above channels and take a minimum of 10 complete scans prior to proceeding to next step. Hand record parameters T-5, T-7, F-3, F-4, F-1, T-15. (DAS procedure 1.4)		
5	.4	Record substrate temperature (T-7) with ARC L&N pyrometer and prism. Record DAS time.	12:38:09 ↓ 12:38:37	
	.5	Remove prism.		
	.6	Set MTS flow rate to 4 g/min. Tylan vernier - 4.440		
	.7	Set Tylan switch SV-1 to "ON". Record DAS time. ~~12:40:53~~	12:40:37	KU
4	.8	After MTS flow rate is stable, hold for 2 min. Hand record parameters T-5, T-7, F-3, F-4, F-1, T-15. Record DAS time	12:43:52	
	.9	Set Tylan switch SV-1 to "OFF". Record DAS time.	12:47:08	
2	.10	After 2 min hand record parameters T-5, T-7, F-3, F-4, F-1, T-15. Record DAS time	12:47:12	
	~~.11~~	Set MTS flow at 5.42 g/min. Tylan vernier - 6.010		
	.12	Set Tylan switch SV-1 to "ON". Record DAS time. 12:51:48		KU
4	~~.13~~	After flow rate is stable for 2 min, hand record parameters, T-5, T-7, F-3, F-4, F-1, T-15. Record DAS time	12:56:33	
2	.14	Set CH_4 flow rate at 6.496 lpm Tylan readout · 6.04 FP Rotameter - 19.9 Tylan vernier 6.090 (Actual 17.6 scfh)		
	~~.15~~	Set Tylan Switch SV-3 to "ON". Record DAS time. 12:58:09		KU
2	~~.16~~	After CH_4 flow rate is stable for 2 min, hand record parameters T-5, T-7, F-3, F-4, F-1, T-15. Record DAS time	13:01:18	
	~~.17~~	Record substrate temperature (T-7) with ARC L&N pyrometer and prism. Record DAS time. 13:04:02		
	~~.18~~	Remove prism. ↓ 13:04:47		

THIS PAGE IS BEST QUALITY PRACTICABLE
FROM COPY FURNISHED TO DDC

TABLE D-IV (continued)

4.6.19	Discontinue DAS scan (DAS procedure 1.4.1). Insert 1 file gap on mag tape (DAS procedure 2.2.1).	____	____
4.7	Coating Run No. 3 15828		
4.7.1	Change Test ID number to ~~15827~~ (DAS procedure 1.2).	____	____
.2	Set DAS to scan channels 00 - 32 (DAS procedure 1.4).	____	____
.3	Set DAS to scan at 5-minute intervals. Record DAS time. (DAS procedure 1.4.6)	17:10:00	____
.4	Hand record and print-out all data at this time & at 15-minute intervals over the next 4 hours (DAS procedure 1.4.4).	____	____
.5	Adjust power as required to maintain T-7 at value measured in 4.6.16. Record DAS time at each adjustment of power.	____	____
6.	After 4 hours, discontinue DAS scan (DAS procedure 1.4.1). Insert 1 file gap on mag tape (DAS procedure 2.2.1).	____	____
4.8	Repeat of 4.3 with increased flow:		
4.8.1	Change Test ID number to ~~15828~~ 15838 (DAS procedure 1.2). 2nd Test ID 15839	____	____
.2	Set DAS to scan channels 06 - 12 (T-5, T-7, F-3, F-4, F-1, T-15) (DAS procedure 1.4). 17:41:00	____	____
.3	Initiate DAS for continuous scan of above channels and take a minimum of 10 complete scans prior to proceeding to next step. Hand record parameters T-5, T-7, F-3, F-4, F-1, T-15. (DAS procedure 1.4).	____	____
.4	Set Tylan switch SV-1 to "OFF". Record DAS time. 17:42:27	____	____
.5	Record substrate temperature (T-7) with ARC L&N pyrometer and prism. Record DAS time. 17:43:20	____	____
.6	Remove prism. 17:44:06	____	____

THIS PAGE IS BEST QUALITY PRACTICABLE
FROM COPY FURNISHED TO DDC

TABLE D-IV (continued)

4.8.7	After 15 minutes from 4.8.4, set Tylan switch SV-3 to "OFF". Record DAS time.	17:58:33	____
.8	Record substrate temperature (T-7) with ARC L&N pyrometer and prism. Record DAS time. 17:58:56	____	____
.9	Remove prism. 17:59:30	____	____
.10	Discontinue DAS scan. (DAS procedure 1.4.1). Insert 1 file gap on mag tape (DAS procedure 2.2.1).	____	____
5.0	Test Termination:		
5.1	Change Test ID number to 15887. Set DAS to scan channels 00 - 32 . Set DAS to scan at 5-minute intervals. Record DAS time. 18:06:00 Hand record all data at this time. (DAS procedures 1.2, 1.4).	____	____
5.2	Turn off furnace power.	____	____
5.2.1	Record DAS time and elapsed time in run logs.	18:10:25	____
.2	Maintain N_2 gas flow rates of previous conditions (Section 4.8).	____	____
.3	Continue hand recording and print-out all data at 15-minute intervals over next hour (DAS procedure 1.4.4).	____	____
5.3	After 1 hour, adjust process N_2 to 200 SCFH.	____	____
5.3.1	Record DAS time and elapsed time in run logs.	19:20:00	____
.2	Discontinue hand recording of data.	____	____
.3	Set all applicable pyrometers to "calibrate" mode. Take 10 scans of DAS of channels 00 - 32 . Using the tape recorder control, add 2 file gaps and rewind the tape. Verify that it has been labeled with the date, test numbers and tape sequence number. Turn off the DAS and tape deck. (DAS procedure 1.4 and 2.2.1).	____	____

THIS PAGE IS BEST QUALITY PRACTICABLE
FROM COPY FURNISHED TO DDC

TABLE D-IV (continued)

.4	Cover all sight ports with cardboard	____	____
.5	Turn off all instruments except 24 VDC power supply.	____	____
.6	Cover all pyrometer heads with plastic bags	____	____
5.5	Purge Tylan MTS System: → OPEN BUBBLER PURGE N_2 ROTAMETER		
5.5.1	Set Valve SV-5 to "BYPASS"	____	____
.2	Set Valve SV-6 to "BYPASS"	____	____
.3	Set Valve 1A and 1B to "OPEN"	____	____
.4	Set Valve SV-4 to "NITROGEN" SET BUBBLER PURGE N_2 ROTAMETER TO 100%	____	____
.5	Set Valve SV-2 to "OPEN"	____	____
.6	Purge with N_2 ~~for 1 hour~~	____	____
FINISH			
.7	Set Valve SV-4 to "OFF"	____	____
.8	Set Valve SV-1A and SV-1B to "CLOSED"	____	____
.9	Set Valve SV-2 to "CLOSED"	____	____
.10	Set Valve SV-3 to "OFF"	____	____
.11	Set Valve SV-6 to "OFF"	____	____

THIS PAGE IS BEST QUALITY PRACTICABLE
FROM COPY FURNISHED TO DDC

TABLE D-V

TEST LOG - COATING TEST SERIES 15800

DAS Time	Remarks
14:10:03	F-5 (WV-8 open) - 26 ± 1. F-5 (WV-8 closed - 22 ± .5.
14:13:55	F-5 (WV-8 open - 26.5 ± .5.
16:05/16:15	Adjusting pyrometers T-5 and T-2 for alignment. Noticed that iris does not converge in center of sight port.
16:32:30	Changed from low to medium range on T-1.
16:45/17:00	Adjusting alignment of T-2 (Channel 13).
17:00/17:15	Adjusting alignment of T-5 (channel 12) and T-7 (channel 11).
17:12:40	Start stabilization; T-7 reads 1738°C.
17:22:00	Increase process N_2 to 940 SCFH.
18:10	Recalibrate T-2 (channel 13) and T-9 (channel 19).
18.36:00	T-15 T/C found to be approx. 0.5 inch out of fitting. Inserted it fully for start of temp profile test.
19:18	Calib T-2 and T-9 (Adjusted T-2 down approx 60°).
19:20	Adjusting position of pyrometer T-9 (channel 19).
20:02	Calib T-2 and T-9 (adjusted T-2 up 35°). ch's 13 and 19.
20:15	Temp stabilized at 1738°C.
21:02	Calib T-2 and T-9 (adj T-2 down approx 80°C).
22:02:31	Stopped cont scan and took all ch scan. Started cont scan of ch 06-12.
22:05	Inadvertantly turned Tylan unit off for approx 1 sec.
22:18	T-8 meter reading has been very low for approx. 30 min. Calib unit and unit now looks ok.
22:22	Calib T-8 again - unit looks ok.
22:27	Calib T-2 and T-9 (Adjusted T-2 down approx 60°)
23:02	Calib T2 and T9: T-2, 20° low, adjusted up. T-9 zero, adjusted down 20°.
23:20	Removed case from T-13 pyrometer head in an attempt to free stuck filter. T-13 off during this period.

TABLE D-V (continued)

DAS Time	Remarks
24:02	T-2 Calib 40° low, adjust up; T-9 zero ok.
23:30	Started to trouble shoot T-13. Data is bad from start of run to now. (Realigned); data should be good after about 0130 hrs.
01:02	T-2 calib 60° high, adjust down; T-9 zero ok.
02:02	T2 calib 20° low, adjust up; T-9 zero ok.
02:15	No file gap after this record.
03:06	T-2 40° low, adjusted up; T-9 zero ok.
03:19	Increased power from 50 + to 51 kw.
03:52	Increased power from 50 + to 51 kw.
04:02	T-2 20° low, adjusted up; T-9 zero ok.
04:18	Increased power from 50 to 52 kw.
04:48	Increased power from 52- to 52 kw.
05:02	T-2 50° high, adjusted down; T-9 zero ok.
05:19	Increased power from 52 to 52 + kw.
05:49	Decreased power from 52 + to 52 kw.
06:02	T-2 30° low, adjusted up; T-9 zero ok.
06:03	Decreased power from 58 to 52 kw.
06:33:30	Decreased power from 52 to 52- kw.
7:02	T-2 40° high, adjust down; T-9 zero ok.
07:33	Increased power from 52 to 55 kw.
07:45	Increased power from 55 to 58 kw.
07:30	Test ID XXXXX dropped the 4 bit (15801).
07:58	Increased power from 58 to 62 kw.
08:02	T-2 10° low, adjusted up; T-9 zero ok.
08:29	Increased power from 60 to 63 kw.

AD-A058 115 LOS ALAMOS SCIENTIFIC LAB N MEX F/G 11/2
DEVELOPMENT OF PYROLYTIC GRAPHITE/SILICON CARBIDE COMPOSITE MAT--ETC(U)
JUN 78 T C WALLACE, G E CORT, J J DAMRAN W-7405-ENG-36
UNCLASSIFIED AFRPL-TR-78-46-VOL-1 NL

3 OF 3
AD A058 115

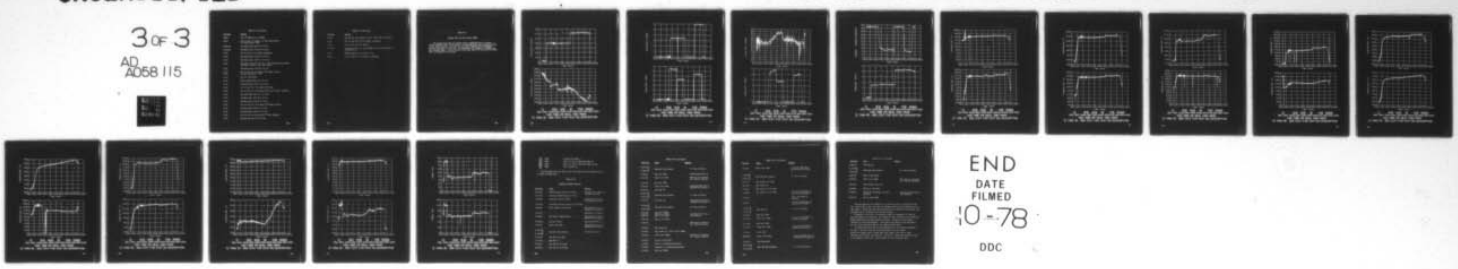

END
DATE FILMED
10-78
DDC

TABLE D-V (continued)

DAS Time	Remarks
08:30	Test ID XXXXX now ok (15805).
09:03	Adj T-2 and T-9 (adjust T-2 down approx 40°C) (T-9 high approx 10°R).
09:06:50	Increased power from 63 to 65 kw.
09:32:00	Decreased power from 64 to 63 kw.
10:06	Cal T-2 and T-9 (no adjust necessary).
10:18	Decreased power from 63 to 62 kw.
10:32	Decreased power from 62 + to 62 kw.
10:25	Increased case flow for 150 to 200 (stuffed locum blanket into hole in RTV at case tube inlet).
10:51	Decreased power from 62 to 61 kw.
11:02	CAL T-2 and T-9 (T-9 approx 20°R high on zero).
11:12	N_2 case increased to 230.
11:15	Cal T-2 (10°R high).
11:30	Begin stabilization for run no 3.
11:33	Increased power from 61 to 62 kw.
12:06	Cal T-2 and T-9; (T-2 approx 40°C low).
13:08	Cal T-2 and T-9; (T-9 approx 60°R low at zero); adjusted.
13:16	Increase power from 61 + to 62 kw.
13:24	Increase power from 62 to 63 kw.
13:36	Increase power from 63 to 64 kw.
14:07	Cal T-2 and T-9; (T-9 approx 10°R high on zero).
14:19	Increase power from 64 to 65 kw.
14:51	Decrease power from 65 to 64 kw.
15:07	Cal T-2 and T-9; both units 20° low; adjusted
15:36	Decrease per from 64 to 63 kw.

TABLE D-V (continued)

DAS Time	Remarks
15:50	Reduced CH_4 rate from 20 to 19.9 SCFH (F&P flow meter).
16:02	Cal T-2 and T-9; (T-2 15° high - adjusted).
17:02	Cal T-2 and T-9; (no adjust).
17:36:39	Turned SV-1 back on. Was thought to have been turned off inadvertently.
18:50	Changed range on T-13 from I to H.
18:53	Cal T-2 and T-9; (T-2 30°low - adjusted).

TABLE D-VJ

REDUCED DATA FOR THE COATING TESTS

The reduced test data are plotted versus normalized time in minutes. A second reference scale at the bottom of each page gives the corresponding DAS or real time in hours. The label on each figure identifies the parameter plotted (see Figs. A-6 and B-1). The parameters are arranged in alphabetical and numerical order. At the bottom of each page there is a circled test number that is referred to in the text.

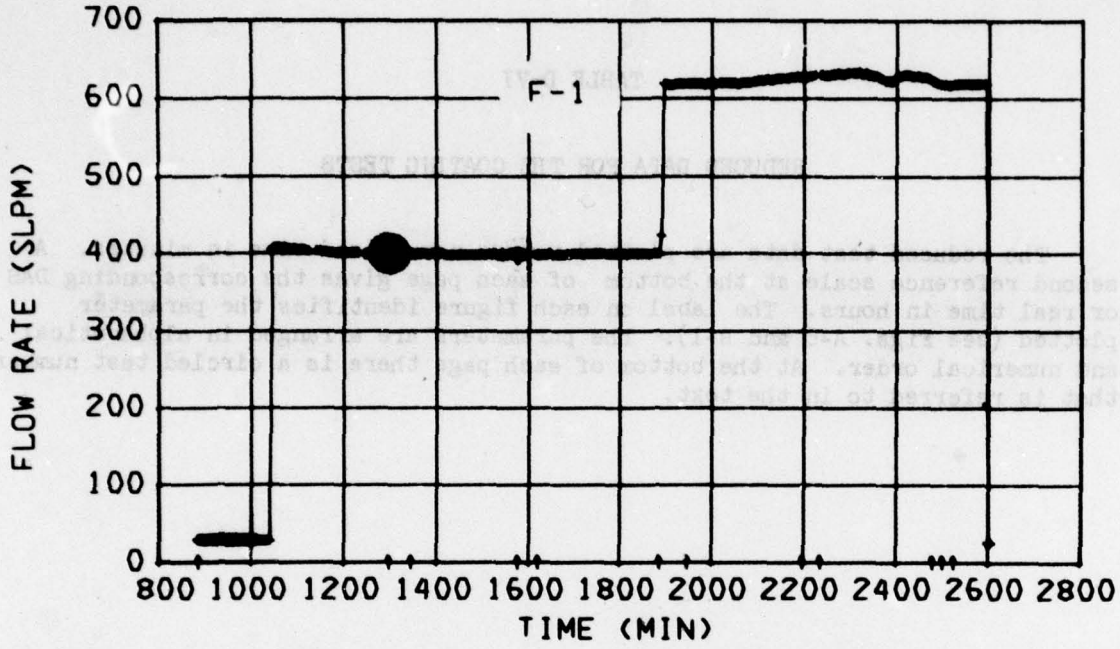

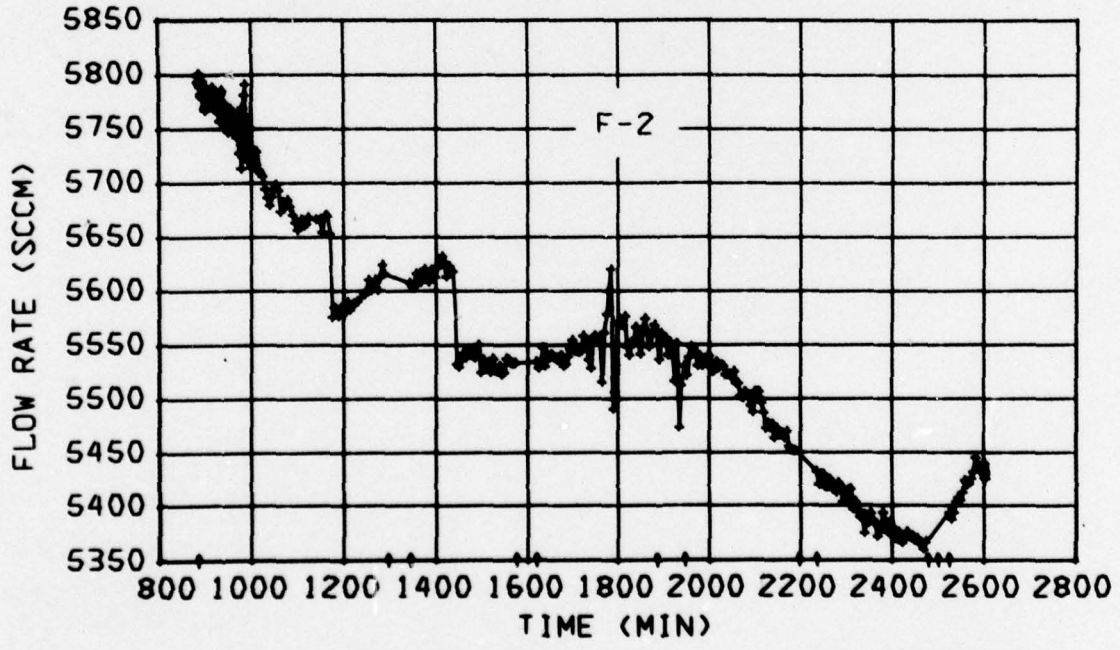

① ②③ ④⑤ ⑥ ⑦⑧ ⑨⑩⑪

1320 1640 2000 2320 0240 0600 0920 1240 1600 1920 2240

DAS TIME OR REAL TIME (HRS)

① THRU ⑪: SEE TEXT FOR TEST NO. DESCRIPTION

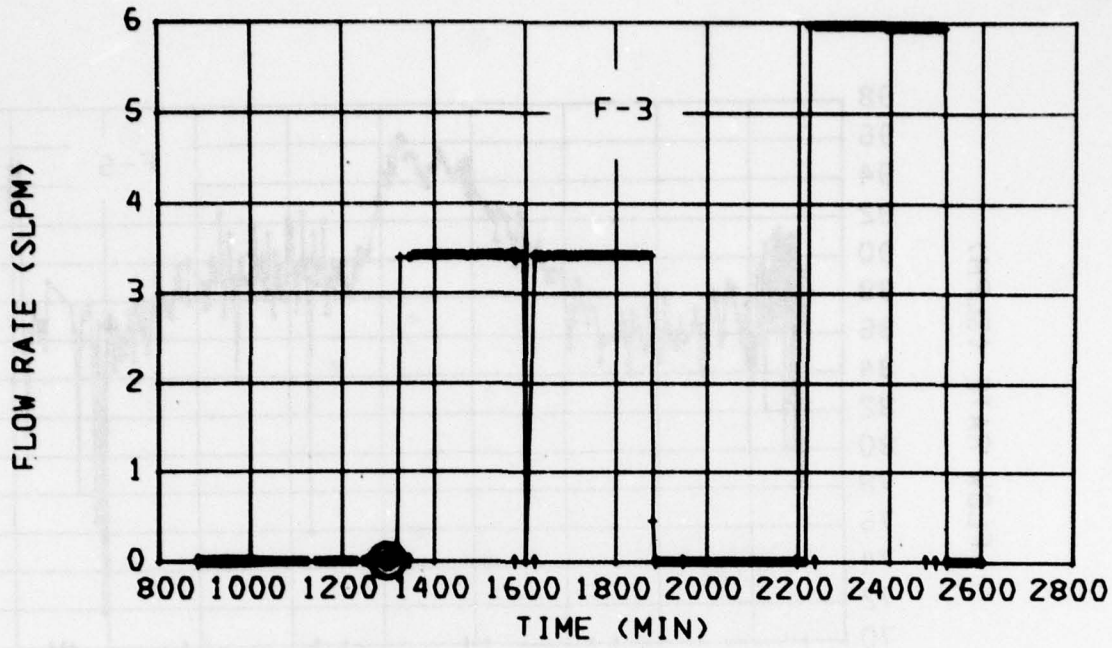

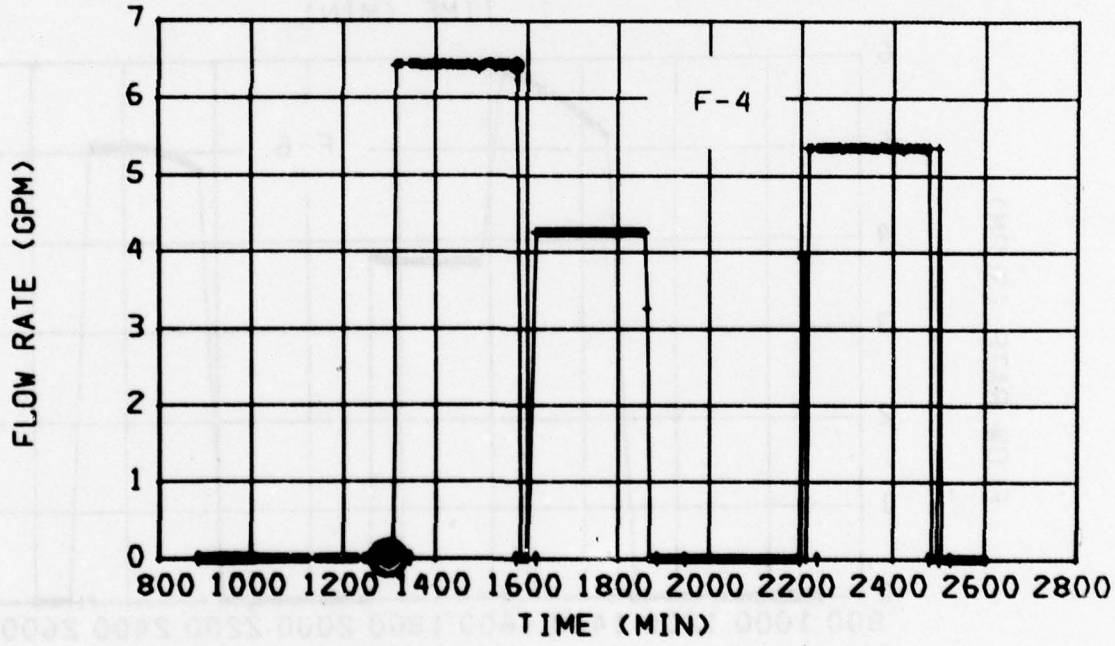

① ②③ ④⑤ ⑥ ⑦⑧ ⑨⑩⑪

1320 1640 2000 2320 0240 0600 0920 1240 1600 1920 2240

DAS TIME OR REAL TIME (HRS)

① THRU ⑪: SEE TEXT FOR TEST NO. DESCRIPTION

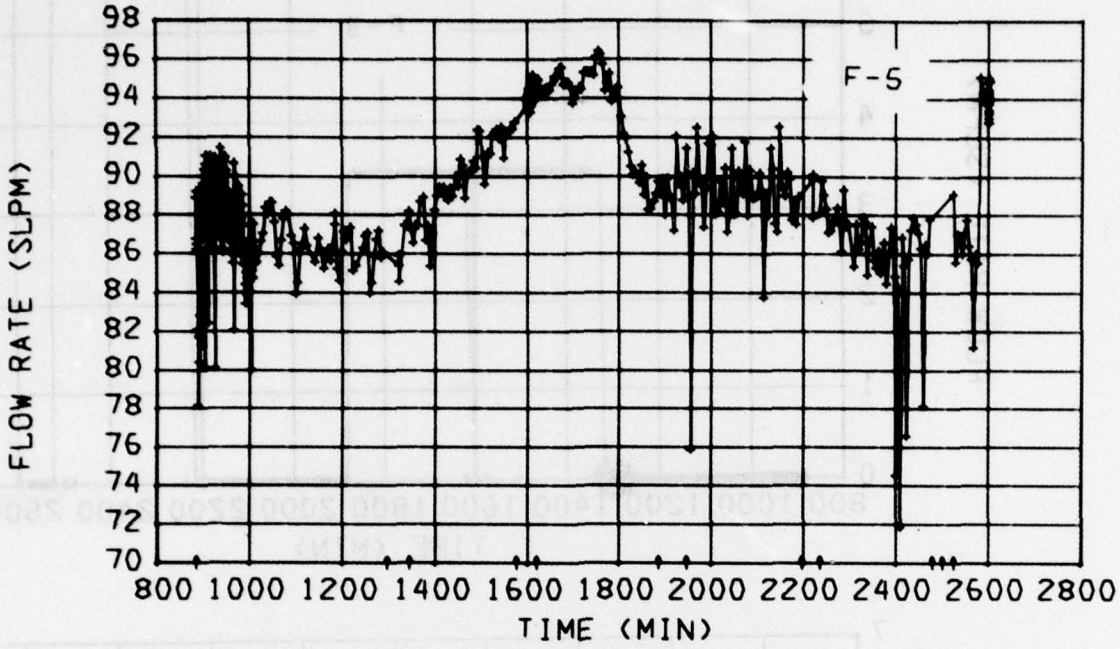

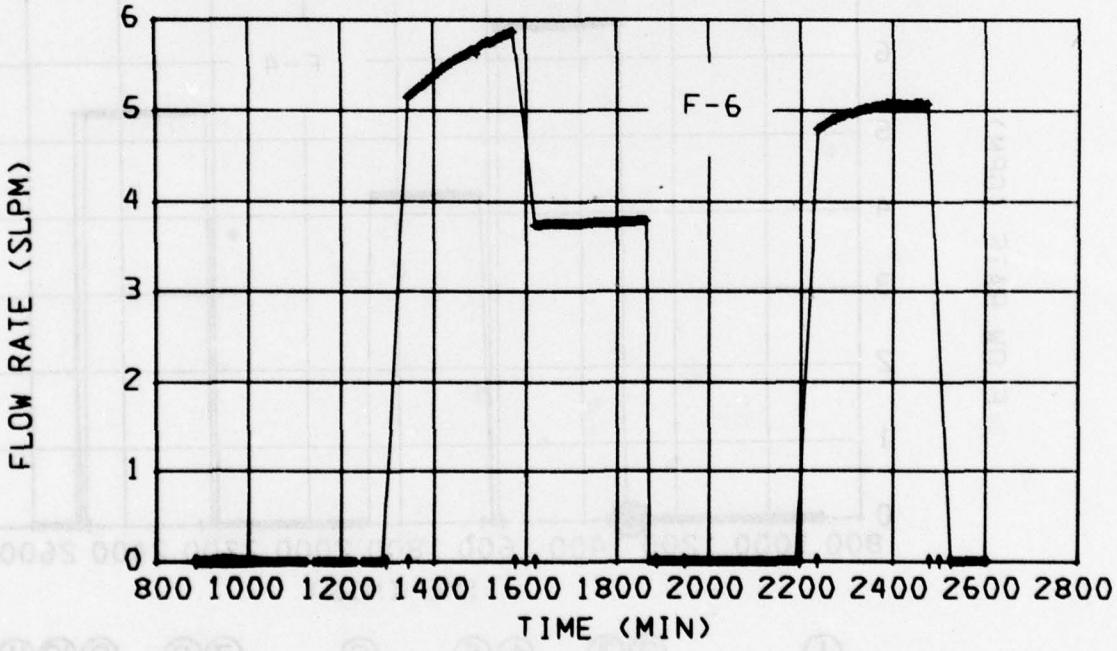

① ②③ ④⑤ ⑥ ⑦⑧ ⑨⑩⑪

1320 1640 2000 2320 0240 0600 0920 1240 1600 1920 2240

DAS TIME OR REAL TIME (HRS)

① THRU ⑪: SEE TEXT FOR TEST NO. DESCRIPTION

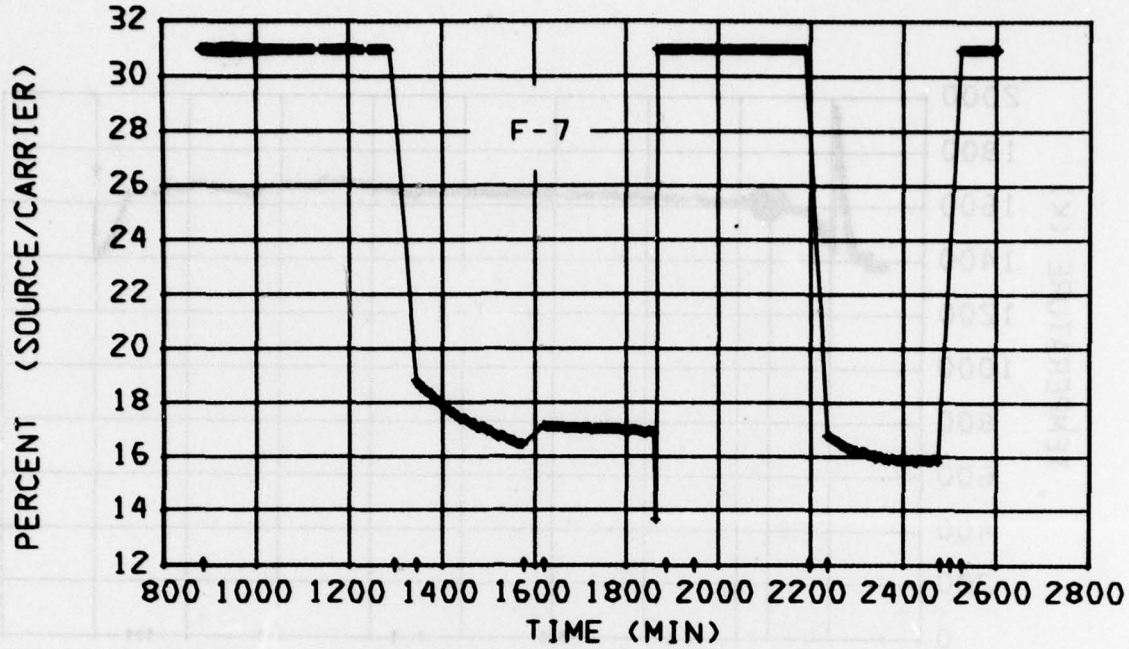

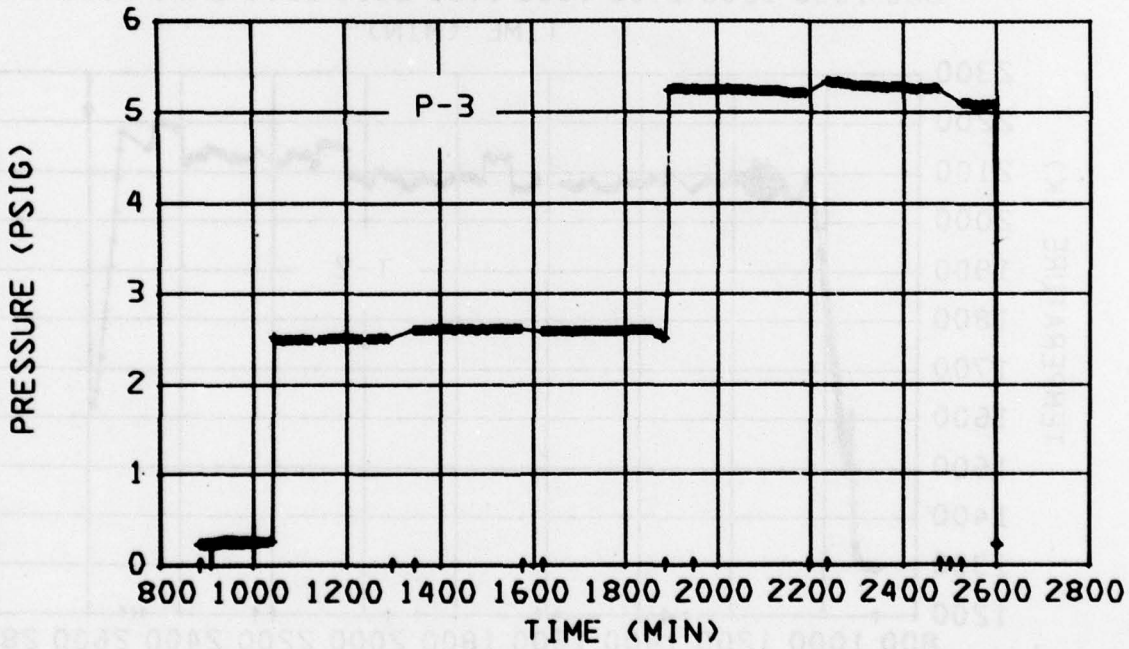

① ②③ ④⑤ ⑥ ⑦⑧ ⑨⑩⑪

1320 1640 2000 2320 0240 0600 0920 1240 1600 1920 2240

DAS TIME OR REAL TIME (HRS)

① THRU ⑪: SEE TEXT FOR TEST NO. DESCRIPTION

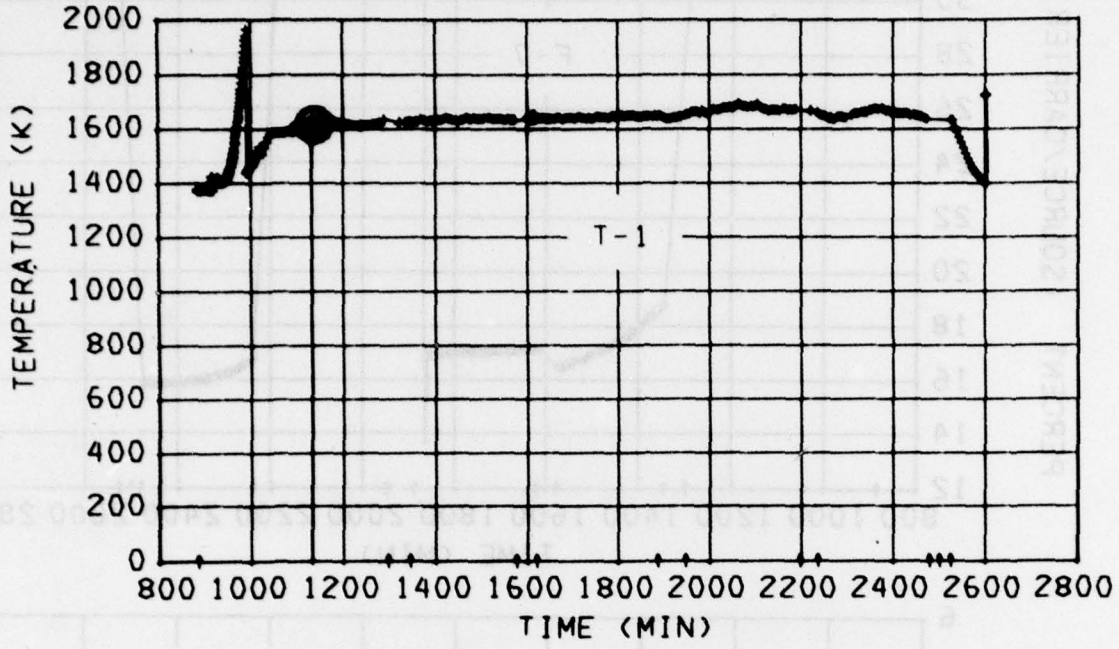

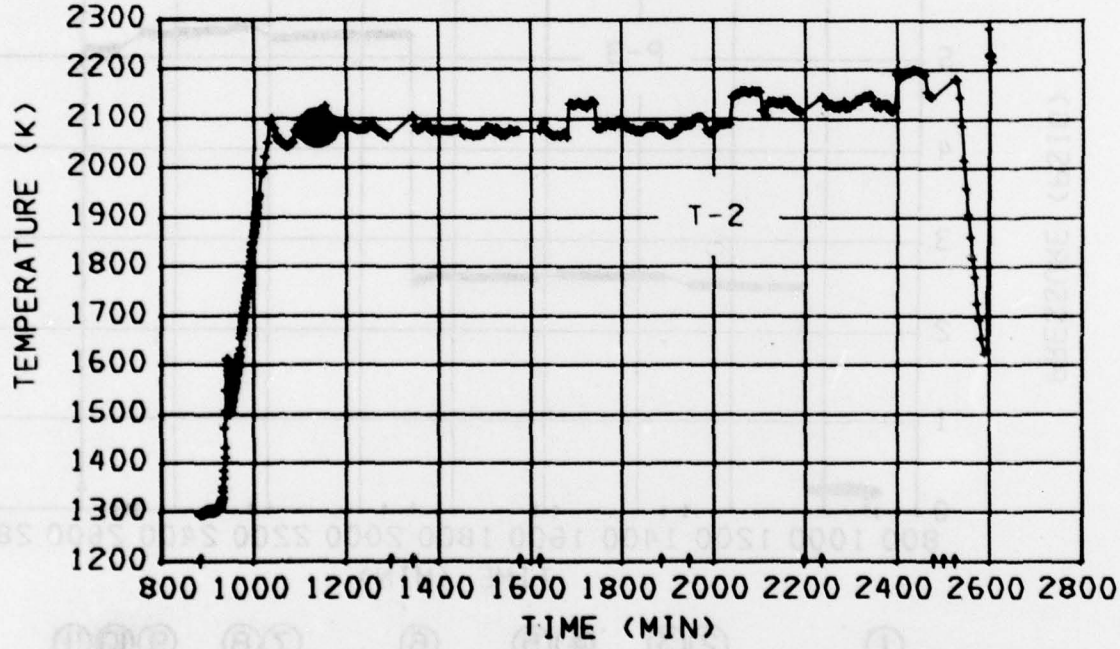

① ②③ ④⑤ ⑥ ⑦⑧ ⑨⑩⑪

1320 1640 2000 2320 0240 0600 0920 1240 1600 1920 2240

DAS TIME OR REAL TIME (HRS)

① THRU ⑪: SEE TEXT FOR TEST NO. DESCRIPTION

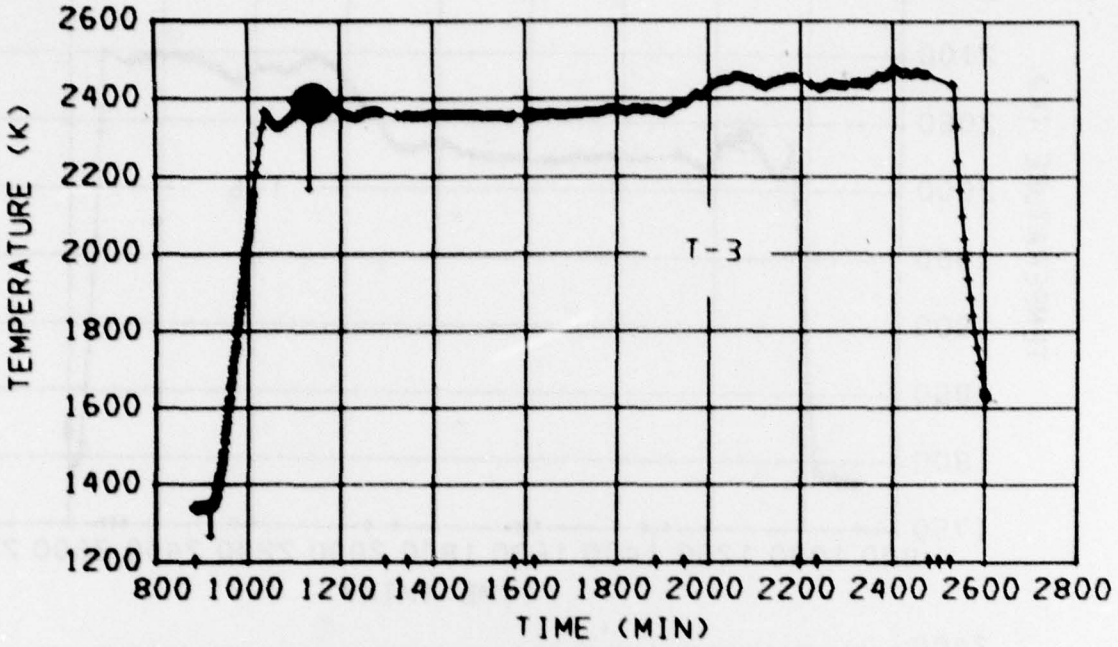

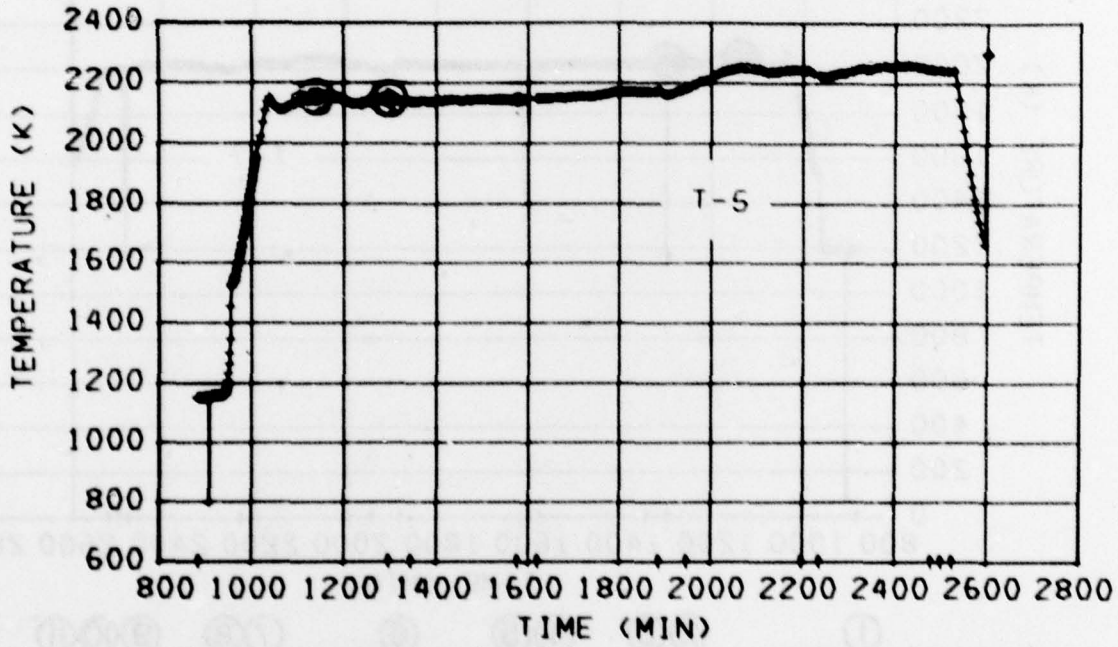

① ②③ ④⑤ ⑥ ⑦⑧ ⑨⑩⑪

1320 1640 2000 2320 0240 0600 0920 1240 1600 1920 2240

DAS TIME OR REAL TIME (HRS)

① THRU ⑪: SEE TEXT FOR TEST NO. DESCRIPTION

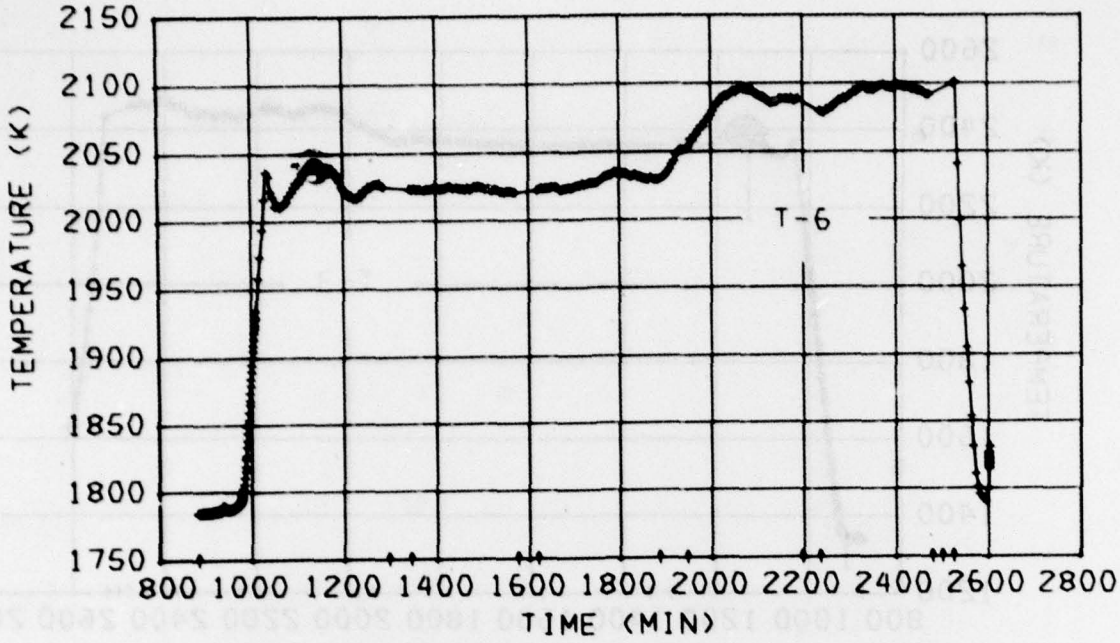

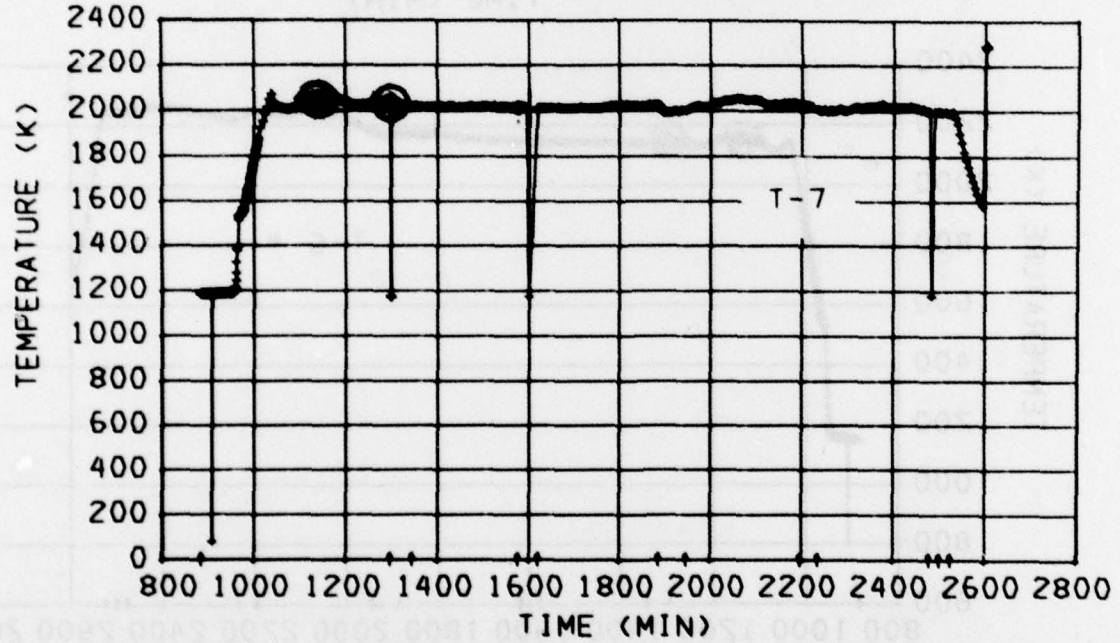

① ②③ ④⑤ ⑥ ⑦⑧ ⑨⑩⑪

1320 1640 2000 2320 0240 0600 0920 1240 1600 1920 2240

DAS TIME OR REAL TIME (HRS)

① THRU ⑪: SEE TEXT FOR TEST NO. DESCRIPTION

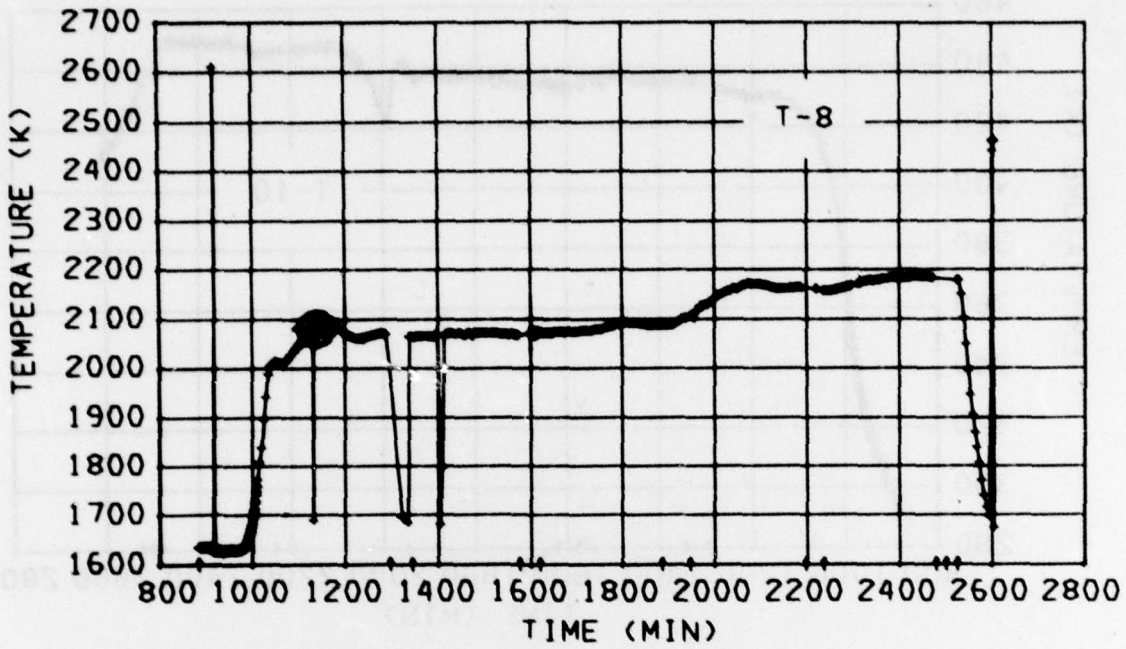

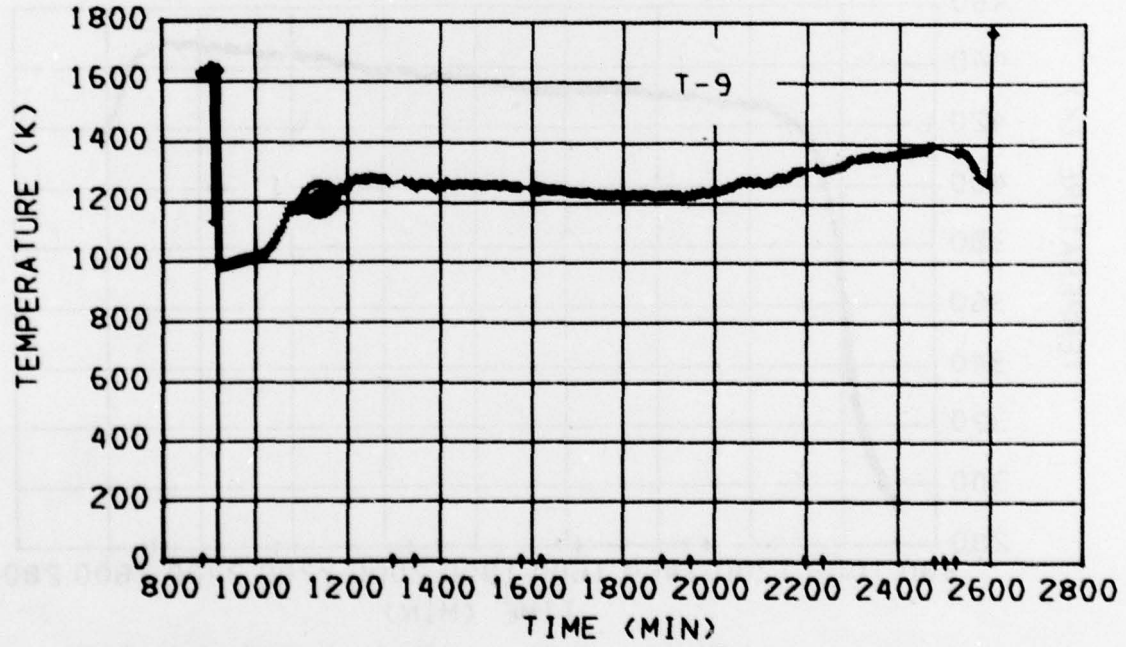

① ②③ ④⑤ ⑥ ⑦⑧ ⑨⑩⑪

1320 1640 2000 2320 0240 0600 0920 1240 1600 1920 2240

DAS TIME OR REAL TIME (HRS)

① THRU ⑪: SEE TEXT FOR TEST NO. DESCRIPTION

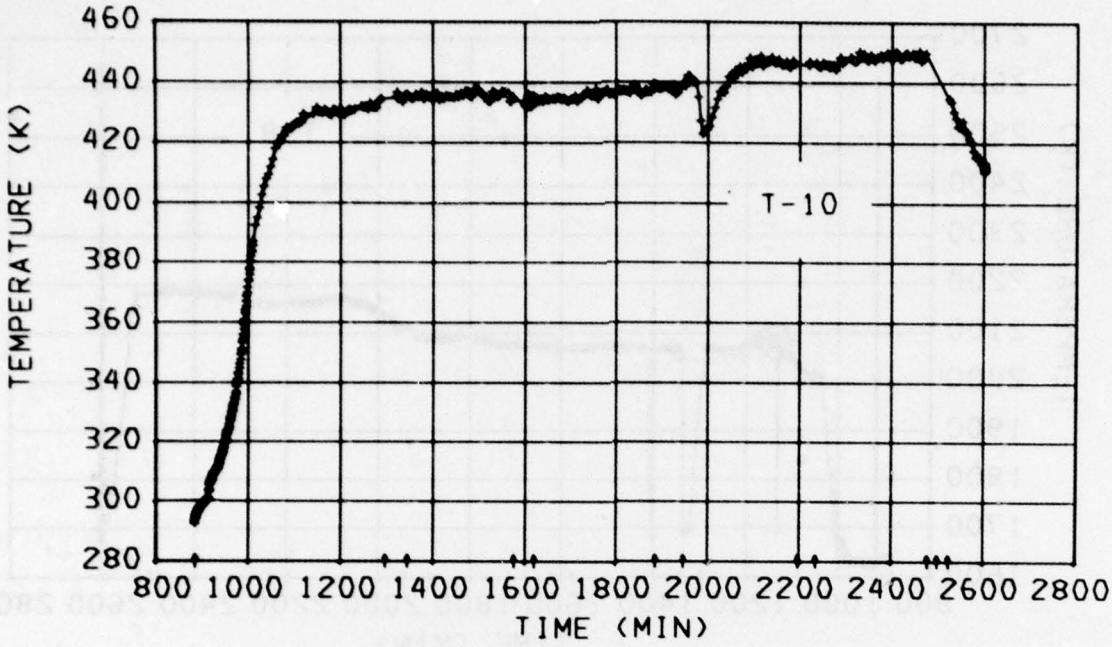

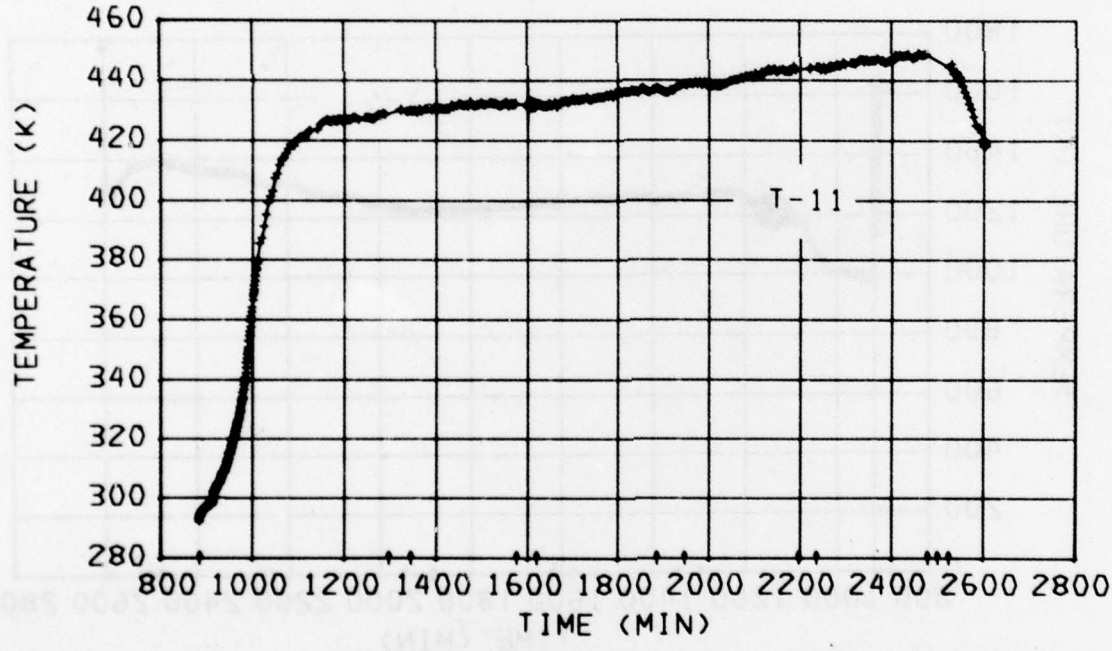

① ②③ ④⑤ ⑥ ⑦⑧ ⑨⑩⑪

1320 1640 2000 2320 0240 0600 0920 1240 1600 1920 2240

DAS TIME OR REAL TIME (HRS)

① THRU ⑪: SEE TEXT FOR TEST NO. DESCRIPTION

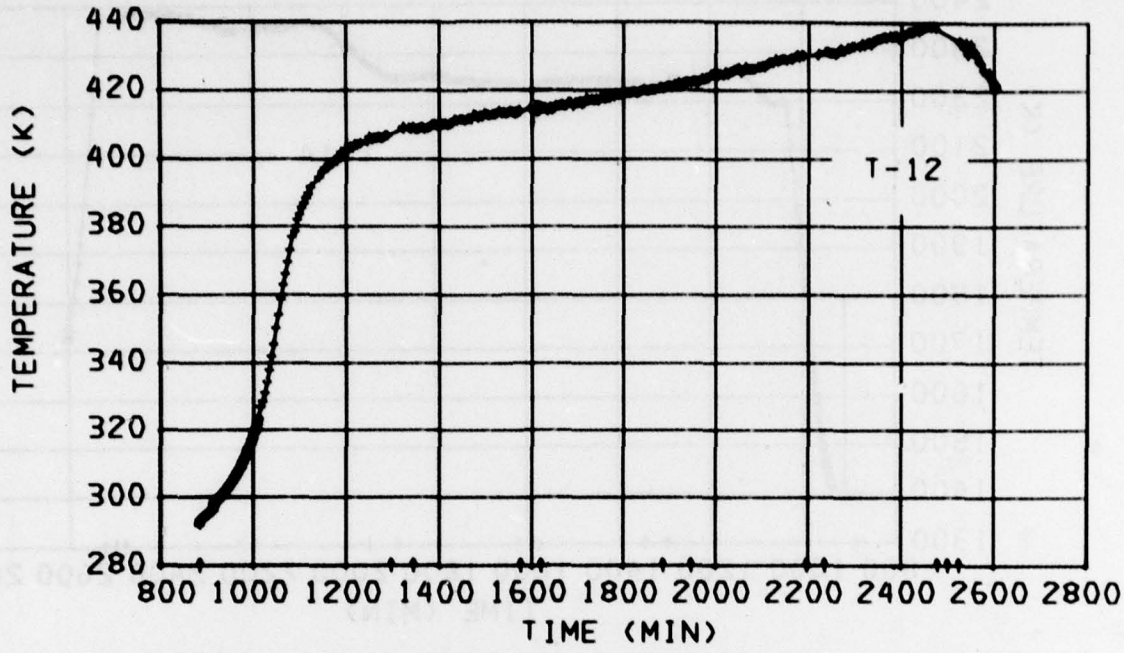

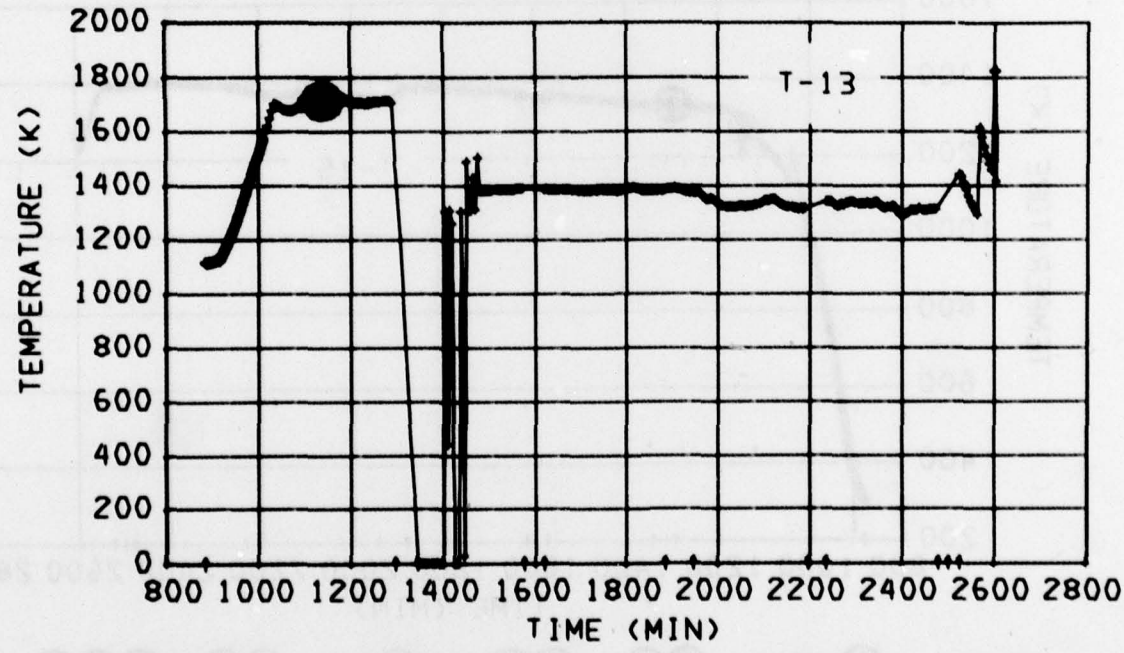

① ②③ ④⑤ ⑥ ⑦⑧ ⑨⑩⑪

1320 1640 2000 2320 0240 0600 0920 1240 1600 1920 2240

DAS TIME OR REAL TIME (HRS)

① THRU ⑪: SEE TEXT FOR TEST NO. DESCRIPTION

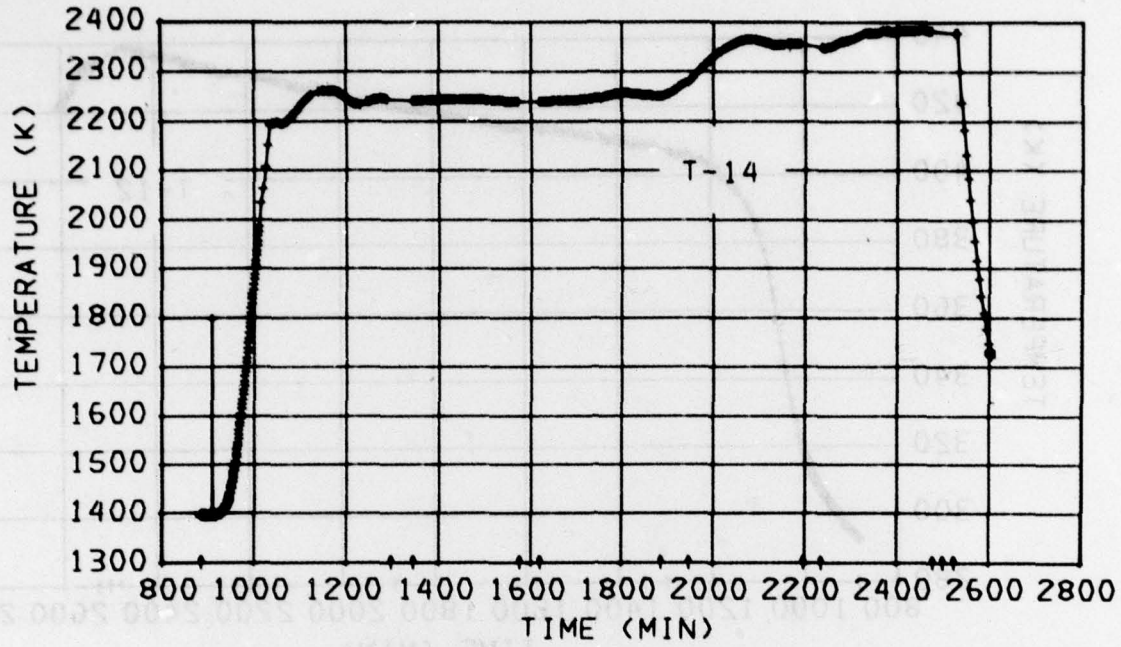

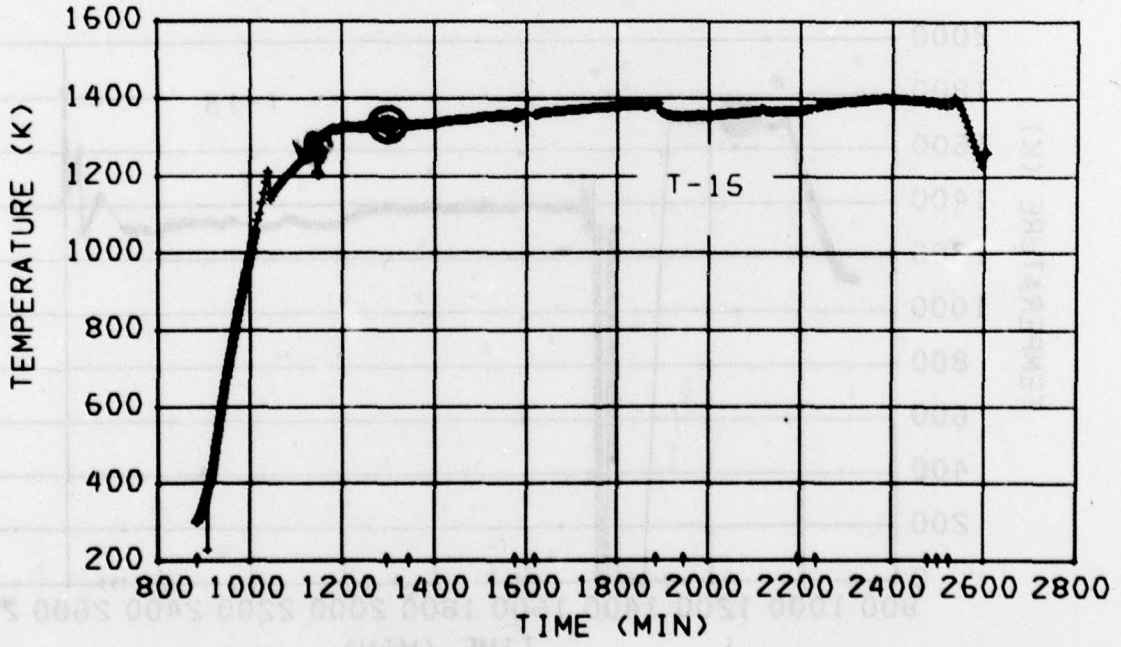

① ②③ ④⑤ ⑥ ⑦⑧ ⑨⑩⑪

1320 1640 2000 2320 0240 0600 0920 1240 1600 1920 2240

DAS TIME OR REAL TIME (HRS)

① THRU ⑪: SEE TEXT FOR TEST NO. DESCRIPTION

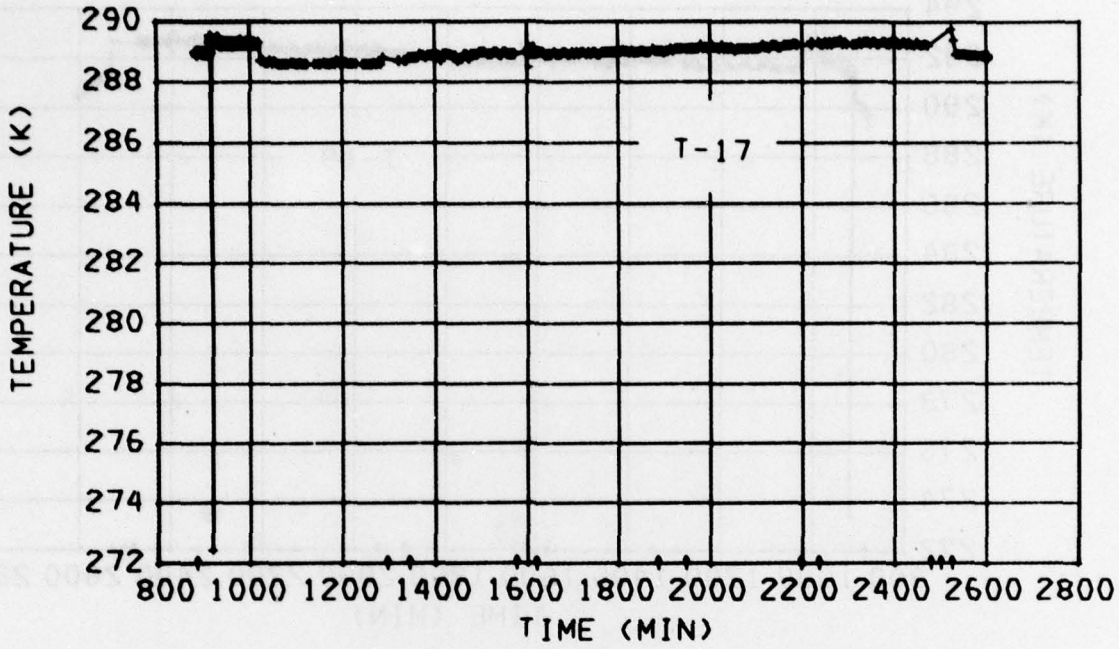

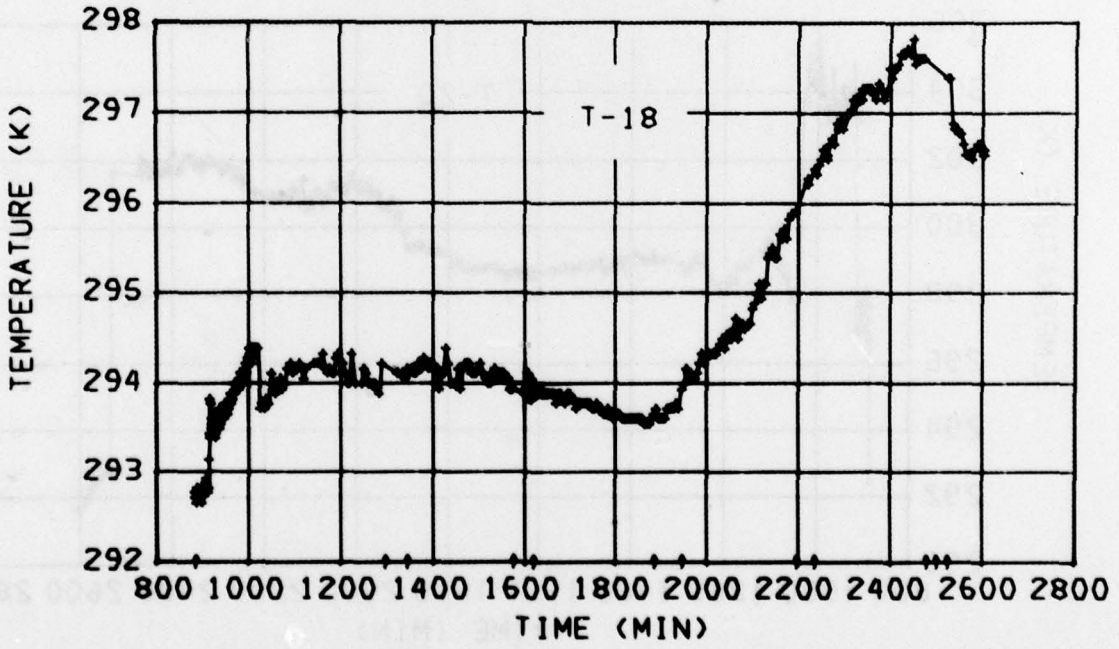

① ②③ ④⑤ ⑥ ⑦⑧ ⑨⑩⑪

1320 1640 2000 2320 0240 0600 0920 1240 1600 1920 2240

DAS TIME OR REAL TIME (HRS)

① THRU ⑪: SEE TEXT FOR TEST NO. DESCRIPTION

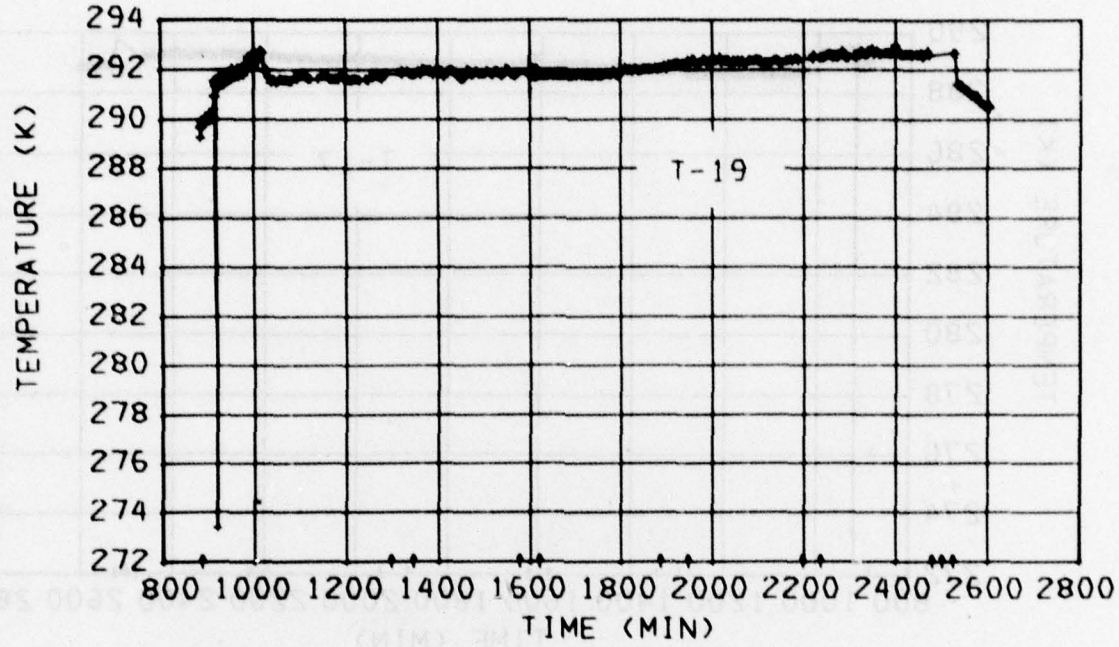

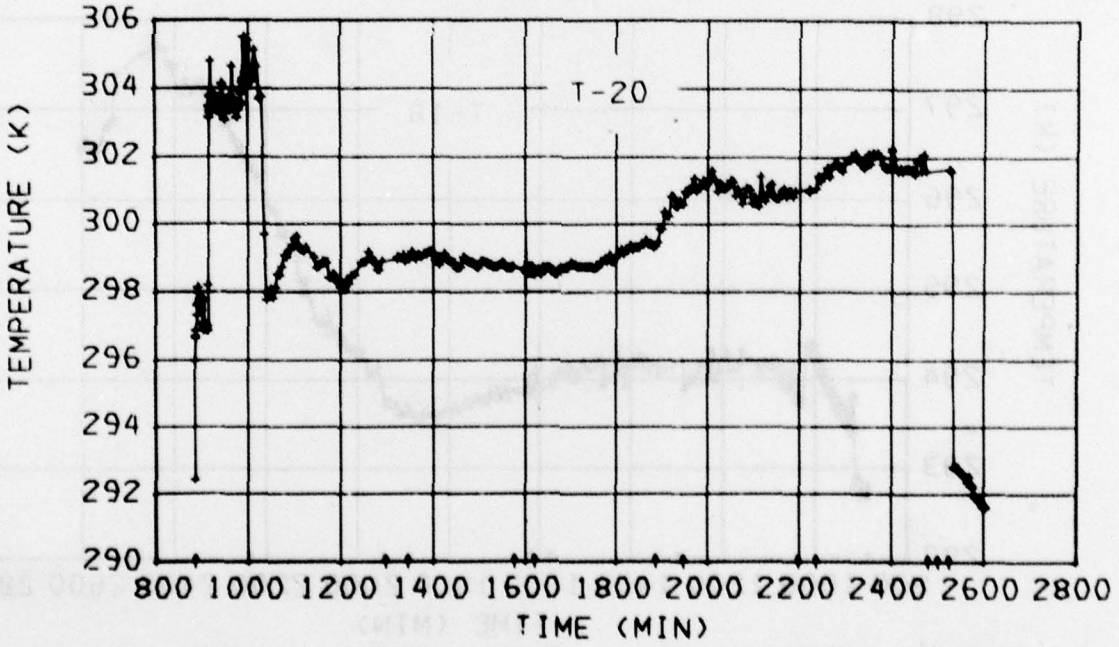

① ②③ ④⑤ ⑥ ⑦⑧ ⑨⑩⑪

1320 1640 2000 2320 0240 0600 0920 1240 1600 1920 2240

DAS TIME OR REAL TIME (HRS)

① THRU ⑪: SEE TEXT FOR TEST NO. DESCRIPTION

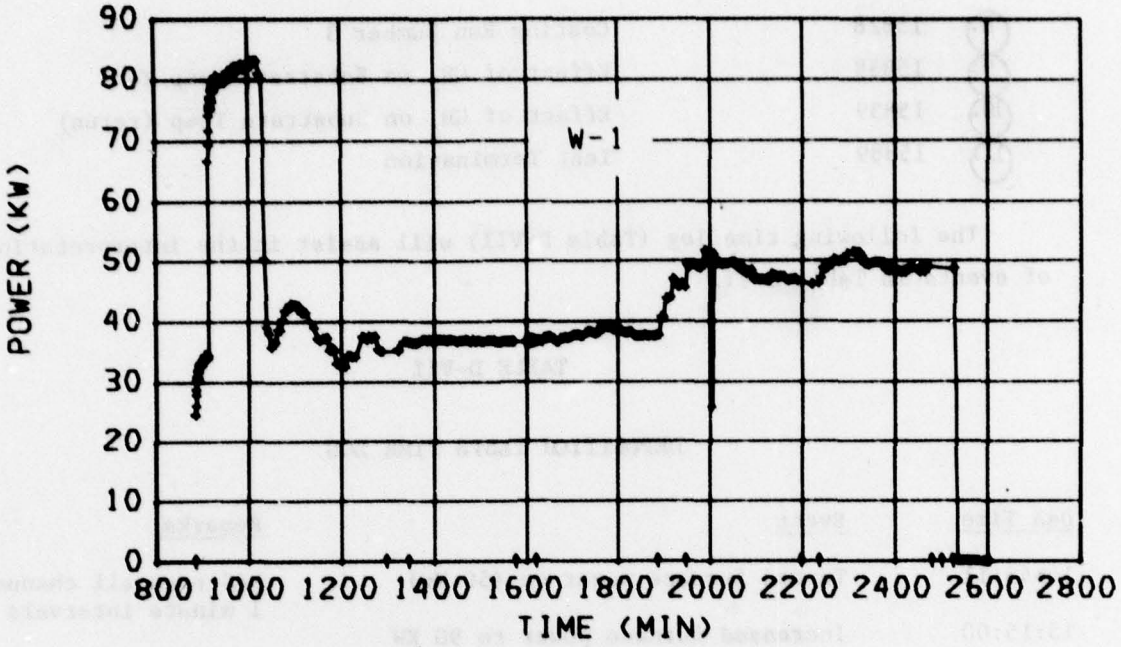

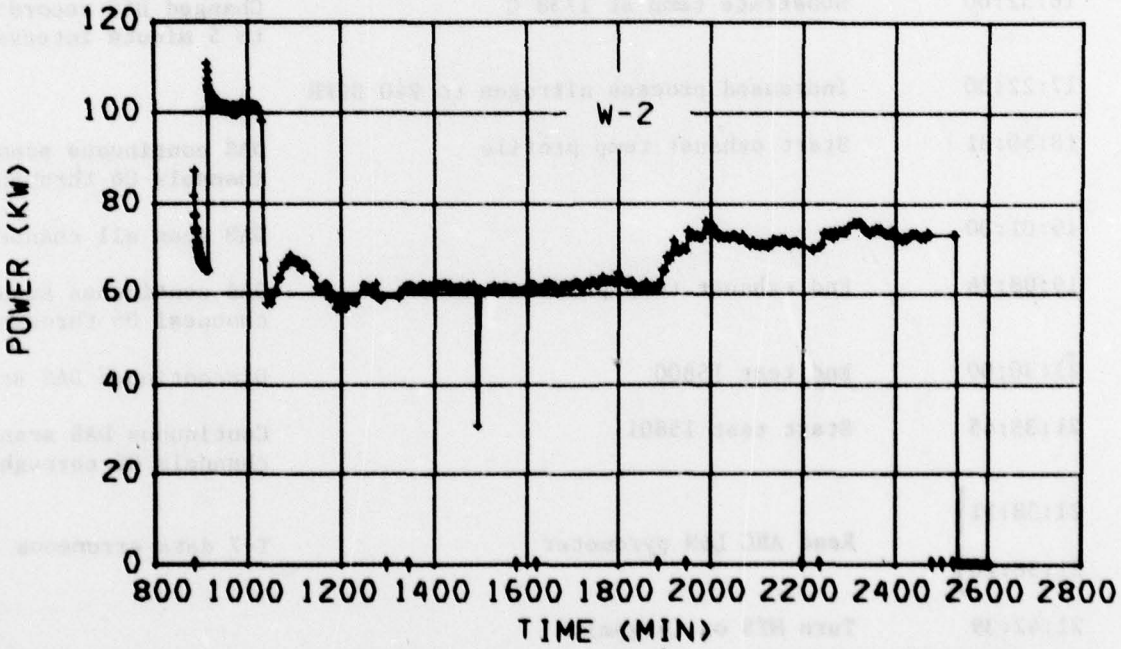

① ②③ ④⑤ ⑥ ⑦⑧ ⑨⑩⑪

1320 1640 2000 2320 0240 0600 0920 1240 1600 1920 2240

DAS TIME OR REAL TIME (HRS)

① THRU ⑪: SEE TEXT FOR TEST NO. DESCRIPTION

8.	15828	Coating Run Number 3
9.	15838	Effect of CH_4 on Substrate Temp T-7
10.	15839	Effect of CH_4 on Substrate Temp (rerun)
11.	15889	Test Termination

The following time log (Table D-VII) will assist in the interpretation of of events in Table D-VI.

TABLE D-VII

DEPOSITION TESTS TIME LOG

DAS Time	Event	Remarks
14:45:11	Turned furnace power on (50 Kw)	DAS scan all channels at 1 minute intervals
15:15:00	Increased furnace power to 90 KW	
16:52:00	Substrate temp at 1738°C	Changed DAS recording to 5 minute intervals
17:22:00	Increased process nitrogen to 940 SCFH	
18:50:31	Start exhaust temp profile	DAS continuous scan of channels 06 through 12
19:01:00		DAS scan all channels
19:08:26	End exhaust temp profile	DAS continuous scan of channesl 06 through 12
21:30;00	End test 15800	Discontinued DAS scan
21:35:45	Start test 15801	Continuous DAS scan of channels 06 through 12
21:38:11	Read ARC L&N pyrometer	T-7 data erroneous
21:38:20		
21:42:39	Turn MTS on (4 gpm)	
21:45:42	Turn MTS off	
21:51:26	Turn MTS on (6.5 gpm)	
21:58:20	Turn CH_4 on (3.48 lpm)	

TABLE D-VII (continued)

DAS Time	Event	Remarks
22:07:27 – 22:08:09	Read ARC L&N pyrometer	T-7 data erroneous
22:08:47	End test 15801	Discontinued DAS scan
22:15:00	Start test 15802	DAS scan all channels at 5 minute intervals
02:15:00	End test 15802	
02:16:08	Start test 15803	Continuous DAS scan of channels 06 through 12
02:22:52	Turn MTS off	
02:25:27 – 02:27:15	Read ARC L&N pyrometer	T-7 data erroneous
02:37:24	Turn CH_4 off	Continuous DAS scans of channels 06 through 12
02:39:46 – 02:40:59	Read ARC L&N pyrometer	T-7 data erroneous
02:41:28	End test 158003	
02:43:30	Start test 158004	Continuous DAS scan of all channels
02:45:14	MTS on (4.3 gpm)	
02:51:19	CH4 on (3.45 lpm)	
03:00:00		DAS scan all channels at 5 minute intervals
07:05:00	MTS turned off	
07:20:00	CH_4 turned off - End of test 158004	
07:25:00	Start test 158005	DAS scan all channels at 5 minute intervals
07:30:00	N_2 set to 1465 SCFH	
11:30:00	Start T-7 stabilization period	
12:30:00	Complete T-7 stabilization period	
12:30:00	End test 158005	

TABLE D-VII (continued)

DAS Time	Event	Remarks
12:36:16	Start test 15818	Continuous DAS scans of channels 06 through 12
12:38:09	Read ARC L&N pyrometer	T-7 data erroneous
12:38:37		
12:40:37	MTS turned on (4 gpm)	
12:47:08	MTS turned off	
12:51:48	MTS turned on (5.42 gpm)	
12:58:08	CH_4 turned on (6.04 lpm)	Continuous DAS scans of channels 06 through 12
13:02:00		Three DAS scans all channels
13:03:23		Continuous DAS scans of channels 06 through 12
13:04:02	Read ARC L&N	T-7 data erroneous
13:04:47		
13:05:44	End test 15818	
13:10:00	Start test 15828	DAS scan all channels at 5 minute intervals
17:15:00	End test 15828	
17:20:01	Start test 15838	Continuous DAS scans of channels 06 through 12
17:39:43	Abort test	
17:41:01	Start test 15839	Continuous DAS scans of channels 06 through 12
17:42:27	MTS Turned off	
17:43:20	Read ARC L&N pyrometer	T-7 data erroneous
17:44:06		

TABLE D-VII (continued)

DAS Time	Event	Remarks
17:58:33	Turn CH_4 off	
17:58:56 to 17:59:30	Read ARC L&N pyrometer	T-7 data erroneous
18:00:33	End of test 15839	
18:06:00	Start test 15889	DAS scan all channels at 5 minute intervals
18:10:25	Turn furnace power off	
19:20:00	Set N_2 at 200 SCFH	
19:22;02	Place all pyrometers in "Cal" position	Continuous DAS scan of all channels
19:24:28	End of test 15889	

The data depicted for paramter T-1 is incorrect prior to 16:32:30 on day 126. This is due to the fact that the pyrometer had not been calibrated in the "low range." Should this data become necessary for analysis of the furnace, the pyrometer will be calibrated and the data reduced.

Subsequent to the test, the pyrometer heads for parameters T-5 and T-6 were discovered to be reversed. The pyrometers were connected to the respective signal conditioners and DAS channels correctly. However, the units were "looking" at the wrong parameter. The reduced data depicts this discrepancy but the correct data was used for the computer model study.

The data from the pyrometer which measured T-13 is erroneous throughout the test. The unit could not be focused properly on the target.
Some of the figures show a single data point spike on day 126 at times 15:10:00, and 15:19:00, and 18:53:09. On day 127 a data spike appears on some of the figures at 02:45:50. These spikes represent erroneous data.